THERMO-PHYSICAL PROPERTIES OF ALKANOLAMINE- ETHANOL HYBRID SOLUTIONS: EXPERIMENTAL MEASUREMENTS AND MODELING

by

Seyedehsaleheh Razavi

BSc (Pure Chemistry), MSc (Physical Chemistry)

Submitted in Fulfillment of the Academic Requirements for **Master of Science in Chemical Engineering**, School of Engineering, College of Agriculture, Engineering and Science (AES), University of KwaZulu-Natal (UKZN)

Durban, South Africa

September 2021

Supervisor: Mr. Elly M. Obwaka

PREFACE

I,…… **Seyedehsaleheh Razavi (217034753)**……., declare that:

(i) The research reported in this thesis, except where otherwise indicated, is my original work.

(ii) This thesis has not been submitted for any degree or examination at any other university.

(iii) This thesis does not contain other persons' data, pictures, graphs, or other information unless specifically acknowledged as being sourced from other persons.

(iv) This thesis does not contain other persons' writing unless specifically acknowledged as being sourced from other researchers. Where other written sources have been quoted, then:

their words have been re-written but the general information attributed to them has been referenced;

where their exact words have been used, their writing has been placed inside quotation marks and referenced.

(v) Where I have reproduced a publication of which I am an author, co-author, or editor, I have indicated in detail which part of the publication was actually written by myself alone and have fully referenced such publications.

(vi) This thesis does not contain text, graphic, or tables copied and pasted from the Internet unless specifically acknowledged, and the source being detailed in the thesis and the Reference sections.

Signed: Seyedehsaleheh Razavi

Date: 27 September 2021

Supervisor:

Mr. Elly M. Obwaka

Signature:

Date: 2 April 2021

ACKNOWLEDGMENTS

In the name of God, the Most Gracious and the Most Merciful.

I thank God for all the opportunities, trials and strength that have been showered on me to finish writing the thesis.

I would like to express my gratitude and warmest thanks to my supervisor, Mr. Elly. M. Obwaka, for his friendly guidance and expert advice throughout all stages of this work. It has been a great pleasure to have him as my supervisor.

I also want to extend my thanks to to staff from the Thermodynamics Research Unit (TRU), especially Mr. A. Khanyile, and also staff from the Analytical Laboratory, especially Mrs. N. Hadebe.

I offer my special thanks to Admin Staff in the School of Engineering, especially Mrs. N. Dlamini and also staff from the College of Agriculture Engineering and Science, especially Mrs. A. Luthuli for their help and support in the administrative works.

My deepest gratitude goes to all of my family members. It would not be possible to write this thesis without the support from them.

ABSTRACT

This study presents the measured densities (ρ), viscosities (η) and refractive indices (n_D) of Monoethanolamine (MEA) + Ethanol (ETOH), N-Methyldiethanolamine (MDEA) + ETOH and Diethanolamine (DEA) + ETOH mixtures over the entire range of amine concentration, at temperatures from 293.15 to 333.15 K, with 5 K intervals and at atmospheric pressure. Densities and viscosities of the studied binary mixtures were measured using the combined DSA 5000 M and Lovis 2000 M/ME. Also, a commercial digital refractometer, Atago, RX-7000 α, was used to measure the refractive indices of the samples studied in the present work.

The experimental data of the pure amines were compared with those reported in literature and the low values of average absolute deviations (%AARD) confirm the reliability of the methods and the equipment applied in this work. The excess molar volume values for the studied mixtures (V^E) were determined through experimental density data and correlated using Redlich- Kister equation as a function of amine mole fraction. The sing and value of excess molar volume provide a better understanding of the structural effect and intermolecular interactions in the binary mixtures. Other thermo-physical properties including partial molar volume ($\overline{V}$), partial molar volume at infinite dilution ($\overline{V}^{\infty}$), and apparent molar volume (V_φ), were also obtained from V^E values and Redlich-Kister adjustable parameters.

The viscosity results were used to calculate the deviation in viscosity of studied mixtures. Also, the values of viscosity deviation were correlated using Redlich-Kister equation as a function of amine mole fraction. The values of V^E for all the solutions were found to be negative that shows the volume contraction of the studied mixtures when an alkanolamine and ethanol are mixed. The values of Δη for all the solutions are negative, which reveals the weak interactions between unlike molecules. Following experimental studies, several well-known and previously reported correlations were applied to calculate the densities, viscosities, and refractive indices of the studied binary systems that are discussed in detail in the subsequent chapters. The accuracies of the applied models were determined by calculating the average absolute deviations. The results show that the models/correlations can represent the experimental data with acceptable accuracies.

Also, several mixing rules were applied to estimate the refractive indices of the studied mixtures. These relations often estimate the refractive indices of mixtures from refractive indices of pure compounds that are practical while experimental data are not available. The estimated values of the refractive indices through mixing rules show excellent agreement with the experimental values of this work.

TABLE OF CONTENTS

LIST OF TABLES

LIST OF FIGURES

NOMENCLATURE

A	Fitting parameter	U	Internal Energy (J), ($m^2 \cdot kg/s^2$)
A_i	Polynomial coefficient	H	Enthalpy (J)
A_i	Redlich–Kister coefficients	S	Entropy (J/K)
F	Force (N)	G	Gibbs free energy (J)
k	Constant		
m	Mass (g)		
M	Molecular weight (g. mol^{-1})		
M_m	Molar parameter		
N	Number of measurements		
n	Number of moles (mol)		
n_D	Refractive index		
p	Pressure		
T	Temperature (K)		
V	Volume (cm^3)		
V^E	excess volume		
V_i	Molar volume of component i ($cm^3.mol^{-1}$)		
$\bar{V}_i^{\infty}$	Partial molar volume of component i at infinite dilution ($cm^3.mol^{-1}$)		
$\bar{V}_i$	Partial molar volume of component i ($cm^3.mol^{-1}$)		
$V_{\varphi,i}$	apparent molar volume of component i ($cm^3.mol^{-1}$)		
x_i	Partial molar volume of component i ($cm^3.mol^{-1}$)		
Y	Physio-chemical property		
Z_i	Regressed coefficient		

Abbreviations

AARD	Average absolute relative deviation
Cal	Calculated
CO_2	Carbon Dioxide
DEA	Diethanolamine
ETOH	Ethanol
Exp	Experimental
Lit	Literature
MDEA	Methyldiethanolamine
MEA	Monoethanolamine
Std	Standard

u(x)	Uncertainty

Greek letters

ρ	Density (g. cm−3)
η	Viscosity (mPa. s)
Φ	Volume fraction
Δ	Deviation
φ	Apparent
θ	Measured Value
δ	Standard deviation

Subscript

i	Component i
1	Component 1, MEA, MDEA,DEA
2	Component 2, EtOH

Superscript

∞	Infinite dilution
Cal	Calculated value
E	Excess property
Exp	Experimental values
id	Ideal property

CHAPTER 1: CO_2 CAPTURE

1. INTRODUCTION

The increase in global warming as a result of atmospheric greenhouse gas (GHG) concentrations is one of the most important environmental challenges and has recently become a topic of public concern. Continuous greenhouse -gas emissions including carbon dioxide, methane, nitrous oxide, and chlorofluorocarbons have been considered a major cause of global warming which in turn leads to severe environmental problems, such as melting of ice and snow cover, average sea-level rise and devastating weather patterns [1].

The atmospheric concentration of GHGs and also the average global temperature has increased steadily within the last century due to the rapid increase of population and world energy consumption. Among the significant greenhouse gases, carbon dioxide (CO_2) is a principal anthropogenic contributor to the greenhouse effect and global warming due to its emission quantity which is accounted for about 60% [2].

The global climate changes have been mainly attributed to increase in emitted CO_2 concentrations in the atmosphere through four potential sources:
(1) industrial processes,
(2) transportation,
(3) combustion of controversial fossil fuels (i.e., coal, petroleum, and natural gas),
(4) de-carbonization (production of hydrogen from carbon-rich feedstock),

At present, among the carbon dioxide emission sources, carbon-based fossil fuels provide almost 80% of the world's commercial energy needs [3]. Given that fossil fuel combustion is the main source of the huge energy demand for humans, strategies to mitigate CO_2 emissions in the atmosphere are urgently needs [4]. The monthly global CO_2 concentration reached 412 parts per million by volume (PPMV) in 2020 from an approximately pre-industrial value of 280 PPMV [4],[5]. Likewise, according to the Intergovernmental Panel on Climate Change (IPCC) ,it has been

predicted that the concentration of atmospheric CO_2 may increase to 570 PPMV by the year 2100 which causes a rise of 1.9 °C in the global temperature and an increase of 3.8 m in the mean sea level [6],[7].

Based on the National Oceanic and Atmospheric Administration (NOAA), the annual concentration of CO_2 in the atmosphere has increased by 3 ppm in the past 5 years. **Figure 1-1** represents the average monthly and annual concentrations of CO_2 from 1980 to 2020.

August 2021: 414.47 ppm
August 2020: 412.78 ppm

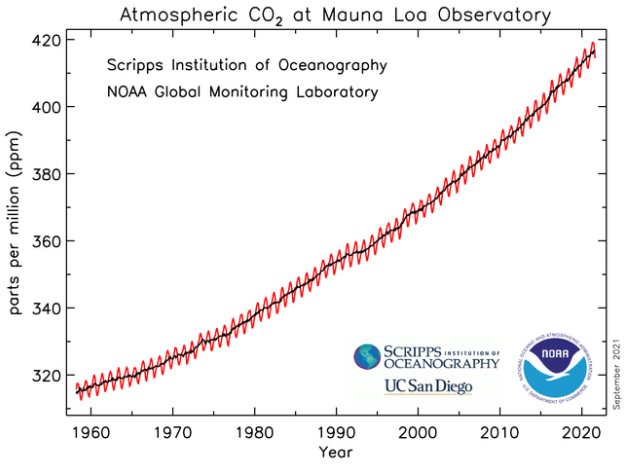

Figure 1-1 Atmospheric concentration of CO_2 from 1980 to 2020 [8]

Concern over the increase in atmospheric CO_2 level has urged scientists to develop technologies to cope with atmospheric carbon dioxide removal demand and consequently reduce the risk of global warming. In general, there are several strategies for CO_2 emission reduction into the atmosphere which is also shown in **Figure 1-2** [9]:

- Control and reduction of energy consumption (improve energy efficiency),
- Substituting coal to the low carbon fuels such as natural gas, hydrogen, and nuclear power,
- Production of energy from non-carbon energy alternatives like renewable resources (hydroelectric, wind, solar and biomass energy) instead of fossil fuels,
- CO_2 capture and storage technique (CCS),

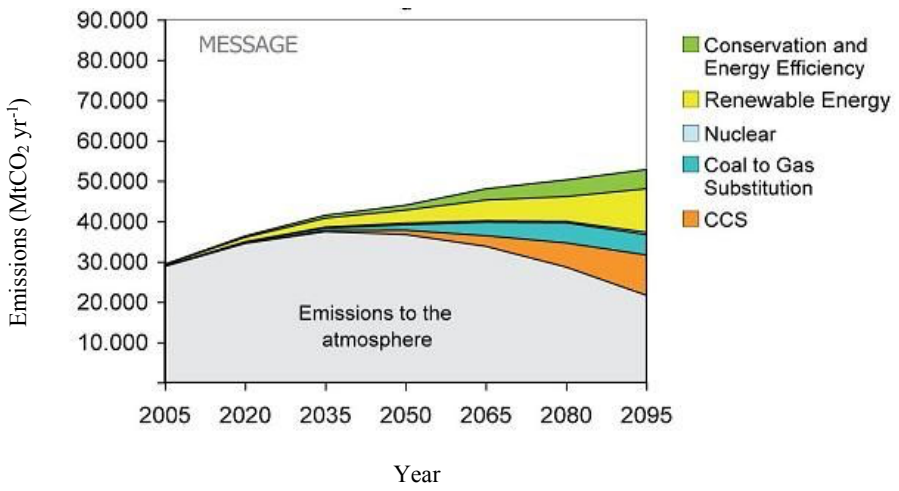

Figure 1-2 Global potential contribution of CCS as part of a mitigation portfolio. This figure shows the global CO_2 emissions in grey and corresponding contributions of main emissions reduction measures in colour [10]

Despite considerable research on renewable energy sources, using these sources as an alternative to fossil fuels is not commercially practical since they cannot meet the energy demands and are still not mature. Hence, fossil fuels are still the main source of energy and will remain the world dominant fuels over the next few decades until the low-carbon and even zero-carbon energy technologies can truthfully be applied. Amongst the different approaches, carbon capturing and storing (CCS) is the widely accepted way of trapping CO_2 from large point emission sources [9]. In the global CCS technology, carbon dioxide is trapped up to 90% from power stations and industrial sites. In this process, the CO_2 is captured from the fuel gas and separated from the sorbent. Then, the highly concentrated CO_2 is compressed and transported to a storage point through pipeline or ship, and finally, the captured CO_2 stored underground so that it does not go through the atmosphere and contribute to climate change. Since the separation and capture of CO_2 is the most costly and energy-consuming step of CCS which is contributing to about 70–80% of the total cost of the full CCS process, many types of research has aimed at improving the current technologies and developing novel methods to separate and capture CO_2 [11].

1.1 CO_2 capture technologies

Efficient capture of CO_2 from industrial sources is the most promising emission reduction approach with important environmental, economic and energy supply security benefits. Power

plants, oil and gas refineries, iron and steel production, as well as certain chemical plants, are the main industrial sources of CO_2. In carbon capture technologies, the regeneration energy of the capturing material is an important factor in determining the efficiency and cost-effectiveness of the process. Furthermore, the capturing materials should possess the capability to remove carbon dioxide from the gas mixture [12]. The CO_2 concentration in the gas stream, the pressure of the gas stream, and the type of the fuel either solid or gas are the key factors in choosing the capture method [13]–[15].There are three main CO_2 capture approaches associated with different combustion processes, including [7]:

(1) pre-combustion,

(2) oxy-combustion,

(3) post-combustion,

These technologies are illustrated in simplified form in **Figure 1-3** and discussed in the following sections [16].

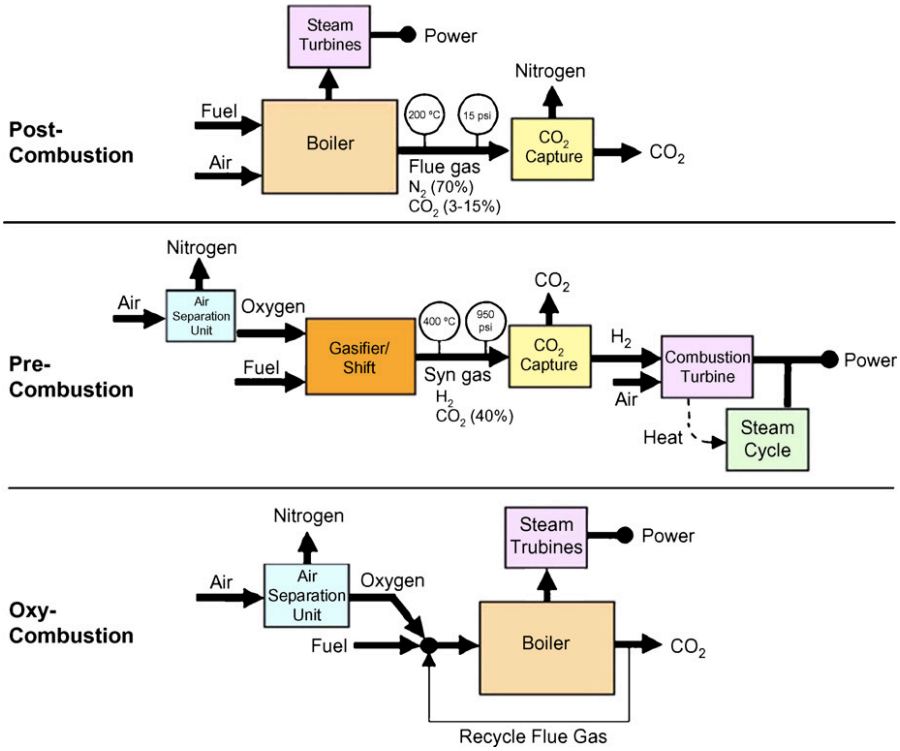

Figure 1-3 Schematic representation of CO_2 capture systems [16]

1.1.1 **Pre-Combustion Capture**

In this process, the fuel (coal or natural gas) is pretreated prior to combustion. Pre-treatment includes gasification and steam reforming for coal and natural gas, respectively. The fuel is then reacted with air/oxygen and steam to partially oxidize under high pressure and slightly elevated temperature to produce synthesis gas, a mixture with key components of CO, H_2, and water. This partial oxidation process provides the required heat to decompose the fuel and produce syngas. The excess steam as an oxidizing agent is then added to syngas in the shift reactor to convert CO to CO_2 and form more H_2. This process, known as water gas shift (WGS) reaction, results in the production of H_2-rich and CO_2- rich gas mixture (R-1) to (R-3).

$$\text{Coal} \xrightarrow{\text{gasification}} CO+H_2 \qquad \text{(R-1)}$$

$$CH_4+H_2O \xrightarrow{\text{reform}} CO+H_2 \qquad \text{(R-2)}$$

$$CO+H_2O \xrightarrow{\text{Water-gas shift}} H_2+CO_2 \qquad \text{(R-3)}$$

CO_2 is then captured from the gas stream, transported, and eventually stored. The remaining hydrogen-rich fuel can be subsequently used to generate electricity and power.

This method has some potential benefits over the post-combustion capture. Given that the gasification is operated at high pressure and the concentration of CO_2 is high in syngas, this technique has the potential of being less expensive than post-combustion capture. In pre-combustion capture, a much smaller volume of gas needs to be treated for the same amount of captured CO_2 in post-combustion which leads to much smaller equipment size. Besides, due to the high CO_2 partial pressure, more efficient capture technologies such as physical absorption can be used which would further reduce the energy penalty. Physical absorption technology uses physical solvents that are available at low cost and requires low regeneration energy [16]. Of the main disadvantages of pre-combustion capture is the high total capital costs due to its applicability mainly to new power plants [15]. Existing plants that will be retrofitted with CO_2 capture will mainly opt for post-combustion capture [17].

1.1.2 **Oxy-Combustion Capture**

Oxygen fired combustion commonly refers to the Oxy-combustion technique that consists of the process of burning carbon-containing fuels in pure oxygen rather than air. In this technique, the cryogenic air separation unit removes N_2 out of the air and produces pure oxygen. Pure oxygen is then injected with the fuel to the chamber where combustion happens. The resulting flue gas from the combustion process is almost totally CO_2 and water vapor. The steam is easily removed by condensation and then is separated from the flue gas. The resulting CO_2-enriched stream is then compressed, transported and eventually stored. The combustion temperature resulting from the burning of fossil fuels with pure oxygen is extremely high compared to conventional combustion in power plants. To avoid high flame temperature, CO_2- rich flue gas can be recycled and fed back into the combustor [15].

One of the advantages of the oxy-fuel combustion is that due to the production of CO_2- rich flue gas (over 80%) the simple process is required for CO_2 purification. Moreover, in this technique, no reagent and solvents are applied since oxy-fuel combustion relies mainly on physical separation processes. Likewise, due to the decreased flue gas volume and high concentration of CO_2, this technique offers low operating costs of carbon capture and causes less environmental problems [7]. The main drawback of oxy-fuel combustion is the need for a large quantity of oxygen coming from the energy-intensive air separation unit which is expensive in both energy consumption and capital cost [16],[15].

1.1.3 **Post-Combustion Capture**

In this method, carbon capture is performed after the combustion of fossil fuel. Fossil fuel is injected in the boiler and directly combusts in air. This produces steam and the flue gas of CO_2, N_2, and water. The resulting CO_2 is captured from the effluent gas of a combustion process using a suitable liquid solvent, which reacts chemically with the CO_2 and preferentially takes it out from the flue gas. The CO_2 in the loaded solvent is desorbed using temperature or pressure change. The resulting CO_2 is then compressed and becomes ready for transport to storage units. The generated steam is also used to power turbines and to make electricity [18] .The resulting solvent which is almost CO_2 free is then recycled and employed for a new cycle of separation.

However, carbon dioxide removal in the post-combustion technique is more challenging. A large quantity of gas should be handled due to the low CO_2 concentration in flue gas (less than 15%) which leads to large equipment size. Also, as the CO_2 level in combustion flue gas is quite low and the required concentration of CO_2 for transport and storage is over 95.5 %, the energy cost of the capture unit to reach this amount of CO_2 are quite expensive [16]. A further drawback of this technique as a result of low CO_2 concentration is that the powerful chemical solvents have to be used to capture CO_2 and consequently, a large amount of energy is required to release the CO_2. Moreover, the low CO_2 partial pressure in the flue gas and relatively high temperature of flue gases creates the additional technical design for the development of cost-effective capture processes. [15],[4]. Despite these disadvantages, post-combustion capture has been considered to be the most technologically mature and commercially viable option to capture CO_2 from fossil fuel because it represents the highest potential to be retrofitted to traditional pulverized coal power plants [19]. **Table 1-1** summarize the advantages and limitations of these different approaches.

Table 1-1 Comparison of different combustion technologies for CO_2 capture [16]		
	Advantages	**Disadvantages**
Pre-combustion	- Gasification is operated at high pressure. -The CO_2 concentration is high in syngas. -The much smaller volume of gas needs to be treated. -Much smaller equipment size is required. - The high partial pressure of CO_2 provides a greater driving force for the separation process and allows for the use of more effective separation technologies.	-High total capital costs of equipment due to its applicability mainly to new power plants. -Extensive modifications requirements to existing plants that can be retrofitted with CO_2 .
Oxy-combustion	-Very high CO_2 concentration in flue gas -Decreased fuel gas volume. -Simple process requirements for CO_2 separation and purification. - No need to use any reagent and solvents. - Low operating costs of carbon capture and fewer environmental problems. - Retrofit and repowering technology option.	-Large oxygen production requirements increase energy consumption as well as capital cost. - Oxy-fuel processes that can also be retrofitted into existing power plants are still unclear. - Decreased process efficiency
Post-combustion	-Applicable to most existing coal-fired power plants -More mature than other alternatives, It can be retrofitted to traditional pulverized coal power plants. - Extensive experience already exists for amine scrubbing from applications in chemical industrial processes [20] - High optimization potential to reduce energy losses -The highest degree of purity of the CO_2 (>99.99%) of all CCS technologies.	-Low CO_2 loading capacity that affects the capture efficiency. -Low CO_2 partial pressure. - High investment costs. -Comparably large environmental impact and Flexible operation mode has yet to be demonstrated

1.2 Technological routes for CO_2 capture

CO_2 capture and separation contribute 75% to the cost of overall CCS [21]. Hence, it is the most important issue for the CCS process to cut down the capture cost to the acceptable cost of the energy industry. Currently, several capture technologies have been established to successfully separate CO_2 from the flue/fuel gas stream prior to transportation. In this section, the main CO_2 separation technologies based on different physical and chemical processes have been described including [22]:

- Absorption in solutions (separation with chemical/physical solvents),
- Adsorption on solids (solid materials can be used to separate gases),
- Membrane technologies (porous or nonporous materials can be used to separate gases)
- Cryogenic distillation (separation of gases takes places based on the difference in their boiling points)
- Hydrate formation

These technologies are represented in **Figure 1-4** and discussed in the following sections.

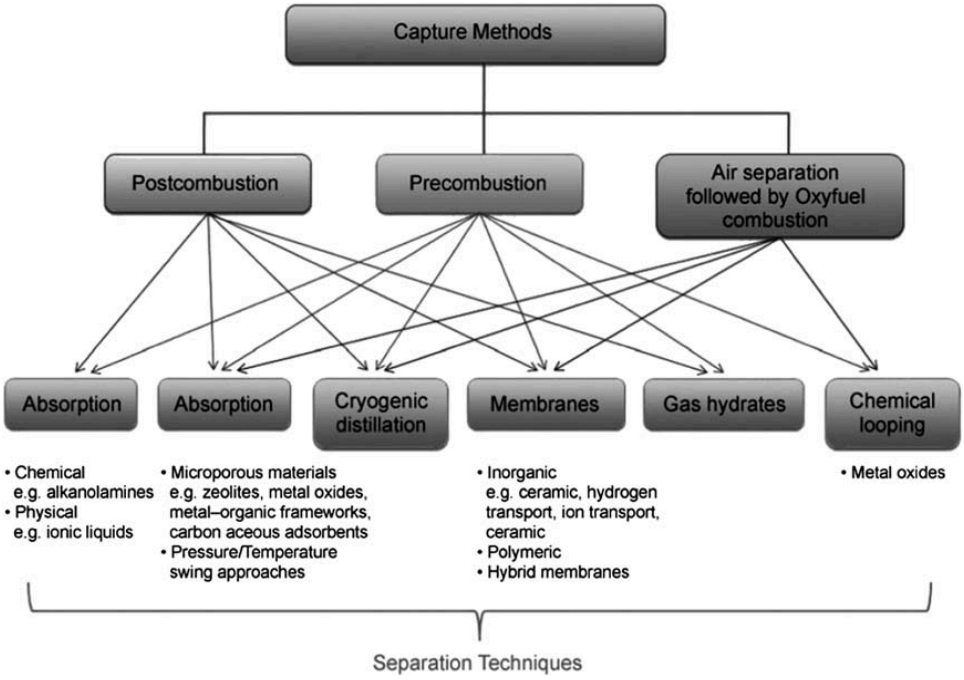

Figure 1-4 Different carbon capture technical methods for the CO_2 capture [23]

1.2.1 **Absorption**

The principal of CO_2 capture using absorption technology is that a liquid solvent is applied to separate the CO_2 from other main flue gas components. The type of solvent and its selection are the main part of the absorption technique. The loaded solvent can be regenerated through a stripping or regenerative process by either reducing pressure, raising the temperature, or a combination of both. The solvent-based absorption method is the most mature and applicable technique for CO_2 capture. In general, solvents are categorized based on their reaction types in the solution [18]. Different types of solvents include chemical, physical, and mixture of solvents which are discussed in the following sections. It is to be noted that based on the investigations by Electric Power Research Institute, the absorption-based processes account for almost 60% of post-combustion CO_2 technology [24]. The available solvents that applied for capturing CO_2 pose several disadvantages such as solvent degradation and loss, high regeneration energy, and corrosiveness. To decrease these drawbacks, different methods have been reported in the literature including the use of alternative solvents and process configuration together with process optimization. The main subject of current research is the use of alternative solvents that are more energy-efficient and environmentally friendly. A brief review of solvent-based CO_2 capture technologies has been reported by Mumford *et al,* 2015 [25]. The authors briefly discussed the utilization of physical and chemical solvents as well as their mixture in the CO_2 capturing process [25]. The ideal solvent for the absorption process must meet several features. For solvent evaluation, the following criteria are proposed [26]:

- CO_2 absorption capacity: the maximum amount of CO_2 absorbed per unit mass of the solvent (kg CO_2 /kg solvent).
- Regeneration energy: The required energy to strip CO_2 from the solvent. This energy is the same amount as the heat released during absorption and reaction. Therefore, the absorption heat (released energy when the solvent absorbs carbon dioxide) and reaction heat (released energy when the CO_2 is absorbed by a chemical solvent) affects the energy required during the regeneration.
- Reaction rate: The chemical reaction rate is an important factor that affects the size of the absorber and stripper in the absorption system. Also, the absorption and regeneration reaction rates impact the required volume of solvent for CO_2 separation. The slower the

absorption and regeneration reaction rates are, the larger amount of solvent is required that leads to an increase in capital and operating cost.

- Degradation rate: Oxidative degradation is a problem that occurs while the solvents like amines contacted with impurities such as O_2, NO_x, and SO_x under elevated temperature. Atmospheric degradation might happen if the solvent reacts with OH radicals during the day. The products of degradation might be toxic and/or volatile.
- Corrosiveness: Equipment corrosiveness strongly depends on the type of solvents. For instance, since most amines are highly corrosive, to reduce the equipment corrosiveness they must be diluted which causes an increase in the operating costs.
- Solvent cost: Solvent cost is an important criterion for solvent evaluation that strongly vary among solvents from cheap and simply available (e.g., NH_3) to very expensive (e.g., ILs).

The desired properties of an ideal solvent for chemical absorption include fast reaction rate to CO_2, high absorption capacity, low regeneration energy which means low heat of reaction with CO_2, high thermal stability, low corrosive behavior, low solvent cost, and low environmental effect [27].

1.2.2 **Adsorption**

The phenomenon of concentration of molecules of a liquid or gas at a solid surface is defined as adsorption. In the adsorption process with the aim of CO_2 capturing, CO_2 from a gas stream attaches itself to the surface of a solid sorbent by either physical (physisorption) or chemical processes (chemisorption) and hence is removed selectively from the gas stream. For applications to CO_2 capture, several physical solid adsorbents have been proposed including, metal-organic frameworks (MOFs), activated carbons, zeolites, and zeolite-like materials [12]. However, to develop a proper CO_2 capture technique, an appropriate adsorbent should satisfy several important criteria, including [28],[12]:

(1) low heat capacity,
(2) low-cost raw materials,
(3) high adsorption-desorption reaction rate,
(4) high surface area,
(5) high selectivity to CO_2,

(6) high CO_2 loading capacity,

(7) high thermal, mechanical, and chemical resistance,

(8) high regeneration ability.

The selective removal of CO_2 from a gas stream can be achieved by three main techniques [28]:

- Reducing pressure (Pressure-Swing Adsorption (PSA))
- Passing an electric current through the adsorbent (Electric swing adsorption (ESA))
- Increasing temperature (Temperature Swing Adsorption (TSA))

1.2.3 **Membranes**

Membranes are especial industrial materials that permit the gases to pass through them selectively. In general, the membrane process depends on the concentration of gas, the nature of the material, and the difference in pressure across the membrane. A membrane should possess several properties to be practical for the capture of carbon dioxide, including [29]:

(1) high permeability and selectivity with respect to CO_2,

(2) High thermal, chemical, and aging stability,

(3) being cost-effective,

Various types of membranes are currently available such as organic (polymeric) membrane, inorganic (zeolite, carbon, ceramic or metallic) membrane, porous or non-porous membrane [12].Main membrane technologies are often classified as gas separation membrane and gas absorption membrane which is described below and shown in **Error! Reference source not found.**.

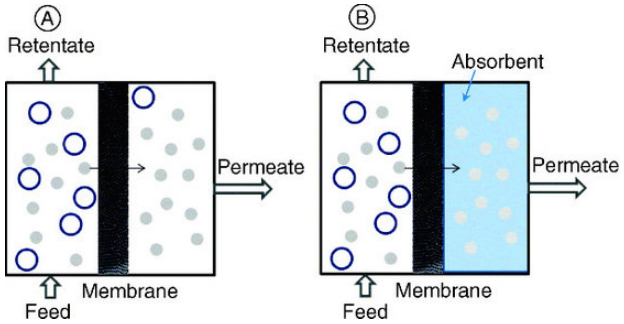

Figure 1-5 a) Gas separation membrane and, b) Gas absorption membrane technology [30]

1.2.3.1 Gas separation membrane

In the gas separation membrane process, a membrane separates specific components preferentially from the exhaust gas of a power plant and generates a certain gas-rich permeate. These semi-permeable barriers perform as filters to extract selectively CO_2 from flue / natural gas in the post-combustion capture process and hydrogen in the pre-combustion capture process. The earliest application of membranes for gas separation technology dates back to the 1980s and since then membranes have been widely applied in many industrial separation processes [12]. The ideal CO_2 separation through the membrane can take place when the gas stream contains a high concentration of CO_2 and low concentration of contaminated gasses and the permeable membrane shows high selectivity with respect to CO_2.In practice, the gas stream has low pressure, low CO_2 concentration, and high impurities. Furthermore, the membranes are not selective enough to CO_2 to achieve the desired purity, hence, multiple stages are required to reach a high degree of CO_2 separation that would noticeably increase complexity, energy consumption and capital costs [31].

1.2.3.2 Gas absorption membrane

In the gas absorption process, the membrane acts as a contacting device to put the flue gas (like CO_2) and the liquid solvent (like MEA) in contact with each other and thereby, enhancing the physical and chemical absorption efficiency. The membrane applied in this process is a porous, hydrophobic membrane and the liquid can be carbonate or amine solutions. The hydrophobic membrane barrier separates the gas phase from the absorption liquid phase. The gas to be separated diffuses through the membrane, and gets absorbed in the liquid [32], [33]. The capital cost in this technology is lower than that of the conventional membrane. The limitation of this process is that the pressure of the gas stream and liquid solvent should be at the same level. In contrast to the gas separation technology that the membrane gives the process its selectivity, in gas absorption technology, it is the liquid that determines the selectivity of the process. In membrane technology, CO_2 can be separated from flue gas through one of the following concepts [33]:

- The difference of the CO_2 partial pressure throughout the membrane
- Reversible chemical reaction with carriers like carbonates, amine, or molten salt hydrates dissolved in the membrane liquid, or porous inorganic materials.

The main drawback related to the limited application of the membrane technology is that high separation efficiency cannot always be achieved in this process due to the low selectivity of these materials. Further disadvantages of membranes include: the lack of stability under the reforming environment (which contains steam and hydrogen sulfide), operational problems of low fluxes and fouling, the challenge of preventing membrane wetting, and finally, they are currently in the research phase of development [29].

1.2.4 **Cryogenic separation**

Cryogenic separation includes the fractional condensation and distillation of gas mixtures in multiple stages at very low temperatures and high pressure to liquefy and purify CO_2. This technology is comparable to other conventional distillation processes except that instead of components of a liquid, the components of a gas mixture are separated using the difference in their boiling points [9].

During cryogenic separation the flue gas including CO_2 is cooled to the very low temperature of -100 to -135 degrees Celsius (slightly above the point where CO_2 forms a solid). At this temperature, CO_2 desublimes or changes from a gas state to a solid-state. The solid CO_2 can thereby be separated from the other light gases, pressurized to the high pressure of 100–200 atm and finally stored. This process allows the pure CO_2 to be recovered in the liquid form. The liquified CO_2 can be transported conveniently or can be pumped to the injection site to enhanced coal-bed methane (ECBM) or enhanced oil recovery (EOR) [9]. Cryogenic separation shows high potential for separation of CO_2 from high-pressure and high CO_2 concentration gas streams, such as in pre-combustion capture processes, or oxy-fuel combustion.

The CryoCell technology uses a cryogenic process to separate CO_2 from the natural gas, while it eliminates corrosion-related issues, water consumption and chemical usage. A simulation and modeling technique in Aspen HYSYS has also been used to evaluate the efficiency of the cryogenic process for producing a high purity, high-pressure CO_2 from oxy-fuel combustion flue gas [34]. Despite several researches on this process, Cryogenic distillation is an energy-intensive process Since the distillation is conducted at extremely low temperatures and high pressures [35].

1.2.5 **Chemical looping**

Chemical-looping is a cycling process and considered one of the promising CO_2 capture technologies accompanied by post-combustion, pre-combustion, and oxy-combustion. In the Chemical-looping process, an oxygen carrier in the form of metal oxide is used to transfer oxygen from the combustion air to the fuel via oxidation-reduction reactions. Metal oxide avoids direct contact between fuel and air. A typical chemical looping combustion process consists of two interconnected reactors, a fuel reactor, and an air reactor. During the process, the metal oxide is reduced to metal in the fuel reactor via a chemical reaction while the fuel is being oxidized to CO_2 and water. The reduced oxygen-carrier (or metal) is further transferred into the air reactor which contains N_2 with unused O_2. The metal is then re-oxidized in the air reactor and recycled in the process. The reactions of the fuel in the fuel reactor and oxygen carrier in the air reactor are provided in reactions 4 and 5, respectively, which Me_xO_y stands for the oxidized oxygen carrier and Me_xO_{y-1} represents the reduced oxygen carrier.

$$\text{Fuel} + n\text{Me}_x\text{O}_y \longrightarrow n\text{Me}_x\text{O}_{y-1} + \text{H}_2\text{O} + \text{CO}_2 \qquad \text{(R-4)}$$

$$\text{Me}_x\text{O}_{y-1} + \tfrac{1}{2}\,\text{O}_2 \longrightarrow \text{Me}_x\text{O}_y \qquad \text{(R-5)}$$

Fuels in chemical-looping can be either gaseous fuels (natural gas, refinery gas, syngas, etc.) or solid fuels (coal, petroleum coke, and biomass). The schematic representation of the chemical-looping combustion process is shown in **Figure 1-6**.

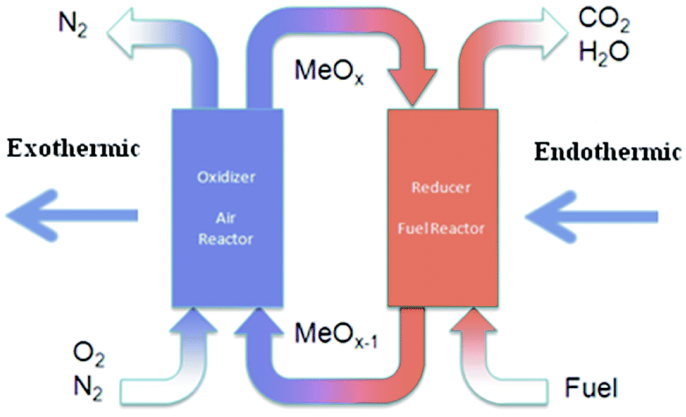

Figure 1-6 Chemical-looping combustion process [36]

After water condensation of gas stream generated from the fuel reactor, almost pure CO_2 can be obtained without the consumption of energy for separation. The overall amount of heat evolved in the CLC process is the same as normal combustion in which the oxygen is in direct contact with the fuel. There is no need of using external capture devices in this process as there has no significant energy penalty for the capture process. Thereby, the chemical looping process is potentially much cheaper than other technologies proposed for CO_2 separation. Further, the large size separation equipment is not required as air and fuel go through different reactors and combustion takes place without flame [37].

The main drawback of the overall chemical looping combustion process is that the oxygen carriers are subjected to strong chemical and thermal stresses in every cycle and the performance could be poor after enough number of cycles in use. The oxygen carrier is mostly composed of a metal oxide (active phase) and support (inert phase). A wide variety of metal oxides have been proposed as promising candidates for this process including Fe_2O_3, NiO, CuO, CdO, and Mn_2O_3 with the advantage of being low-cost and suitable [38]. The inert phase acts as porous support and can be used to optimize the performance of the metal oxides by providing a higher surface area for the reaction and enhanced mechanical strength of the particles [39].

Various researchers have investigated the effectiveness of different metal oxides in the Chemical looping process [40],[39]. In particular, oxygen carriers for chemical looping process should possess the following properties [39], [40]:

- Fast reactivity during reduction by fuel and oxidation by air,
- High chemical, structural, and mechanical resistance to tolerate the stresses resulting from a high number of reduction-oxidation cycles,
- Resistant to agglomeration,
- Resistant to carbon formation,
- Low-cost production,
- Nonthreatening environmental impact,

1.2.6 **Clathrate hydrate**

Amongst the new concepts for CO_2 capture, gas hydrate crystallization has received great attention both from the industry and academic researchers during the last two decades. The discovery of gas hydrates (or clathrates) is credited to Sir Humphrey Davy in the early 19th century [18]. Clathrate hydrates are ice-like inclusion crystals formed in mixtures of water and non-polar or slightly polar low molecular weight gases or volatile liquids at low temperature, specified (generally high) pressure, and material availability condition [41]. Clathrate hydrates are formed once hydrogen-bonded water molecules form structures resembling cages (host) containing cavities. These structures are thermodynamically unstable without the presence of the hydrate forming molecules in the cavities. To stabilize the cage-like structures, the cavities have to be filled with the hydrate forming molecules also known as guest molecules. The size ratio of the guest molecule to the cavity determines whether or not the guest molecule can form a stable hydrate structure. To achieve a stable hydrate structure the ratio should be almost 0.9 [42]. Stable hydrates structures cannot be formed in case the size ratio is notably less or over unity. The guest molecules can be either non-polar or slightly polar and include CO_2, O_2, N_2, H_2, and natural gas components. It is to be noted that there is no chemical bonding between the host and guest molecules. The cage is held together by hydrogen bonds between water molecules and inside the cage, guest molecules interact with water molecules by van der Waals forces. In fact, this Van der Waals force makes the gas hydrate very stable. The clathrate hydrate is more stable than hexagonal ice. Only one guest molecule can be trapped in each cavity. However, some researches on the gas hydrate have shown that more than one H_2 molecule can be trapped in one cavity under certain pressure and temperature conditions [43], [44].

The basis for the use of clathrate hydrate formation/decomposition as a separation process is the concentration of the gases in the hydrate crystals is different from that in the original gases mixture [45],[46].

Different structures of clathrate hydrates can be formed based on the chemical properties and the size of the guest molecule in the mixture. Furthermore, the types of formed cavities and the distribution of these cavities in a unit cell are used to distinguish the structures of clathrate hydrates [45].

Clathrate Hydrates crystallise in three predominant structures based on the geometries of their constituent water cages. Structure (type) I (SI) and Structure (type) II (SII) both crystallize in a cubic system and structure (type) H crystallise within a hexagonal framework. Five types of hydrate cages are known. The smallest hydrate cage which is defined as pentagonal dodecahedra is formed by twelve five-sided polygons (5^{12}). This type of hydrate cage is present in all three structures of gas hydrates. By linking two, four, or eight hexagonal faces (6^2, 6^4, 6^8), three more types of hydrate cages can be formed with larger diameters. These types of cages denote as $5^{12}6^2$ in structure I, $5^{12}6^4$ in structure II, and $5^{12}6^8$ in structure H. Besides, structure H has a medium cavity with three square, six pentagonal, and three hexagonal faces (4^3 5^6 6^3). A unit cell of structure I is composed of 46 water molecules forming six large cavities with the shape of tetradecahedron ($5^{12}6^2$) and two small cavities with the shape of a pentagonal dodecahedron (5^{12}). Molecules with a molecular diameter less than 6 Å, such as methane, ethane, hydrogen sulfide, and carbon dioxide can form structure I. However, nitrogen with diameter of less than 4 Å and other small molecules are considered as exceptions and they form structure II [47]. A unit cell of structure II is composed of 16 small cavities (5^{12}) and 8 large cavities with the shape of hexadecahedron ($5^{12}6^4$) which are created by 136 water molecules. Structure II is formed with molecules with a diameter less than 4 Å and greater than 6 Å up to 7 Å such as hydrogen, nitrogen, and propane. Structure H forms a more complicated crystal containing three types of cavities. A unit cell of structure H is composed of 34 water molecules forming 3 small cavities of 5^{12}, 2 medium cavities of 4^3 5^6 $6^{3,}$ and 1 large cavity of $5^{12}6^8$ [47]. The large cavity in structure H is estimated to fit guests with diameter of 8 to 9 Å. Small molecules such as methane, xenon, or hydrogen sulfide, can fill the two small cavities in structure H [47].

The shapes of all the formed cavities in structures I, II, and H are indicated in **Figure 1-7**. Furthermore, **Table 1-2** provides a quick comparison among different hydrate structures of type I, II, and H.

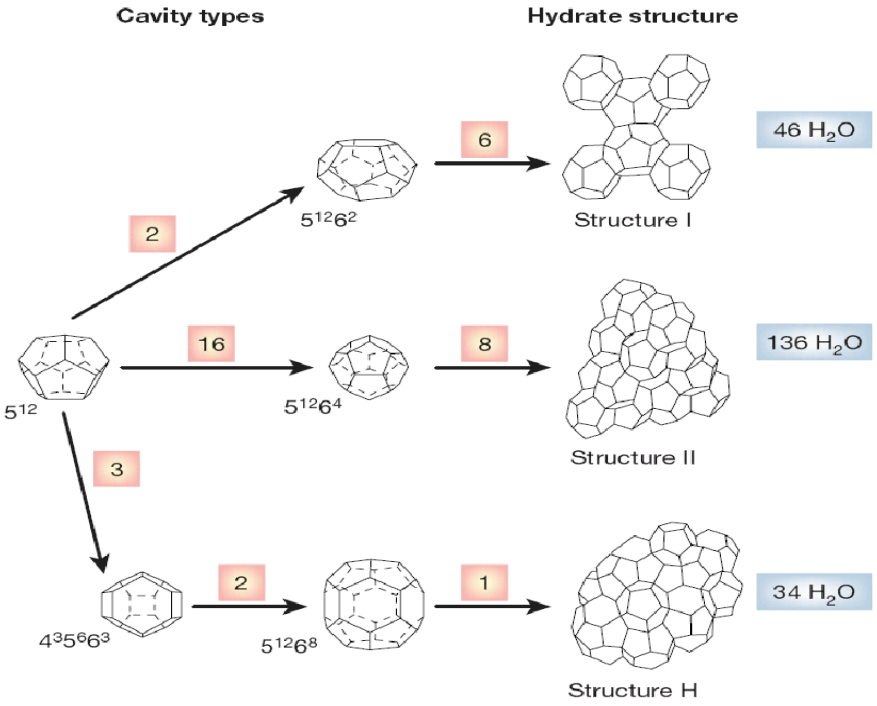

Figure 1-7 Gas hydrate cavity structure [48]

Table 1-2 Structural properties of hydrates [48]

Hydrate crystal structure	I		II		H		
Cavity	Small	Large	Small	Large	Small	Medium	Large
Description	5^{12}	$5^{12}6^2$	5^{12}	$5^{12}6^4$	5^{12}	$4^35^66^3$	$5^{12}6^8$
Number of cavities per unit cell	2	6	16	8	3	2	1
Average cavity radius (Å)	3.95	4.33	3.91	4.73	3.91†	4.06†	5.71†
Coordination number*	20	24	20	28	20	20	36
Number of waters per unit cell	46		136		34		

1.3 Research objective

The main purpose of this MSc program is to study thermo-physical properties of a simple and cost-effective hybrid alkanolamine solvent for chemical absorption of CO_2, as the most commonly used CO_2 capture process in industry. Hybrid solvents, mixture of alkanolamines and alcohol, have been employed in this study mainly due to their less solvent regeneration energy over chemical solvents.

Since ethanol is an environmentally friendly alcohol with low toxicity and it is easily available, it can be a proper physical solvent to mix with alkanolamines for the CO_2 absorption process. Hence, in this study, the mixture of commonly used alkanolamines was selected in CO_2 capturing together with ethanol as the solvent.

A comprehensive experimental and theoretical study on the three binary hybrid solvents of alkanolamines (MEA, DEA, MDEA) and ethanol has been performed in this research. To this end, the following objectives are outlined:

1- To measure the thermo-physical properties of the selected mixtures to contribute to the data bank of thermodynamic properties of amine-based solutions.
2- To measure the experimental values of density, viscosity and refractive index of selected binary solvents of alkanolamines and ethanol over the entire range of mole fraction at various temperatures T= (293.15 to 333.15 K) and at atmospheric pressure along with estimating the experimental uncertainties.
3- To measure the physio-chemical properties of the studied solutions including excess molar volume, partial molar volume, partial molar volume at infinite dilution, and apparent molar volume from the density experimental data.
4- To correlate:
   a) the obtained density, viscosity, and refractive index values,
   b) the excess thermodynamic properties including excess molar volume
   c) the viscosity and refractive index deviation using the several well-known predictive empirical models.

1.4 The novelty of this study

Volumetric and viscometric properties of the solutions as well as other thermo-physical properties such as refractive index are of utmost importance in the design and optimization of CO_2 capture equipment. As mentioned earlier in this chapter, a considerable amount of research has been conducted on the thermo-physical properties of aqueous amine-based solutions. However, few authors have reported on the application of non-aqueous alkanolamines solvents for CO_2 absorption, and studies on the experimental density and viscosity of alkanolamines in alcoholic solutions including methanol and ethanol is still lacking. Also, it is to be noted that there has been no data reported in the literature for the refractive index of the mixtures of alkanolamines and ethanol solutions used in this study until now.

For the selected solvents in this study including MEA-ETOH and MDEA-ETOH, only two previous studies have been reported on the density and viscosity of these mixtures and for a non-aqueous mixture of DEA-ETOH, no research has been conducted so far. Also, no investigations have been done on the refractive index of these hybrid solvents. Comprehensive literature review on the correlation of thermo-physical properties of the selected solvents in this study showed that only the excess volume of these mixtures (except for DEA-ETOH) have been correlated earlier using Redlich-Kister equation and the rest of the empirical models that applied in this study have not been reported for these mixtures as yet.

Hence, the current study is the only research that has reported refractive index of the MEA-ETOH, MDEA-ETOH and DEA-ETOH solutions at different temperatures of 293.15 to 333.15 K and has conducted a comprehensive study on the correlation of density, viscosity, refractive index and refractive index deviation using several well-known predictive empirical models.

1.5 Overview of this thesis

In this thesis, extensive investigations of the interactions between three different mixtures of the Monoethanolamine (MEA) + Ethanol (ETOH), N-Methyldiethanolamine (MDEA) + ETOH and Diethanolamine (DEA) + ETOH, over the entire range of amine concentration, at atmospheric pressure and temperature range from 293.15 to 333.15 K, with 5 K intervals, were carried out.

Chapter one focuses on the technologies to capture CO_2 from flue gas as well as the common technological routes for CO_2 capture.

In chapter two, an overall literature review including absorption techniques to capture CO_2 as well as different types of solvents for the absorption process is discussed. Chemical, physical and hybrid solvents together with amine-based solvents are reviewed.

Chapter three represents a comprehensive study on the solution thermodynamic theory. Also, a brief review of different data correlation techniques for density, viscosity, and the refractive index of binary liquid mixtures are presented in this chapter.

In chapter four, a brief review of some physio-chemical properties of the solvent including density, viscosity, and refractive index along with their measurement methods have been reviewed.

Chapter 5 describes the materials used to prepare the different solutions and also the experimental equipment applied to measure the physical properties of all pure components and the corresponding mixtures. A detailed explanation of the procedures to carry out the experiments is discussed in this chapter.

Chapter six presents the results of the experimental runs for different systems in the present study such as pure amine solvents and binary systems. This chapter includes all experimental and correlation, results and discussions on different systems under study.

Chapter seven summarizes the thesis with conclusions and recommendations for future work.

CHAPTER TWO: OVERALL LITERATURE REVIEW

2. Literature review

In this chapter, an overall literature review including absorption techniques for capturing CO_2 as well as different types of solvents for the absorption process is discussed. Chemical, physical and hybrid solvents as well as amine-based solvents are included. Also, a brief review of some physio-chemical properties of the solvent including density, viscosity, and refractive index along with their measurement methods have been reviewed.

2.1 Review on absorption technique

Solvent-based absorption technology is the most commonly used process in natural gas, petroleum, and chemical industries for CO_2 capturing [49]. The selection of the solvent is the main part of the absorption technique. In general, solvents can be categorized based on their reaction types in the solution. Different types of solvents include chemical, physical, and mixture of solvents which are discussed in the following sections.

2.2 Chemical absorption

The chemical absorption process is considered to be by far the most commonly used technique to capture CO_2 from low to moderate pressure and low concentration of flue gases [50]. This is due to the exceptional ability of reactive solvents in selectively capturing CO_2 from flue gas, high CO_2 loading capacities and, high mass transfer coefficient of absorption and desorption processes. Besides the mentioned advantages of chemical solvents, there are several drawbacks reported for chemical solvents in the literature including high solvent regeneration energy, high solvents cost, high corrosive behavior, high absorption heat, and some environmental impact [28]. It is to be noted that the regeneration energy cost plays an important role (up to 70% of the total operating costs) in the entire operating cost of CO_2 capture [51],[52].

As mentioned above, the consumed energy for solvent regeneration in the chemical absorption process is quite high which accounts for 80% of the total energy consumption in an absorption

process [13]. As the regeneration unit consumes the majority of energy in the chemical absorption process, several researches have been done to decrease energy consumption by optimizing and designing different configurations for the regeneration unit.

Since CO_2 is an acid gas, using a basic solvent can capture CO_2 from the gas stream. The basic principle of chemical absorption is the reversible, exothermic acid-base neutralization reaction between a weak acid and a weak base that results in the formation of water-soluble salts. Since chemical absorption shows the most potential for valid CO_2 control, and it has been commercialized for many decades, this process has been investigated widely for post-combustion CO_2 capture [53]. Lately, the most widely studied and used chemical solvent technology to reduce carbon dioxide concentrations in industrial processes such as fossil fuel power plants, iron /steel manufacturing, and cement productions is amine-based chemical absorption [54].

The most widely used category of amine-based solvents is alkanolamines which are combinations of alcohol (-OH functional group) and amine (-NH_2, NHR, NR_2 functional groups). The role of the hydroxyl group in alkanolamines is to reduce the vapor pressure and therefore enhances the water solubility of them. On the other hand, amine groups in alkanolamines provide the required alkalinity in aqueous solutions to promote the acid gas reaction. It has been reported that the amine-based absorption technique accounts for almost 95% of U.S. natural gas purification operations [55]. The reaction of alkanolamines with CO_2 is selective and reversible. The development of alkanolamines aqueous solutions started with the work done by R.R. Bottoms [56]. Many studies have been carried out on the chemistry and kinetic reactions of the alkanolamines as well as their thermodynamic and process modeling in the different types of unit operations. The most commonly used amine-based solvents are given in **Table 2-1**[52], [57]–[64] :

Table 2-1 Types of alkanolamines	
Type of alkanolamines	**Example**
Primary amines	Monoethanolamine(MEA), Diglycolamine(DGA)
Secondary amines	Diethanolamine (DEA), Diisopropanolamine (DIPA)
Tertiary amines	Methyl-diethanolamine (MDEA), Triethanolamine (TEA)
Primary sterically hindered amines	2-amino-2-methyl-1-propanol (AMP)
Polyamines	Piperazine (PZ), Aminoethylethanolamine (AEEA), Diethylenetriamine (DETA),Triethylenetetramine (TETA), Tetraethylenepentamine (TEPA),

A typical flow sheet of an amine-based carbon capture process is shown in **Figure 2-1**. The flue gas is introduced to the bottom of the absorber and contacts counter-currently with a CO_2 lean or liquid solvent. The CO_2 gas is preferentially absorbed by the solution. When the solution has reached the intended CO_2 loading, it leaves at the bottom of the absorber, and the CO_2 free flue gas escapes from the top of the absorber. The CO_2- enriched solution then passes through the top of the desorption column and flows downward. The reboiler at the bottom of the desorber heats the solvent to reverse the chemical reaction and releases the CO_2 from the solvent. The water vapor is condensed using the condenser on the top of the desorber column, leaving high concentrated CO_2 stream for subsequent transportation and storage. From the top of the desorber column, the high purity CO_2 gas stream is produced, and from the bottom, the solvent is cooled and recycled back to the absorption column to contact additional gas.

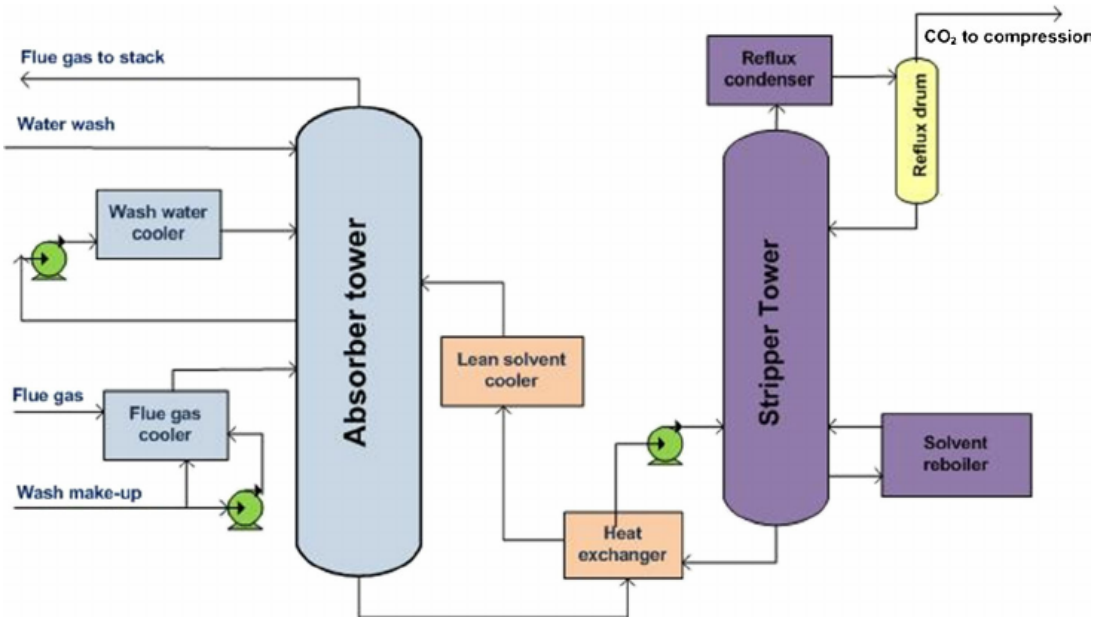

Figure 2-1 Process flow for amine-based capture from flue gas [4]

- **Primary alkanolamines:** Primary amines contain hydroxyl group and primary amino functional group (R can be alkyl or aromatic) on an alkane backbone. Monoethanolamine (MEA) is the first generation and most well-known alkanolamines in the natural gas industry .It has been industrially employed for over 60 years [15] . MEA is appropriate for the gas stream with low CO_2 concentrations as it is relatively cheap, shows fast reaction rate with CO_2 and it has high alkalinity. However, it still poses several disadvantages including low CO_2 loading capacity, high thermal and oxidative degradation, high corrosiveness, high vapor pressure, and most importantly high reaction heat and high solvent regeneration cost [65][22].

2-(2-aminoethoxy)ethanol, commercially known as Diglycolamine (DGA) is also a primary alkanolamine that represents similar properties to MEA in many aspects, however, due to its low vapor pressure, it is used at higher concentrations in aqueous solution [50]. To address the drawbacks of MEA and the development of efficient solvents with high absorption-desorption capacity, high oxidative and thermal stability, and energy-efficient performance, several principal alkanolamines have been commercially employed, including diethanolamine (DEA), N-methyldiethanolamine (MDEA).

- Secondary alkanolamines: Secondary alkanolamines contain hydroxyl group and secondary amine functional group (R can be alkyl, aryl, or both) on an alkane backbone. Secondary alkanolamines such as diethanolamine (DEA) and diisopropanolamine (DIPA), considered to be a proper alternative to MEA due to the representation of intermediate properties over primary amines. DEA has low vapor pressure, lower level of degradation, and more resistance to corrosion compared to MEA, while DIPA requires lower solvent regeneration energy than MEA [50].

- Tertiary alkanolamines: In this group of alkanolamines, nitrogen is connected to three organic substituents, like triethanolamine (TEA) or methyldiethanolamine (MDEA), the CO_2 loading capacity and reaction rate is low, the regeneration cost is lower than that in MEA, whereas they show high resistance to corrosion and degradation [50].

The reaction rate of primary and secondary amines with CO_2 is faster than in tertiary amines and follows the order: primary, secondary, and tertiary amines [66],[67]. This is due to the formation of stable carbamate in CO_2-Primary/secondary Alkanolamines- H_2O solution. However, the fast reaction rates in primary and secondary amines lead to an increase in solvent regeneration cost since very high heating is needed in the desorber [21]. The most accepted reaction mechanism for primary and secondary amines (including sterically hindered amines) is the zwitterion mechanism which was first proposed by Caplow in 1968 [68]. As shown in reaction (R-6) and (R-7), the primary and secondary amines (denoted here as AmH) react with CO_2 to form zwitterion first and then an additional free base (denoted here as B) which can be either amine, water or OH^{-1} in an aqueous solution is used to form the stable carbamate.

$$CO_2 + AmH \leftrightharpoons AmH^+COO^- \qquad \text{(R-6)}$$

$$AmH^+COO^- + B \rightarrow AmCOO^- + BH^+ \qquad \text{(R-7)}$$

If the base in the reaction (R-7) is amine itself then, for the overall reaction of carbamate formation in a solution 2 mole of alkanolamine is required per mole of CO_2.

$$CO_2 + 2\ AmH \leftrightharpoons AmCOO^- + AmH_2^+ \qquad \text{(R-8)}$$

For the sterically hindered amines, the stability of the carbamate compound is lower than primary and secondary amine due to the restriction of larger substituents to rotate around the amino-carbamate group. The carbamate, therefore, undergoes hydrolysis more easily than reaction with an amine, and bicarbonate formation takes place. Meanwhile, free amine molecules are released for additional reaction with CO_2 that increases the CO_2 loading capacity to 1.0 mol of CO_2 per mol of amine [69].

$$AmH^+COO^- + H_2O \rightarrow HCO_3^- + AmH_2^+ \quad \text{(R-9)}$$

Then, the overall reaction of bicarbonate formation is shown as follows:

$$CO_2 + AmH + H_2O \leftrightharpoons HCO_3^- + AmH_2^+ \quad \text{(R-10)}$$

The reaction of the ternary amine with CO_2 leads to base-catalyzed hydration of CO_2 to form bicarbonate ion [70]. This reaction can be represented as:

$$R_3N + H_2O + CO_2 \rightarrow HCO_3^- + R_3N^+H \quad \text{(R-11)}$$

For tertiary amines, the rate of this base-catalyzed bicarbonate formation reaction is lower than those of the zwitterion mechanism for primary and secondary amines which results in low solvent regeneration cost that is considered as an advantage of tertiary amines. Besides, the formation of carbamate anion and bicarbonate ion has a major effect on the CO_2 solubility in aqueous alkanolamines solutions. The more carbamate is produced, the higher capacity of free amine exists in the solution, leading to the re-reaction of free amines with CO_2 molecules and raising the CO_2 loading capacity. The overall reaction stoichiometry indicates that for primary and secondary amines, the CO_2 loading capacity lies in the range of 0.5-1 mole of CO_2 per mole of amine, whereas for tertiary amines and sterically hindered amines it is the one-to-one ratio, showing higher loading capacity. According to the work done by Henni *et al*, (2013), the increase in hindrance to the amino groups increases the loading capacity in the order of Primary amines < Hindered amines < Secondary amines < Tertiary amines [19].

High CO_2 loading capacity (1.0 mol of CO_2 per mol of amine), high thermal stability, and low regeneration energy of tertiary amine (MDEA) make this amine more important than that of lower order amines. Besides these advantageous, tertiary amine (MDEA) has a low reaction rate and

therefore it can only perform well in the presence of activators such as MEA, DEA, PZ, and other fasting reacting solvents to enhance the absorption rate. Since these amines still show several drawbacks, the specialty hindered amines (2-amino-2-methyl-1-propanol (AMP))[71] and cyclic diamine (piperazine (PZ)) [72] have emerged.

- Sterically hindered amines: These amines are a different class of acid gas absorbent in which the nitrogen atom of the amine molecule is partially shielded by neighboring groups so that larger molecules cannot easily approach and react with the nitrogen.The general reaction mechanism for sterically hindered amine is described earlier in (R-7) and (R-8) and follows the zwitterion mechanism. AMP, the primary sterically hindered amine, has great absorption and desorption characteristics, such as lower desorption energy consumption up to 15% [73], higher resistance against degradation lower regeneration energy up to 20% [73], and higher loading capacity (1.0 mol of CO_2 per mol of amine) compared to common primary and secondary amines. These advantages, however, partly offset by the low reaction rate of AMP. At typical stripping temperatures, most of the sterically hindered amines are also non-corrosive to carbon steel even in the oxidative atmosphere. The other factors are comparable to MEA [26].

Diamine: Piperazine (PZ) is a cyclic amine with two secondary amine groups in its structure generally used as a promotor/activator to add into the high absorption capacity solvents with the capability of bicarbonate formation like tertiary and/or sterically hindered amines to enhance the overall absorption rate [74]–[76].The reaction rate of PZ with CO_2 is significantly high due to the presence of multiple amino groups in its structure, besides, its regeneration energy is 10 to 20% less than the regeneration energy for MEA [77],[59],[78]. The resistance of PZ to thermal degradation is high and is negligible up to the temperature of 423.15 K. It also has an effective resistance to oxidative degradation. The solubility of PZ, however, in water is very low, for example, at 293K the solubility of PZ is 14wt%, therefore, CO_2 capture by a high PZ content solution is required to perform at high temperatures [28]. The reaction rate of Piperazine is much faster than MEA, however, due to its larger volatility, its application in CO_2 absorption is much more expensive than MEA and is still under development [79].

Besides the above-mentioned alkanolamines, new amines have also used in the chemical absorption process. The modification in the structure of new amines enhances their effectiveness in CO_2 capture processes. Aminoethylethanolamine (AEEA), Diethylenetriamine (DETA), Methylaminopropylamine (MAPA) are some examples of new amines [58]–[64]. Several amine solvents have recently been experimentally investigated as a promising alternative solvent to evaluate their abilities in CO_2 capture applications [80]–[87]. In addition to current amines, novel amine solvents have been continually produced to determine their potentials in CO_2 capture technology [88]–[92],[62]. However, the regeneration of newly developed amine solvents is still performed at elevated temperatures and the regeneration energy cost is therefore high [93].

Ammonia: a single solvent for the chemical absorption process, has the advantage of higher CO_2 loading capacity and lower regeneration energy than MEA. Ammonia shows a lower price in comparison with other amines. Furthermore, aqueous ammonia can capture all three major acid gases including NO_x, SO_x, and CO_2 from flue gas in a coal-fired power plant which is a cost-effective process. However, low absorption rate and high volatility of ammonia are considered to be significant problems to reach a low-cost CO_2 capture. On the other hand, the mitigation of NH_3 vaporization to the atmosphere should be carried out due to the toxicity of ammonia [94].

CO_2 capturing using ammonia is classified into two processes based on the temperature applied in the system: Conventional and chilled process. In conventional ammonia process, CO_2 can be captured from flue gas at temperatures ranging from 25 to 40 degrees Celsius [95]. Chen *et al*, (2010) investigated the kinetics of CO_2 absorption in an aqueous ammonia solution at temperatures of 25 to 49 degrees Celsius [96]. Several researches have been carried out on the experiment and modeling of VLE behavior of CO_2 absorption in aqueous ammonia solution and equilibrium behavior of CO_2 absorption at low temperature [97]. Also, the mass transfer coefficient of amine and CO_2 absorption in CO_2 capture were studied by Shangchen *et al*,(2016) [98]. The chilled ammonia process is the other type of CO_2 absorption process at low temperatures of about 2 to10 degrees Celsius [95] .This low-temperature process supports the decrease of the ammonia slip in the absorber and helps to reduce the volume of the flue gas [95]. In the research done by Hanak *et al*,(2015) a closed-loop rate-based model was developed for the chilled ammonia process model [99].

- Salt solutions: Another category of chemical solvents that are reported in literature are salt solutions that are naturally salt and once dissolved in the water they can produce electrolyte. Carbonate solution (potassium or sodium)[100]–[102], hydroxide (potassium, sodium or calcium hydroxide) [103], [104] amino acids [105]–[107] are some examples of salt solutions that are utilised for capturing CO_2 from the gas stream.

2.2.1 **Physical absorption**

Physical solvents are highly recommended for the application at the pre-combustion capture process where the fuel gases containing high CO_2 concentrations and are at elevated pressures. During the physical absorption process, CO_2 is absorbed in a liquid solvent based on Henry's Law. This process relies on physical bonds (Van der Waals type or electrostatic) between the organic solvent and CO_2 molecules. The resulting physical bonds are pretty weaker than that of chemical bonds in the chemical absorption procedure. The removal of CO_2 by physical absorption is based on the solubility of CO_2 and the solvents. The amount of CO_2 absorbed strongly depends on both the temperature and the partial pressure of the feed gas. Higher the pressure and lower the temperature, the more CO_2 gas can be physically absorbed. The desorption (solvent regeneration) is achieved by heating and/or depressurization. Since the interaction between CO_2 and the physical solvent is weak compared to chemical solvent, less energy is required for solvent regeneration.

Physical solvents have higher absorption capacity compared to chemical solvents. The selectivity of physical solvents among acid gases is another advantage over chemical solvents. However, in physical solvents, the partial pressure of acid gas must be high and the presence of the low concentration of inert gas in the system is necessary [108].

Physical absorption has been widely applied to several industrial processes to remove CO_2 and acid gas from syngas and natural gas, respectively. The physical solvents must meet several requirements to be economically usable. These criteria include: being non-corrosive to metals, have high acid gas selectivity, low vapor pressure, viscosity, and thermal stability [109].
Most common processes that utilize the solvents that meet all the mentioned criteria are listed as follows:

- **Selexol process**: this process uses Union Carbide Selexol solvent, which is a mixture of dimethyl ether of polyethylene glycol (DMPEG) to physically absorb CO_2 and H_2S from a variety of natural and synthesis gas streams. Selexol is non-corrosive, relatively non-toxic, has high solubility of CO_2, and low vapor pressure. The operating temperature for the system that uses this solvent is relatively high between -20 to 40 degrees Celsius [109].
- **Rectisol process**: This process is the earliest commercial process based on an organic physical solvent. Low-temperature methanol (cold methanol) is used as an absorbent to remove H_2S, COS, and bulk CO_2 from syngas whereby both inorganic and organic impurities are removed as well [109]. The appropriate operation temperature for this solvent is −59.5 to −73.3 degrees Celsius [56] .Utilizing methanol can prevent the formation and dehydration of hydrate and ice at low temperatures. The availability of methanol, its low cost as well as its non-toxicity makes this solvent very attractive for gas processing.
- **Flure process**: In this method, the active solvent is propylene carbonate (PC) which is employed to remove bulk CO_2, H_2S, COS, and CS_2 from natural gas. This process is appropriate for flue gas with the partial pressure of CO_2 higher than 60 psi. The operational temperature of the absorber that uses propylene carbonate is within -17 to 65 degrees Celsius. Besides, in this process, the high solubility of CO_2 in the PC can be reached [109].
- **Purisol process:** This method uses N-methyl 2 Pyrrolidone (NMP) as a solvent process to remove CO_2 and H_2S. The operational temperature for this process can be either room temperature or very low temperature of -15 degrees Celsius. This solvent shows high selectivity to H_2S [109].

Physical solvent absorption is best applied to pressurized gas streams with high CO_2 concentrations and is generally not suited for post-combustion capture. Physical solvents are appropriate for the application at a pre-combustion capture plant where the fuel gases contain CO_2 concentrations of 35-40% and are at elevated pressures [31].

-Ionic liquids: Another type of solvent that has been recently applied for the CO_2 capturing process are Ionic liquids that show both physical and chemical behavior [110]. These solvents have distinct properties that make them practical solvents in different areas. These properties include:

applicability in a wide range of temperatures, high thermal stability, low melting point below room temperature, negligible vapor pressure, inflammability, and environmentally friendly behavior [111].Ionic liquids composed of both anion and cation parts. The possibility of altering the combination of anion and cation parts make these solvents suitable for particular applications [112]. The high viscosity of Ionic liquids compared to other conventional solvents is a drawback that makes these solvents less applicable for CO_2 capturing. The high viscosity leads to the lower mass transfer rate therefore, by proper combination of cations and onions the desired viscosity (low viscosity) of Ionic liquids can be obtained [113]. According to Boot Handford *et al*,(2014) ILs are classified in 3 different types including Task-Specific ILs (TSILs), ILs at Room Temperature (RTILs), and Reversible ILs (RILs) [114]. A considerable number of review papers on the application of ILs as solvents for CO_2 capture have been reported so far [115]–[120]. A brief review of the Utilization of ILs for CO_2 capture has been reported by Zeng *et al*,(2017) [120]. Their study covered all the important review papers on ILs based CO_2 absorption.

2.2.2 **Mixture of chemical solvents**

Generally, no single solvent can show all the desired properties in CO_2 capture technology. Hence, it is particularly critical to develop the promising alternative solvents which not only have fast reaction kinetics and high CO_2 absorption capacity but also be capable of reducing the operational cost. Currently, a large number of solvent blends systems have been proposed to address the underlying shortcomings with the CO_2 absorption behavior. A number of studies have been reported on the absorption of CO_2 using different classes of chemical solvent mixtures.

2.2.2.1 Promoted Ammonia and promoted carbonate

Promoted Ammonia and promoted carbonate are two examples of chemical solvents. Adding the activator to carbonate solutions leads to the increase in the rate of reaction with CO_2 based on the research done by Savage *et al*, (1984) [121].The most important promotors for carbonate solutions are amines and amino acids [122]–[124]. For Ammonia solution the best promotor that considerably enhances the CO_2 rate absorption is Piperazine [125].Yu *et al*, (2012) indicate that the PZ,1-methyl piperazine, and sarcosine sodium salt promoted CO_2 absorption in aqueous

ammonia considerably higher than the other additives [126],[127]. Since the main subject of the current study is amines we focused on the studies that have been done on the amines.

2.2.2.2 Mixture of alkanolamines

The application of amine-based blends was primarily proposed by Chakravarty *et al*,(1985) to combine the benefits of the fast reaction rate of monoamines (primary and secondary amine) or polyamines (e.g. PZ) and the high absorption capacity and low solvent regeneration energy of tertiary or sterically hindered alkanolamine (e.g. MDEA, AMP) [128]. To this end, various researchers have studied amine blended solvents and confirmed the enhancement of the overall behavior of these solvents in terms of fast reaction rate, high CO_2 loading capacity, high thermal degradation, and low regeneration energy. For instance, fast reacting amines such as MEA, DEA have been used as promoters for MDEA to enhance the overall reaction rate (MEA−MDEA, DEA−MDEA) [129]. Due to the high absorption rate and capacity of PZ, the mixture of PZ as an activator to tertiary amines and hindered amines have been investigated [130]–[132].

Likewise, the increase in the reaction rate of fast solvent like MEA is possible by adding a small amount of faster solvent like PZ as a promotor (MEA-PZ) [133],[134]. The blend of PZ, MEA, and DEA with AMP are also promising alternatives to MEA due to combining the advantages of fast-reacting solvents with high CO_2 absorption capacity solvent.(AMP-PZ [74],[75], DEA-AMP [135], MEA−AMP [129], AMP – PZ – MEA [136]. PZ-AEPD [137]) . Based on Rayer *et al*, (2012) studies, addition of the hindered amine to MDEA increases the reaction rate of CO_2 and enhances the CO_2 loading capacity to the highest amount [138]. The work on the modeling of the CO_2 absorption in an absorber stripper system has been carried out by shih and chang ,(2005) using the aqueous mixture of MDEA and DGA [139].

Also, 2-isopropylaminoethanol (IPAE) has shown a high reaction rate together with the small regeneration energy. Based on the research done by Goto *et al*, (2011), the regeneration energy for the mixture of IPAE+ amine is as low as 2.5 MJ/kg CO_2 [140].
N-(2-aminoethyl) ethanolamine (AEEA) has a high absorption capacity for CO_2 among amines due to two amine groups in its structure, thus, it can be a proper promotor for the tertiary amines.

A study carried out on the aqueous mixture of MDEA with five different additives showed that the aqueous mixture of MDEA and AEEA has the highest CO_2 absorption rate [141].
Despite performances of the amine blends solvents are generally superior over individual amine solvents in CO_2 absorption technology, this process still poses serious economic and environmental problems including high corrosion rate of the equipment, high energy consumption during high-temperature absorbent regeneration, large equipment size, amine loss by evaporation and thermal and oxidative degradation by SO_2, NO_2, and oxygen in the flue gas.

2.2.3 **Mixture of chemical and physical solvents (Hybrid solvent)**

This solvent is a mixture of amine together with physical solvents to take advantage of the best characteristics of both. With the combination of physical solvent and amine, the nearly complete H2S, CO_2, and organic sulfur removal can occur. Some advantages of hybrid solvents over other solvents are higher loading capacity of CO_2, lower regeneration energy that leads to the reduction of the overall cost in the industry, lower rate of corrosion, and faster absorption rate. The most famous hybrid solvent process is Sulfinol process that employs the mixture of amine and sulfolane. Sulfinol-D and Sulfinol-M solvents are a mixture of sulfolane -DIPA and sulfolane -MDEA, respectively. The sulfinol process can selectively remove Mercaptan, RSH, COS, and other organic sulfur compounds [90],[109].

The mixture of amines and ILs (as mentioned earlier shows both physical and chemical behavior) is another sample of hybrid solvent. In this solvent, the viscosity of ILs that is an issue for the CO_2 capturing process is reduced by mixing these solvents with amines and the CO_2 capacity is, therefore, improved [142]. In other words, the solubility of CO_2 in this type of solvent is enhanced by an increase in amine concentration. Density, Viscosity, and Performances of CO_2 Capture in 16 Absorbents of Amine + Ionic Liquid have been determined by Zhao *et al*, (2010) [143]. The authors reported better performance of these solvents in CO_2 capture as a result of the presence of ILs. Moreover, the viscosities in these systems are lower than that of current ILs and the regeneration energy of these absorbents is less than that of current amine absorbents. In the other research done by Bernard *et al*, (2016) the CO_2 absorption behavior and corrosion of the mixed solvent of Amines-ILs have been investigated. The authors concluded that the corrosion rate of the

MEA solution is reduced in the presence of ILs [144]. Moreover, it is reported in the literature that the addition of ILs to the MEA solution can reduce the losses of MEA per ton of captured CO_2 and decrease the regeneration energy of the solvent compared to aqueous MEA solution [145],[146]. Another category of hybrid solvents is a mixture of alkanolamines and alcohol. This group of solvent has shown great attention because of the low boiling point and thereby low solvent regeneration energy as well as low corrosiveness compared to the traditional solvents. Also, as the basicity of alkanolamines solution increases with the addition of the hydroxyl group from alcohol, the loading capacity of CO_2 into the solvent of alkanolamines improves in the presence of alcohol.

As comparative research, Rayer *et al*, (2013) investigated experimentally the CO_2 absorption kinetics by N-(2-hydroxyethyl)ethylenediamine in aqueous and non-aqueous systems of methanol and ethanol using the stopped-flow technique [147].The mixture of primary amines with alcohol as a solvent are used widely in the Amisol process. Park *et al*, (2006) investigated the reaction kinetics of carbon dioxide with hybrid solvents of TEA–methanol, ethanol, n-propanol, n-butanol, ethylene glycol propylene glycol, propylene carbonate, and water using chemical absorption technique [148]. Moreover, they presented an empirical correlation between the reaction rate constants and the solubility parameter of the solvent. Tan *et al*,(2013) investigated the CO_2 capture process using the non-aqueous mixture of PZ and diethylenglycol. The authors reported the decrees in the regeneration energy of the solvent as a result of the absence of water [149]. The performance of the hybrid solvent of MEA–triethylene glycol (TEG) in the solubility of CO_2 was investigated by Lue *et al* ,(2011) [150]. The results were an indicator of the relatively lower temperatures for the absorption and desorption process that results in less energy consumption with lower solvent evaporation as well as a reduction in thermal degradation of MEA caused by the high-temperature operation. Spasojevic *et al,* (2014) reported the study on the measurement of densities, viscosities, and refractive indices of 1-amino-2-propanol with 1-butanol and 2- butanol solutions at the temperature range from 288.15 to 333.15 K and over the whole range of concentration. Also, measured results were correlated using the Redlich−Kister relation [151]. In the study done by Dubay *et al*, (2011) the thermodynamic properties of binary liquid mixtures of diethylenetriamine with 2-methyl-1-propanol, 2-propanol, and 1-butanol at different temperatures were investigated. A Redlich–Kister equation was applied to correlate the excess molar volumes and deviations of measured properties [152].

Among the alcohols, methanol has been widely used as a physical solvent in the CO_2 capture process (Rectisol and Amisol) as it takes advantage of two potential characteristics including high physical CO_2 solubility and low solvent regeneration energy. The hybrid solution of MEA-MeOH has shown better performance in the process of CO_2 capturing than MEA-H_2O solution. The reason behind this is the less regeneration energy of the MEA-MEOH solvent that reduces the operating temperature and therefore, the MEA thermal degradation is notably reduced. However, as the vapor pressure of MeOH is high, the CO_2 absorption into the MEA–MeOH must be conducted at a low temperature to minimize the vaporization of MeOH in the absorption and regeneration process [153].

For the reason of minimizing the methanol vaporization, Jie *et al*, (2016) investigated two types of hybrid solutions including the mixtures of MEA with TEA and methanol and MEA with glycerol and methanol. The performance of the tertiary mixtures then compared with aqueous MEA and MEA-MeOH solution. The authors reported that the solution of MEA-glycerol-methanol has shown better absorption property than aqueous MEA solution while MEA-TEA-methanol solution did not show the proper CO_2 absorption rate. Also, addition of TEA and glycerol to the mixture of MEA-MeOH cannot improve the performance of MEA- MeOH for CO_2 absorption [154]. In the study done by Fu *et al*, (2015) the performance of CO_2 absorption into a hybrid solvent of MEA–MeOH was experimentally studied. The authors reported that the hybrid of MEA–MeOH has shown better CO_2 absorption property over the MEA-H_2O [153]. Henni *et al* ,(1995) studied the CO_2 solubility of tertiary aqueous solvent of MDEA- MeOH at 40 and 100 degrees Celsius and partial pressures of the acid gas up to 7.04 MPa [155]. Tounsi *et al,*(2005) measured the solubility of CO_2 in an aqueous mixture of DEA-MeOH over the temperature ranging from 323.15 to 393.15 K and pressure up to 3.6 MPa [156]. The study done by Tamajon *et al,*(2016) on the CO_2 absorption into MDEA-MeOH solvent showed the improvement of CO_2 diffusivity and solubility using physical absorption [157].

Besides the researchers conducted on the CO_2 solubility of the mixture of alkanolamines and methanol, studies on the thermo-physical properties of these solvents are still lacking. It is to be noted that for design and optimization of the CO_2 capture process, knowing the thermodynamic properties of the multicomponent systems is essential as the cost and efficiency of the process can

be optimized by modeling of these parameters. To this end, Fu et al, (2018) investigated the viscosity and surface tension of the aqueous solutions of MEA-MeOH and DEA-MeOH experimentally and theoretically [93]. Valtz *et al*, (2005) investigated the density of the mixture of MEA–MeOH at different temperatures of 283.15 to 353.15 K and over the entire range of concentration. Also, the Redlich-Kister equation was employed to correlate the excess molar volume of this mixture [158].

Despite several advantages of methanol as an organic solvent, due to its high vapor pressure and thereby rapid evaporation, cooling systems should be applied that causes the increase in the operational and capital cost of the system. Also, methanol is mostly produced from natural gas which is a non-renewable source. It is highly toxic and can cause methanol poisoning in case of ingestion, breathing, and skin exposure. It is, therefore, clear that a better alternative should replace methanol. Ethanol is a suitable substitute for methanol as it is produced normally through fermentation from biomass which is a renewable source. Hence, ethanol is far more environmentally friendly than methanol. On the other hand, the toxicity of ethanol is lower than methanol that makes this alcohol a better substitution for methanol [159]. The use of ethanol as a physical solvent in the chemical absorption processes could be interesting since certain studies on the hybrid solvents of amine-MeOH (as discussed above) have indicated the improvement of the experimental results compared to aqueous amine solutions. Despite the considerable research on the thermo-physical properties of aqueous alkanolamines, few papers are reporting the thermo-physical properties of non-aqueous solutions of alkanolamines and ethanol. Versteeg *et al*,(1998) investigated the absorption of CO_2 in a solution of MDEA in ethanol [160]. Densities and viscosities of MEA-H_2O, MEA-ETOH, and MEA-2-propanol at different temperatures of 303.15, 313.15, and 323.15 K were measured by Lee *et al,* (1995). The authors reported the excess molar volumes and viscosity deviations as well as their correlations using a Redlich-Kister equation [161]. In the study done by La Rubia *et al*, (2009) density and speed of sound of ternary systems of aqueous MDEA- ETOH and TEA-ETOH at different temperatures were measured. The authors also calculated the isentropic compressibility value through measured experimental values of these physical properties [162]. La Rubia also studied the density and speed of sound of binary mixtures of MDEA and TEA with Ethanol over the entire range of concentration and at different temperatures. The isentropic compressibility values were also reported in this study [163]. Alvarez

et al, (2008) reported the study on the surface tensions of binary mixtures of MDEA-ETOH and TEA-ETOH at temperatures ranging from 288.15 to 313.15 K over the entire range of concentrations. Furthermore, the Redlich–Kister equation was used to correlate the excess volume and isentropic compressibility [164]. The density and viscosity of the binary mixture MDEA-ETOH at 40 °C were investigated by Tontiwachwuthikul *et al*, (2000). Also, the authors reported the derived excess molar volumes and viscosity deviations together with the correlation of these properties as a function of composition [165]. Volumetric and viscometric properties of binary mixtures of 1-amino-2-propanol - ethanol, N-(2-aminoethyl)ethanolamine - ethanol, 3-amino-1-propanol-ethanol, and N-(2-aminoethyl)-1,2-ethanediamine ethanol were measure at the temperatures of 293.15−323.15 K + Ethanol by Zhu *et al* , (2017)[166]. Chen *et al,* (2018) have recently calculated the density of the binary mixture of MEA with two different types of alcohol including straight-chain alcohol (ethanol, n- propanol and n-butanol) and branched-chain alcohol (isopropanol, isobutanol, and tertbutanol) at temperatures ranging from 293.15 to 333.15 K at 0.1 MPa. The molar volume, excess molar volume, and thermal expansion coefficient were also determined in this study [167]. In the study done by Zho *et al*, (2019) the density and viscosity of ternary solutions of MDEA-MEA-ETOH at different temperatures of 293.15 to 323.15K were calculated. The excess molar volume and deviation of viscosity were measured for both binary and tertiary solutions and the obtained values were correlated using Redich-Kister type of equation [168]. The detail of the studies done on the binary solution of alkanolamines and ethanol are summarized in **Table 2-2**.

Table 2-2 Experimental and theoretical studies on the thermo-physical properties of some alkanolamines+ ETOH

Reference	System	T(K)	Study	Observation
Lee *et al*, (1995)[161]	MEA+H_2O MEA+ETOH MEA+2-propanol	303.15 - 323.15K	Measurement of the density, viscosity and kinetic viscosity of studied systems	- The excess volumes and viscosity deviations were calculated and correlated using Redlich-Kister equation. - Kinematic viscosities were also correlated using McAllister's models
La Rubia *et al,* (2007)[163]	MDEA+ETOH TEA+ETOH	288.15 - 313.15K	Measurement of density, speed of sound, excess volume, isentropic compressibility and isentropic compressibility deviation of binary studied systems	- Increase in both density and sound velocity with increase in amine mole fraction and decrease with increase in temperature. negative values for excess volume and isentropic compressibility deviation were observed for both systems for all mixtures and temperatures
La Rubia *et al*, (2009) [162]	H_2O+MDEA+ETOH H_2O+TEA+ETOH	288.15- 323.15K	Measurement of density, speed of sound, excess volume, isentropic compressibility and isentropic compressibility deviation of tertiary studied systems	- Increase in density with increase in amine mole fraction and decrease in density with increase in temperature. - A constant value for the sound velocity was observed for TEA system with high amine concentration while MDEA system showed the reverse trend. - Large negative values for both excess volume and isentropic compressibility deviation were observed that were indicative of the strong hydrogen bonding interactions among unlike molecules.
Alvarez *et al,*(2008) [164]	MDEA+ETOH TEA+ETOH	288.15 - 313.15K	Measurement of the surface tension and deviation of surface tension of the selected binary mixtures	- Increase in value of surface tension with increase in the amine concentration in both mixtures - Decrease in value of surface tension with increase in temperature for both mixtures

				- Positive deviations were observed for mixtures of MDEA+ETOH, while negative deviation was obtained for the mixture of TEA+ETOH - The trends were different while compared to aqueous mixtures of MDEA and TEA at the comparable conditions - The surface tension deviations were correlated using Redlich-Kister equation
Tontiwachwuthikul *et al,*(2000)[165]	MDEA+ETOH	323.15K	Measurement of the density, viscosity, excess molar volume and viscosity deviation of the selected binary mixtures.	- Negative values for both excess volume and viscosity deviation were observed - The derived excess molar volumes and viscosity deviations were correlated using Redlich-Kister equation - The Grunberg-Nissan interaction energy constants were reported.
Zhu *et al,* (2017) [166]	MIPA+ETOH AEEA+ETOH 3-AP+ETOH DETA+ETOH	293.15−323.15K	Measurement of the densities, viscosities, the volumetric and viscometric properties of selected binary mixtures.	-Negative values for excess molar volume of all mixtures were observed that were attributed to the dipole-dipole and hydrogen bond interactions among unlike molecules and the packing effect. - Negative values for viscosity deviation of MIPA+ETOH, AEEA+ETOH, 3-AP+ETOH mixtures were observed that were indicative of stronger interaction between the same molecules than, unlike molecules. - Positive values for viscosity deviation of DETA+ETOH mixtures were observed that were attributed to the stronger interaction between unlike molecules. - The derived excess molar volumes and viscosity deviations were correlated using Redlich-Kister equation

Chen *et al,* (2019) [167]	MEA+ETOH MEA+n- propanol MEA+n-butanol	293.15- 333.15 K	Measurement of the density, molar volume, excess molar volume and thermal expansion coefficient for selected mixtures	-Increase in the density of binary mixture with increase in MEA concentration and decrease in density with the increase in temperature. - Negative values for excess molar volume were observed which was attributed to the hydrogen bonding and steric effect. - The magnitude of excess molar volume follows the order MEA +ETOH < MEA+ n-propanol < MEA n-butanol for straight-chain alcohol and MEA+ tertbutanol < MEA + isobutanol < MEA + n-butanol for branched-chain alcohol mixtures
Zho *et al,*(2019) [168]	MDEA+ETOH MEA+ETOH MDEA+MEA MDEA+MEA+ETOH	293.15-323.15K	Measurement of the density, viscosity, volumetric and viscometric properties of the selected tertiary mixture	- Negative values for excess molar volume and viscosity deviation of binary mixtures of MDEA+ETOH and MEA+ETOH and tertiary mixture were observed that were attributed to strong hydrogen bond interactions among unlike molecules and the packing effect. - The viscosity deviation and excess molar volume of binary mixtures of MDEA+ETOH and MEA+ETOH and tertiary mixture were correlated using Redlich-Kister equation.

As discussed earlier, there are few published papers on the thermo-physical properties of MEA-ETOH and MDEA-ETOH at comparable conditions, while no data is available in the literature for the mixture of DEA-ETOH. Also, no data reported for the refractive index of the selected mixtures in this study.

In this research, according to the importance of physical solvent in the improvement of the experimental results compared to results obtained from aqueous solutions, density, viscosity and refractive index of hybrid solvents of MEA, MDEA and DEA with ethanol were examined over the entire range of concentration and at the temperature ranging from 293.15 to 333.15K, with 5K intervals. The volumetric properties including the molar volume, excess molar volume, partial molar volume, apparent molar volume, and partial molar volume at infinite dilution were calculated. The deviation in the viscosity and refractive index was also investigated. All the experimental values were correlated using several well-known correlations which are discussed in detail in chapter 6. According to the importance of thermo-physical properties of the multicomponent systems on design and optimization of CO_2 capturing process and based on the role of the thermodynamic modeling of these properties in efficiency and cost of the absorption process, a brief review on some thermo-physical properties and their measurement techniques as well as a review on some well-known correlation of these properties have been presented in the following chapters.

CHAPTER THREE: THEORETICAL SECTION

3. Theory of Solution

The information of this chapter including all the equations is taken from the book entailed " Introduction to Chemical Engineering Thermodynamics" by J.M. Smith and Hendrick Van Ness [169].

A solution in thermodynamics refers to a homogeneous system of two or more chemical components. In such a mixture, the component that is present in the greatest amount is known as a solvent in which the solute, component in the lesser amount, is dissolved. To characterize a solution, it is necessary to introduce the variables specifying the composition of the different chemical components of the solution. The first important composition variable refers to a mole number which is denoted by n_i (mol) for the system of N components. For the multi-component system, the more practical composition variable is mole fraction, x_i, which is defined as the number of mol of solute i in the solution divided by the total number of moles,n_{tot}, in the solution.

$$\mathbf{x_i = \frac{n_i}{n_{tot}} \ with \ n_{tot} = \sum_i n_i} \qquad 3\text{-}1$$

The atomic percent of component i is the other important composition variable which is often denoted by $(at\%)_i$, and is equal to 100 times the mole fraction x_i.

The third composition variable of importance is the concentration of the solution which refers to the amount of solute dissolved in a given volume of solvent and defined as the number of moles of component i, n_i (mol), divided by the volume of solution, V (lit).

$$\mathbf{c_i = \frac{n_i}{V} \ [\frac{mol}{dm^3}]} \qquad 3\text{-}2$$

The maximum amount of solute that can be dissolved in a solvent at equilibrium state is described as solubility. Three types of intermolecular interactions are involved in the formation of a solution including the solute-solvent, solvent-solvent, and solute-solute interaction. Solvent-solute

interactions determine if a substance can dissolve in a particular solvent. Dissolution often occurs when the magnitude of solute-solvent interactions is either comparable to or greater than solvent-solvent and solute-solute interactions. The overall enthalpy changes and change in entropy must be considered while predicting if a solution will form. Exothermic ($\Delta H_{soln}<0$) processes and an increase in entropy favor dissolution. It should be mentioned that the aforementioned discussion on solubility is typically restricted to solid-liquid equilibria although in this case magnitude of enthalpy of fusion should be also considered. Note that the mixtures studied in this work reveal full and unlimited solubility.

3.1 The thermodynamic description of the solution

In the chemical, petroleum, and pharmaceutical industries multicomponent gases or liquids normally undergo composition changes during mixing, separation, inter-phase transfer, and chemical reaction processes. Hence, in addition to T and P, composition also plays an important role in the thermodynamic description of such systems. Thermo-physical and thermodynamic investigations have increased remarkably during the last decades to introduce a new class of fundamental properties for homogeneous solutions of variable composition. Of the separate class of properties relevant to multi-component and multi-phase systems, the partial molar property and the chemical potential are particularly important. A new class of solution properties known as excess properties is of great importance which is based on an idealization of solution behavior called the ideal solution. The experimental data of excess thermodynamic properties of liquid solutions provide a deep understanding of the molecular interactions and can be used in developing reliable predictive thermodynamic models.

3.2 Partial molar quantities

For a given pressure and temperature, more than one phase and composition are possible and it becomes important to evaluate the contribution of each component to the different thermodynamic properties. When two substances are combined into a mixture, the overall property of the mixture is not composed of a weighted average of the same property of the pure substances. Mixing has introduced a new variable whose intensity changes with the composition of the solution. To fully

characterize the equilibrium state of a multi-component system, it is, therefore, necessary to specify the number of moles of the different components in the solution in addition to T and P. The total value of any extensive property M (V, U, H, S, A, G) is defined as following general property relation:

$$\boldsymbol{M_m = nM = M(T, P, n_1, n_2 \ldots\ldots n_i \ldots\ldots n_N)} \qquad 3\text{-}3$$

Where N and n refer to the total number of chemical components in the system and the total number of moles in the system, respectively. The subscript m denotes for the molar parameters. Taking the total differential of nM from equation 3-3:

$$\boldsymbol{d(nM) = \left[\frac{\delta(nM)}{\delta p}\right]_{T,n} dp + \left[\frac{\delta(nM)}{\delta T}\right]_{P,n} dT + \left[\frac{\delta(nM)}{\delta n_i}\right]_{T,P,n_{i\neq j}} dn_i} \qquad 3\text{-}4$$

The term$\left[\frac{\delta(nM)}{\delta n_i}\right]_{T,P,n_{i\neq j}}$, the change of total extensive property, nM, with the differential amount of species i added to the finite amount of solution when T, P and all mole numbers exceptn_i are constant, is defined as the partial molar property of species i and is denoted by the generic symbol $\bar{M}_i$.

Symbol $\bar{M}_i$ may stand for the partial molar internal energy $\bar{U}_i$,the partial molar enthalpy $\bar{H}_i$, the partial molar entropy $\bar{S}_i$, or the partial molar Gibbs energy $\bar{G}_i$.It should be noted that the partial molar Gibbs energy is defined as the chemical potential of species i in the mixture.

$$\bar{G}_i = \left[\frac{\delta(nG)}{\delta n_i}\right]_{T,P,n_{i\neq j}} = \mu_i \qquad 3\text{-}5$$

Chemical potentials play a key role in chemical thermodynamics. The thermodynamic properties may then be obtained from the chemical potential of each component. Chemical equilibrium and equilibrium between phases can be determined using μ_i. Also, if we know the properties of chemical potentials relative to the temperature, pressure, and composition of the system, we can

obtain all the molar and the thermodynamic properties of the solution. As shown below, the partial derivatives of μ_i with respect to T and P become:

$$\left[\frac{\delta \mu_i}{\delta T}\right]_{P,n_i} = \left[\frac{\delta \bar{G}_i}{\delta T}\right]_{P,n_i} = -\bar{S}_i \qquad 3\text{-}6$$

then using $\mu_i = \bar{H}_i - T\bar{S}_i$, $\bar{H}_i$ is obtained. Substituting $\bar{H}_i$ in $\bar{U}_i = \bar{H}_i - P\bar{V}_i$ and $\left[\frac{\delta \bar{H}_i}{\delta T}\right]_{P,n_i}$ give $\bar{U}_i$ and $\bar{C}_{p,i}$, respectively. Knowing the partial molar quantities of μ_i, $\bar{V}_i$, $\bar{S}_i$, we will be able to obtain thermodynamic properties of the solution such as $G = \sum_i n_i \bar{G}_i$, $S = \sum_i n_i \bar{S}_i$, $V = \sum_i n_i \bar{V}_i$ and so on. Equation 3-4 has the simpler form of:

$$(nM) = n\left[\frac{\delta M}{\delta p}\right]_{T,x} dp + n\left[\frac{\delta M}{\delta T}\right]_{P,x} dT + \sum_i \bar{M}_i \, dn_i \qquad 3\text{-}7$$

Where subscript x denotes differential at constant composition.

In general, the partial molar property of a substance in a mixture differs from the molar property of the same substance in a pure system at the same temperature and pressure. This owing to the fact that while in a pure system the molecules interact with their own species, in a solution molecule may be subjected to different interactions with dissimilar molecules. This may render the value of a molar property different in mixed and pure states.

Since $n_i = x_i n$,

$$dn_i = x_i dn + n dx_i \qquad 3\text{-}8$$

$$d(nM) = n dM + M dn \qquad 3\text{-}9$$

When dn_i and d(nM) are replaced by the above equations, then equation 3-7 Becomes:

$$n dM + M dn = n\left[\frac{\delta M}{\delta p}\right]_{T,x} dp + n\left[\frac{\delta M}{\delta T}\right]_{P,x} dT + \sum_i \bar{M}_i \, (x_i dn + n dx_i) \qquad 3\text{-}10$$

$$\left[dM - \left[\frac{\delta M}{\delta p}\right]_{T,x} dp - \left[\frac{\delta M}{\delta T}\right]_{P,x} dT - \sum_i \bar{M}_i \, dx_i\right] n + \left[M - \sum_i \bar{M}_i \, x_i\right] dn = 0 \qquad 3\text{-}11$$

As n and dn are independent of each other, equation 3-11 can only be valid if each term in bracket

is zero. On putting the coefficients to zero the following equations obtain:

$$dM = \left[\frac{\delta M}{\delta p}\right]_{T,x} dp + \left[\frac{\delta M}{\delta T}\right]_{P,x} dT - \sum_i \bar{M}_i \, dx_i \qquad 3\text{-}12$$

$$M = \sum_i \bar{M}_i \, x_i \qquad 3\text{-}13$$

$$nM = N \sum_i \bar{M}_i \, x_i \qquad 3\text{-}14$$

These equations are of central importance as they calculate mixture properties using partial properties. One further important equation that follows directly from equations 3-12 and 3-13 is:

$$dM = \sum_i x_i \, d\bar{M}_i + \sum_i \bar{M}_i \, dx_i \qquad 3\text{-}15$$

Comparing equations 3-12 and 3-15 yields the well-known Gibbs-Duhem equation (GDE):

$$\left[\frac{\delta M}{\delta p}\right]_{T,x} dP + \left[\frac{\delta M}{\delta T}\right]_{P,x} dT - \sum_i x_i \, d\bar{M}_i = 0 \qquad 3\text{-}16$$

This equation must be satisfied for all changes in P, T, and the M_i caused by changes of state in a homogeneous phase. For the important special case of changes at constant T and P, it simplifies to:

$$\sum_i x_i \, d\bar{M}_i = 0 \qquad 3\text{-}17$$

The significance of the Gibbs-Duhem equation is that the chemical potential of a component in a mixture cannot change independently of the chemical potential of the other components.
For binary systems, the sumability relation becomes:

$$M = x_1 \bar{M}_1 + x_2 \bar{M}_2 \qquad 3\text{-}18$$

$$dM = x_1 d\bar{M}_1 + M_1 \bar{M}_1 + \sum_i \bar{M}_i \, dx_i \qquad 3\text{-}19$$

Considering G-D equation at constant T and P and since for system of two components $x_1+x_2=1$ and $dx_1=-dx_2$, the following equations can be obtained:

$$\bar{M}_1 = M + x_2 \frac{dM}{dx_1} \quad 3\text{-}20$$

$$\bar{M}_2 = M - x_1 \frac{dM}{dx_1} \quad 3\text{-}21$$

3.3 Mixing process and thermodynamic of mixing

Knowing the thermodynamics of mixing is important as it will give us information about how much the thermodynamic quantities change when going from an unmixed state to a mixed state. When the two or more pure components mix spontaneously at constant pressure they form a single homogeneous phase and the thermodynamic quantities of the system experience a change as a result of the mixing [170] .Based on the foregoing considerations one may define an isothermal molar property change of mixing as the value of M for the multi-component system minus the value of the same property in the pure substances at the same P and T. So, ΔM_{mix} is given by:

$$\Delta M_{mix}(T,P) = M(T,P) - \sum x_i \, M_i(T,P) = \sum x_i \, (\bar{M}_i - M_i) \quad 3\text{-}22$$

Where M (can be = V, U, H, S, A, G) is a molar solution property and M_i is a molar pure components property at the same value of T and P [169].Because the mixing function is linear it permutes with other linear operators such as derivatives [171], so from $V = \left[\frac{\delta G}{\delta P}\right]_{T,n_i}$, we obtain:

$$\Delta V_{mix} = -\left[\frac{\delta \Delta G_{mix}}{\delta P}\right]_{T,n_i} \quad 3\text{-}23$$

Similarly, the following important relations can be obtained

$$\Delta S_{mix} = -\left[\frac{\delta \Delta G_{mix}}{\delta T}\right]_{P,n_i} \quad 3\text{-}24$$

$$\Delta H_{mix} = -T^2 \left[\frac{\delta(\Delta G_{mix}/T)}{\delta T}\right]_{P,n_i} \quad 3\text{-}25$$

$$\Delta U_{mix} = P\Delta V_{mix} - \Delta H_{mix} \quad 3\text{-}26$$

Of mixing quantities such as ΔS_{mix} , ΔH_{mix} and ΔV_{mix} can obtain useful information about the intermolecular interactions of the solution in comparison to pure components.

3.4 Ideal solution

An ideal solution is a solution with thermodynamic properties similar to those of a mixture of ideal gases. In an ideal solution, the interactions and entropies between molecules of the components does not differ from the interactions and entropies between the molecules of each component. Normally**,** this is a solution that each component obeys Raoult's Law. Raoult's Law, established by French chemist Raoult (1887), states that for closely related liquids the partial vapor pressure (P_i) (Pascal) of each component in a solution is given by the product of the vapor pressure of the corresponding pure component (P_i^*) at the same temperature and its mole fraction (x_i) in the solvent:

$$P_i = x_i P_i^* \quad 3\text{-}27$$

3.4.1 The chemical potential of ideal liquid solutions

For an ideal solution the chemical potential of all solution components in all concentrations and for the specific range of T and P follows the equation below:

$$\mu_i(l) = \mu_i^*(l) + RT\ln\left[\frac{P}{P_i^*}\right] \quad 3\text{-}28$$

where μ_i and μ_i^* denote the chemical potential of component i and chemical potential of pure component i in the ideal solution, respectively. P_i is the vapor pressure of substance i and P_i^* is the vapor pressure of the pure component i at the same T. In all cases, the notation * means the pure

component. Since in ideal solution each component (i) obeys Raoult's Law, the chemical potential can be expressed as:

$$\mu_i(l) = \mu_i^*(l) + RT\ lnx_i \qquad 3\text{-}29$$

Mixtures that follow this rule throughout the whole composition range are called ideal solutions. Many liquid solutions significantly deviate from the ideal behavior predicted by Raoul's Law.

3.4.2 Mixing properties of an ideal solution

From the definition of μ_i in the equation 3-29 all the mixing properties can be easily obtained. Based on

$$\Delta G_{mix} = G - G^* = \sum_i x_i (\mu_i - \mu_i^*) \qquad 3\text{-}30$$

The Gibbs free energy of mixing for ideal solutions follows immediately:

$$\boldsymbol{\Delta G_{mix} = RT \sum n_i\ lnx_i} \qquad 3\text{-}31$$

Since x_i is the mole fraction of component i and in mixtures, all mole fractions are between 0 and 1, the logarithm of x_i will be negative, in conclusion, ΔG_{mix} will have a negative amount as well. According to the Second Law at constant P and T mixing is a spontaneous process. Based on equation (3-26), at T and P constant, $\Delta V_{mix} = \left[\frac{\delta \Delta G_{mix}}{\delta P}\right]_{T,n_i} = 0$.

As we expect from the definition of an ideal solution, the formation of an ideal solution of its pure components at constant T and P, does not involve any changes in volume. The change in the molar entropy of the system is expressed by the following equation:

$$\boldsymbol{\Delta S_{mix} = \left[\frac{\delta \Delta G_{mix}}{\delta T}\right]_{P,n_i} = -R \sum n_i\ lnx_i} \qquad 3\text{-}32$$

Based on equation $\Delta G_{mix} = \Delta H_{mix} - T\Delta S_{mix}$ and equations 3-31 and 3-32, the change of enthalpy for an ideal solution is zero. The zero-enthalpy change means that the ideal solution at constant T and P is not associated with any heat exchange. However, the reverse is not always true. If the ΔH_{mix} and ΔV_{mix} are zero the solution can be both ideal and non-ideal solution. Similarly, based on equation (3-126), and $\Delta H_{mix} = 0$ and $\Delta V_{mix} = 0$, the following relation can be obtained:

$$\mathbf{\Delta U_{mix} = 0} \qquad \text{3-33}$$

3.4.3 Partial molar properties of an ideal solution

Based on chemical potentials $\mu_i = \mu_i^* + RT\ \ln x_i$, $\bar{S}_i = -\left(\frac{\partial \mu_i}{\partial T}\right)_{p,n_i}$, $\bar{V}_i = \left(\frac{\partial \mu_i}{\partial P}\right)_{T,n_i}$ and $\bar{H}_i = \mu_i + T\bar{S}_i$ all other thermodynamic partial molar properties for an ideal solution can be obtained straightforwardly.

$$\mathbf{\bar{S}_i = S_i^* - R\ ln x_i} \qquad \text{3-34}$$

in equation 3-34 $\ln x_i$ is negative in a mixture, therefore the partial molar entropy of a component of an ideal mixture is greater than the molar entropy of the pure substance at the same T and p.

$$\mathbf{\bar{V}_i = \left(\frac{\partial \mu_i}{\partial P}\right)_{T,n_i} = V_i^*} \qquad \text{3-35}$$

$$\mathbf{\bar{H}_i = \mu_i^*{}_i + TS_i^* = H_i^*} \qquad \text{3-36}$$

$$\mathbf{\bar{U}_i = H_i^*{}_i + PV_i^* = U_i^*} \qquad \text{3-37}$$

It is to be noted that in an ideal mixture the partial molar quantities of $\bar{V}_i$, $\bar{H}_i$ and $\bar{U}_i$ are independent of the mixture composition and is equal to the molar quantities of pure component i at the same T and p as the mixture. These results are consistent with $\Delta V_{mix} = 0, \Delta H_{mix} = 0$ and $\Delta S_{mix} \neq 0$. Note that $\Delta H_{mix} = 0$ does not mean that there are no interactions, it means that the interactions in the mixture are the same as those in either pure substance.

3.4.4 Ideal dilute solution

The ideal dilute solution is so dilute that the solute molecules interact mainly with solvent molecules. Many liquid solutions deviate from the ideal behavior predicted by Raoult's Law. William Henry, an English chemist, found experimentally that for real solutions at low solute concentrations, despite the vapor pressure of the solute is proportional to the mole fraction,

contrary to Raoul's law the constant of proportionality is not the same as the vapor pressure of the pure material. This relationship is defined as Henry's Law and expressed by the equation below:

$$\mathbf{P_B = x_B K_B} \quad 3\text{-}38$$

where K_B is an empirically determined constant with the units of pressure and X_B is the mole fraction of the solute. B refers to the component B.

Henry's law constant can often be written in terms of the molarity and molality:

$$\mathbf{P_i = K_{i,c} C_i} \quad 3\text{-}39$$

$$\mathbf{P_i = K_{i,m} x_i} \quad 3\text{-}40$$

where $K_{i,c}$ and $K_{i,m}$ are related to K_i .The subscripts c and m refer to the morality and molality, respectively. Ideal-dilute solutions are those for which the solute obeys Henry's law and the solvent obeys Raoult's Law. The reason that the solvent and solute are remarkably different in their behavior arises from the fact that in dilute solution the solvent molecules which are in large excess are surrounded by other solvent molecules so that they experience the environment very much like a pure liquid. (the solvent obeys Raoult's Law). On the other hand, the solute which is in low concentration tends to be surrounded by solvent molecules and consequently, their environment and thermodynamic behavior are quite different from a pure one (The solute obeys Henry's Law).

3.4.5 **Partial molar quantities in ideal-dilute solutions**

The partial molar properties for the solvent and solute in ideal-dilute solutions are described as follows:

Solvent (A):

$$\mathbf{\bar{H}_A = H^*_A} \quad 3\text{-}41$$

$$\mathbf{\bar{V}_A = V^*_A} \quad 3\text{-}42$$

$$\mathbf{\bar{S}_A = S^*_A - R \ln x_A} \quad 3\text{-}43$$

Solute (B):

$$\mathbf{\bar{S}_B = S^*_B - R \ln x_B} \quad 3\text{-}44$$

$$\bar{V}_i = \left(\frac{\partial \mu_i^o}{\partial P}\right)_T$$ 3-45

Based on $\bar{S}_i = -\left(\frac{\partial \mu_i^o}{\partial T}\right)_{P,ni}$ and $\bar{H}_i = \mu_i + T\bar{S}_i$, partial enthalpy, and entropy will be obtained:

$$\bar{\mathbf{V}}_{\boldsymbol{B}} = \bar{\mathbf{V}}^{\circ}{}_{\boldsymbol{B}} = \bar{\mathbf{V}}^{\infty}{}_{\boldsymbol{B}}$$ 3-46

$$\bar{\mathbf{H}}_{\boldsymbol{B}} = \bar{\mathbf{H}}^{\circ}{}_{\boldsymbol{B}} = \bar{\mathbf{H}}^{\infty}{}_{\boldsymbol{B}}$$ 3-47

The partial molar volume and internal energy of the solute are constant in the ideal-dilute range and are equal to the values at infinite dilution ($\bar{M}^{\infty}{}_B, (M = V, H)$). When the pressure is equal to the standard pressure p∘, the ($\bar{M}^{\infty}{}_B$) quantities are equal to the standard values ($\bar{M}^{\circ}{}_B$).

$$\bar{\mathbf{S}}_{\boldsymbol{B}} = \mathbf{S}^{*}{}_{\boldsymbol{B}} - \mathbf{R}\ln \mathbf{x}_{\boldsymbol{B}}$$ 3-48

$$\bar{\mathbf{S}}_{\boldsymbol{B}} = \bar{\mathbf{S}}^{\circ}{}_{\boldsymbol{B}} - \mathbf{R}\ln \mathbf{x}_{\boldsymbol{B}}$$ 3-49

3.5 Non-ideal solution

Solutions of liquids that its components do not obey Raoul's law at every range of concentration and all temperatures are called non-ideal solutions. It is typically the solution in which solvent and solute molecules interact with each other with a different force than forces of interaction between the molecules of the pure compounds. In other words, real solutions are composed of particles for which A-A, A-B, and B-B interactions are all different (The molecules of the pure compounds interact with each other with different force than forces between solvent and solute molecules). On the other hand, the deviations from ideality (Raoult's law) cannot only be explained in the framework of molecular interactions only. Let us consider the following example -mixture of two n-alkanes, differing as to the length, i.e. n-hexane and n-hexadecane. All the interactions between like and unlike molecules are practically the same, but this mixture exhibits significant negative deviations from ideality.

In real solutions, there may be volume and enthalpy changes when liquids mix. $\Delta H_{mix} \neq 0$ means heat is absorbed or released during the mixing process. We can express the behavior in real solutions as a deviation from Raoul's law. Deviation from Raoult's Law can be positive or negative.

3.5.1 **Positive deviation from Raoult's Law**

In this case, the vapor pressure of the mixture is always greater than that expected by Raoult's Law. The intermolecular forces between dissimilar molecules of A and B are less strong than those in pure liquids. Thus, the tendency of each component to pass to the vapor phase increases.

$f_i > f_i^* x_i$ or $P_i > P_i^* x_i$

Molecules in this case are breaking away more easily than they do in pure one. Indeed, the resulting solution has a larger enthalpy of the solution than pure components of the solution, thus the solution process needs heat to be absorbed to move forward which states the process is endothermic. If the change of enthalpy in the solution process is large and positive, then the liquids may be immiscible.

3.5.2 **Negative deviation from Raoult's Law**

In this case, the intermolecular forces between dissimilar molecules are greater than those in pure liquids. Thus, the tendency of each component to pass to the vapor phase is low.

$f_i < f_i^* x_i$ *or* $P_i < P_i^* x_i$

It states that the vapor pressures of the mixture are less than that would be expected for an ideal mixture via Raoult's Law. In negative deviation from Raoult's Law, the solution process is accompanying by releasing more energy in the form of heat which results in making the reaction process exothermic. It means more heat is given out when the new stronger bonds are made than was used in breaking the original weaker ones.

3.5.3 **Chemical potential of non-ideal solutions**

If a mixture is not ideal, we can write a more accurate description of the chemical potentials of each component in condensed solutions after an activity coefficient γ_i is introduced within the logarithm. The chemical potential is then written as:

$$\boldsymbol{\mu_i = \mu_i^\circ + RT\ln(\gamma_i x_i)} \quad 3\text{-}50$$

Where μ_i° is the chemical potential of constituent i in the standards state. The activity coefficient of component i γ_i is a dimensionless factor that takes into account the deviation from ideal behavior in the solution [170]. This coefficient considers the non-ideal characteristics of a mixture and it is between 0 and 1. For an ideal solution γ_i approaches 1 and then the Raoult's Law is accurate. If $\gamma_i > 1$ or $\gamma_i < 1$ then the substance i shows negative or positive deviation from ideality/Raoult's Law respectively. By substituting the product $\gamma_i x_i$ to the variable a_i which is known as the activity of component i the chemical potential is rewritten as:

$$\boldsymbol{\mu_i = \mu_i^\circ + RT\ln(a_i)} \quad 3\text{-}51$$

3.5.4 **Thermodynamic of mixing for non-ideal solution**

Based on $\Delta G_{mix} = G - G^* = \sum_i x_i\,(\mu_i - \mu_i^*)$, and the definition of μ_i for the non-ideal solution the Gibbs free energy of mixing for non-ideal solutions is written as follows:

$$\boldsymbol{\Delta G_{mix} = RT \sum n_i \ln a_i} \quad 3\text{-}52$$

all other thermodynamic mixing properties for non-ideal solutions are listed as follows

$$\Delta S_{mix} = \left[\frac{\partial \Delta G_{mix}}{\partial T}\right]_P = -RT \sum_i x_i \left(\frac{\delta \ln a_i}{\partial T}\right)_P - R \sum_i x_i \ln a_i \quad 3\text{-}53$$

$$\Delta H_{mix} = \Delta G_{mix} + T\Delta S_{mix} = -RT^2 \sum_i x_i \left(\frac{\delta \ln a_i}{\partial T}\right)_P \quad 3\text{-}54$$

$$\Delta V_{mix} = \left[\frac{\delta \Delta G_{mix}}{\delta P}\right]_{T,n_i} = RT \sum_i x_i \left(\frac{\delta \ln \gamma_i}{\partial P}\right)_T \quad 3\text{-}55$$

3.5.5 **Excess functions**

The deviation from ideal behavior is well understood by the thermodynamic excess property/function. It can provide information about the nature of intermolecular interactions, i.e.,

attraction or repulsion. Excess quantities are properties of mixtures that characterize their non-ideal behavior. If M represents the molar value of any extensive property, then an excess quantity M^E of a mixture is defined as the difference between the value of the extensive property of the real mixture and the value it would have if the solution is ideal [169] at the same temperature, pressure, and composition. Therefore,

$$\mathbf{M^E = M - M^{id}} \quad \text{3-56}$$

for example: $G^E = G - G^{id}$, similar definitions hold for other excess properties:

$$\mathrm{H^E = H - H^{id}} \quad \text{3-57}$$

$$\mathrm{S^E = S - S^{id}} \quad \text{3-58}$$

$$\mathrm{V^E = V - V^{id}} \quad \text{3-59}$$

Moreover, subtraction of $\mathrm{G^{id} = H^{id} - TS^{id}}$ from $\mathrm{G = H - TS}$ gives $\mathrm{G^E = H^E - TS^E}$.
The excess property bears a relationship to the property change of mixing.

$$\Delta\mathrm{M = M - \sum_i x_i M_i} \quad \text{3-60}$$

$$\mathrm{G^E = G - G^{id} = G - (\sum_i x_i G_i + RT \sum_i x_i \ln x_i} \quad \text{3-61}$$

$$\text{Thus,} \quad \mathrm{G^E = \Delta G_{mix} - RT \sum_i x_i \ln x_i} \quad \text{3-62}$$

$$\mathrm{S^E = \Delta S_{mix} + RT \sum_i x_i \ln x_i} \quad \text{3-63}$$

The excess enthalpy and volume are both equal to the observed enthalpy and volume of mixing, because the ideal values are zero in each case thus,$V^E = \Delta V_{mix}$ and$H^E = \Delta H_{mix}$. As for ideal solutions, the excess properties are equal to zero, thus,

$$\mathrm{\Delta G_{mix} = RT \sum_i x_i \ln x_i} \quad \text{3-64}$$

$$\mathrm{\Delta S_{mix} = -RT \sum_i x_i \ln x_i} \quad \text{3-65}$$

$$\mathrm{\Delta V_{mix} = 0, \Delta H_{mix} = 0} \quad \text{3-66}$$

Subtracting $\Delta M(id) = M(id) - \sum_i x_i M_i$ from $\Delta M = M - \sum_i x_i M_i$ gives us the following equation that represents the excess properties and states that the property changes of mixing are readily calculated one from the other.

$$M^E = \Delta M - \Delta M^{id} \quad (3\text{-}67)$$

3.5.5.1 Excess chemical potential

$$\mu_i^E = \mu_R - \mu_{id} \quad (3\text{-}68)$$

Based on $\mu_i^\circ(real) = \mu_i^\circ(ideal)$ then:

$$\mu_i^E = (\mu_i^\circ - RTlna_i) - (\mu_i^\circ - RTlnx_i) = RTln\gamma_i \quad (3\text{-}69)$$

$$G_i^E = G_R - G_{id} = RT\sum_i x_i lna_i - RT\sum_i x_i lnx_i = RT\sum_i x_i ln\gamma_i \quad (3\text{-}70)$$

Similarly, other important relations include:

$$S^E = -\left(\frac{\partial G_i^E}{\partial T}\right)_P = -R\sum_i n_i\left(\frac{\partial ln\gamma_i}{\partial T}\right)_P \quad (3\text{-}71)$$

$$H^E = G_i^E - TS_i^E = -RT^2\sum_i n_i\left(\frac{\partial ln\gamma_i}{\partial T}\right)_P \quad (3\text{-}72)$$

$$\Delta V^E = -\left(\frac{\partial G_i^E}{\partial P}\right)_T = -RT^2\sum_i n_i\left(\frac{\partial ln\gamma_i}{\partial P}\right)_T \quad (3\text{-}73)$$

The nonzero values of the excess functions are due to the fact that interactions between particles of different components are different from the interactions between particles of the same component.

3.5.5.2 Partial molar volume

In a system that contains at least two substances, the total value of any extensive property of the system is the sum of the contribution of each substance to that property. The contribution of one

mole of a substance to the volume of a mixture is called the partial molar volume of that component. At constant T and P:

$$\mathrm{V} = \mathrm{n}_1\left(\frac{\partial \mathrm{V}}{\partial \mathrm{n}_1}\right) + \mathrm{n}_2\left(\frac{\partial \mathrm{V}}{\partial \mathrm{n}_2}\right) \quad 3\text{-}74$$

$$V_{1,m} = n_1\left(\frac{\partial V}{\partial n_1}\right)_{T,P,n_2} + n_2\left(\frac{\partial V}{\partial n_2}\right)_{T,P,n_1} \quad 3\text{-}75$$

$$V_{1,m} = \left(\frac{\partial V}{\partial n_1}\right)_{T,P,n_2} \quad 3\text{-}76$$

$$V_{2,m} = \left(\frac{\partial V}{\partial n_2}\right)_{T,P,n_1} \quad 3\text{-}77$$

The partial molar volume for the pure components is $\mathrm{V_{1,m}}^{*} = \frac{\mathrm{m_1}}{\rho_1}$ and are $\mathrm{V_{2,m}}^{*} = \frac{\mathrm{m_2}}{\rho_2}$. The total molar volume and molar volume of components can be obtained from

$$V_m = x_1\,V_{1,m} + x_2\,V_{2,m} = \left(V_{1,m} - V_{2,m}\right)x_1 + V_{2,m} \quad 3\text{-}78$$

so,

$$V_{1,m} = V_m + x_2\left(\frac{\partial V_m}{\partial x_1}\right) \quad 3\text{-}79$$

$$V_{2,m} = V_m + x_1\left(\frac{\partial V_m}{\partial x_1}\right) \quad 3\text{-}80$$

$$\Delta V_{mix} = V^E = \Delta V_2 + x_1\left(\frac{\partial V^E}{\partial x_1}\right) = \Delta V_1 - x_2\left(\frac{\partial V^E}{\partial x_1}\right) \quad 3\text{-}81$$

The most common method of measuring partial molar volumes is to measure the dependence of the volume of a solution upon its composition. The observed volume can then be fitted to a function of the composition (usually using a computer), and the slope of this function can be determined at any composition of interest by differentiation.

3.5.5.3 Excess molar volume

Volume changes on mixing at constant pressure and temperature are an indicator of the non-idealities present in real mixtures. The change in volume on mixing two liquids, especially two

polar liquids, 1 and 2 can be attributed to several procedures including : (a) the breakdown of 1 - 1 and 2 - 2 intermolecular interactions which have a positive effect on the volume, (b) the formation of 1 - 2 intermolecular interactions which results in a volume contraction of the mixture, (c) packing effects caused by a difference in the size shape of the component species and which may have a positive or negative effect on the value, and (d) formation of new chemical species.

The excess molar volume upon mixing has been determined via two principal methods, directly and indirectly. The direct measurements involve mixing the liquids and observing the resultant volume change in dilatometers and the indirect measurements involve measuring the density of the pure liquid as well as the density of the mixture using densitometers or pycnometers. The dilatometer is filled with known masses of pure liquids, which are separated by mercury. The height of mercury in the calibrated graduated column is noted. The liquids are mixed by rotating the dilatometer and the volume change on mixing is indicated by the change in the height of the mercury in the calibrated capillary.

The indirect determination of excess volume for a binary mixture can be determined from density measurements of components in the pure and mixed state using the following equation:

$$V^E = \frac{(x_1 M_1 + x_2 M_2)}{\rho_{12}} - \left(\frac{x_1 M_1}{\rho_1}\right) - \left(\frac{x_2 M_2}{\rho_2}\right) \qquad 3\text{-}82$$

where x_1 and x_2 are the mole fractions, M_1 and M_2 are molar masses, ρ_1, ρ_2 and ρ are the densities where 1 and 2 refer to the component 1 and 2, respectively and ρ is the density of the mixture. A brief review of density measurement techniques has been discussed in the following chapter.

3.6 Correlations

Precise representation of experimental data on thermo-physical properties is pre-requisite to design the accurate equipment for many chemical processing including CO_2 capture and storage process. This need leads researchers to develop the models to correlate the experimental data. These correlation equations can predict the physio-chemical properties of the mixture when the laboratory report is not available. Some well-known correlations for densities, viscosities, and the refractive indices of binary liquid mixtures have been reported in the literature. A brief review of these correlations is presented in this section.

3.6.1 **Density correlation**

The density of a solution is a significant factor in the experimental data analysis. For the correlation of the density of liquid mixtures, several models have been proposed in the literature. Idem *et al* (2016), applied the Weiland equation to correlate the density of the loaded and unloaded aqueous mixtures of amines including DEAB, MDEA, and MEA [172]. Also, Liu *et al,* (2017) reported a study on the correlation of density of the binary EAE+H_2O and ternary CO_2+EAE+H_2O systems using Weiland model, Redlich−Kister equation (explained below)[173]. The densities of the unloaded solution of aqueous MEA were measured and correlated with Weiland model and Redlich−Kister equation [174]. In the study performed by Zhang *et al* ,(2015) the densities of partially carbonated aqueous tertiary amine-based solvents (DMAE and DEAE) at temperatures from 298.15 to 353.15 K were measured and correlated using Redlich−Kister equation and the equation that Weiland proposed [175]. In the study performed by Eimer *et al*,(2016) the Jouyban-Acree model was applied for correlation of the densities of aqueous 3A1P solutions [176]. Below are some correlation models for density that were used in this study:

3.6.1.1 Weiland Model

Weiland et al, (1998) introduced an expression for calculation of the density of the CO_2 loaded alkanolamine solutions. [177].

One common method to correlate the density of liquid mixtures is through the excess molar volume. In general, the density of a solution is given by the ratio of the average molar weight of the solution to its total molar volume.

$$\rho = \frac{\sum_i^n x_i M_i}{V} \qquad 3\text{-}83$$

Where ρ and V are the density and molar volume of the solution,x_i and$M_i$are the mole fractions and molecular weights of the pure components in the solution, respectively.

The molar volume of the ideal solution is the sum of the partial molar volumes of the component multiplied by their molar fractions. As the solutions of alkanolamines show deviation from the ideality, the molar volume of these solutions is associated with the extra parameter that is stated as the excess molar volume and is calculated from the following equation [168]:

$$V^E = V - \sum_{i=1}^{n} x_i V_i \qquad 3\text{-}84$$

Here, V_i is the molar volume of pure component i and is calculated from experimental density. This way, the excess molar volume of the unloaded amine solutions can be calculated to analyze the density of the system. One of the mathematical equation that is widely used in the correlation of experimental data of binary solutions is the Redlich–Kister equation [178].

$$\mathrm{Y^E} = \mathrm{x_1 x_2} \sum_{\mathrm{p=0}}^{\mathrm{m}} \mathrm{A_p} (\mathrm{x_1} - \mathrm{x_2})^{\mathrm{p}} \qquad 3\text{-}85$$

Where Y^E can be any excess property or thermodynamic change of property (V^E, $\Delta\eta$,…), therefore:

$$\mathrm{V^E} = \mathrm{x_1 x_2} \sum_{\mathrm{p=0}}^{\mathrm{m}} \mathrm{A_p} (\mathrm{x_1} - \mathrm{x_2})^{\mathrm{p}} \qquad 3\text{-}86$$

where A_p is the polynomial coefficient andx_1 andx_2 are mole fractions of components 1 and 2, respectively. $\mathrm{A_p}$is a temperature-dependent fitting parameter, hence, $\mathrm{Y^E}$can be rewritten as equation below [178]:

$$\mathrm{Y^E} = \mathrm{x_1 x_2} \sum_{\mathrm{i=0}}^{\mathrm{k}} (\sum_{\mathrm{j=0}}^{2} \mathrm{B_{ij}\, T^j})\, (\mathrm{x_1} - \mathrm{x_2})^{\mathrm{i}} \qquad 3\text{-}87$$

The value of $\mathrm{A_P}$ is obtained by using unweighted Least-Square Method and fitting of equations (3-85) or (3-86) to the experimental results.

For ternary mixtures the Redlich-Kister equation is defined as follows [178] :

$$\mathrm{Y_{123}{}^E} = \mathrm{x_1 x_2} \textstyle\sum_{\mathrm{v=0}}^{\mathrm{r}} (\mathrm{A_v})_{12} (\mathrm{x_1} - \mathrm{x_2})^{\mathrm{v}} + \mathrm{x_1 x_3} \textstyle\sum_{\mathrm{v=0}}^{\mathrm{r}} (\mathrm{A_v})_{13} (\mathrm{x_1} - \mathrm{x_3})^{\mathrm{v}} + \mathrm{x_2 x_3} \textstyle\sum_{\mathrm{v=0}}^{\mathrm{r}} (\mathrm{A_v})_{23} (\mathrm{x_2} - \mathrm{x_3})^{\mathrm{v}} \qquad 3\text{-}88$$

where $\mathrm{x_i}$ is the mole fraction of component i, and $(\mathrm{A_v})_{ij}$ are adjustable coefficients for the binary mixture i, j obtained by the least-squares method.

The ability to change the number of adjustable parameters adapt the Redlich-Kister equation into a flexible equation. The optimum number of coefficients is determined from an approximation of the variation in the standard deviation σ with [168]:

$$\sigma = \left[\frac{\sum_{n=1}^{N}(Y_{exp}-Y_{cal})^2}{(N-(m+1))}\right]^{1/2} \quad 3\text{-}89$$

where subscripts n and m represent the experimental and calculated values, respectively, using Redlich-Kister equation for property Y. N and m are the number of experimental data points and the number of adjustable coefficients, respectively.

3.6.1.2 Modified Graber equation

Graber *et al*, (2004) first proposed an empirical model as a function of both temperature and concentration to correlate the density of the multicomponent systems [179]. The two-variable correlation equation helps in representing the data at different temperatures and concentrations. Therefore, a single equation derived from applied correlations is applied to represent the data. Several researches have been conducted on the correlation of the experimental density data using the modified Graber equation [54], [180]–[183].

The Graber equation can be stated as given below:

$$Y = w \exp\left(Z_1 + Z_2 T^{0.5} + Z_3 w^{0.5}\right) + Z_4 + Z_5 T^{0.5} + Z_6 w^{0.5} \quad 3\text{-}90$$

In which Y represents density or other physio-chemical properties, w is the mass fraction of corresponding component in the system and, parametersZ_i (i=1-6) are the regressed coefficients investigated by fitting the experimental data of density by minimizing of the % AARD value between experimental and correlated data. However, in this equation, only the concentration of one component of the mixture is applied. Hence, to characterize the effect of the concentration of both components on the physio-chemical properties of the mixture (density, refractive index), Murshied *et al* , (2017)[183] proposed a new equation that is further improved form of equation (3-90).

$$Y = (w_1 + w_2)\exp\left(Z_1 + Z_2 T^{0.5} + Z_3 w_1^{0.5} + Z_4 w_2^{0.5}\right) + Z_5 + Z_5 T^{0.5} + Z_6 w_1^{0.5} + Z_7 w_2^{0.5} + Z_8 T^{0.5} \quad 3\text{-}91$$

3.6.1.3 Jouyban−Acree Model

Besides, densities of the solutions can be correlated using Jouyban−Acree model (JAM) as a function of temperature and concentration through the following equation [184]:

$$\ln \rho_m = x_1 \ln \rho_1 + x_2 \ln \rho_2 + x_1 x_2 \sum_{i=0}^{n} \left| \frac{B_i (x_1 - x_2)^n}{T} \right| \quad 3\text{-}92$$

Where ρ_m, ρ_1 ,and ρ_2 are the density of the mixture and density of pure components 1 and 2, andx_1 andx_2 are mole fraction of components 1 and 2, respectively. B_i is the fitting parameters obtained from the Least-Square Method. The optimum number of fitting parameters is determined with %AARD expressed in equation (3-93) and when %AARD does not show significant changes with the increase in the order of the equation.

$$\text{AARD\%} = 100\% \frac{1}{n} \sum_{i=1}^{n} \left| \frac{Y_{exp,i} - Y_{cal,i}}{Y_{exp,i}} \right| \quad 3\text{-}93$$

This equation as well as the Graber equation can be used widely for correlation of different physio-chemical properties.

3.6.2 Viscosity correlation

Calculation of the viscosity of the liquid mixtures through the properties of the pure components using the correlation equations is of great importance in practical problems of fluid flow and heat and mass transfer. Several semi-empirical models have been proposed in the literature so far to predict the viscosity of amine-based binaries and ternaries liquid mixtures.

Lee *et al*, (1995) studied the viscosity of MEA-H_2O, MEA-ETOH, and MEA-2-Propanol at temperatures ranging from 303.15 to 323.15 K. The viscosity deviations for all the mixtures were correlated using Redlich-Kister equation. Also, the authors applied the McAllister's model to correlate the kinematic viscosity of the studied mixtures [161]. In the study done by Øi *et al*, (2020) the three-body McAllister's model was applied to correlate determined kinematic viscosities of MDEA -H_2O, DMEA- H_2O, and DEEA - H_2O Mixtures from dynamic viscosity data [185].

The viscosity measurement of the unloaded and loaded mixture of MEA-H_2O at higher concentrations was performed by Eimer *et al*,(2017) [186]. The authors applied four different models including Heric and Brewer, Jouyban-Acree, Herraez et al and Redlich-Kister to correlate the viscosity of unloaded studied mixtures. In another study performed by Eimer *et al*, (2018) the new viscosity data for loaded and unloaded aqueous solutions of 3A1P at different temperatures ranging from 298.15 to 373.15 K were examined. Also, Heric and Brewer model was applied to correlate the viscosity of unloaded aqueous solutions of 3A1P [187]. Idem *et al*,(2016) applied the Grunberg and Niassan equation to correlate the viscosity of the unloaded aqueous mixtures of amines including DEAB, MDEA, and MEA [172]. Fu *et al*,(2012) performed experiments on the viscosity of carbonated MDEA-MEA aqueous solution at temperatures ranging from 293.15 to 343.15 K and correlated the viscosities of solutions with modified Grunberg–Nissan equation [188]. The viscosities of the binary and ternary systems including MEA and their correlations with Grunberg and Nissan model were performed by Li *et al,*(1995)[189]. Mandal *et al*, (2003) measured viscosities for aqueous mixtures of MEA + MDEA, MEA + AMP, DEA + MDEA, DEA + AMP for different temperature ranges. The viscosity data were correlated using by Grunberg-Nissan model [190].

Hartono *et al* , (2014) measured the viscosity of aqueous MEA solutions and carbonated MEA solutions and correlated their deviation using Redlich-Kister equation [174]. In the study done by Fu *et al* ,(2014) the viscosities of carbonated AMP-PZ solutions were measured and correlated using the model proposed by Weiland [191].

Below are some of the equations which have been used in this work to correlate the viscosity data of the studied solutions.

3.6.2.1 McAllister Model

A well-known correlation for experimental viscosities of binary systems was developed by McAllister (1960) [192]:

$$\ln \nu_m = x_1^3 \ln \nu_1 + 3x_1^2 x_2 \ln \nu_{12} + 3x_1 x_2^2 \ln \nu_{21} + x_2^3 \ln \nu_2 - \ln\left(x_1 + x_2 \frac{M_2}{M_1}\right) + 3x_1^2 x_2 \ln\left[\left(2 + \frac{M_2}{M_1}\right)/3\right] + 3x_2^2 x_1 \ln\left[\left(1 + \frac{2M_2}{M_1}\right)/3\right] + x_2^3 \ln\left(\frac{M_2}{M_1}\right) \quad 3\text{-}94$$

Here ν_m is the kinematic viscosity of the binary mixture, x_1 and x_2 are the mole fractions, ν_1 and ν_2 are the kinematic viscosities of the pure components, and M_1 and M_2 are the molar masses of components 1 and 2.The interaction parameters ν_{21} and ν_{12} were determined using the least square regression method.

3.6.2.2 Heric and Brewer Model

Another semi-empirical method to correlate the viscosity of the liquid mixture is the Heric and Brewer correlation model [193].In this model, the viscosity of the mixture is calculated using the Following equation:

$$\ln \eta = x_1 \ln \eta_1 + x_2 \ln \eta_2 + x_1 \ln M_1 + x_2 \ln M_2 - \ln(x_1 M_1 + x_2 M_2) + x_1 x_2 \left[\sum_{i=0}^{i} A_i (x_1 - x_2)^i\right] \quad 3\text{-}95$$

In the equations above, η, x, M and A_i refer to the dynamic viscosity, mole fraction, molecular weight, and model's fitting parameters, respectively. Integer 1 and 2 refer to the components 1 and 2.

3.6.2.3 Jouyban-Acree Model

Besides, the viscosity of the solutions can be correlated using Jouyban−Acree model (JAM) as a function of both temperature and concentration through the following equation [184].

$$\ln \eta = x_1 \ln \eta_1 + x_2 \ln \eta_2 + x_1 x_2 \sum_{i=0}^{n} \left[\frac{A_i (x_1 - x_2)^n}{T}\right] \quad 3\text{-}96$$

Where η, η_1 and η_2 are the viscosity of the mixture and viscosity of pure component 1 and 2, and x_1 and x_2 are mole fraction of component 1 and 2, respectively. A_i is the fitting parameters obtained from the Least-Square Method. The optimum number of fitting parameters is determined with %AARD expressed by equation (3-93) and it is obtained when %AARD does not show significant changes with the increase in the order of the equation.

3.6.2.4 Herraez Model

Herraez *et al*, (2008) presented a new model for measuring the viscosities of liquid mixtures. This model is based on the linear behavior of liquid mixtures, where they used the corrective polynomial as an exponential function of the molar fraction. This equation is given as follows [194]**:**

$$\eta = \eta_1 + (\eta_2 - \eta_1) x_2^{\left(\sum_{i=0}^{n} (B_i . {x_2}^i)\right)} \quad \text{3-97}$$

Where η, η_1 andη_2 are the viscosity of the mixture and the pure components 1 and 2, andx_1 andx_2 are mole fraction of component 1 and 2, respectively. A_i is the fitting parameters obtained from the Least-Square Method.

3.6.2.5 Grunberg and Niassan Model

The following equation proposed by Grunberg and Niassan, was applied to correlate the viscosity of liquid mixture[195] :

$$\ln \eta = x_1 \ln \eta_1 + x_2 \ln \eta_2 + G_{12} x_1 x_2 \quad \text{3-98}$$

In the above equations, G_{12} refer to the model's adjustable parameters. The number of parameters,G_{12}, are selected from i = 0,1,2, to n and can be derived by fitting to the experimental data.

3.6.2.6 Redlich-Kister equation

One of the mathematical equation that is used in the correlation of experimental viscosity of binary solutions is the Redlich–Kister equation [178]. The details of this equation have been discussed earlier in section 3.6.1.1.

3.6.3 Refractive index correlation

The refractive index is an essential physical property that is employed for accurate identification of a liquid component, confirmation of the sample's purity, and determination of the concentration of solute in a solution. Several correlations have been proposed in the literature for the prediction

of the refractive indices of binary or multi-component mixtures while the experimental data is not available. Out of which Gladstone-Dale [196], Lorentz-Lorenz [197], Heller [198], Weiner [199], Arago-Biot [200], Newton[201], Eykman [202]and Eyring-John [203] and Oster [204]are the most commonly used equations which are given in Equations (3-99) to (3-107).

3.6.3.1 Gladstone-Dale (G-D)

Gladstone-Dale relation for correlating the refractive index of a binary mixture is given as follows [196]:

$$\frac{n_m - 1}{\rho} = \sum_{i=1}^{r} \frac{n_i - 1}{\rho_i} w_i \qquad 3\text{-}99$$

3.6.3.2 Lorentz-Lorenz (L-L)

Lorentz-Lorenz equation for the refractive index is based on the molecular interaction change with volume fraction [197]:

$$\frac{n_m^2 - 1}{n_m^2 + 2} = \sum_{i=1}^{r} \frac{n_i - 1}{n_i^2 + 2} \phi_i \qquad 3\text{-}100$$

3.6.3.3 Heller (H)

Heller's (H) equation is represented as the following equation [198]:

$$\frac{n_m - n_1}{n_1} = \sum_{i=1}^{r} \frac{n_i^2 - 1}{n_i^2 + 2} \phi_i \qquad 3\text{-}101$$

3.6.3.4 Weiner (W)

Weiner proposed the following relation for the refractive index of binary liquid mixtures [199]:

$$\frac{n_m^2 - n_1^2}{n_m^2 - 2n_1^2} = \sum_{i=1}^{r} \frac{n_i^2 - n_1^2}{n_i^2 + 2n_1^2} \phi_i \qquad 3\text{-}102$$

3.6.3.5 Arago-Biot (A-B)

Arago-Biot equation for the refractive index of liquid mixtures is given as follows [200]:

$$n_m = \sum_{i=1}^{r} n_i \, \phi_i \qquad 3\text{-}103$$

3.6.3.6 Eykman

Below is the Eykman equation for the refractive index of liquid mixtures [202]:

$$\frac{{n_m}^2 - 1}{n_m + 0.4} = \frac{n_1^2 - 1}{n_1 + 0.4}\phi_1 + \frac{n_2^2 - 1}{n_2 + 0.4}\phi_2 \qquad 3\text{-}104$$

3.6.3.7 Newton (N)

Newton proposed the following relation for the refractive index of binary liquid mixtures [201]:

$${n_m}^2 - 1 = (n_1^2 - 1)\phi_1 + (n_2^2 - 1)\phi_2 \qquad 3\text{-}105$$

3.6.3.8 Eyring-John

Eyring-John equation is as follows [203]:

$$n_m = n_1\phi_1^2 + 2(n_1 n_2)^{\frac{1}{2}}\phi_1\phi_2 + \, n_2\phi_2^2 \qquad 3\text{-}106$$

3.6.3.9 Oster

Eyring-John equation is as follows [204]:

$$\frac{{n_m}^2 - 1}{{n_m}^2}\,(2n_1^2 + 1) = \frac{n_1^2 - 1}{n_1^2}\,(2n_1^2 + 1)\phi_1 + \frac{n_2^2 - 1}{n_2^2}(2n_2^2 + 1)\phi_2 \qquad 3\text{-}107$$

In which for all the equations, n_m, n_i (i=1,2) and w_i refer to the refractive index of a mixture, the refractive index of pure components and weight fraction of pure components 1 and 2, respectively.

Also, ϕ_i (i=1,2) refer to the volume fractions of pure components. In addition to the above-mentioned equation, Redlich-Kister equation was also employed to correlate the refractive index data. In the study performed by Mundhwa *et al,* (2006) the Redlich- Kister type of equation was used to predict the refractive index of aqueous solution of 2-((2-aminoethyl) amino) ethanol at temperatures ranging from 298.15 to 333.15 K [205].

Idem *et al*, (2008) investigated the refractive index of the binary solutions of MEA-H_2O, MDEA-H_2O, MEA-MDEA, and tertiary solutions of MEA-MDEA-H2O, MEA-H_2O-CO_2, and MDEA-H_2O-CO_2 at different temperatures from 295 to 333K. Also, the experimental results were correlated with different empirical relations [206].

The refractive indices of the solutions in this study were correlated with all the above-mentioned empirical equations at different temperatures. A literature survey indicates that there is not sufficient data or even no data available on the correlation of the density, viscosity and refractive index of the hybrid mixtures studied in this research including MEA+ETOH, MDEA+ETOH, and DEA+ETOH binary systems.

4. Experimental Equipment and Techniques

4.1 Introduction to density

Density is a fundamental characteristic of materials that must be accurately measured due to its wide application in science and technology. The density of a substance is the proportion of its exact mass, m, and the volume it occupies, v. The most common symbol to denote density in physical science, is the Greek letter, ρ. Density can be mathematically defined as Equation (4-1) and is usually expressed in the SI unit of kg/m³ [207] .

$$\rho = \frac{m}{v} \qquad 4\text{-}1$$

The density of a material typically depends on temperature and pressure. For liquids, temperature is a central factor that can affect density [207]. It is, therefore, significant to state the density of a substance at a given temperature. The density is also termed the absolute density to differentiate it from the dimensionless quantity of relative density [207].

Relative density is the ratio between the density of the material and that of the standard substance under the same conditions of T and P [207],[208].

$$\text{Relative density} = \frac{\text{Density of material}}{\text{Density of the reference substance}} \qquad 4\text{-}2$$

Both the temperature of the material and standard substances must be specified. The relative density indicates if a material sinks or floats in the standard substance. Typically, water is used as the standard substance for liquids. A relative density less than one, therefore, means the substance will float in water [209].

4.1.1 Density measurement techniques

Despite the apparent simplicity of density definition, the accurate measurement of the density of fluids is complex and many novel techniques have been developed. Several principals on density

measurements of liquids have been reported in the literature [210], [209]. There are different types of manual and automated density measuring instruments (Densitometers) used in various process applications which are based on these operating principals. The selection of the densitometer type normally depends on the performance requirement, application, and budget. Although not a complete list, in this section, I focused on some laboratory methods that are most often used in research and quality.

4.1.1.1 Oscillating U-tube

The oscillating U-tube is a technique used for density determination of flowing systems based on an electronic measurement of the oscillation frequency, from which the density value is measured [207]. It usually consists of a mechanical oscillator constructed in the form of a U-tube (oscillating U-tube) with fix mounted ends. The u-shaped tube is vibrated at the resonance frequency of the oscillator. The eigenfrequency of the oscillation of the U-tube is influenced by the sample 's mass and therefore by the density of the sample [211]. The resonance frequency, ω, is inversely proportional to the square root of the total mass of the tube which is the sum of the masses of u-tube and the inner contents of the tube [207]. Typically, the oscillation period, τ, (1 divided by resonance frequency), measured instead of the frequency. This period can be measured with high resolution in a simple relation to the density of the sample in the oscillator according to the following formula:

$$\rho = A.\tau^2 - B \qquad 4\text{-}3$$

Where A and B are the relevant constants of each oscillator [212]. Based on equation (4-3), the density is calculated by knowing the period of oscillations of the U-tube and the reference oscillator quantities. Since the quantities of both the tube mass and the tube's inner volume are known, the vibrating tube method enables calculating the density of unknown fluids after performing a proper apparatuses calibration with two fluids (usually water and air) [213].Despite modern devices that indicate digital density values, in older instruments, the density must be calculated from the measured period of oscillations and the calibration constants [209].

4.1.1.2 Pycnometry

Pycnometery is a technique that uses a defined volume filled with a liquid to determine the liquid density and specific gravity by weighing the mass. Density is then calculated using the equation (4-1) and specific gravity is determined by dividing the density of a substance to the density of water at a defined temperature [214],[215]. The instrument based on this technique is called a pycnometer which is a glass or metal container with a close-fitting ground glass stopper having a capillary hole through it so that air bubbles can escape from the equipment [214]. This enables the accurate measurement of the density of a fluid by reference to an appropriate calibration liquid such as water or mercury [215]. Pycnometers are commonly used under ambient conditions for measuring the density and specific gravity of different materials. The density of the sample can be calculated from the difference in weight between the full and empty pycnometer divided by its known volume [214].

4.1.1.3 Hydrostatic methods

The hydrostatic method is based on Archimedes' principle which states the buoyant force experienced by an immersed object is equivalent to the weight of the fluid it displaces [207], [214]. This method covers density measurements using the following techniques:

4.1.1.3.1 Buoyancy

The buoyancy method is often used to determine the density of bodies and liquids. The liquid density can be determined by measuring either the upward buoyant force of the body or measuring the immersion depth. Through this principle, the volume and therefore the density of an irregularly shaped object can also be obtained by calculating its mass in air and its actual mass while immersed in water. Accurate density measurement, therefore, is highly dependent upon precise weight values [209].

4.1.1.3.2 Hydrostatic balance

A hydrostatic balance is a very accurate balance with a sinker of precisely defined volume. The sinker is attached to a scale pan with shorter stirrup via a hook. The sinker is submerged in the

liquid sample, afterward, the apparent weight loss of the sinker is determined. Based on the Archimedes principle, the apparent weight loss of the sinker is equal to the weight of the fluid it displaces so that the precise volume and precise weight are known [209],[214].

4.1.1.3.3 Hydrometer

A hydrometer measures directly the density and specific gravity of liquids from the immersion depth. Hydrometers operate based on the Archimedes Principle or the principle of flotation There are different types of hydrometers; however, the most common form includes a sealed, long-necked glass cylinder with a bulb filled with a metal weight at one end and scale going up at upper part. Based on the depth of hydrometer flotation into the liquid, the density and specific gravity can be read from the scale on the neck. Hence, a hydrometer sinks deeper into a low-density liquid than into that of high density[209],[214].

4.1.1.3.4 Hydrostatic pressure (pressure sensor method)

Hydrostatic pressure is the pressure exerted by the weight of the liquid above a measurement point of the static liquid. By measuring the hydrostatic pressure using a pressure sensor, the density can be calculated from the following very general formula:

$$\rho = \frac{P}{hg} \qquad 4\text{-}4$$

where

p = pressure in fluid (Pa)

ρ = density of the liquid (kg/m^3)

g = gravimetrical acceleration (9.81 m/s^2)

h = height between the liquid level and pressure sensor (m)

For closed systems, two pressure sensors are placed at the height of Δh from each other. In such systems, the liquid density can be determined by measuring the vertical distance between two pressure sensors, Δh, and the pressure difference, Δp [207].

4.2 Introduction to Viscosity

Viscosity is an important physical property of the fluid which opposes the relative motion between the two adjacent layers of the fluid that are moving at different velocities. In simple terms, viscosity gives information on how thick a fluid is and how easily it flows. The defined quantity is sometimes called dynamic viscosity, absolute viscosity, or simple viscosity. A mathematical description of viscosity can be pictured by the two-plates model. Consider a liquid placed between two parallel plates as shown in **Figure 4-1**. A force exerted on the upper plate causes the fluid nearby the upper plate to be dragged in the direction of F. The applied force is communicated to neighboring below layers of fluid and leads to the progressive decrease in velocity of each fluid layer which is away from the upper plate. In this system, the force F applied to the top layer divided by the boundary surface of the fluid A is called shear stress, τ. The quotient of F and A results in unit N/m^2, which is named pascal [Pa] [216].

$$\tau = \frac{F}{A}\left[\frac{N}{m^2}\right] \qquad 4\text{-}5$$

Figure 4-1 A mathematical description of viscosity by the two-plates model [216]

The two-plates model allows for calculating the resulting deformation rate of fluid which is called the shear rate. The shear rate, D, is defined as the velocity of the top plate divided by the distance between the two plates [216].

$$D = \frac{v}{L}\left[\frac{m}{s.\,m}\right] \qquad 4\text{-}6$$

Based on Newton's Law, the shear stress is proportional to shear rate and the proportionality factor is referred to dynamic viscosity [216].

$$\tau = \eta * D \quad \text{4-7}$$

To obtain dynamic viscosity, one must reformulate newton law.

Only Newtonian liquids can be described by this simple relation. A fluid is Newtonian if the viscosity is independent of the external force -i.e. shear rate at a given temperature. In other words, when the shear stress is linearly dependent on the share rate, then the fluid is Newtonian fluid and is obeying Newton's law. The other type of fluid is called Non-Newtonian fluid, which does not obey Newton's law, and the viscosity of this type changes with the shear rate, and in this case for exact definition, one has to specify the apparent viscosity [216].

4.2.1 **Temperature dependence of viscosity**

The viscosity depends on the thermodynamic state of the fluid and is usually specified by the pairs of variables (T, P) or (T, ρ) for a pure fluid, to which must be added a composition dependence in the case of mixtures. A fluid's viscosity strongly affected by its temperature. Due to the inversely proportional relation between viscosity and temperature, and increases in temperature cause a fluid's viscosity to decrease and vice versa. Viscosity is typically independent of pressure at low or medium pressure, however, under extreme pressure liquids often experience an increase in viscosity [216].

4.2.2 **Types of viscosity**

4.2.2.1 Dynamic viscosity

As mentioned earlier, the dynamic viscosity η (eta), called absolute viscosity or just viscosity, is calculated by reformulation of the Newton's Law through dividing the shear stress by shear rate [216].

$$\eta = \frac{\tau}{D} \quad \text{4-8}$$

The SI unit of viscosity is the pascal-second [Pa.s] or [mPa.s] millipascal-second. Other commonly used units are [P] Poise or [cP] centipoise. The relation between units:

P = 100 cP,1 cP = 1 mPa.s.

4.2.2.2 Kinematic viscosity

The other type of viscosity is called kinematic viscosity (represented by the Greek letter ν "nu") which is a measure of the substance's flow under the influence of gravitational force. The ratio of the dynamic viscosity of a fluid to its density is referred to Kinematic viscosity [216].

$$v = \frac{\eta}{\rho} \qquad 4\text{-}9$$

The SI unit of kinetic viscosity is [m^2/s] square meters per second or [mm^2/s] square millimeters per second.

4.2.2.3 Apparent viscosity

Ideally viscous or Newtonian fluids have constant viscosity for all shear rate values at a given temperature. On the other hand, for shear-dependent fluids, the viscosity changes as the shear rate are varied. Hence, to have a meaningful viscosity measurement, the shear rate must be stated or defined. This is the "apparent viscosity" or "apparent shear viscosity". Each apparent value is one point of the viscosity function (eta over shear rate). Apparent viscosity has the SI derived unit of Pa·s [216] .

4.2.3 Viscosity measurement techniques

Since a precise viscosity measurement is fundamental to correctly analyze many engineering situations that involve fluid flow, various methods have been developed to obtain the viscosity over the years. Generally, the simplicity, accuracy, and suitability of the method for certain types of fluid are important factors in choosing the proper viscosity measurement technique. Various theories that have been developed for prediction or estimation of viscosity must be verified using experimental data. This section outlines various types of viscometers with the further discussion regarding their operation modes. Viscometers can be generally classified into five categories based on their designs and experimental techniques used, including capillary, rotational, oscillatory-body, falling-body, and vibrating wire viscometers. This list is by no means thorough, there are other types of viscometers, however, not all of them are useful for industrial processes.

4.2.3.1 Capillary viscometer

Capillary viscometer is one of the earliest widely used viscometers to precisely determine the kinematic viscosity of Newtonian fluids [217]. These types of viscometers are very simple in operation, need a small volume of liquid and inexpensive. The prior knowledge of the volume and density of the sample is required for the determination of the viscosity. These viscometers measure the time taken for a defined quantity of fluid to travel between two graduation marks through a capillary tube of known length, width, and very small diameter. The liquid flows through the capillary tube either under gravitational force (Gravimetric Capillary Viscometer) or under an external force. In the viscometer where an external force is applied, the liquid is forced to travel a specific distance at a determined rate through the capillary and the pressure drop across the capillary is measured. Kinetic viscosity can be calculated from the measured flow time (t_f) multiply by the so-called capillary constant (K_C) [217].

$$v=K_C \cdot t_f \qquad 4\text{-}10$$

For most of the capillary viscometers, K_C is obtained by calibrating the capillary using one or more reference fluid of known viscosity and density. A typical capillary viscometer basically consists of a liquid reservoir, a capillary of known dimensions, a pressure controller, the flow rate meter, and a thermostat to keep the required temperature. The essential component used in capillary viscometers is a “U-shaped” glass which gives them the commonly associated name, the U-tube capillaries. Based on the type of glass used in viscometers, glass capillaries are classified into reverse-flow and direct-flow models. For reverse-flow types, the reservoir is positioned above the distance marks while in direct-flow capillaries the sample reservoir is placed below [217].
The established types of glass capillaries are shown in **Figure 4-2**:

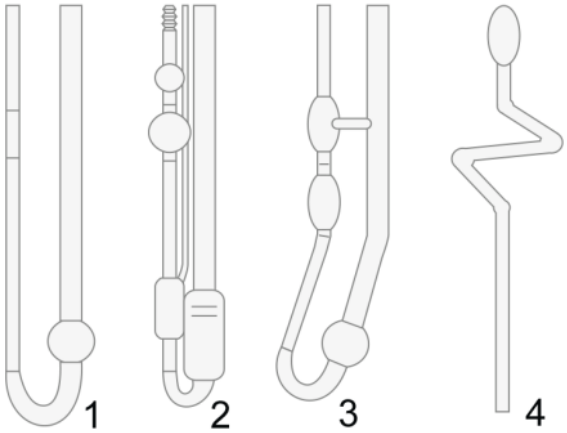

Figure 4-2 Types of glass capillaries [217]

1. Ostwald capillary
2. Ubbelohde capillary
3. Cannon-Fenske capillary
4. Houillon capillary

With the development of the automatic gravimetric capillary viscometer, utilizing the stop watch for measuring manually the flow time was replaced with automatic registration of the fluid.
The most advanced models automatically fill, measure, clean, and dry. Moreover, some advantages of automatic gravimetric capillary viscometer include eliminating human reading errors, utilizing less measuring volume than the original types, and covering an extended viscosity range. Such automatic viscometers mainly coupled with a thermoelectric system, for temperature control [217].

4.2.3.2 Rotational viscometers

The operational principle of Rotational viscometers relies on the idea that the amount of power (torque) required to turn a spindle in the fluid at a known speed is directly proportional to the viscosity of that fluid. These viscometers use a motor drive, which is considerably stronger than the earth's gravitational force. They can, therefore, be used to measure the viscosity of more highly viscous substances. Since these instruments do not use the force of gravity to function, their measurements are based on the fluid's internal shear stress. Rotational viscometers measure dynamic viscosity that is sometimes also referred to as shear viscosity. The shear stress remains

constant throughout the fluid sample; therefore, these viscometers are most suitable for studying non-Newtonian fluids. Different types of rotational viscometers are commercially available based on their geometries [217].

These viscometers can be classified into three general categories including Coaxial-Cylinder Viscometer, Cone and Plate Viscometer, Coni-Cylinder Viscometer [218], as shown in **Figure 4-3**.

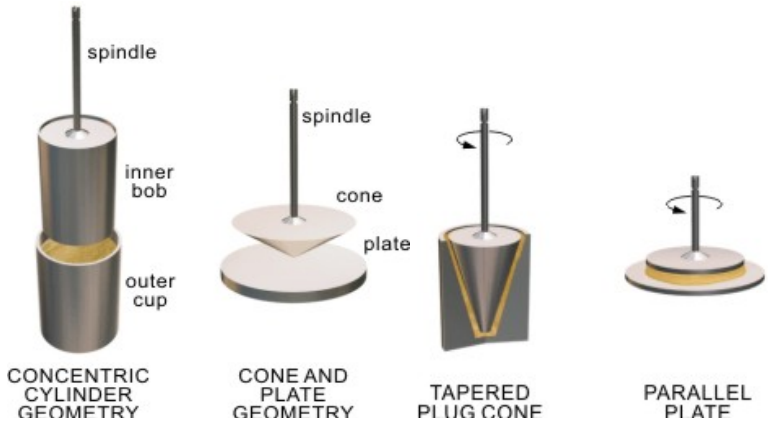

Figure 4-3 Types of rotational viscometers [219]

A typical rotational viscometer basically consists of a sample cup, a head unit with a motor, and a bob or spindle driven by the motor. The viscosity is determined by measuring the resistance of a bob rotating in the sample-filled cup. There are two main principles in use based on which part is driven by motor [217]:

-**The Couette principle:** The motor rotates the sample-filled cup around the stationary measuring spindle.

-**The Searle principle:** The instrument's motor turns the measuring spindle inside a fixed sample-filled vessel.

In most commercial Rotational viscometers, the theory of the operation is based on the Searle principle. Two different sets up are used to measure viscosity using Rotational viscometers [217].

- Spring Motor

The Spring instruments utilize a stepper motor to drive the main shaft. A spring and pivot assembly rotate on the shaft. The spindle hangs from this assembly. The spring is deflected by the viscosity

of the sample under test when the spindle rotates. The type of spring totally depends on the viscosity of the substances. For the high viscosity samples, the spring needs to be more robust while for substances in the low viscosity range a more sensitive spring is required [217].

- Servo Motor

The servo device uses a precision servo motor to drive the main shaft and a digital encoder to record the rotational speed. The Spindle is attached directly to the shaft. High-speed microprocessors measure the speed from a digital encoder and calculate the current required to drive the rotor at the test speed. The required current is proportional to the viscosity of the sample under test. servo motor viscometers cover a wider measuring range compared to spring instruments and are more robust. Moreover, the digital encoder and motor allow for wider speed and torque range and therefore a wider range of viscosity than is possible with a spring viscometer. However, the measurement accuracy at low speeds and low viscosity is lower than for spring viscometers [217].

4.2.3.3 Falling-body viscometers

Falling body methods that are used to measure viscosity include the falling ball, falling sinker, and rolling ball type methods[220]. A falling -ball viscometer is based on the gravimetrical force as a drive. This type of viscometer is used to measure the falling time of a ball of a defined diameter and density traveling a specified distance through a sample-filled glass tube with a defined inner diameter. The viscosity can be directly measured based on this time, and calibration tests using the viscosity of standard fluids. The more viscous the fluid is, the more time takes the fluid pass a distance between two specified lines on the cylindrical tube. The inclination angle of the capillary allows for adjusting the driving force. Dynamic viscosity with the standard dimension of [mPa.s] is measured using falling ball viscometers. The Hoppler viscometer, named after Fritz Hoppler, is the worldwide firs falling-ball viscometer to determine dynamic viscosity which states an inclination angle of exactly 80° [221]. When the ball moves through the fluid, a portion of the gravitational force drives the ball downwards. The buoyancy and friction act as the upward forces and slow down the ball movement. According to Newton’s law of motion for a falling ball, that

states there are gravitational force, buoyancy force, and friction force, and these three forces reach a net force of zero, the viscosity is calculated using the following equation [217], [220]:

$$\eta = \mathrm{K}.(\rho_b - \rho_s).\mathrm{t_r} \qquad 4\text{-}11$$

Where η is the dynamic viscosity[mpa.s], K is the proportionality constant, ρ_b andρ_s are the density of ball and sample[g/cm^3], respectively. For $K = \frac{g.d^2}{18.l}$ d is the radius of the ball, l is the distance,t_r is falling time through distance l [s] [220]. Equation (4-11) shows the relation between the viscosity of a fluid and the terminal velocity of a falling ball through it.

4.2.3.4 Oscillating-Body viscometers

The oscillating-body viscometer consists of an axially symmetrical body suspended from an elastic strand that is immersed in a fluid medium. The oscillating system is gently rotated in a fluid to start the harmonic oscillation motion. The fluid applies a viscous drag on the oscillator causing the change in angular frequency of the oscillation and the damping decrement of the resulting harmonic compared with those in a vacuum. The magnitude of the change depends on the fluid's viscosity and density as well as the physical characteristics properties of the suspension system. In other words, the viscosity of a fluid can be measured by observation of the decay of damped harmonic oscillations of the oscillating system. Oscillating Cylinder viscometers, Oscillating spheres viscometers, and Oscillating disks viscometers are the most commonly used examples of these viscometers [222].

4.2.3.5 Vibrating viscometer

In the vibrating viscometers, the oscillations include periodic distortions of the solid body itself, which is in contact with the test fluid. Vibrational viscometers measure the damping of an oscillating electromechanical resonator immersed in the fluid whose viscosity to be determined. The resonator may be a cantilever beam, oscillating sphere, or tuning fork which generally oscillates in torsion or transversely in the test fluid. The higher the viscosity, the larger the damping imposed on the resonator [223]. The resonator's damping can be determined by one of the following methods [223]:

- Measuring the power input required to keep the oscillator vibrating at a constant amplitude. The higher the viscosity, the more power is needed to maintain the amplitude of oscillation. The vibrating probe accelerates the fluid and power input is proportional to the product of viscosity and density.
- Measuring the decay time of the oscillation when the vibration of the resonator is switched off. The higher the viscosity, the faster the signal decays.
- Measuring the frequency of the resonator as a function of the phase angle between excitation and response waveforms. The higher the viscosity, the larger the frequency change for a given phase change.

The main advantage of vibrating viscometers is the small volume of sample required for their use that leads to ease of operation over extreme conditions of temperatures and pressures. Furthermore, these instruments are of simple mechanical construction than those of oscillatory bodies. Easy cleanout and prospect of construction with easily available materials is another important feature of vibrational viscometers [223].

4.3 Introduction to the refractive index

The refractive index of a substance is a factor that explains how light passes through the medium. In general, refractive index is the ratio of the velocity of light in the vacuum (c) to its velocity in a specified medium(v). The refractive index is measured for various reasons including identification of a liquid component, confirmation of the sample's purity, and determination of the concentration of dissolved particles in a solution. There are some benefits associated with the measurement of the refractive index. Using a refractometer, the sugar concentration of fluids like drinks and foods, shown by the Brix scale, can be controlled and monitored through measuring the refractive index continuously. Common industrial applications involve fruit juices, jams, syrups, concentrates and purees, compotes, and other pasty fluids as well as micro-emulsions, biotechnical liquids, and pharmacological materials [224].

4.3.1 **Types of refractometer**

Measurement of the refractive index has been used for many years to identify and characterize liquids and solids .as refractive index measurements are quick and liable, they have become the state of the art in various industries around the world. Due to the different requirements for refractometers, these instruments have generated with different designs, operation, and precision. There are different types of refractometer including abbe refractometer, the digital refractometer, automatic refractometer and hand refractometer [224].

4.3.1.1 Abbe refractometer

The first laboratory bench-top device for the high precision determination of the refractive index of liquids was the Abbe refractometer. The measuring principle of this refractometer is based on the principle of total reflection. This way the purity of the substances and the concentration of the solution can be determined. For the measurement, two prisms that are made of glasses are used between which the sample should be tested is placed. These prisms are called illuminating and refracting prisms. The light from a radiation source is allowed to enter the apparatus and hits the sample from the illuminating prism, gets reflected at a critical angle at the bottom surface of reflecting prism. The refractive index of the refracting prism is high about 1.75 and the samples used in this refractometer should have a refractive index less than that of refracting prism. The incident light rays propagate through the double prism and sample only if their angles of incidence at the interface are less than the critical angle of total reflection. A microscope and a mirror are used to measure the position of the border between light and dark areas. A compensator knob is used to make the edge of light and dark area clear/sharp. Also, with the help of a rotary knob, the light and dark portion at the intersection of the microscope's crosshairs is adjusted. The resultant refractive indexes can then be read from a Vernier scale piece. Furthermore, a pipe with an inlet and outlet as well as a thermometer is employed in this instrument to circulate water to control instrument and fluid temperatures [224].

4.3.1.2 Handheld refractometers

The handheld refractometers are cost-effective and simple to use with rapid concentration measurement of liquids and semi-solid samples. These refractometers are popular in a multitude of applications including determination of salt content in marine aquaria, water content in honey, serum protein content and Brix, and potential alcohol content. These cylinder-shaped refractometers do not require any battery for operation. Handheld refractometers have an illuminator flap instead of an illuminating prism which creates a diffused light and keeps the sample in place. The light propagates through the sample and enters the measuring prism. To measure the refractive index of the sample, only a small drop of liquid is sufficient. The corresponding refractive indexes can be then read from the eyepiece scale while the device is placed refractometer in the direction of some light source (such as lamp or sun). The measured refractive index can be converted into other units such as Brix degrees, alcohol or glycol %, etc. For temperature compensation of liquids, handheld refractometers offer integrated Automatic Temperature Correction (ATC) [224].

4.3.1.3 Digital refractometer

Digital refractometers operate in the same way as handheld refractometers, except they are provided with an automatic determination and readout of the boundary line. They offer reduced inter-operator variability, and higher precision than manual handheld refractometers, and are typically available with a selection of common scales [224].

4.3.1.4 Automatic refractometer

Automatic refractometers eliminate differences in measured results between operators and provide the highest level of accuracy. In contrast to manual refractometric measurements under uncontrolled environmental conditions, it is possible, for example, to measure the refractive index of the sample at different temperatures or light wavelengths. Automatic refractometers are found mainly in laboratory applications, where precise measurement under highly controlled conditions is required. Modern instruments are equipped with light-emitting diodes (LEDs) as light sources,

which have largely replaced older tungsten halogen or sodium vapor lamps because of their exceptionally long lifetime of 100 000 hours. An interference filter guarantees the maintenance of the correct wavelength. To enable comparability refractometric measurements, these are usually carried out at the standard wavelength of 589.3 nm (sodium D-line). The measuring principle is the same as other refractometers, where monochromatic light is incident at different angles of incidence on the prism and the sample. The intensity of the reflected light is determined by a charge-coupled device (CCD) scanner and the resulting position of the light / dark boundary is determined automatically. Dark, cloudy, and even opaque samples such as mustard, ketchup, or mayonnaise can easily be measured with the help of a fully automated, modern refractometer. For these applications, 2-3 drops or a few grams of sample needed to be applied using a pipette or a spatula onto the measuring prism. To avoid stray light and evaporation, a sample cover is placed over the sample and prism. After measurement, the sample is removed by wiping with a soft paper cloth. The arduous purification of two prism halves (as is necessary for conventional refractometers) is thus avoided. Automatic refractometers are used in diverse industries in the processing of food and drinks to determine sugar content and for quality control. Refractive index is often represented on the Brix scale (° Brix) for these applications. This value, which is displayed directly on the device, technically refers to the content of the sucrose-dry substance in a pure water solution. However, it is also used as the characteristic value in the quality control of juices and other food products, and sometimes even in the analysis of other products, such as petroleum [224].

CHAPTER FIVE: EXPERIMENTAL SECTION

5. Methods and experimental section

Knowing the physical properties of amine solutions are essential for the design of the CO_2 capture unit, modeling, and operation of the equipment [189]. Also, physical properties such as density and viscosity are required to measure some properties like reaction rate constant, the solubility of free-gas, and liquid diffusivities [225]. Another essential physical property is the refractive index that is used for the identification of a liquid component, confirmation of the sample's purity, and determination of the concentration of solute in a solution.

The purpose of the present chapter is to provide information on the chemicals used to prepare the different solutions and also describe the experimental equipment used to measure the physical properties of all pure components as well as the corresponding mixtures. Furthermore, this chapter deals with a detailed explanation of the procedures and the steps taken to carry out the experiments. It should be mentioned that the equipment was chosen based on their availability in our department.

5.1 Material used

The chemical used in the present study were purchased from Sigma-Aldrich Company. These chemicals include MEA, MDEA, DEA, TEA, and ETOH. **Table 5-1** reports the specifications of the used chemicals. The purity of all chemicals was checked by comparing their measured density and viscosity with those reported in the literature. As will be described in the next chapter, the measured results indicate a good agreement with literature values, hence, all chemicals were used as received without any further purification. The difference between the experimental and literature values for the above thermos-physical properties was within the experimental error.

Table 5-1 Details of the chemicals used in this work				
Chemical	**Source**	**Purity**	**Molecular weight**	**Chemical formula**
MEA	Sigma-Aldrich	≥ 99%	61.08	C_2H_7NO
DEA	Sigma-Aldrich	≥ 99%	105.14	$C_4H_{11}NO_2$
MDEA	Sigma-Aldrich	≥ 99%	119.16	$C_5H_{13}NO_2$
ETOH	Sigma-Aldrich	≥ 99%	46.07	C_2H_5OH

5.2 Sample preparation

All mixtures were prepared gravimetrically at ambient temperature and pressure. In this procedure, the glass bottle was first washed with distilled water, ethanol, and then acetone. The vacuum pump was then used to dry the bottle. The binary mixtures were prepared by transferring the pure components via a syringe into a stoppered bottle. This helps to prevent evaporation of the mixture and contamination with the CO_2 from the air. During the preparation of each mixture, a glass bottle was placed empty on the balance and was set to zero. The pure component with the lower vapor pressure was first introduced to the bottle slowly until the desired mass was reached. Next, the weight of the component was recorded. Then, the balance was set to zero again and the same procedure as the first component was used for the other component, and the weight of the second component was recorded. Lastly, the composition of the solution was determined from the recorded weights of two components. An OHAUS analytical mass balance with maximum capacity of 6100 g, an uncertainty of ± 10^{-4} g and, readability of 0.001 g was applied to determine the masse of each component of the mixture. The mixtures were then shaken to ensure complete homogeneity of the two compounds. These samples were used to measure the thermo-physical properties at temperatures ranging from 293.15 K to 333.15 K.

The amine concentrations used in this work are given below:
Concentration for MEA+ETOH: 0.201,0.4,0.602,0.8 x MEA
Concentration for MDEA+ETOH: 0.2,0.401,0.599,0.8 x MDEA
Concentration for DEA+ETOH: 0.2,0.4,0.6,0.8 x DEA

5.3 Measuring equipment and method

Different measuring equipment including densitometer, viscometer, and refractometer were used to measure the thermos-physical properties of the mixtures in the studied temperature range.

5.3.1 Density measurement

An Anton Paar vibrating U-tube densimeter (DSA 5000 M) with an accuracy of ±0.02 K in temperature was employed in the present study to measure the density of the pure components and all prepared mixtures. The capacity of instrument to measure ρ is within the range of 0 to 3g.cm^{-3} and a temperature range of 0 – 70 °C with pressure variation from 0 to 0.3 MPa. The accuracy and repeatability of density in experimental measurements were found ± 7.10^{-6} g.cm^{-3} and ± 1.10^{-6} g.cm^{-3}, respectively. Also, the reproducibility of the digital vibrating tube densimeter is ± 5.10^{-6} g.cm^{-3}.

The calibration for the DSA 5000 M was done with Anton Paar ultrapure water and dry air at 298.15 K. DSA 5000 M measures two independent properties of density and sound velocity in one setup simultaneously and under the same conditions. This two in one instrument is equipped with a density cell and a sound velocity cell thus combining the proven Anton Paar oscillating U-tube method with highly accurate measurements. Both cells are temperature-controlled by a built-in Peltier thermostat. The sample automatically runs through both measuring cells. For one run, only 3.5 mL of sample is required to get all these parameters. The sample is introduced into a U-shaped tube made from borosilicate glass that is excited to vibrate at its characteristic frequency. The characteristic frequency changes are directly related to the density of the sample. After reaching a stable oscillation, the excitation is switched off and the oscillation fades out freely. This excitation and fade-out pattern are repeated continuously. By evaluating this pattern, highly precise density results are obtained, the effects of viscosity compensated, the sample´s viscosity is even measured and air bubbles or particles are detected [226].

5.3.1.1 Accuracy

(i) The period of oscillation of the U-tube is measured by optical pickups.
(ii) Two integrated Pt 100 platinum thermometers together with Peltier elements provide an extremely precise thermostat of the sample.
(iii) Thermobalance: An additional reference oscillator provides long-term stability and enables precise measurements over the whole temperature range of the instrument with the only adjustment at 20° C.
(iv) Based on an additional measuring cell made of stainless steel and high-resolution electronics, the velocity of the sound of the filled-in sample can also be determined accurately [227] .

5.3.1.2 Error detection

Filling errors are a kind of measuring errors when using a density and sound velocity meter which is caused by bubbles or particles in both measuring cells. To ensure results are not distorted by filling errors, DSA 5000 M comes with two features to verify that samples are properly filled.
(i) Filling Check™: This feature automatically detects filling errors generating by bubbles or particles in the filled U-tube and gives a warning message.
(ii) U-View™: The U-View™ camera with zoom function shows high- resolution live images of the U-tube sensor and the entire filled-in sample [227].

5.3.2 Viscosity measurement

Viscosities were measured using Lovis 2000 M/ME micro viscometer from Anton Paar with an accuracy of ± 2.10^{-3} for viscosity and ± 0.02 K for temperature. The repeatability and reproducibility of the viscometer are ± $2. 10^{-3}$ and ± $1 .10^{-3}$ mPa.s, respectively.
It is a small measuring module which is inserted into a DMA Generation M/ DSA Generation M density meter for the combined measurement of density and viscosity. Lovis 2000 M/ME is a rolling-ball viscometer that measures the time taken by a ball to roll through opaque or transparent liquids based on Hoeppler's falling ball principle. This viscometer features viscosity measurement in a measurement temperature range of 5 to 100 degrees C with pressure variation from 0 to 0.3 MPa. A sample volume of less than 100 µL is required to deliver efficient measuring operations. Results are given in three categories of dynamic viscosity, intrinsic viscosity, and

kinematic viscosity in one cycle. Lovis 2000 M/ME is compact and economical, that is, saves both space and money. Lovis 2000 M/ME is a closed system, therefore, prevents the sample from evaporation and contamination. Furthermore, it includes a variable measurement angle for the calculation of zero-shear viscosity. For this viscometer three capillaries were available from the manufacturer with diameters 1.59, 1.8 and 3.0 mm [228].

5.3.3 **Procedure for combined DSA 5000 M and Lovis 2000 ME**

Before introducing the sample into DSA 5000 M measuring cell and the capillary of Lovis 2000 ME, a proper cleaning liquid for the relevant sample has to be found. A suitable cleaning solvent has to miscible with the sample easily. Generally, cleaning the measuring cell of DSA 5000 M and Lovis capillary should be carried out with two cleaning liquids: Cleaning liquid 1 which dissolves and removes sample residues in the measuring cell and cleaning liquid 2 that has to be a good solvent for cleaning liquid 1 and be easily evaporated by dry air. In the present study, according to the sample used, the cleaning liquid 1 was Ethanol, and Acetone was used as cleaning liquid 2.
Before each experimental run, both densimeter cell and capillary were first flushed with ethanol and then acetone. Afterward, a compressed stream of dry air was blown through the cell via an air pump until the constant readings were displayed on the screen. The deionised water was then introduced to the cell to check the density. The correct value for the density of the dried air and water at the respective temperature indicates that everything is in order.

After verifying the accuracy of the densitometer operation, the sample was filled to the U-tube cell and capillary using a syringe and at the same time. The syringe was inserted directly into the inlet adapter of the DSA 5000 M measuring cell. The outlet of the DSA 5000 M measuring cell was connected with the inlet of the Lovis 2000 ME capillary block. The hose from its outlet was connected to a waste vessel (see **Figure 5-1**).

The injection had to be done slowly to prevent the formation of an air bubble inside both U-tube cell and capillary. The sample was always filled past its nodal points and the syringe was left in place at the nodal point during each measurement. Following injection, the sample is left for a while to reach thermal equilibrium. Once equilibrium was reached, two consecutive readings were

recorded which differed only in one or two digits. The average reading was calculated and then reported as a final result.

This procedure was carried out for all samples at atmospheric pressure, and ten investigated temperatures ranging from 293.15K to 338.15 K with a regular interval of 5 K. The U-View™ camera displayed high-resolution image of U-tube cell during each measurement. The density of air and water was set for the calibration. Density values of water, pure solvents, and air were determined between each solution injection to check both the sample purity and densitometer operation. For viscosity measurements of light sample, the 1.59 mm glass capillary with steel balls and for viscose sample the 1.8 mm glass capillary were applied.

Figure 5-1 Combined DSA 5000 M and Rolling ball viscometer Lovis 2000 ME

5.3.4 **Refractive index**

The refractive indices of the samples in present work were measured using a digital refractometer Atago, RX-7000 α (see **Figure 5-2**). The Atago, Rx-7000α is a digital benchtop refractometer for refractive index measurement (1.3250 to 1.7000 n_D), and Brix (0.00 to 100.00%) concentration of liquid samples. The unit has a digital, LED-illuminated, backlit display of refractive index and % Brix in degrees C with a top and bottom limit bar for set control range in targeted temperature. A

refractometer measures the refractive index of a liquid or solid sample, converts it to concentration in units of percent by weight, and shows the results. This refractometer features refractive index measurement in a measurement temperature range of 5 to 70 degrees C. It has a high measurement accuracy of ±0.001 for Brix and ± 0.00001 for n_D. The unit provides measurement value automatically right after the sample reaches its target temperature. It has automatic temperature compensation (ATC) for accuracy, as well as manual calibration to adjust standard liquid values and to correct differences in measurement values between instruments. Atago, RX-7000α refractometer has a built-in Peltier thermo-module that maintains a constant temperature which eliminates the need for an external constant temperature water bath. It is housed in a durable, die-cast aluminum metal body for resistance to heat and organic solvents. The sample well cover plate blocks outside light for measurement accuracy. The well is made of stainless steel 316 for durability [229] .

Figure 5-2 Atago digital refractometer RX-7000α [229]

5.3.4.1 Procedure

As for the measurements of density and viscosity, the Atago, RX-7000α was first cleaned with ethanol and then with acetone to remove any residues left at the surface of the prism for better results. All the experiments were performed at atmospheric pressure and temperature range of 293.15–338.15 K, with a regular interval of 5 K. The refractive index of deionized water was set for the calibration. Furthermore, the refractive index value of water was determined between each solution injection to check the refractive index operation. The temperature was adjusted and samples were injected into the stainless steel well using a syringe (4-6 drops). The sample was covered by a black plate as a lid to prevent exposure of samples to outside light. Each sample was measured three times at a wavelength of 589 nm and the average of these readings was considered as the final result. The technical specification of DSA 5000m [226], Lovis 2000M/ME [228], and Atago 7000 alpha [229],are given in **Table 5-2** to Table **5-4**.

Table 5-2 Technical specification for densitometer DSA 5000 M	
Technical Specifications	
Measuring range	
Density	0 to 3 g/cm^3
Sound velocity	1000 to 2000 m/s
Temperature range	0 °C to 100 °C (32 °F to 212 °F)
Pressure range	0 bar to 8 bar (0 psi to 116 psi)
Accuracy	
Density*	0.000007 g/cm^3
Concentration determination	Typically, 0.01 to 0.1 % (application-dependent)
Digital Resolution	
Density	0.000001 g/cm^3
Sound velocity	0.01 m/s
Repeatability s.d.**	
Density	0.000001 g/cm^3
Sound velocity	0.1 m/s
Temperature	0.001 °C
0 to 100 % H_2SO_4	0.02 % H_2SO_4
0 to 28 % free SO_3	0.04 % free SO_3
28 to 65 % free SO_3	0.1 % free SO_3
Additional information	
Integrated tables and functions	• Ethanol tables • Extract/sugar tables • Acid/base tables • 20 freely programmable user functions
Available options	• ISO 17025 calibration providing full traceability to SI units • Cooling kit for low-temperature measurement
Amount of sample in the measuring cells	3 mL
Measuring time per sample	1 to 4 minutes
Interfaces	RS-232, 4 x USB, CAN, VGA, Ethernet
Display	Bright 10.4" TFT PCAP touchscreen (640 x 480 px) with customizable display layout

Wetted parts	PTFE, borosilicate glass, stainless steel DIN 1.4539/UNS N08904
Dimensions	495 x 330 x 230 mm
Weight	22.5 kg (49.6 lbs)

Table 5-3 Technical specification for Rolling-ball viscometer Lovis 2000 M/ME

Technical Specifications	
Viscosity	
Viscosity range	0.3 mPa.s to 10,000 mPa.s
Repeatability s.d.	up to 0.1 % [1)]
Accuracy	up to 0.5 % [1) 2)]
Temperature	
Temperature range	+ 5 °C to 100 °C
Repeatability s.d.	0.005 °C
Accuracy	0.02 °C
Measuring time	
Resolution	0.001 s
Accuracy	0.05 %
Further specifications	
Test duration	minimal 30 s, typical 3 min
Sample volume	0.1 mL to 0.8 mL
Inclination	15° to 80° in 1° steps
Repeatability s.d.	0.02 °
Accuracy	0.1 °
Shear rate	0.5 s^{-1} to 1000 s^{-1} influenced by capillary size and inclination

Table 5-4 Technical specification for digital refractometer Atago 7000 alpha	
Technical Specifications	
Model	RX-7000α
Cat.No.	3262
Range	Refractive index (n_D): 1.29980 to 1.71500 Brix: 0.00 to 100.00%
Resolution	Refractive index (n_D): 0.00001 (0.0001) Brix: 0.01% (0.1%) Temperature: 0.01°C
Accuracy	Refractive index (n_D): ±0.0001 Brix: ±0.1%
Temperature control range	5.00 to 70.00°C
Dimensions & Weight	37×26×14cm, 6.8kg
Output terminals	• Printer (for ATAGO digital printers) • Computer - RS-232C Connection to a USB port requires a USB to RS-232 adapter (optional)
Warranty	2 years standard (3 years with product registration)

5.4 Experimental Uncertainties Calculation

5.4.1 Combined standard uncertainty for ρ, η, n_D

The combined standard uncertainty of the measured variable, suggested symbol u(Θ), in this study is calculated from any of the two categories of uncertainty type A or type B. Type A evaluation of standard uncertainty is based on the statistical method for testing data in which the mean is taken to represent the true value [230].The type A uncertainty is calculated through the following equation:

$$u_i(\Theta) = \frac{\delta}{\sqrt{n}} \quad 5\text{-}1$$

Where δ represents the standard deviation and n is the number of measured values. The standard uncertainty of type B is evaluated based on scientific judgments such as available measurement data and specifications provided by the manufacturer (accuracy and repeatability). The overall standard uncertainty is expressed as:

$$u_i(\Theta) = \frac{\Delta a}{\sqrt{3}} \quad 5\text{-}2$$

Δa is the half of the interval width. The rectangular distribution model is the default model in the absence of any other information [230]. Hence, the combined standard uncertainty for measured thermo-physical properties is determined by:

$$u_c(\Theta) = \pm\sqrt{u_a(\Theta)^2 + u_{rep}(\Theta)^2 + u_b(\Theta)^2} \quad 5\text{-}3$$

where Θ is the thermo-physical properties such as ρ, η, and n_D. u_a and u_b represents the accuracy and reproducibility of the instrument, respectively and $u_{rep}(\Theta)$ denotes the standard uncertainty related to the repeatability of the measurement. The combined expanded uncertainty is then calculated by multiplying the combined standard uncertainty by a factor of 2 [231].

The combined standard uncertainties and combined expanded uncertainties for ρ, η, n_D, V^E and $\Delta\eta$ for the systems of interest are listed in Table 5-5.

Table 5-5 **Combined uncertainties for ρ, η, n_D,** x_i **,**V^E and $\Delta\eta$

	ρ (g.cm^{-3})	**η (mPa.s)**	**n_D**	**x_i**	**V^E(cm^3.mol^{-1})**	**$\Delta\eta$(mPa. s)**
combined standard uncertainty u (θ)	± 0.0001	± 0.0015	± 0.00005	±0.0001	±0.01	±0.01
combined expanded uncertainty U (θ)	± 0.0002	± 0.003	± 0.0001	±0.0002	±0.02	±0.02

CHAPTER SIX: RESULTS AND DISCUSSION

6. Experimental Results and Discussion

Results of experimental runs for different systems investigated in the present study such as pure amine solvents, pure ethanol and binary system are presented and discussed in this chapter. Several reported correlations gathered from literature were used to correlate the experimental and actual data. In order to evaluate the deviations between experimental data/actual and those available in the literature, average absolute relative deviations were calculated.

6.1 Pure MEA, DEA, MDEA and ETOH

Density, viscosity, and refractive index of pure MEA, DEA, MDEA and ETOH were measured at atmospheric pressure and temperature range of 293.15–338.15 K, with a regular interval of 5 K using DSA 5000 M/Lovis 2000M/ME and Atago 7000 a, respectively.

All the measured results are listed in **Table 6-1** to **Table 6-4** and represented in **Figure 6-1**. Also, the experimental data of pure amines were compared with the literature data and the AARDs are reported in **Table 6-1** to **Table 6-4**. These low values of AARD's confirm the reliability of the methods and experimental equipment applied in this work.

Figure 6-1-a shows the density of pure MEA, DEA, MDEA and ETOH at temperatures 293.15–338.15 K and pressure of 0.1 mPa. This figure shows that after Ethanol, MEA has the least and DEA has the highest density values. Furthermore, it can be seen that density shows a decreasing trend with temperature for all amine solvents.

Figure 6-1-b displays the viscosity of pure MEA, DEA, MDEA and ETOH in temperature range under study and atmospheric pressure. All viscosities are a decreasing function of temperature. MEA and DEA have the least and the greatest viscosity values, respectively.

The refractive indices of pure MEA, DEA, MDEA and ETOH over the temperature range of study are reported in **Figure 6-1-c**. According to this figure, the refractive index also decreases with increase in temperature for all solvents.

Table 6-1: Densities (ρ), viscosities (η) and Refractive indices (n_D)of MEA at T = (293.15 to 343.15) K and P = 0.101MPa							
Sample	**T/K**	**[a]ρ/g·cm^{-3}**		**[b]η/mPa·s**		**[c]n_D**	
		exp	**lit**	**exp**	**lit**	**exp**	**lit**
MEA	**293.15**	1.01634	1.0179[232] 1.0164[233] 1.01665[234] 1.01610[158] 1.0161[235] 1.01593[236] 1.01630[237] 1.01647[167]	23.260	24.614[234] 24.14[235] 24.231[236] 23.40[237] 24.10[190]	1.45446	1.45601[238] 1.4539[239] 1.4545[240]
	298.15	1.01249	1.0125[233] 1.0121[235] 1.01198[236] 1.01253[167] 1.0123[241]	18.256	18.89[235] 18.740[236] 18.98[190] 17.90[242]	1.45256	1.452[243] 1.45432[238] 1.4521[239] 1.4525[240]
	303.15	1.00822	1.0085[233] 1.00874[234] 1.00817[158] 1.0084[235] 1.00802[236] 1.00802[237] 1.00847[167]	14.642	14.956[234] 14.88[235] 14.986[236] 14.71[237] 15.11[190] 14.423[242]	1.45069	1.45066[244] 1.45273[238] 1.4503[239]
	308.15	1.00434	1.0046[233] 1.00449[167] 1.0041[242] 1.0042[245]	11.923	12.28[190] 11.86[245]	1.44806	
	313.15	1.00021	1.0006[233] 1.00077[234] 1.00021[158] 1.0001[235] 1.00006[236] 0.99998[237] 1.00050[167]	9.778	9.839[234] 9.93[235] 9.776[236] 9.77[237] 10.02[190] 9.61[241] 9.562[242]	1.44605	1.4468[244] 1.4449[234]
	318.15	0.99632	0.99639[167] 0.996[242] 0.9962[245]	8.193	8.455[190] 7.91[245]	1.44422	
	323.15	0.99227	0.99275[234] 0.99219[158]	6.945	6.902[234] 6.89[235]	1.44230	

Table 6-1 (continued)

			0.9919[235] 0.99205[236] 0.99197[237] 0.99241[167]		6.765[236] 6.83[237] 6.972[190] 6.72[241]		
	328.15	0.98831	0.9883[242] 0.9887[245]	5.930	5.047[190] 5.74[245]	1.44052	
	333.15	0.98432	0.98410[158] 0.9836[235] 0.985[242]	4.980	4.97[235] 4.814[242]	1.43863	
%AARD		**0.0282**		**2.0700**		**0.0547**	

[a]U(T) = 0.02 K; U(ρ) = 0.00020 g.cm^{-3}, data recorded at 0.101MPa, U(P) = 0.001 MPa.

[b]U(T) = 0.02 K; U(η) = 0.003 mPa.s , data recorded at 0.101MPa, U(P) = 0.001 MPa

[c]U(T) = 0.02 K ; U(n_D) = 0.00010; data recorded at 0.101MPa and a standard wavelength of 589 nm, U(P) = 0.001 MPa.

Table 6-2: Densities (ρ), viscosities (η) and Refractive indices (n_D) of MDEA at T = (293.15 to 343.15) K and P = 0.101MPa.							
Sample	**T/K**	**[a]ρ/g·cm^{-3}**		**[b]η/mPa·s**		**[c]n_D**	
		exp	**lit**	**exp**	**lit**	**exp**	**Lit**
MDEA	**293.15**	1.0406	1.03966[246] 1.04006[247] 1.04050[237] 1.0406[248],[249]	103.050	103.091 [246] 103.04[237] 104.5[190] 103.3[248] 102.7[250]	1.46927	1.4689[251] 1.46935[252]
	298.15	1.03618	1.0368[249] 1.0369[253] 1.0359[254] 1.0379[252] 1.0371[251]	77.650	77.19[190] 77.85[255]	1.46727	1.4671[251] 1.46724[252]
	303.15	1.03261	1.032468[247] 1.03260[237] 1.0328[248] 1.0332[249] 1.032[254] 1.03325[256] 1.0341[252]	57.370	57.28[237] 57.86[190] 57.615[246] 57.3[248]	1.46539	1.46532[255],[252] 1.46796[256] 1.4653[251] 1.46498[257]
	308.15	1.02765	1.0294[249] 1.02901[253] 1.0303[252] 1.0298[251]	43.850	44.14[190] 43.90[255]	1.4639	1.4625,[251] 1.4631[252]
	313.15	1.0248	1.024862[247] 1.02476[237] 1.0254[248] 1.0256[249] 1.0244[254] 102565[256]	33.980	33.94[237] 34.31[190] 34.043[246] 34.1[248] 34.02[250] 34.150[57]	1.46197	1.46074[255] 1.46438[256] 1.4607[251] 1.46099[257]
	318.15	1.02096	1.0218[249] 1.02264[253] 1.0227[252] 1.0221[251]	27.450	26.53[190] 27.44[255] 27.575[249]	1.45909	1.4589[251] 1.45892[255]
	323.15	1.01732	1.017212[247] 1.01712[237] 1.0178[248] 1.0167[254] 1.0185[251]	21.860	21.31[237] 21.67[190] 21.466[246] 21.6[248] 21.50[250]	1.45713	1.4570[251] 1.45708[255] 1.45680[257]

Table 6-2 (continued)

	328.15	1.01456	1.0141[249] 1.0150[252]	18.065	17.89[255] 18.024[249]	1.45522	1.45513[252]
	333.15	1.01092	1.009506[247] 1.009[254] 1.010[248] 1.0103[249]	14.430	14.179[246] 14.39[190] 14.3[248] 14.84[57] 14.377[258]	1.45274	1.45287[255] 1.45252[257]
%AARD		**0.0808**		**0.8116**		**0.0401**	

[a] U(T) = 0.02 K; U(ρ) = 0.00020 g.cm^{-3}, data recorded at 0.101MPa, U(P) = 0.001 MPa.

[b]U(T) = 0.02 K; U(η) = 0.003 mPa.s , data recorded at 0.101MPa, U(P) = 0.001 MPa

[c]U(T) = 0.02 K ; U(n_D) = 0.00010; data recorded at 0.101MPa and a standard wavelength of 589 nm, U(P) = 0.001 MPa.

Table 6-3: Densities (ρ), viscosities (η) , and Refractive indices (n_D) of DEA at T = (293.15 to 343.15) K and P = 0.101MPa							
Sample	**T/K**	**[a]ρ/g·cm^{-3}**		**[b]η/mPa·s**		**[c]n_D**	
		Exp	**lit**	**exp**	**lit**	**exp**	**Lit**
DEA	**293.15**	1.0973	1.0974[248] 1.0975[251] 1.09725[259] 1.0968[239] 1.09642[260]	890.500	855.25[260] 890.5[190] 892.037[236]	1.47724	1.4766[22] 1.4776[239] 1.47788[260]
	293.15	1.0939	1.0936[240] 1.0939[251] 1.09402[259] 10935[239] 1.09322[260] 1.09337[236]	561.000	562.315[261] 566.57[260] 566.3[190] 562.7[236]	1.47588	1.4759[22] 1.4764[260] 1.4760[239]
	303.15	1.09087	1.0909[240] 1.0902[248] 1.0907[251] 1.09078[259] 1.08999[260] 1.0894[262]	380.500	380.5[262] 383.9[190] 380.18[261] 386.6[248] 384.84[260] 394.200[236]	1.47444	1.4735[251] 1.4746[239] 1.4749[260]
	308.15	1.08764	1.0875[259] 1.0870[251] 1.0867[262]	268.500	267.51[260] 262.4[190]	1.47297	1.4726[251] 1.4734[260]
	313.15	1.08383	1.0838[240] 1.0842[259] 1.0841[251] 1.0839[248] 1.08343[260] 1.0829[262]	190.340	192.85[261] 188.2[190] 189.7[248] 189.86[260] 191.317[236]	1.47148	1.4714[251] 1.47188[260]
	318.15	1.08051	1.0808[251] 1.0811[240] 1.08022[260] 1.08086[259] 1.0803[262]	140.000	137.48[260] 145.6[190]	1.46985	1.4695[251] 1.47035[260]
	323.15	1.07808	1.0775[251] 1.0771[240],[248] 1.07697[260]	102.500	106.94[261] 119.5[190] 101.2[248] 101.45[260] 102.722[236]	1.46817	1.4672[251] 1.46883[260]

Table 6-3 (continued)

	328.15	1.07474	1.0744[262] 1.07367[260] 1.0736[240]	77.000	76.189[260]	1.46651	1.46883 1.46730[260]
	333.15	1.0713	1.0703[248] 1.07034[260] 1.070[240] 1.0699[262]	59.500	57.9[248] 61.36[262] 57.69[190] 58.407[260] 57.304[261]	1.46442	1.46578[260]
%AARD		**0.0405**		**1.8614**		**0.0302**	

[a] U(T) = 0.02 K; U(ρ) = 0.00020 g.cm^{-3}, data recorded at 0.101MPa, U(P) = 0.001 MPa.

[b]U(T) = 0.02 K; U(η) = 0.003 mPa.s , data recorded at 0.101MPa, U(P) = 0.001 MPa

[c]U(T) = 0.02 K ; U(n_D) = 0.00010; data recorded at 0.101MPa and a standard wavelength of 589 nm, U(P) = 0.001 MPa.

Table 6-4: Densities (ρ), viscosities (η) , and Refractive indices (n_D)of ETOH at T = (293.15 to 343.15) K and P = 0.101MPa							
Sample	**T/K**	**[a]ρ/g·cm^{-3}**		**[b]η/mPa·s**		**[c]n_D**	
		exp	**lit**	**exp**	**lit**	**exp**	**lit**
ETOH	**293.15**	0.78949	0.78954[234] 0.78824[263] 0.78946[265] 0.78940[167]	1.162	1.17[166] 1.160[263] 1.116[234]	1.36161	1.3616[234]
	298.15	0.78531	0.78510[264] 0.78520[265] 0.78513[167] 0.78506[266]	1.077	1.079[266] 1.077[267] 1.08[268] 1.093[264]	1.35994	1.35923[267] 1.3610[269]
	303.15	0.78068	0.780904[234] 0.78073[263] 0.78075[265] 0.78075[167]	0.982	0.97[166] 0.99[161] 0.968[263] 0.9502[234]	1.35792	1.3574[234]
	308.15	0.77642	0.77643[264] 0.77642[265] 0.77641[167]	0.897	0.902[264]	1.35599	
	313.15	0.77223	0.77220[234] 0.77198[263] 0.77181[265] 0.77204[167]	0.836	0.832[165] 0.824[266] 0.834[161]	1.35397	1.3532[234]
	318.15	0.76754	0.76762[264] 0.76752[167] 0.76738[265]	0.761	0.77[268] 0.759[264]	1.35189	
	323.15	0.76353	0.7635[161] 0.76329[234] 0.76304[167]	0.703	0.701[161] 0.69[166]	1.34979	1.3493[234]
	328.15	0.75868	0.75860[264]	0.638	0.644[264]	1.34769	
	333.15	0.7546		0.591		1.34523	
%AARD		**0.1332**		**1.4374**		**0.0437**	

[a] U(T) = 0.02 K; U(ρ) = 0.00020 g.cm^{-3}, data recorded at 0.101MPa, U(P) = 0.001 MPa.

[b]U(T) = 0.02 K; U(η) = 0.003 mPa.s , data recorded at 0.101MPa, U(P) = 0.001 MPa

[c]U(T) = 0.02 K ; U(n_D) = 0.00010; data recorded at 0.101MPa and a standard wavelength of 589 nm, U(P) = 0.001 MPa.

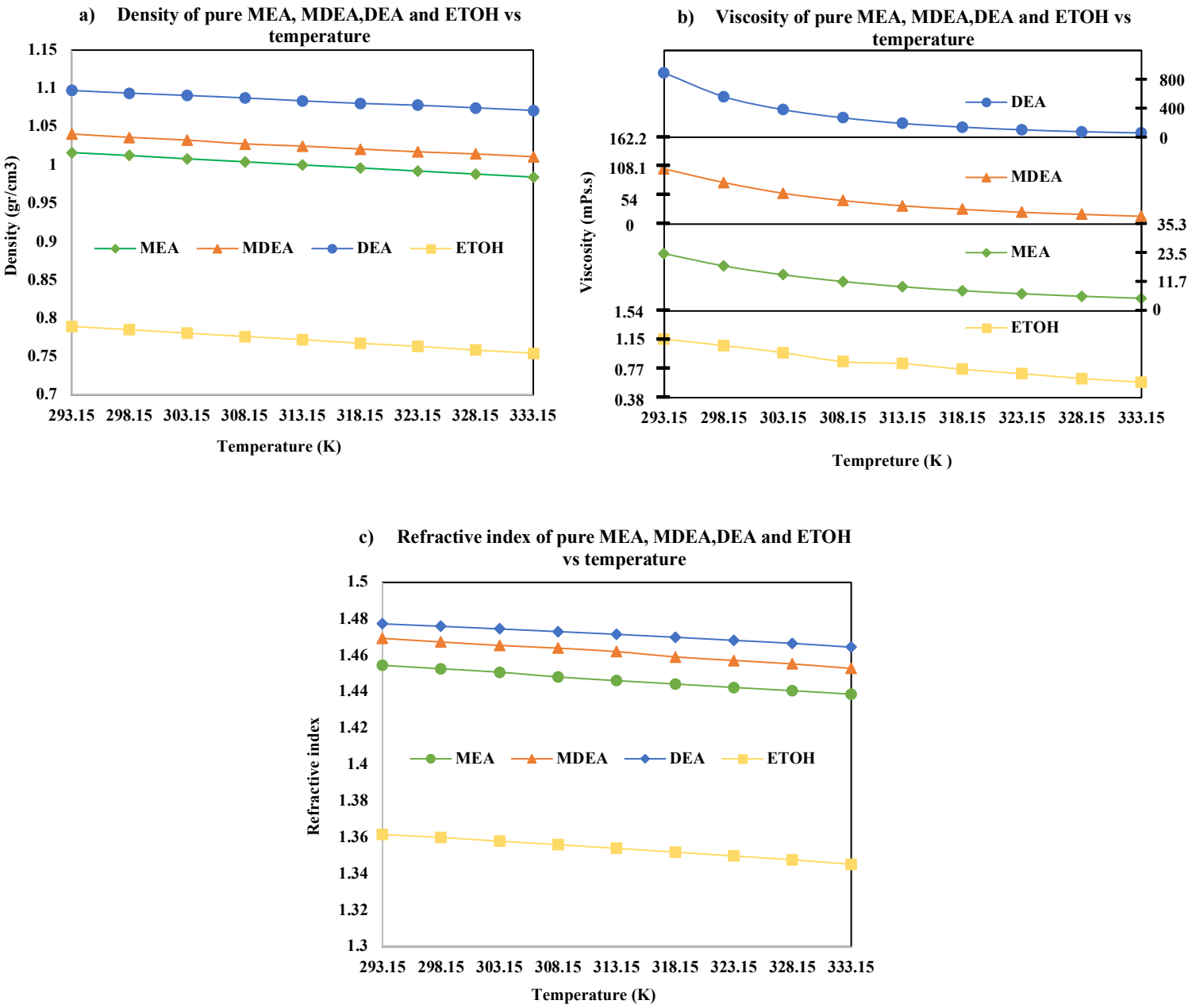

Figure 6-1 : Pure amine solvents and ethanol at temperatures from 293.15 K to 333.15 K and P=0.1 MPa

a) Density, b) Viscosity, and c) Refractive index

6.2 Binary Mixtures

Non-aqueous solutions of MEA, DEA, MDEA with ETOH at different concentrations of amines were prepared. Density, viscosity and refractive index of the studied blends were measured over temperatures range from 293.15 K to 338.15 K. The results are listed in

Table 6-5.

The composition and temperature dependencies of density, viscosity and refractive index of MEA+ETOH, MDEA+ETOH and DEA+ETOH are shown in **Figure 6-2** , respectively. As it can be seen from the figure, the density of the studied solutions increases with the increase of amines concentration at all temperatures. This is attributed to the higher molar mass of amines against ethanol that causes increase in density of the mixture with adding a greater number of amines. From this figure, it can be also observed that the density of the solutions decreases with increasing the temperature. The decrease in mixture density can be attributed to the increase in volume of the solution while the mass stays constant. It is concluded that the density of the studied solutions is the function of both temperature and mixture composition

Table 6-5 : Densities (ρ), viscosities (η), and Refractive indices (n_D) of binary mixtures at T = (293.15 to 343.15) K and P = 0.101MPa

MEA+ETOH									
[d]X1	T=293.15 K	T=298.15 K	T=303.15 K	T=308.15 K	T=313.15 K	T=318.15 K	T=323.15 K	T=328.15 K	T=333.15 K
[a]ρ (g.cm $^{-3}$)									
0	0.78949	0.78513	0.78068	0.77642	0.77223	0.76754	0.76353	0.75868	0.7546
0.2010	0.84371	0.83920	0.83451	0.83000	0.82556	0.82072	0.81646	0.81154	0.80722
0.4004	0.89293	0.88844	0.88371	0.87924	0.87471	0.87000	0.86560	0.86073	0.85640
0.6020	0.93816	0.93381	0.92909	0.92478	0.92032	0.91577	0.91139	0.90665	0.90234
0.8006	0.97892	0.97465	0.97034	0.96618	0.96179	0.95751	0.95328	0.94880	0.94456
1	1.0163	1.0125	1.0082	1.0043	1.0002	0.9963	0.9923	0.9883	0.9843
[b]η (mPa.s)									
0	1.162	1.077	0.982	0.863	0.836	0.761	0.703	0.638	0.591
0.2010	2.140	1.910	1.700	1.500	1.360	1.210	1.100	1.020	0.920
0.4004	3.893	3.383	2.920	2.534	2.304	2.039	1.816	1.625	1.440
0.6020	7.409	6.164	5.327	4.389	3.756	3.279	2.857	2.462	2.128
0.8006	13.470	10.725	9.032	7.481	6.132	5.312	4.530	3.812	3.261
1	23.260	18.256	14.642	11.923	9.778	8.193	6.945	5.930	4.980
[c]n_D									
0	1.36161	1.35994	1.35792	1.35599	1.35397	1.35189	1.34979	1.34769	1.34523
0.2010	1.38515	1.38359	1.38171	1.3799	1.37821	1.3767	1.3756	1.3743	1.37333
0.4004	1.40489	1.40357	1.40185	1.39992	1.39813	1.39675	1.39522	1.39389	1.3927
0.6020	1.42257	1.42087	1.41923	1.41738	1.41541	1.41364	1.41231	1.41092	1.4093
0.8006	1.43885	1.43726	1.43546	1.43363	1.43183	1.43007	1.42885	1.42765	1.42627
1	1.45446	1.45256	1.45069	1.44806	1.44605	1.44422	1.4423	1.44052	1.43863

MDEA+ETOH									
[a]ρ (g.cm $^{-3}$)									
0	0.78949	0.78513	0.78068	0.77642	0.77223	0.76754	0.76353	0.75868	0.7546
0.2002	0.87854	0.87392	0.86936	0.8646	0.86047	0.85565	0.8515	0.84691	0.84267
0.4013	0.9396	0.935	0.93072	0.92585	0.92209	0.9175	0.91343	0.90937	0.90527
0.5998	0.98328	0.97858	0.97452	0.96955	0.96614	0.96176	0.95778	0.95419	0.95021
0.8000	1.01625	1.01171	1.00786	1.0028	0.99966	0.99546	0.99161	0.9884	0.98455
1	1.0406	1.03618	1.03261	1.02765	1.0248	1.02096	1.01732	1.01456	1.01092
[b]η (mPa.s)									
0	1.162	1.077	0.982	0.863	0.836	0.7606	0.7034	0.638	0.5909
0.2002	3.295	2.895	2.561	2.269	1.984	1.799	1.565	1.354	1.251
0.4013	8.525	7.188	6.188	5.468	4.466	4.315	3.618	2.952	2.699
0.5998	21.286	17.490	14.175	11.690	9.700	8.606	7.040	5.993	4.819
0.8000	49.480	40.860	29.630	23.670	18.810	16.026	12.990	10.930	8.340
1	103.05	77.650	57.370	43.850	33.980	27.450	21.860	18.065	14.430
[c]n_D									
0	1.3616	1.35994	1.35792	1.35599	1.35397	1.35189	1.34979	1.34769	1.34523
0.2002	1.40067	1.39895	1.39708	1.39542	1.39376	1.39283	1.39182	1.39105	1.39
0.4013	1.426	1.42435	1.42272	1.42165	1.42023	1.4191	1.41835	1.41776	1.41694
0.5998	1.44424	1.44269	1.4411	1.44009	1.43835	1.43765	1.43629	1.43543	1.43432
0.8000	1.45776	1.45528	1.45335	1.45198	1.45036	1.44813	1.44686	1.44523	1.44383
1	1.46927	1.46727	1.46539	1.4639	1.46197	1.45909	1.45713	1.45522	1.45274
DEA+ETOH									
[a]ρ (g.cm $^{-3}$)									
0	0.78949	0.78513	0.78068	0.77642	0.77223	0.76754	0.76353	0.75868	0.7546
0.2002	0.88481	0.8805	0.87615	0.87188	0.86753	0.86291	0.85905	0.85427	0.85019

0.4001	0.95754	0.95338	0.94929	0.9452	0.94088	0.93654	0.93299	0.92851	0.92449
0.6000	1.01506	1.01115	1.00738	1.00352	0.9993	0.99527	0.99208	0.98798	0.98409
0.8000	1.06061	1.05682	1.05339	1.04987	1.04588	1.04219	1.03931	1.03562	1.03194
1	1.0973	1.0939	1.0909	1.0876	1.0838	1.0805	1.0781	1.0747	1.0713
[b]η (mPa.s)									
0	1.162	1.077	0.982	0.863	0.836	0.7606	0.7034	0.638	0.5909
0.2002	5.347	4.630	4.034	3.254	3.125	2.873	2.493	2.269	2.083
0.4001	20.000	17.140	13.560	11.350	8.930	7.560	6.770	6.060	5.920
0.6000	86.500	59.480	44.980	36.070	28.540	23.060	18.450	14.770	12.280
0.8000	318.900	210.500	143.000	106.000	80.500	62.00	46.370	32.990	26.500
1	890.500	561.000	380.500	268.500	190.340	140.000	102.500	77.000	59.500
[c]n_D									
0	1.3616	1.35994	1.35792	1.35599	1.35397	1.35189	1.34979	1.34769	1.34523
0.2002	1.41723	1.41716	1.41637	1.41532	1.41362	1.41302	1.41238	1.41177	1.41054
0.4001	1.44416	1.44295	1.44245	1.44031	1.43902	1.43822	1.43743	1.43586	1.43516
0.6000	1.45002	1.44823	1.44672	1.44524	1.44424	1.44335	1.44267	1.44195	1.44177
0.8000	1.4653	1.46369	1.46218	1.46067	1.45907	1.45815	1.45737	1.4567	1.45557
1	1.47724	1.47588	1.47444	1.47297	1.47148	1.46985	1.46817	1.46651	1.46442

[a]U(T) = 0.02 K; U(ρ) = 0.00020 g.cm^{-3}, data recorded at 0.101MPa, U(P) = 0.001 MPa.

[b]U(T) = 0.02 K; U(η) = 0.003 mPa.s , data recorded at 0.101MPa, U(P) = 0.001 MPa

[c]U(T) = 0.02 K ; U(n_D) = 0.00010; data recorded at 0.101MPa and a standard wavelength of 589 nm, U(P) = 0.001 MPa.

[d]U(x_i)=0.0002

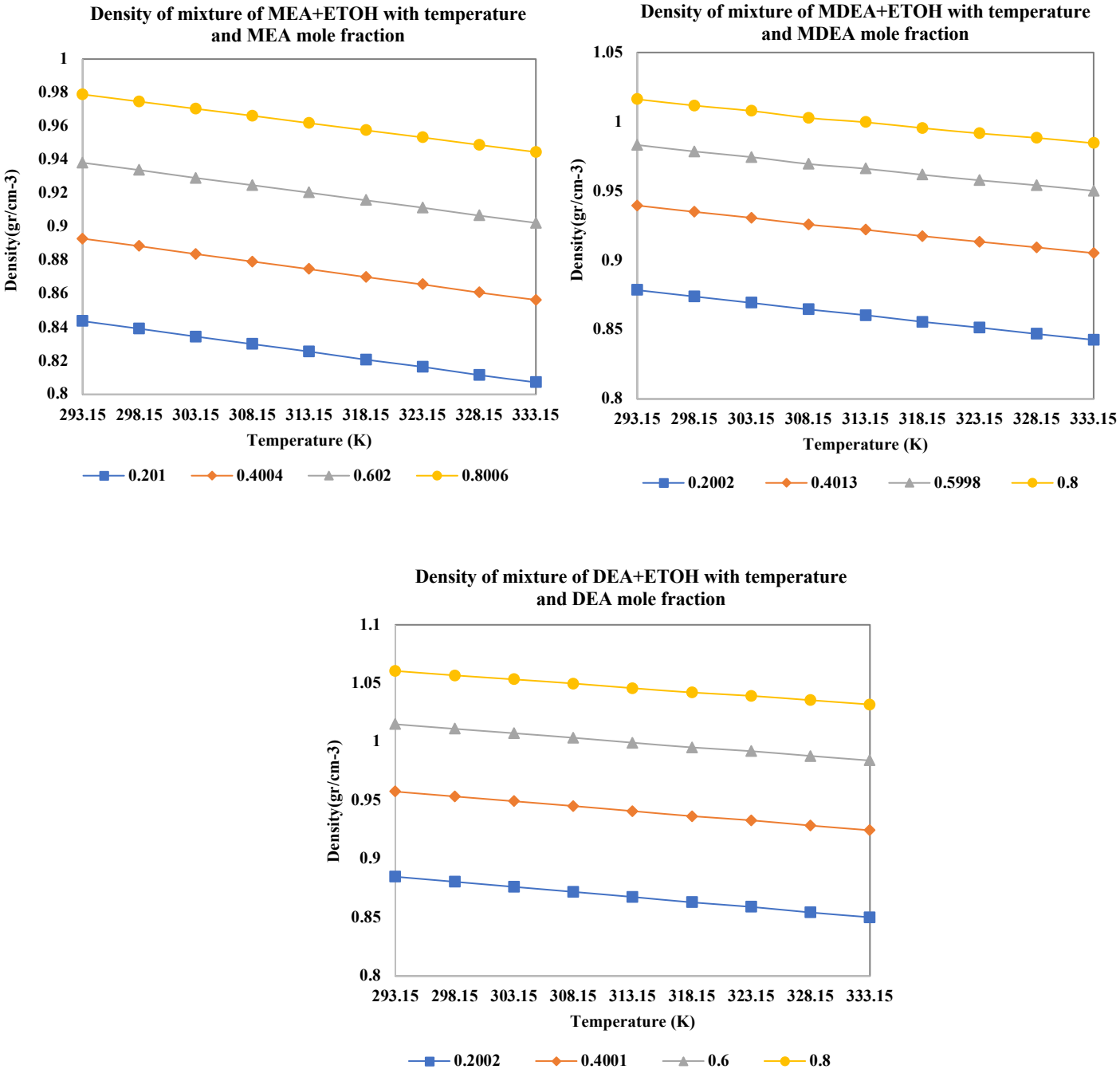

Figure 6-2 : Composition and temperature dependency of density of the alkanol amines and ethanol solutions

The trend of changes in viscosity with temperature and concentration of binary mixtures are presented in **Figure 6-3**. At any constant temperature, the viscosity value of the studied solution increases upon increase in concentration of each studied alkanolamines due to the higher viscosity of them compared to ethanol.

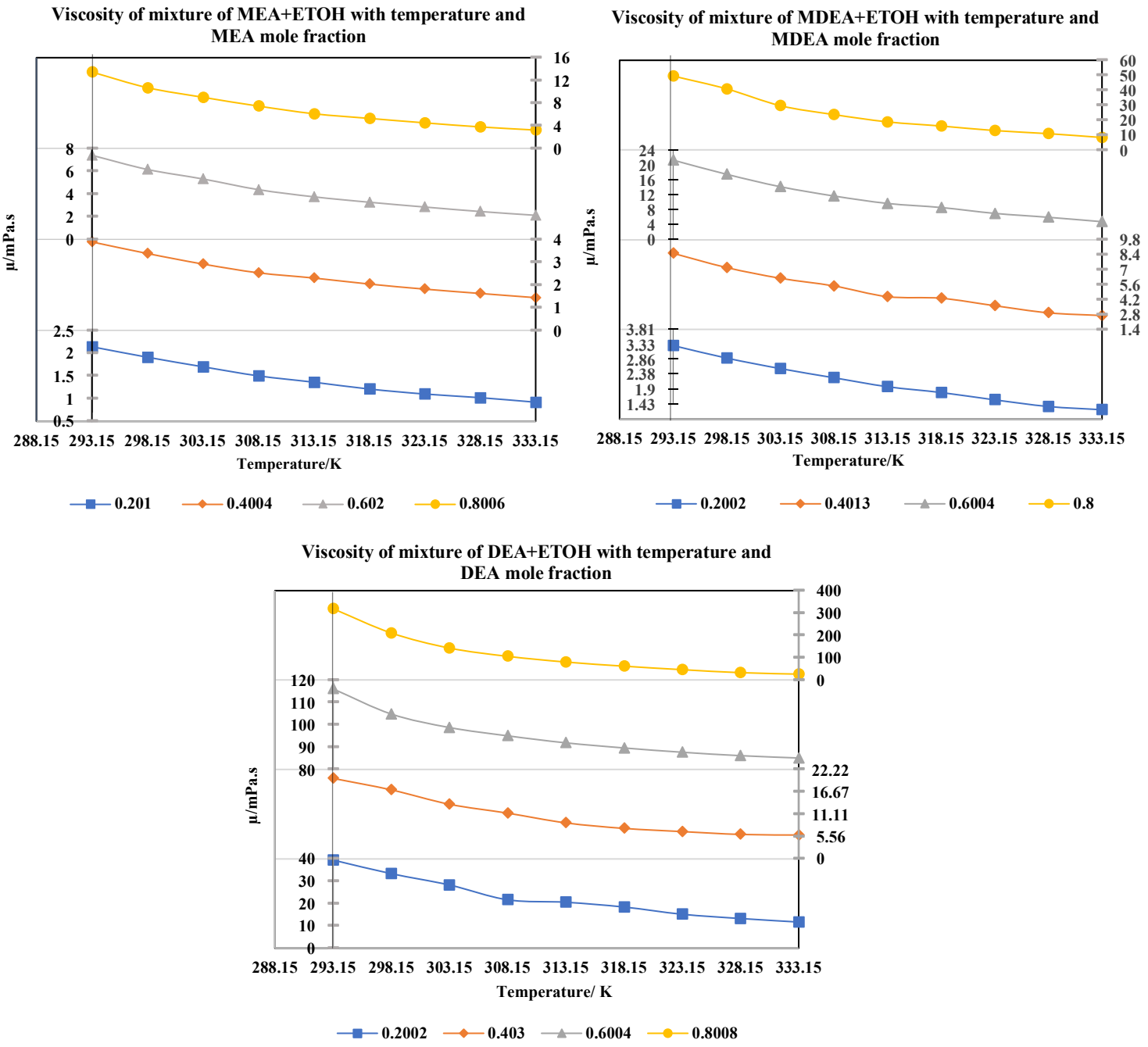

Figure 6-3 :Composition and temperature dependency of viscosity of the alkanolamines and ethanol solutions

However, an increase in temperature at any constant concentration leads to decrease in the viscosity value of the system. This decreasing behavior of viscosity (resistance against mobility) is due to the increase in mobility of the system with increase in temperature.

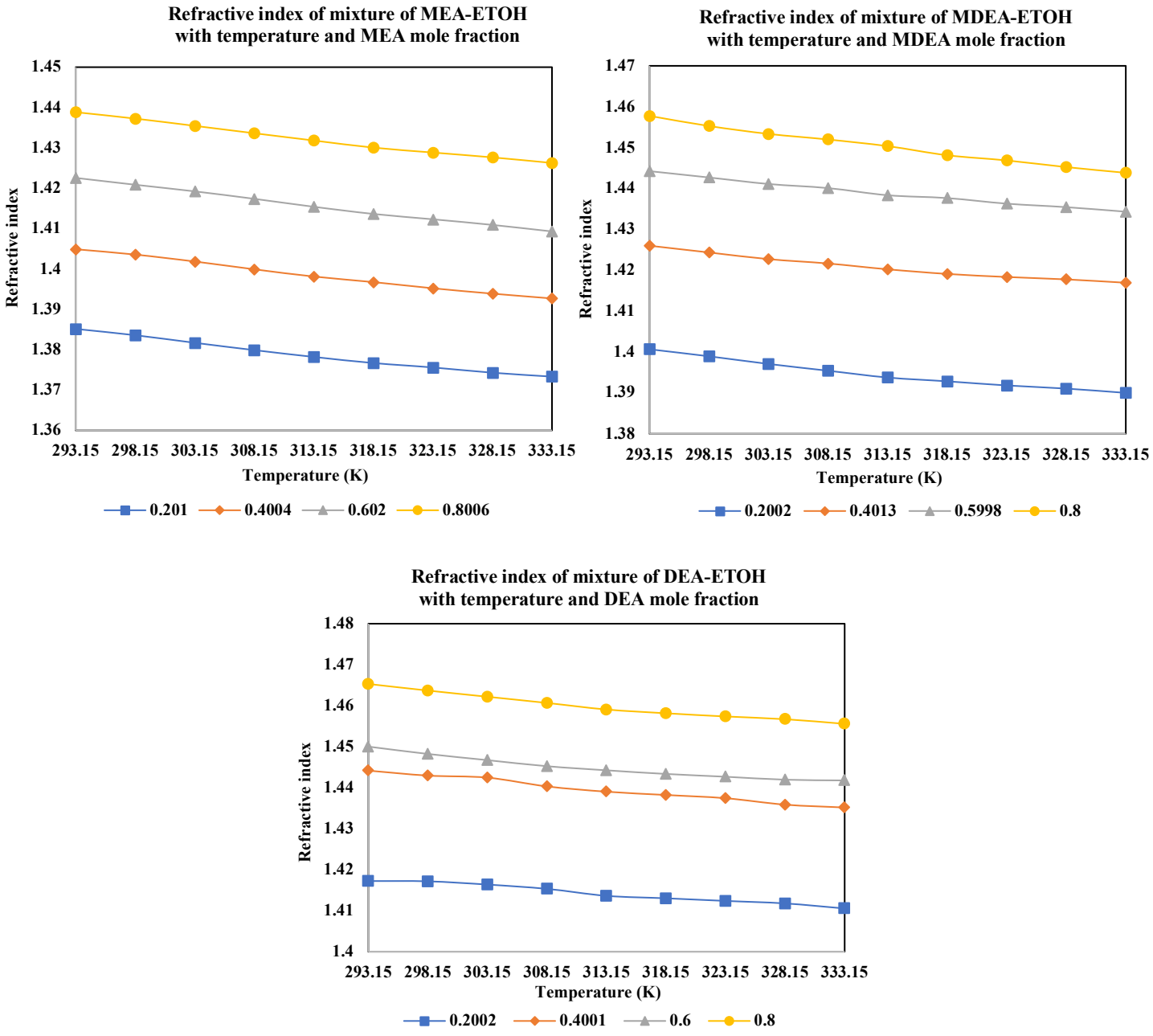

Figure 6-4: Composition and temperature dependency of Refractive index of the alkanolamines and ethanol solutions

From **Figure 6-4**, it can be seen that refractive index values of the solutions decrease upon increasing the temperature at any constant concentration but increases with the increase in the concentration of alkanolamines at any constant temperature.

Despite there is a considerable number of reports on the aqueous solution of alkanolamines, the research on the non-aqueous amine solutions are still lacking. To the best of my knowledge, there are only a few works done on investigation of the physical properties of the amine-ethanol solutions [270],[161],[168],[167].

The experimental density and viscosity of the binary mixture of alkanolamine-ethanol at different temperatures and amine's mole fractions are compared with the data reported in literature and listed in **Table 6-6**. Furthermore, there has not been reported any results for the refractive index of studied alkanolamine-ethanol mixture so far.

Table 6-6: Comparison of the experimental and literature data for mixture of a) MEA + Ethanol and b)MEDA +Ethanol with literature data

a) MEA(x_1) - Ethanol

x_1=0.2

T/K	This work		Literature			
			Lee et al [161]		Zhu et al.[168]	
	ρ	η	ρ	η	ρ	η
293.15	0.84371	2.14			0.84368	2.12
298.15	0.8392	1.91				
303.15	0.83451	1.7	0.8345	1.73	0.83494	1.68
308.15	0.83000	1.5				
313.15	0.82556	1.36	0.8262	1.42	0.82534	1.36
318.15	0.82072	1.21				
323.15	0.81646	1.1	0.8174	1.19	0.81735	1.11
%AARD			**0.0646**	**4.7861**	**0.0624**	**0.6952**

x_1=0.4

T/K	This work		Literature			
			Lee et al [161]		Zhu et al.[168]	
	ρ	η	ρ	η	ρ	η
293.15	0.89293	3.89			0.89315	3.96
298.15	0.88844	3.38				
303.15	0.88371	2.92	0.8844	3.05	0.88454	2.98
308.15	0.87924	2.53				
313.15	0.87471	2.30	0.8759	2.34	0.87469	2.29
318.15	0.87	2.04				
323.15	0.8656	1.82	0.8670	1.85	0.86658	1.80
%AARD			**0.1253**	**2.6132**	**0.0698**	**1.1962**

x_1=0.6

T/K	This work		Literature			
			Lee et al [161]		Zhu et al.[168]	
	ρ	η	ρ	η	ρ	η
293.15	0.93816	7.41			0.93802	7.45
298.15	0.93381	6.16				
303.15	0.92909	5.33	0.9296	5.37	0,92938	5.23
308.15	0.92478	4.39				
313.15	0.92032	3.76	0.9212	3.93	0.91984	3.80
318.15	0.91577	3.28				
323.15	0.91139	2.86	0.9123	2.95	0.91188	2.87
%AARD			**0.0835**	**2.8062**	**0.0457**	**1.0966**

x_1=0.8

T/K	This work		Literature			
			Lee et al [161]		Zhu et al.[168]	
	ρ	η	ρ	η	ρ	η
293.15	0.97892	13.47			0.97896	13.74
298.15	0.97465	10.72				
303.15	0.97034	9.03	0.9705	9.05	0.97081	9.05
308.15	0.96618	7.48				
313.15	0.96179	6.13	0.9626	6.32	0.96195	6.17
318.15	0.95751	5.31				
323.15	0.95328	4.53	0.9541	4.54	0.95382	4.48
%AARD			**0.0622**	**1.1806**	**0.0406**	**0.6593**

b) MDEA(x_1) - Ethanol

x_1=0.2

T/K	This work		Literature				
			Rubia et al. [270]	Tontiwachwuthikul et al [161]		Zhu et al.[168]	
	ρ	η	ρ	ρ	η	ρ	η
293.15	0.87854	3.29	0.87900			0.87956	3.23
298.15	0.87392	2.89	0.87436				
303.15	0.86936	2.56	0.86983			0.86979	2.45
308.15	0.8646	2.27	0.86464				
313.15	0.86047	1.98	0.86034	0.8666	2.13	0.86028	1.94
318.15	0.85565	1.8					
323.15	0.8515	1.56				0.85257	1.52
%AARD			**0.0353**	**0.7124**	**7.5758**	**0.0179**	**1.5793**

x_1=0.4

T/K	This work		Literature				
			Rubia et al. [270]	Tontiwachwuthikul et al [161]		Zhu et al.[168]	
	ρ	η	ρ	ρ	η	ρ	η
293.15	0.9396	8.52	0.94750			0.94142	8.77
298.15	0.935	7.19	0.94270				
303.15	0.93072	6.19	0.93824			0.93067	6.08
308.15	0.92585	5.47	0.93317				
313.15	0.92209	4.47	0.92865	0.92186	4.2	0.92143	4.5
318.15	0.9175	4.31					
323.15	0.91343	3.62				0.91345	3.32
%AARD			**0.7949**	**0.0249**	**6.0403**	**0.0192**	**0.6121**

x_1=0.6

T/K	This work		Literature				
			Rubia et al. [270]	Tontiwachwuthikul et al [161]		Zhu et al.[168]	
	ρ	η	ρ	ρ	η	ρ	η
293.15	0.98328	21.286	0.98670			0.98481	21.94
298.15	0.97858	17.49	0.98208				
303.15	0.97452	14.175	0.97752			0.97463	14.14
308.15	0.96955	11.69	0.97275				
313.15	0.96614	9.7	0.96798	0.96676	9	0.96586	9.68
318.15	0.96176	8.606					
323.15	0.95778	7.04				0.95792	6.79
%AARD			**0.3068**	**0.0642**	**7.2165**	**0.0101**	**0.1133**

x_1=0.8

T/K	This work		Literature				
			Rubia et al. [270]	Tontiwachwuthikul et al [161]		Zhu et al.[168]	
	ρ	η	ρ	ρ	η	ρ	η
293.15	1.01625	49.48	1.01988			1.01676	49.39
298.15	1.01171	40.86	1.01530				
303.15	1.00786	29.63	1.01124			1.00751	29.56
308.15	1.0028	23.67	1.00679				
313.15	0.99966	18.81	1.00249	1.00083	17.8	0.99913	18.85
318.15	0.99546	16.026					
323.15	0.99161	12.99				0.99130	12.44
%AARD			**0.3457**	**0.1170**	**5.3695**	**0.0219**	**0.1122**

6.3 Volumetric properties

The excess molar volume V^E of a binary mixture is defined as deviation between the real and the ideal solution and can be calculated from the density and using the following equation:

$$V^E = \frac{(x_1 M_1 + x_2 M_2)}{\rho_{12}} - \left(\frac{x_1 M_1}{\rho_1}\right) - \left(\frac{x_2 M_2}{\rho_2}\right) \qquad 6\text{-}1$$

Where x_i, M_i and ρ_i (i=1,2) are the mole fraction, molar mass and the density of pure components i, respectively. In this equation, ρ_{12} is the density of the mixture.

The results of V^E for the investigated binary mixtures at different temperatures and over the whole range of composition are listed in **Table 6-7**. The excess molar volume versus mole fraction of studied alkanolamines (x_1) at temperatures from 303.15 to 323.15 K are graphically represented in **Figure 6-5**. Also, the comparison between V^E of these systems at 298.15 K for different systems are also depicted in this figure.

As it can be seen from the diagrams, the value of V^E for all the solutions are negative and absolute value of V^E decrease with increase in temperature. The negative values of V^E point out that the volume shrinkage takes place when alkanolamines and ethanol are mixed.

The magnitude and sign of V^E can arise from the several factors: chemical, physical, and structural [271]. Chemical contribution is due to the formation of the complex structure between unlike molecules as a result of strong intermolecular interaction (charge-transfer, dipole- dipole interaction and hydrogen bonding) between alkanolamine and ethanol through N···H-O and H-O···H-O bond. With the formation of the complex, the volume contraction takes place in the mixture. Therefore, chemical effect contributes negatively to V^E [272]. Contrarily, depolymerization of the alkanolamines and ethanol, and the disruption of the bonds in self associated alcohol and alkanolamines molecules lead to the volume expansion of the mixture. This factor that is also classified as the chemical contribution makes the positive contribution towards V^E [166],[273]. It should be mentioned that the physical effect originates from "normal" physical interactions, both attractive or repulsive. In the latter case, it is sometimes called as a structural

effect. The physical (attractive) contribution does not have to be positive although usually it happens so. It depends on the differences between unlike and like interactions.

The geometrical effect includes the size and shape of the molecules, the molecule strict hindrance as well as the packing effect between unlike molecules [272]. This effect is contributing negatively on the V^E of the system due to the volume contraction obtained in the mixture [166]. In general, the larger the difference in molecular volume of the components are, the more negative deviation of the real mixture from ideality can be seen [274].
For investigated alkanolamines, the number of alkyl groups linked to the N atom, and the size of them reflect the value of V^E. The more the number of the alkyl group and the larger the size, the value of V^E become more negative [275].

The value and sign of V^E depend on which of the above factors in the mixture are predominant over the others. Hence, according to the negative value of V^E , it can be concluded that the chemical and geometrical factors dominate over physical factor in the investigated systems [166].

Further considering Figure 6-5 reveals that the absolute value of V^E for the mixture of ethanol with MEA is larger than other studied systems and follows the order: MEA> MDEA >DEA. The trend for the mixture of MEA and MDEA with ethanol is accordant with the research done by Zhu,*et al*,(2019) [168].

MEA, DEA and MDEA are highly polar. At pure state, both alkanolamine and ethanol are self-associated through N···H-O and O-H… O-H bonds, respectively. DEA and MDEA are secondary alkanolamines with two O-H groups in their structure. The presence of two hydroxyl groups leads to the stronger self-associated bonds for DEA and MDEA compared to MEA. Moreover, the intermolecular H-bond for DEA is much stronger than MDEA. This can be explained by the fact that the methyl group attached to the N atom of MDEA cause the steric hindrance effect that makes the self-associated bond weaken [275]. With addition of Ethanol in alkanolamine, a complex structure is formed as a result of the interaction between hydroxyl group of ethanol, and nitrogen and hydroxyl group of alkanolamines. As the self- associated bonds of MEA molecules are weaker than that in DEA and MDEA, at certain temperature, the number of available MEA species to form

a cross complex with ethanol is larger than DEA and MDEA. Therefore, the volume contraction is MEA-ETOH mixture is larger than that of MDEA-ETOH and DEA-ETOH. With the similar interpretation, the number of available MDEA species at the certain temperature is higher than DEA due to weaker intermolecular hydrogen bonds and hence, volume contraction is larger for MDEA-ETOH mixture than DEA-ETOH mixture. On the other hand, based on the geometrical effect, the larger the deviation in molecular volume of the components are, the better packing in the more open structure of the larger molecule takes place that leads to increase in the volume contraction as well as the absolute value of V^E. Therefore, it is expected that the smaller molecule of ethanol can be better packed in the voids presents in large molecule of MDEA and DEA (with molar volumes of 115.002 and 96.115 respectively) compared to MEA (with molar volume of 60.327) [168].

The value of V^E is in the order of MDEA>DEA>MEA. From **Figure 6-5** , it is clearly seen that the trend for MDEA and DEA is in the order and the overall V^E of the MDEA is more negative that DEA due to the crowded structure of MDEA and its size. However, the overall V^E of MEA is the most negative among all amines. This trend indicates that the chemical effect seems to be dominant in the presently investigated mixtures.

From **Figure 6-5**, it can be clearly seen that the value of V^E becomes less negative with increase in temperature [276]. In fact, this trend is also a competition between chemical and geometrical factors. When temperature increases the self- and cross-associated bonds of the components decrease and the value of V^E become less negative [168].

Table 6-7: Values of excess molar volume (V^E), partial molar volume ($\bar{V}_i$), and apparent molar volume ($V_{\varphi,i}$) for the studied amines and ethanol mixtures at 293.15–333.15 K and P=0.101MPa

x_1	V^E(cm^3.mol^{-1})	$\bar{V}_1$(cm^3.mol^{-1})	$\bar{V}_2$(cm^3.mol^{-1})	$V_{\varphi,1}$ (cm^3.mol^{-1})	$V_{\varphi,2}$ (cm^3.mol^{-1})
MEA+ETOH					
T=293.15 K					
0.2010	-0.523	58.184	58.179	57.497	57.700
0.4004	-0.728	59.192	57.753	58.280	57.140
0.6020	-0.661	59.764	57.188	59.001	56.694
0.8006	-0.424	60.027	56.581	59.569	56.230
T=298.15 K					
0.2010	-0.515	58.424	58.510	57.764	58.033
0.4004	-0.718	59.426	58.086	58.788	57.480
0.6020	-0.654	60.008	57.511	59.730	57.036
0.8006	-0.415	60.266	56.916	60.549	56.598
T=303.15 K					
0.2010	-0.505	58.731	58.842	58.071	58.381
0.4004	-0.708	59.699	58.434	58.815	57.833
0.6020	-0.641	60.247	57.891	59.518	57.403
0.8006	-0.407	60.508	57.290	60.074	56.974
T=308.15 K					
0.2010	-0.491	58.988	59.178	58.374	58.722
0.4004	-0.696	59.929	58.779	59.078	58.176
0.6020	-0.634	60.484	58.230	59.763	57.744
0.8006	-0.401	60.746	57.626	60.316	57.327
T=313.15 K					
0.2010	-0.480	59.239	59.506	58.677	59.057
0.4004	-0.683	60.180	59.115	59.362	58.520
0.6020	-0.624	60.735	58.570	60.030	58.090
0.8006	-0.392	60.997	57.975	60.578	57.693

T=318.15 K					
0.2010	-0.469	59.524	59.880	58.972	59.436
0.4004	-0.675	60.429	59.494	59.621	58.898
0.6020	-0.615	60.987	58.942	60.283	58.477
0.8006	-0.385	61.245	58.351	60.824	58.090
T=323.15 K					
0.2010	-0.459	59.817	60.196	59.271	59.763
0.4004	-0.660	60.700	59.821	59.908	59.238
0.6020	-0.602	61.240	59.286	60.555	58.825
0.8006	-0.380	61.493	58.704	61.082	58.435
T=328.15 K					
0.2010	-0.452	60.088	60.585	59.553	60.158
0.4004	-0.649	60.968	60.210	60.181	59.641
0.6020	-0.588	61.506	59.678	60.826	59.247
0.8006	-0.366	61.749	59.123	61.346	58.890
T=333.15 K					
0.2010	-0.442	60.355	60.922	59.856	60.499
0.4004	-0.640	61.221	60.552	60.454	59.985
0.6020	-0.579	61.766	60.012	61.090	59.596
0.8006	-0.357	62.007	59.466	61.607	59.262
MDEA+ETOH **T=293.15 K**					
0.2002	-0.502	112.879	58.139	112.005	57.726
0.4013	-0.647	113.773	57.774	112.915	57.283
0.5998	-0.599	114.139	57.414	113.516	56.859
0.8000	-0.409	114.379	56.834	114.002	56.308
T=298.15 K					
0.2002	-0.494	113.389	58.486	112.536	58.061
0.4013	-0.637	114.282	58.109	113.812	57.614
0.5998	-0.582	114.643	57.767	114.986	57.224

0.8000	-0.403	114.873	57.547	115.776	56.665
T=303.15 K					
0.2002	-0.476	113.809	58.807	113.021	58.417
0.4013	-0.626	114.688	58.447	113.840	57.967
0.5998	-0.571	115.054	58.088	114.447	57.585
0.8000	-0.394	115.279	57.545	114.908	57.044
T=308.15 K					
0.2002	-0.462	114.384	59.149	113.648	58.759
0.4013	-0.617	115.237	58.797	114.419	58.306
0.5998	-0.562	115.623	58.418	115.019	57.931
0.8000	-0.381	115.849	57.879	115.481	57.434
T=313.15 K					
0.2002	-0.444	114.707	59.488	114.064	59.104
0.4013	-0.605	115.560	59.149	114.772	58.648
0.5998	-0.553	115.945	58.755	115.353	58.270
0.8000	-0.374	116.172	58.206	115.811	57.786
T=318.15 K					
0.2002	-0.429	115.185	59.866	114.573	59.486
0.4013	-0.592	115.992	59.529	115.241	59.034
0.5998	-0.541	116.407	59.120	115.814	58.670
0.8000	-0.357	116.632	58.594	116.271	58.239
T=323.15 K					
0.2002	-0.419	115.624	60.188	115.041	59.814
0.4013	-0.582	116.419	59.855	115.683	59.366
0.5998	-0.530	116.838	59.443	116.250	59.013
0.8000	-0.346	117.057	58.932	116.702	58.607
T=328.15 K					
0.2002	-0.405	115.956	60.589	115.431	60.218
0.4013	-0.572	116.732	60.261	116.027	59.768
0.5998	-0.523	117.166	59.832	116.582	59.418

0.8000	-0.336	117.386	59.325	117.033	59.043
T=333.15 K					
0.2002	-0.392	116.395	60.929	115.920	60.563
0.4013	-0.563	117.155	60.607	116.473	60.112
0.5998	-0.513	117.601	60.165	117.021	59.771
0.8000	-0.326	117.819	59.667	117.469	59.424
DEA+ETOH					
T=293.15 K					
0.2002	-0.439	94.429	58.150	93.624	57.805
0.4001	-0.552	95.253	57.817	94.437	57.434
0.6000	-0.485	95.555	57.524	95.008	57.141
0.8000	-0.325	95.722	57.122	95.411	56.731
T=298.15 K					
0.2002	-0.431	94.753	58.498	93.962	58.139
0.4001	-0.541	95.563	58.159	95.027	57.776
0.6000	-0.476	95.860	57.883	95.879	57.489
0.8000	-0.317	96.022	57.788	96.614	57.092
T=303.15 K					
0.2002	-0.424	95.023	58.821	94.261	58.483
0.4001	-0.533	95.832	58.492	95.047	58.124
0.6000	-0.469	96.142	58.191	95.598	57.840
0.8000	-0.304	96.299	57.817	95.999	57.494
T=308.15 K					
0.2002	-0.410	95.341	59.156	94.624	58.824
0.4001	-0.521	96.127	58.835	95.369	58.468
0.6000	-0.458	96.443	58.529	95.907	58.190
0.8000	-0.295	96.598	58.160	96.303	57.861
T=313.15 K					
0.2002	-0.392	95.680	59.488	95.052	59.168
0.4001	-0.507	96.466	59.181	95.742	58.812

0.6000	-0.444	96.781	58.878	96.271	58.548
0.8000	-0.290	96.937	58.508	96.648	58.208
T=318.15 K					
0.2002	-0.384	96.043	59.858	95.389	59.543
0.4001	-0.494	96.773	59.559	96.072	59.199
0.6000	-0.439	97.078	59.262	96.575	58.925
0.8000	-0.285	97.234	58.893	96.951	58.598
T=323.15 K					
0.2002	-0.371	96.279	60.183	95.670	59.874
0.4001	-0.487	96.990	59.890	96.307	59.527
0.6000	-0.429	97.301	59.587	96.809	59.267
0.8000	-0.279	97.457	59.222	97.175	58.943
T=328.15 K					
0.2002	-0.359	96.602	60.579	96.039	60.275
0.4001	-0.480	97.300	60.290	96.632	59.924
0.6000	-0.418	97.622	59.976	97.135	59.679
0.8000	-0.270	97.775	59.621	97.494	59.374
T=333.15 K					
0.2002	-0.350	96.932	60.912	96.394	60.615
0.4001	-0.473	97.616	60.629	96.959	60.263
0.6000	-0.409	97.937	60.316	97.461	60.030
0.8000	-0.265	98.088	59.965	97.811	59.727

The combined expanded uncertainties $U(V^E)=0.020$, $U(x_i)=0.0002$

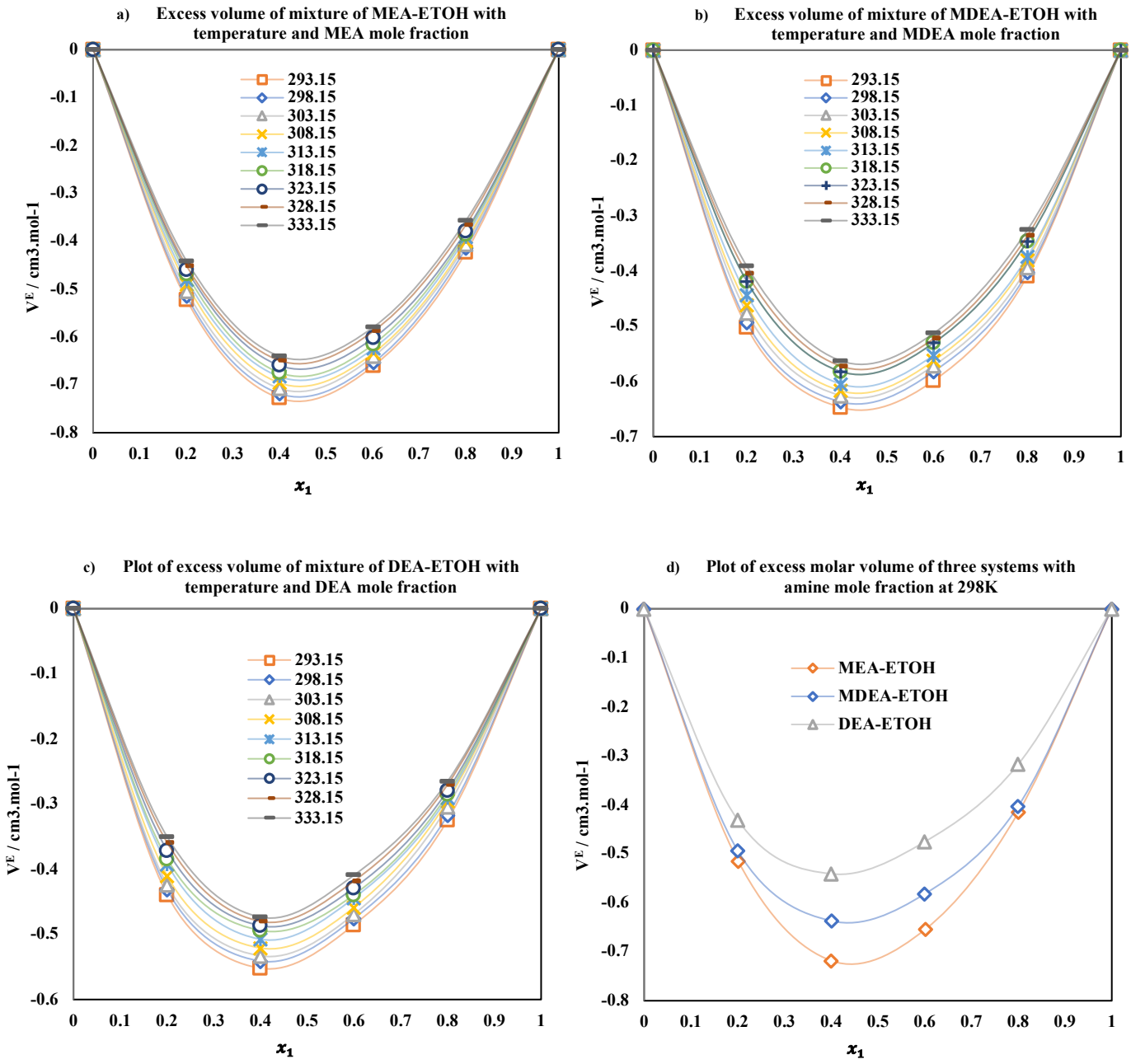

Figure 6-5 :Composition and temperature dependency of excess molar volume of the alkanolamines and ethanol solutions (a, b and c) and comparison of the excess molar volume of three system versus mole fraction of alkanolamines at 298K

All the values of excess molar volumes were correlated using the Redlich–Kister equation [178].

$$V^E = x_1 x_2 \sum_{p=0}^{m} A_p (x_1 - x_2)^p \qquad 6\text{-}2$$

Where A_p are adjustable parameters which are determined using Least-squares method and p is the polynomial expansion degree. The optimization of the number of adjustable parameters is necessary for minimizing the risk of over-fitting and mal-prediction of the data. Thus, despite the higher order of polynomial can cause better fitting, in order to avoid over-determination of data, the optimum number of adjustable parameters should be determined using the Least-Square Method.

The standard deviation of the related quantity is calculated by the following expression:

$$\boldsymbol{\sigma} = \left[\frac{\sum_{n=1}^{N} (Y_{exp} - Y_{cal})^2}{(N - (m+1))} \right]^{1/2} \qquad 6\text{-}3$$

Where m and N are the number of data points and estimated parameters, respectively. The optimum number of adjustable parameters in this work is considered three regarding there is no significant decrease in the standard deviation with the increase in the order of polynomial. The regressed values of A_p along with the standard deviation at different temperatures are presented in **Table 6-8.**

Table 6-8: Redlich− Kister fitting coefficient of the excess volume and Standard Deviations (σ) for the Binary Mixtures at T = 293.15− 323.15 K and P = 0.101MPa									
T (K)	**293.15**	**298.15**	**303.15**	**308.15**	**313.15**	**318.15**	**323.15**	**328.15**	**333.15**
MEA-ETOH									
A_0	-2.893	-2.862	-2.808	-2.772	-2.723	-2.693	-2.633	-2.583	-2.550
A_1	0.585	0.599	0.534	0.491	0.474	0.457	0.438	0.474	0.466
A_2	-0.074	0.011	-0.105	-0.033	-0.003	0.070	0.039	0.082	0.156
σ	0.005	0.003	0.007	0.007	0.006	0.007	0.007	0.008	0.008
MDEA-ETOH									
A_0	-2.561	-2.520	-2.474	-2.435	-2.399	-2.349	-2.307	-2.276	-2.240
A_1	0.454	0.487	0.485	0.453	0.389	0.406	0.411	0.388	0.377
A_2	-0.794	-0.780	-0.702	-0.550	-0.433	-0.295	-0.231	-0.109	-0.002
σ	0.006	0.005	0.007	0.006	0.007	0.006	0.007	0.007	0.008
DEA-ETOH									
A_0	-2.133	-2.090	-2.064	-2.020	-1.964	-1.926	-1.891	-1.859	-1.827
A_1	0.615	0.609	0.633	0.608	0.556	0.526	0.503	0.499	0.487
A_2	-0.702	-0.687	-0.582	-0.506	-0.464	-0.457	-0.386	-0.294	-0.262
σ	0.004	0.004	0.002	0.002	0.006	0.002	0.005	0.008	0.008

Another property that is used to describe the deviation between the real and ideal solution is partial molar volume [166]. It is the contribution of a component to the total volume of the mixture. Although the molar volume can have only the positive value, partial molar volume can be a positive or negative quantity. This property is calculated from the equations below [166]:

$$\bar{V}_1 = V^E + V_1 + (1 - x_1)\left(\frac{\partial V^E}{\partial x_1}\right)_{T,P} \quad 6\text{-}4$$

$$\bar{V}_2 = V^E + V_2 - x_1\left(\frac{\partial V^E}{\partial x_1}\right)_{T,P} \quad 6\text{-}5$$

Where $\bar{V}_1$ and $\bar{V}_2$ are the molar volumes of the pure components of 1 and 2 in the system. By substitution of Equation 4-1 into Equations 4-3 and 4-4, the following equations for component 1 and 2 can be obtained:

$$\bar{V}_1 = V_1 + (1 - x_1)^2 \sum_{p=0}^{m} A_p\,(2x_1 - 1)^p + 2x_1(1 - x_1)^2 \sum_{p=1}^{m} A_p\,(p)(2x_1 - 1)^{p-1} \quad 6\text{-}6$$

$$\bar{V}_2 = V_2 + (x_1)^2 \sum_{p=0}^{m} A_p\,(2x_1 - 1)^p - 2{x_1}^2(1 - x_1) \sum_{p=1}^{m} A_p\,(p)(2x_1 - 1)^{p-1} \quad 6\text{-}7$$

Where A_p are the coefficients of the Redlich-Kister equation listed in **Table 6-8**.

Partial molar volume at infinite dilution ($\bar{V}_i^{\infty}$) is another important property of the solution that can be estimated directly from partial molar volume.

By setting x_1= 0 in equation 6-6, the partial molar volume of component 1 (alkanolamines) at infinite dilution in component 2 (alcohol) can be calculated [166], [277].

$$\bar{V}_1^{\infty} = V_1 + \sum_{p=0}^{m} A_p\,(-1)^p \quad 6\text{-}8$$

Similarly, setting x_1=1 in equation 6-7 leads to the partial molar volume of component 2 at infinite dilution in component 1 [166],[277].

$$\bar{V}_2^{\infty} = V_2 + \sum_{p=0}^{m} {A_p}^p \quad 6\text{-}9$$

In equations 6-8 and 6-9, $\bar{V}_1^{\infty}$ and $\bar{V}_2^{\infty}$ represent the partial molar volume of alkanolamine at infinite dilution in ethanol and partial molar volume of ethanol at infinite dilution in alkanolamine, respectively.

Another approach to calculate the partial molar volume at infinite dilution without use of Redlich-Kister parameters, is through the extrapolation of the apparent molar volume ($V_{\varphi,i}$). Apparent molar volume is defined as the deviation between the volume of the pure solvent per mole of the solute and the volume of the solution. The apparent molar volume of component 1 and 2 can be calculated as [277]:

$$V_{\varphi,1} = V_1 + \frac{V^E}{x_1} \quad 6\text{-}10$$

$$V_{\varphi,2} = V_2 + \frac{V^E}{(1 - x_1)} \quad 6\text{-}11$$

In which $V_{\varphi,1}$and $V_{\varphi,2}$ are the apparent molar volumes of alkanolamines in ethanol and ethanol in alkanolamines, respectively.

By extrapolation the $V_{\varphi,1}$ to $x_1 \rightarrow 0$ and $V_{\varphi,2}$ to $x_2 \rightarrow 0$, the partial molar volume of component 1 and 2 at infinite dilution can be obtained [277]. The extrapolations were applied using the Excel Trend Function. At each constant temperature, x_i refers to mole fractions and y_i refers to the apparent molar volumes.(i= component 1 and 2)

Results of the $\bar{V}_1^{\infty}$ and $\bar{V}_2^{\infty}$ calculated using two methods along with the molar volumes of two components at different temperatures are listed in **Table 6-9**. The values of the partial molar volumes at infinite dilution for alkanolamines and ethanol which are calculated from equations 6-8 and 6-9 are in a good agreement with the values obtained from equations 6-10 and 6-11. Further considering **Table 6-9**, it can be also seen that at the constant temperature, all values of the partial molar volumes at infinite dilution are less than corresponding molar volumes of pure components. This trend can be attributed to the packing effect and formation of hydrogen bond between solvent and solute [278].It is also clear that both apparent and partial molar volumes are the increasing function of temperature and the values of partial molar volumes are slightly higher than corresponding apparent molar volumes.

Table 6-9:Molar volumes of the pure components and partial molar volumes at infinite dilution and at T= 293.15− 323.15 K and P = 0.101MPa						
T (K)	**V_1(cm^3.mol^{-1})**	**V_2(cm^3.mol^{-1})**	**$\overline{V_1}^{\infty}$(cm^3.mol^{-1}) (eq 6-8)**	**$\overline{V_2}^{\infty}$(cm^3.mol^{-1}) (eq 6-9)**	**$\overline{V_1}^{\infty}$(cm^3.mol^{-1}) (eq 6-10)**	**$\overline{V_2}^{\infty}$(cm^3.mol^{-1}) (eq 6-11)**
MEA(x_1)-ETOH						
293.15	60.098	58.354	56.546	55.972	56.850	55.730
298.15	60.327	58.678	56.877	56.426	56.879	56.102
303.15	60.582	59.013	57.136	56.634	57.438	56.487
308.15	60.816	59.336	57.521	57.023	57.752	56.841
313.15	61.067	59.658	57.867	57.407	58.066	57.212
318.15	61.306	60.023	58.225	57.857	58.368	57.613
323.15	61.556	60.338	58.523	58.182	58.681	57.968
328.15	61.802	60.724	58.828	58.697	58.968	58.436
333.15	62.053	61.052	59.193	59.124	59.276	58.812
MDEA(x_1)-ETOH						
293.15	114.514	58.354	110.704	55.453	111.459	55.874
298.15	115.002	58.678	111.216	55.865	111.549	56.246
303.15	115.400	59.013	111.738	56.321	112.484	56.627
308.150	115.957	59.336	112.520	56.805	113.114	57.020
313.15	116.279	59.658	113.058	57.215	113.541	57.369
318.15	116.717	60.023	113.666	57.785	114.055	57.831
323.15	117.134	60.338	114.186	58.211	114.529	58.207
328.15	117.453	60.724	114.680	58.728	114.925	58.643
333.15	117.876	61.052	115.257	59.187	115.420	59.027
DEA(x_1)-ETOH						
293.15	95.817	58.354	92.367	56.134	93.137	56.399
298.15	96.115	58.678	92.728	56.511	93.167	56.767
303.15	96.379	59.013	93.100	57.000	93.784	57.172
308.15	96.672	59.336	93.537	57.419	94.156	57.545
313.15	97.011	59.658	94.027	57.787	94.599	57.898
318.15	97.307	60.023	94.399	58.166	94.949	58.289
323.15	97.523	60.338	94.742	58.564	95.236	58.639
328.15	97.832	60.724	95.180	59.070	95.607	59.076
333.15	98.142	61.052	95.567	59.450	95.968	59.435

6.4 Correlations

Accurate representation of experimental data on thermo-physical properties are pre-requisites to design the perfect equipment for many chemical processes including CO_2 capture and storage processes. This need leads researchers to develop precise models to correlate the experimental data. As such, a number of methods have been proposed to correlate experimental data of unloaded amine-based solutions, which has been explained in chapter 3 section 3-6. In this study, after measurement of the experimental data for density, viscosity and refractive index of the investigated binary mixtures at different temperatures, some correlations were used to correlate the experimental data which are discussed in the following sections.

6.4.1 **Density correlation**

In this study, three methods were evaluated to correlate the density data of binary solutions. Densities of the mixtures of MEA, MDEA and DEA with ethanol were correlated using the modified Graber equations and Jouyban-Acree model as represented by equations 3-90 to 3-92, respectively. All the equations are a function of temperature and concentration.

The objective function (%AARD) was minimized to calculate the regressed coefficients of these equations. Experimental density values were fitted to modified Graber equations and Jouyban-Acree model by Least-Square Method to investigate the corresponding regressed coefficients.

The optimization of the number of regressed coefficients is necessary for minimizing the risk of over-fitting and mal-prediction of the data. Thus, despite the higher order of polynomial can cause better fitting, in order to avoid over-determination of data, the optimum number of regressed coefficients should be determined using the Least-Square Method. The optimum number of adjustable parameters for Jouyban-Acree Model was considered three after there was no significant decrease in the standard deviation with the increase in the order of polynomial.

Table 6-10, Table 6-12 and **Table 6-14** present the calculated density values of binary mixture of MEA-ETOH, MDEA-ETOH and DEA-ETOH from correlations at temperatures ranging from 293.15 to 333.15 K. As such, the values of regressed parameters of these equations for the studied systems together with the values for %AARD are tabulated in **Table 6-11**, **Table 6-13** and ,**Table 6-15.**

The studied models discussed in this work are able to correlate densities of amines- Ethanol solutions with minimal average deviations. Comparison of the %AARD for MEA-ETOH, MDEA-ETOH and DEA-ETOH solutions between the studied models in this work are listed in Table 6-16. As it can be seen from **Table 6-16**, the %AARD values obtained from the Modified Graber methods are very close for all three mixtures. Hence, it can be concluded that the concentration of the second component, which is ethanol in this study, does not impact the density properties of the mixtures noticeably. Also, the %AARD of Jouyban−Acree method are larger than Graber methods for MDEA-ETOH and DEA-ETOH, however, this amount is the lowest for MEA-ETOH mixture.

Table 6-10 :Density results for binary mixture of MEA(x_1)-ETOH at T = (293.15 to 343.15) K and P = 0.101MPa					
T(K)	**x_1**	**Experimental density**	**Calculated density using Modified Graber equation (8 parameters) Eq (3-91)**	**Calculated density using Modified Graber equation (6 parameters) Eq (3-90)**	**Calculated density using Jouyban-Acree Model Eq (3-92)**
293.15	**0.2010**	0.84371	0.84355	0.84345	0.84388
	0.4004	0.89293	0.89205	0.89234	0.89322
	0.6020	0.93816	0.93805	0.93800	0.93879
	0.8006	0.97892	0.97922	0.97904	0.97930
298.15	**0.2010**	0.83920	0.83900	0.83894	0.83930
	0.4004	0.88844	0.88754	0.88788	0.88859
	0.6020	0.93381	0.93357	0.93357	0.93429
	0.8006	0.97465	0.97477	0.97465	0.97507
303.15	**0.2010**	0.83451	0.83449	0.83447	0.83458
	0.4004	0.88371	0.88307	0.88345	0.88374
	0.6020	0.92909	0.92913	0.92919	0.92948
	0.8006	0.97034	0.97035	0.97030	0.97044
308.15	**0.2010**	0.83000	0.83002	0.83003	0.83008
	0.4004	0.87924	0.87864	0.87906	0.87917
	0.6020	0.92478	0.92473	0.92484	0.92499
	0.8006	0.96618	0.96597	0.96599	0.96618
313.15	**0.2010**	0.82556	0.82559	0.82563	0.82563
	0.4004	0.87471	0.87424	0.87470	0.87459
	0.6020	0.92032	0.92036	0.92052	0.92044
	0.8006	0.96179	0.96163	0.96171	0.96179
318.15	**0.2010**	0.82072	0.82119	0.82127	0.82079
	0.4004	0.87000	0.86988	0.87038	0.86975
	0.6020	0.91577	0.91603	0.91624	0.91577
	0.8006	0.95751	0.95732	0.95747	0.95744
323.15	**0.2010**	0.81646	0.81682	0.81694	0.81652
	0.4004	0.86560	0.86555	0.86610	0.86536
	0.6020	0.91139	0.91173	0.91200	0.91138

	0.8006	0.95328	0.95304	0.95326	0.95318
328.15	**0.2010**	0.81154	0.81249	0.81264	0.81154
	0.4004	0.86073	0.86126	0.86184	0.86040
	0.6020	0.90665	0.90747	0.90778	0.90661
	0.8006	0.94880	0.94880	0.94908	0.94873
333.15	**0.2010**	0.80722	0.80819	0.80838	0.80723
	0.4004	0.85640	0.85699	0.85762	0.85598
	0.6020	0.90234	0.90323	0.90360	0.90221
	0.8006	0.94456	0.94459	0.94493	0.94448

Table 6-11 : Regressed Parameters of different methods for the MEA-ETOH mixture at 293.15–333.15 K and P=0.101MPa

Modified Graber equation (8 parameters) Eq (3-91)		**Modified Graber equation (6 parameters) Eq (3-90)**		**Jouyban-Acree Model Eq (3-92)**	
A_1	-3.21565	**A_1**	-1.74277	**A_0**	26.5331
A_2	0.00516	**A_2**	0.00631	**A_1**	-3.65468
A_3	1.83922	**A_3**	0.14265	**A_2**	0.088514
A_4	0.39819	**A_4**	1.32645		
A_5	1.39775	**A_5**	-0.03135		
A_6	-0.10667	**A_6**	0.00234		
A_7	-0.12376				
A_8	-0.03207				
%AARD	**0.0436**	**%AARD**	**0.0450**	**%AARD**	**0.0118**

Table 6-12: Density results for binary mixture of MDEA(x_1)-ETOH at T = (293.15 to 343.15) K and P = 0.101MPa					
T(K)	**x_1**	**Experimental density**	**Calculated density using Modified Graber equation (8 parameters) Eq (3-91)**	**Calculated density using Modified Graber equation (6 parameters) Eq (3-90)**	**Calculated density using Jouyban-Acree Model Eq (3-92)**
293.15	**0.2002**	0.87854	0.87777	0.87725	0.88016
	0.4013	0.93960	0.93860	0.93897	0.94263
	0.5998	0.98328	0.98269	0.98274	0.98612
	0.8000	1.01625	1.01606	1.01586	1.01866
298.15	**0.2002**	0.87392	0.87335	0.87289	0.87472
	0.4013	0.93500	0.93433	0.93470	0.93683
	0.5998	0.97858	0.97851	0.97854	0.98051
	0.8000	1.01171	1.01193	1.01171	1.01350
303.15	**0.2002**	0.86936	0.86898	0.86856	0.86942
	0.4013	0.93072	0.93009	0.93046	0.93138
	0.5998	0.97452	0.97436	0.97438	0.97534
	0.8000	1.00786	1.00784	1.00760	1.00900
308.15	**0.2002**	0.86460	0.86464	0.86427	0.86407
	0.4013	0.92585	0.92588	0.92627	0.92558
	0.5998	0.96955	0.97024	0.97025	0.96954
	0.8000	1.00280	1.00379	1.00352	1.00349
313.15	**0.2002**	0.86047	0.86033	0.86001	0.85916
	0.4013	0.92209	0.92171	0.92210	0.92063
	0.5998	0.96614	0.96616	0.96615	0.96500
	0.8000	0.99966	0.99977	0.99947	0.99966
318.15	**0.2002**	0.85565	0.85606	0.85579	0.85367
	0.4013	0.91750	0.91758	0.91797	0.91500
	0.5998	0.96176	0.96212	0.96209	0.95968
	0.8000	0.99546	0.99578	0.99546	0.99495
323.15	**0.2002**	0.85150	0.85183	0.85160	0.84885
	0.4013	0.91343	0.91347	0.91388	0.90997
	0.5998	0.95778	0.95810	0.95805	0.95485

	0.8000	0.99161	0.99183	0.99148	0.99060
328.15	**0.2002**	0.84691	0.84762	0.84744	0.84345
	0.4013	0.90937	0.90941	0.90981	0.90468
	0.5998	0.95419	0.95412	0.95406	0.95012
	0.8000	0.98840	0.98791	0.98753	0.98672
333.15	**0.2002**	0.84267	0.84346	0.84332	0.83861
	0.4013	0.90527	0.90537	0.90578	0.89967
	0.5998	0.95021	0.95017	0.95009	0.94532
	0.8000	0.98455	0.98401	0.98361	0.98238

Table 6-13: Regressed Parameters of different Methods for the MDEA-ETOH mixture at 293.15–333.15 K and P=0.101MPa

Modified Graber equation (8 parameters) Eq (3-91)		**Modified Graber equation (6 parameters) Eq (3-90)**		**Jouyban-Acree Model Eq (3-92)**	
A_1	-3.60089	**A_1**	-1.91565	**A_0**	74.64438
A_2	0.01555	**A_2**	0.01074	**A_1**	-29.74322
A_3	2.12277	**A_3**	0.34447	**A_2**	14.87511
A_4	0.23742	**A_4**	1.31949		
A_5	1.37914	**A_5**	-0.03095		
A_6	-0.07251	**A_6**	0.00205		
A_7	-0.07057				
A_8	-0.03289				
%AARD	**0.0461**	**%AARD**	**0.0464**	**%AARD**	**0.1443**

Table 6-14: Density results for binary mixture of DEA(x_1)-ETOH at T = (293.15 to 343.15) K and P = 0.101MPa					
T(K)	**x_1**	**Experimental density**	**Calculated density using Modified Graber equation (8 parameters) Eq (3-91)**	**Calculated density using Modified Graber equation (6 parameters) Eq (3-90)**	**Calculated density using Jouyban-Acree Model Eq (3-92)**
293.15	**0.2002**	0.88481	0.88432	0.88297	0.88743
	0.4001	0.95754	0.95694	0.95696	0.96216
	0.600	1.01506	1.01506	1.01504	1.01945
	0.800	1.06061	1.06122	1.06077	1.06402
298.15	**0.2002**	0.88050	0.88007	0.87874	0.88220
	0.4001	0.95338	0.95286	0.95295	0.95672
	0.600	1.01115	1.01111	1.01120	1.01431
	0.800	1.05682	1.05736	1.05706	1.05959
303.15	**0.2002**	0.87615	0.87587	0.87455	0.87699
	0.4001	0.94929	0.94882	0.94897	0.95140
	0.600	1.00738	1.00719	1.00739	1.00939
	0.800	1.05339	1.05353	1.05339	1.05546
308.15	**0.2002**	0.87188	0.87169	0.87039	0.87194
	0.4001	0.94520	0.94481	0.94503	0.94616
	0.600	1.00352	1.00331	1.00362	1.00446
	0.800	1.04987	1.04973	1.04975	1.05121
313.15	**0.2002**	0.86753	0.86755	0.86627	0.86689
	0.4001	0.94088	0.94084	0.94112	0.94083
	0.600	0.99930	0.99946	0.99988	0.99930
	0.800	1.04588	1.04597	1.04614	1.04657
318.15	**0.2002**	0.86291	0.86345	0.86218	0.86150
	0.4001	0.93654	0.93690	0.93725	0.93534
	0.600	0.99527	0.99564	0.99617	0.99418
	0.800	1.04219	1.04224	1.04256	1.04219
323.15	**0.2002**	0.85905	0.85938	0.85812	0.85689
	0.4001	0.93299	0.93299	0.93340	0.93069

	0.600	0.99208	0.99185	0.99249	0.98994
	0.800	1.03931	1.03854	1.03902	1.03871
328.15	**0.2002**	0.85427	0.85534	0.85410	0.85140
	0.4001	0.92851	0.92911	0.92959	0.92514
	0.600	0.98798	0.98809	0.98884	0.98480
	0.800	1.03562	1.03487	1.03550	1.03431
333.15	**0.2002**	0.85019	0.85133	0.85011	0.84662
	0.4001	0.92449	0.92527	0.92580	0.92015
	0.600	0.98409	0.98437	0.98522	0.98002
	0.800	1.03194	1.03123	1.03201	1.03007

Table 6-15: Regressed Parameters of different Methods for the DEA-ETOH mixture at 293.15–333.15 K and P=0.101MPa

Modified Graber equation (8 parameters) Eq (3-91)		**Modified Graber equation (6 parameters) Eq (3-90)**		**Jouyban-Acree Model Eq (3-92)**	
A_1	-3.50451	**A_1**	-2.02219	**A_0**	75.46181
A_2	0.01582	**A_2**	0.02026	**A_1**	-24.3512
A_3	2.20800	**A_3**	0.48939	**A_2**	9.34433
A_4	0.20484	**A_4**	1.31954		
A_5	1.37064	**A_5**	-0.03095		
A_6	-0.08253	**A_6**	0.00234		
A_7	-0.08148				
A_8	-0.03199				
%AARD	**0.0464**	**%AARD**	**0.0587**	**%AARD**	**0.1415**

Table 6-16: Comparison of the %AARD between the studied models for MEA-ETOH, MDEA-ETOH and DEA-ETOH solutions						
Models	**MEA-ETOH**		**MDEA-ETOH**		**DEA-ETOH**	
	%AARD	**SD**	**%AARD**	**SD**	**%AARD**	**SD**
Modified Graber equation (8 parameters) Eq(3-91)	0.0436	0.0005	0.0462	0.0007	0.0464	0.0007
Modified Graber equation (6 parameters) Eq(3-90)	0.0450	0.0006	0.0464	0.0006	0.0587	0.0008
Jouyban−Acree Eq(3-92)	0.0118	0.001	0.1443	0.0022	0.1415	0.0020

In addition, comparison the correlated densities for studied systems obtained from Modified Graber equation(8 parameters), Modified Graber equation(6 parameters) and Jouyban-Acree Model to the experimental densities are shown in **Figure 6-6**, **Figure 6-7** and**, Figure 6-8.**

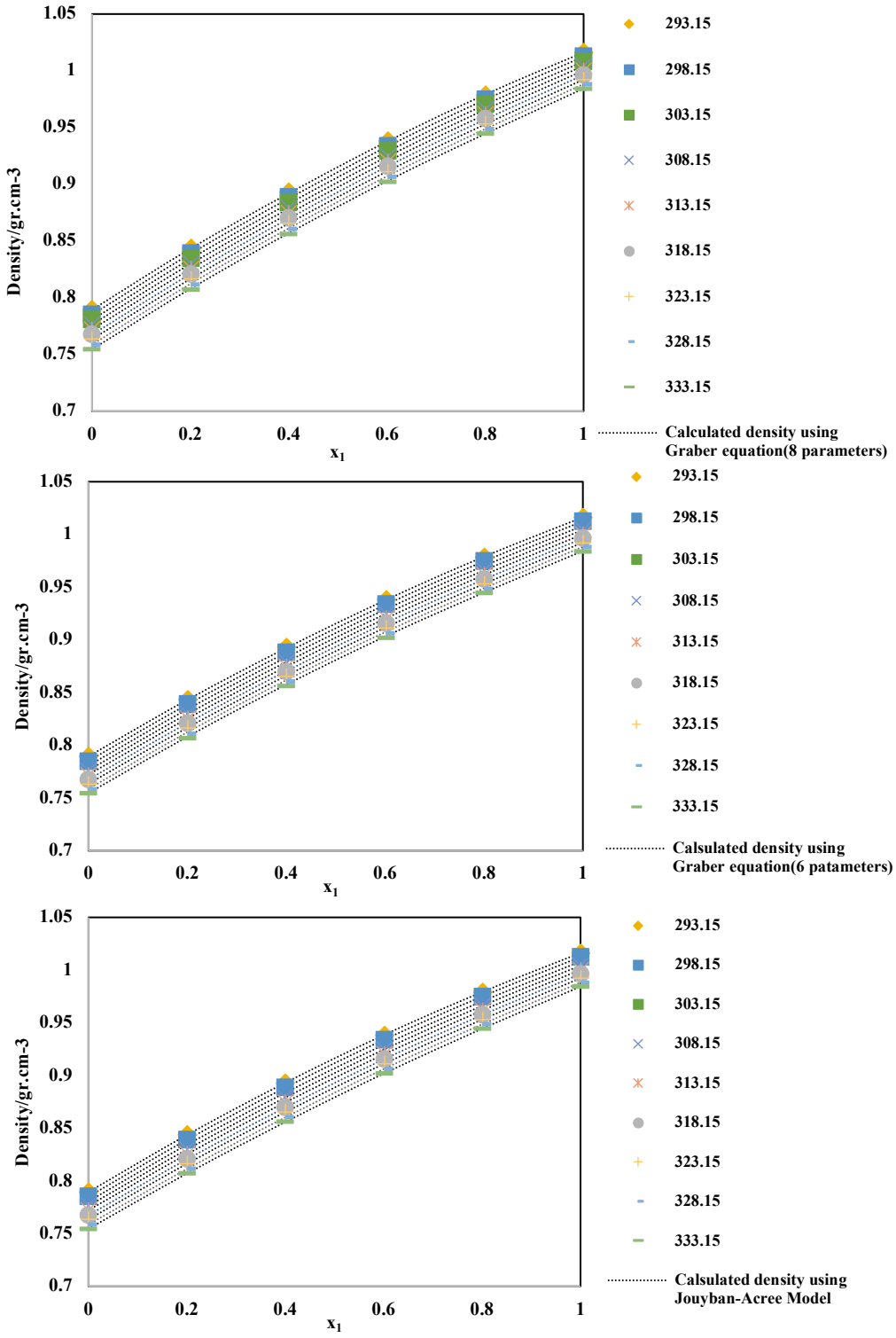

Figure 6-6 :Comparison of the calculated densities using studied models to experimental values for MEA(x_1)-ETOH solution

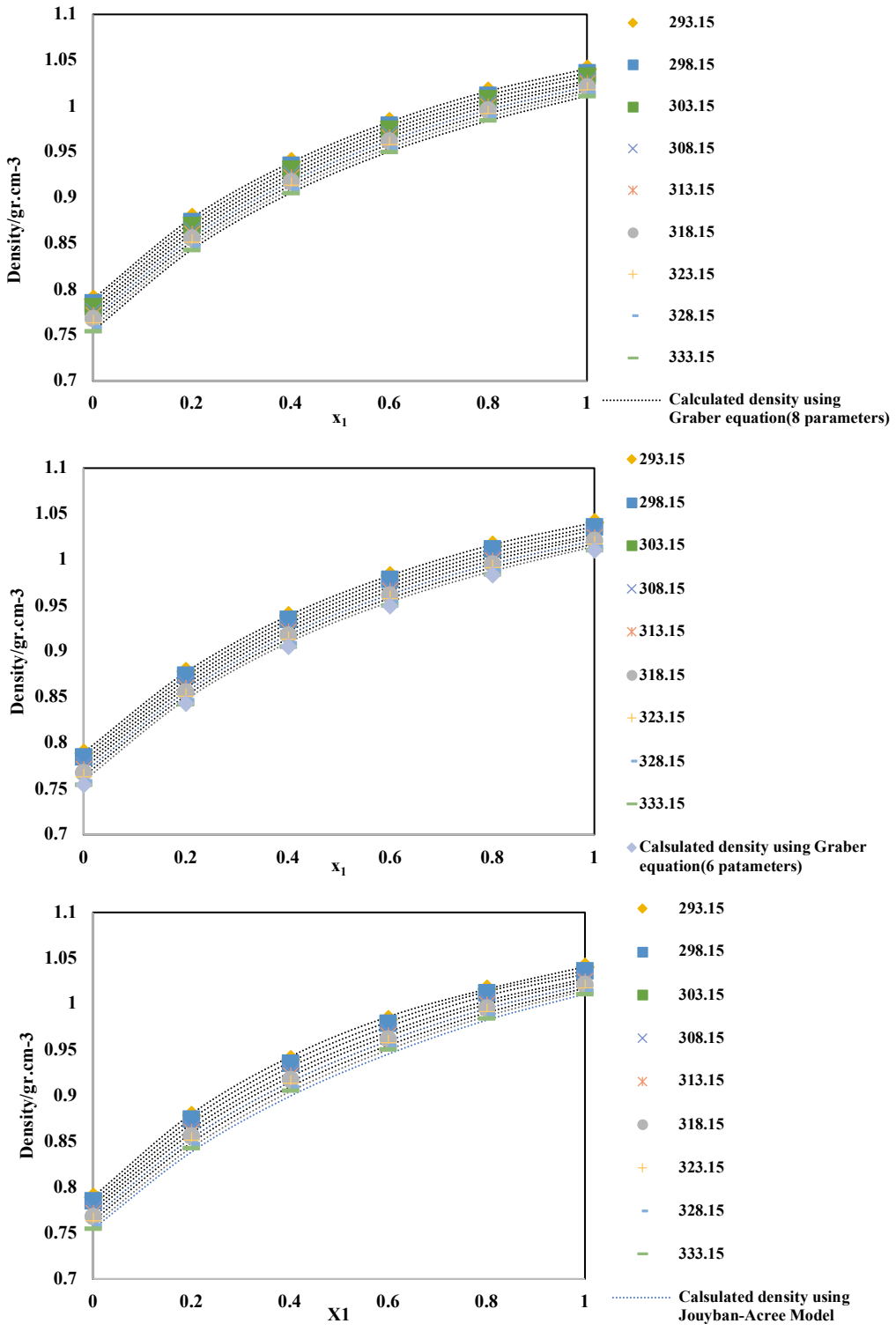

Figure 6-7 :Comparison of the calculated densities using studied models to experimental values for MDEA(x_1)-ETOH solution

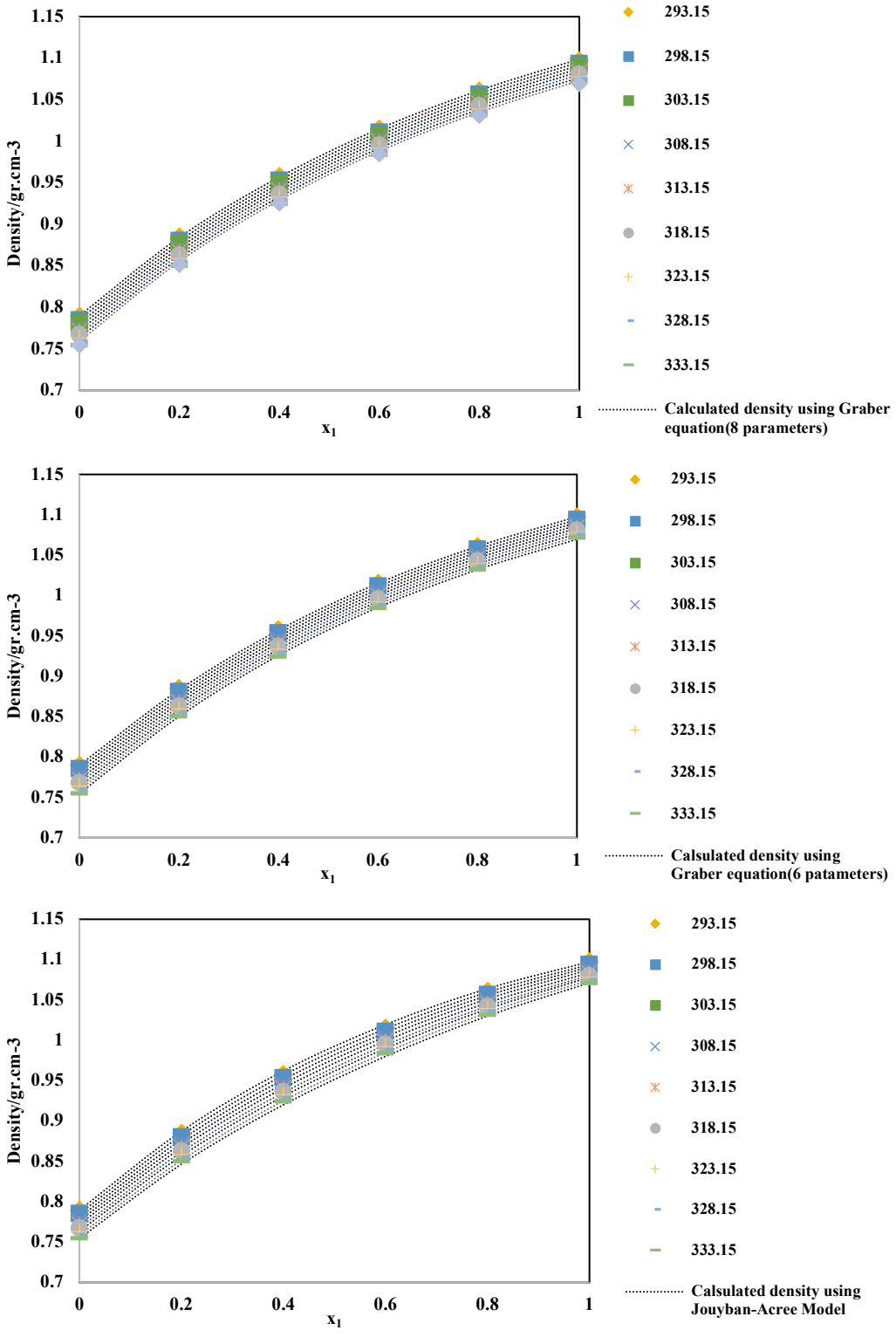

Figure 6-8 :Comparison of the calculated densities using studied models to experimental values for DEA(x_1)-ETOH solution

6.4.2 **Viscosity correlation**

In this study, the viscosity deviation of the binary mixtures of MEA-ETOH, MDEA-ETOH and DEA-ETOH were measured in the temperature range of 293.15 to 333.15 K and correlated with the Redlich-Kister type of equation. The viscosity deviation $\Delta\eta$ of binary mixtures were calculated using the following equation [166] :

$$\Delta\eta = \eta - \sum_{i=1}^{n} x_i \eta_i \qquad 6\text{-}12$$

Where η is the viscosity of mixture, η_i and $x_i$are the viscosity and mole fraction of pure components, and n is the number of components which is 2 in this study.

The results of $\Delta\eta$ for the binary solutions at different temperatures and over the whole range of composition are listed in **Table 6-17**.

The viscosity deviation versus mole fraction of studied alkanolamines (x_1) at temperatures from 303.15 to 323.15 K are graphically represented in **Figure 6-9**.

As it can be seen from this figure, the value of $\Delta\eta$ for all the solutions are negative throughout the entire mole fraction and the viscosity deviations increase with increase of temperature for all mixtures.

The viscosity of the mixture is dependent on the strength of the self-association bonds as well as the strength of the interaction between unlike molecules. Therefore, the positive or negative values of Δη depend on the competition of these two interactions. The mixtures without strong interactions between unlike molecules show negative viscosity deviations, whilst mixtures with strong cross-interactions present positive viscosity deviations [168],[166].The negative values of viscosity deviations of MEA-ethanol, MDEA-ethanol and DEA-ethanol are attributed to the weak interactions between unlike molecules. Also, the difference in the molecular size of the unlike components affects the sign and value of viscosity deviation. The larger the size difference of unlike molecules, the more negative value of viscosity deviation occurs. Hence, in this study, the smallest value (negative deviation) of viscosity deviation is corresponded to DEA-ETOH and the largest value is related to MEA-ETOH binary mixture. The variation trends of viscosity deviation for the mixtures of MDEA-ethanol and MEA-ethanol are almost coincident with those in the literature [168].

Table 6-17 :Viscosity deviations (Δη) of binary mixtures at T = (293.15 to 333.15) K and P = 0.101MPa									
Δη/mPa.s									
MEA(x_1)-ETOH									
x_1	**293.15 K**	**298.15 K**	**303.15 K**	**308.15 K**	**313.15 K**	**318.15 K**	**323.15 K**	**328.15 K**	**333.15 K**
0.2010	-3.464	-2.620	-2.028	-1.586	-1.273	-1.045	-0.858	-0.682	-0.553
0.4004	-6.117	-4.573	-3.532	-2.757	-2.112	-1.698	-1.387	-1.132	-0.908
0.6020	-7.056	-5.255	-3.878	-3.132	-2.463	-1.956	-1.604	-1.362	-1.105
0.8006	-5.384	-4.106	-2.886	-2.237	-1.863	-1.399	-1.170	-1.063	-0.844
MDEA(x_1)-ETOH									
0.2002	-18.265	-13.512	-9.710	-7.200	-5.487	-4.305	-3.374	-2.773	-2.111
0.4013	-33.525	-24.618	-17.423	-12.646	-9.671	-7.156	-5.576	-4.680	-3.446
0.5998	-40.988	-29.515	-20.629	-14.957	-11.016	-8.163	-6.353	-5.098	-4.073
0.8000	-33.192	-21.475	-16.462	-11.583	-8.541	-6.086	-4.639	-3.650	-3.322
DEA(x_1)-ETOH									
0.2002	-173.860	-108.540	-72.928	-51.190	-35.650	-25.763	-18.590	-13.657	-10.302
0.4001	-336.990	-207.960	-139.270	-96.595	-67.727	-48.910	-34.662	-25.130	-18.240
0.6000	-448.260	-277.550	-183.710	-125.380	-85.998	-61.244	-43.331	-31.685	-23.656
0.8000	-393.730	-238.520	-161.600	-108.970	-71.939	-50.152	-35.771	-28.738	-21.218

The combined expanded uncertainty U(**Δη**)= 0.020 mPa.s

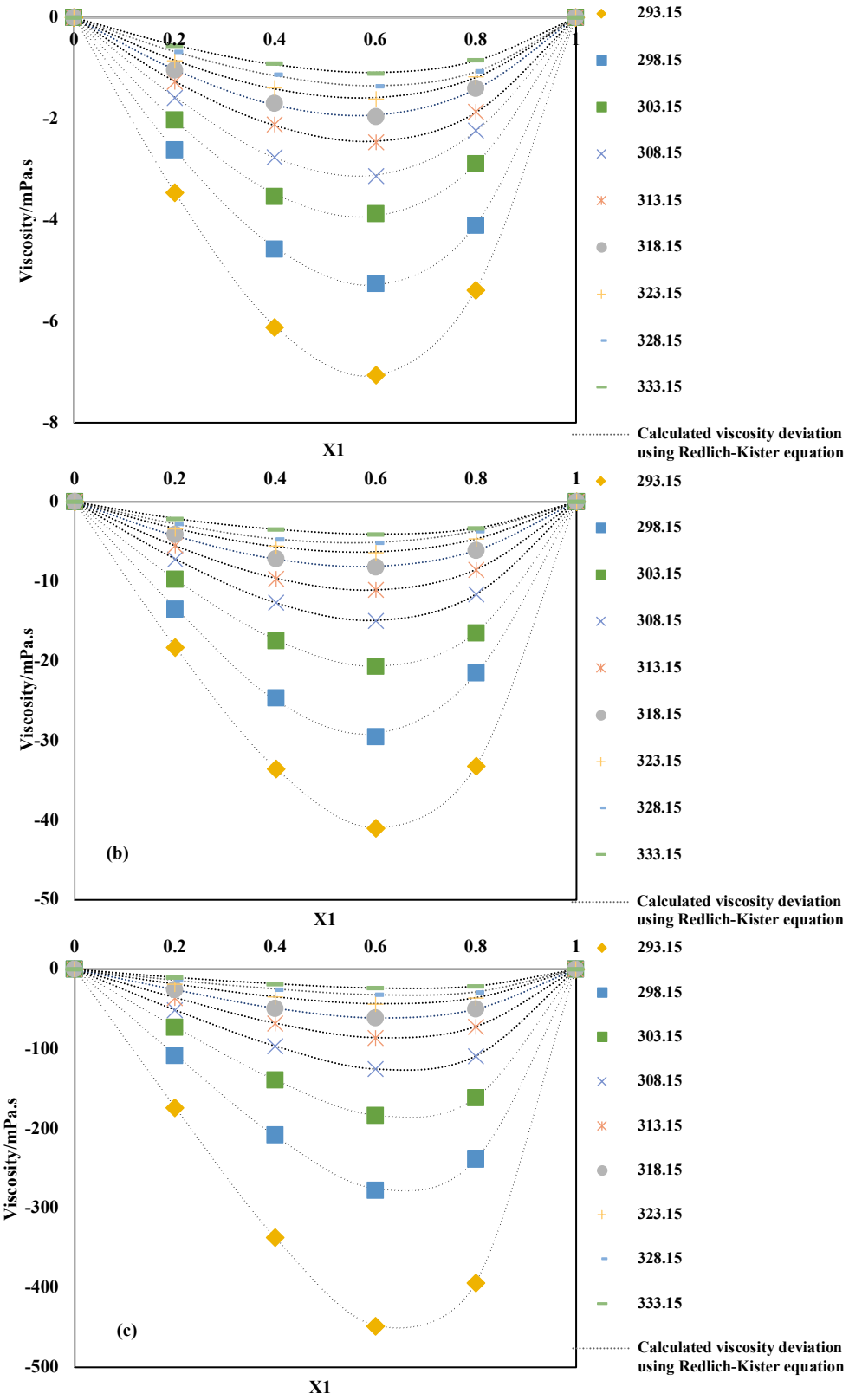

Figure 6-9: Comparison of the calculated viscosity deviation using Redlich-Kister equation to experimental values for a) MEA(x_1)-ETOH, b) MDEA(x_1)-ETOH and, c) DEA(x_1)-ETOH solutions

In addition, Redlich-Kister equation was used to correlate the viscosity deviation of binary solutions at all temperatures as shown by equation 6-13 [178] :

$$\Delta\eta = x_1 x_2 \sum_{p=0}^{m} A_p (x_1 - x_2)^p \qquad 6\text{-}13$$

Where A_p are adjustable parameters which are determined using Least-squares method and p is the polynomial expansion degree which is equal to 2 for all mixtures in this study. The polynomial parameters and standard deviations of equation 6-13 are listed in **Table 6-18**.

Table 6-18: Redlich− Kister fitting coefficient of the viscosity deviations and Standard Deviations (σ) for the Binary Mixtures at T = 293.15− 323.15 K and P = 0.101MPa

T(K)	293.15	298.15	303.15	308.15	313.15	318.15	323.15	328.15	333.15
MEA-ETOH									
A_0	-27.416	-20.403	-15.437	-12.313	-9.498	-7.609	-6.217	-5.162	-4.172
A_1	-10.076	-7.697	-4.538	-3.550	-3.229	-2.051	-1.783	-2.088	-1.639
A_2	-0.592	-1.668	-0.007	1.042	-0.826	-0.061	-0.328	-0.797	-0.530
σ	0.020	0.030	0.031	0.021	0.024	0.036	0.027	0.017	0.022
MDEA-ETOH									
A_0	-154.361	-113.075	-78.873	-57.294	-42.960	-31.814	-24.804	-20.387	-15.484
A_1	-77.989	-43.546	-34.934	-23.157	-15.589	-9.560	-6.921	-4.551	-6.376
A_2	-17.749	10.492	-8.020	-3.838	-2.397	-1.797	-0.632	0.903	-4.134
σ	0.027	0.092	0.061	0.064	0.060	0.046	0.056	0.01	0.010
DEA-ETOH									
A_0	-1618.606	-1002.278	-665.328	-457.663	-318.247	-228.507	-161.552	-116.593	-85.876
A_1	-1148.804	-687.101	-462.404	-300.963	-189.443	-127.443	-89.736	-76.554	-56.810
A_2	-429.388	-227.637	-187.093	-118.571	-49.608	-24.023	-22.971	-44.040	-34.991
σ	0.052	0.075	0.044	0.049	0.055	0.061	0.034	0.044	0.019

The combined expanded uncertainty U(**Δη**)= 0.020 mPa.s

Also, the viscosity of the studied binary mixtures was correlated using different models including McAllister Model, Jouyban-Acree Model, Herraez Model, and Redlich-Kister equation (section 3-6-2).

Comparison of correlated viscosities of binary mixture of MEA-ETOH, MDEA-ETOH and, DEA-ETOH from different correlations to experimental viscosity at temperatures ranging from 293.15 to 333.15 K and P=0.101MPa are presented in **Table 6-19**.

Table 6-19: Comparison the experimental Viscosity of studied binary mixtures to the calculated viscosity of different models at 293.15–333.15 K and P=0.101MPa						
T(K)	**X_1**	**Exp**	**Jouyban-Acree Eq (3-96)**	**Redlich -Kister Eq(3-85)**	**Herreaz Eq(3-97)**	**Mc-Allister (Three -body) Eq(3-94)**
MEA(x_1) -ETOH						
293.15	**0.201**	2.14	2.166	2.14	2.138	2.536
	0.4004	3.893	3.999	3.893	3.896	4.46
	0.6020	7.409	7.374	7.409	7.407	7.901
	0.8006	13.47	13.264	13.526	13.471	13.695
298.15	**0.201**	1.91	1.942	1.91	1.91	2.276
	0.4004	3.383	3.468	3.371	3.392	3.843
	0.6020	6.164	6.183	6.164	6.161	6.551
	0.8006	10.725	10.76	10.88	10.736	11.003
303.15	**0.201**	1.7	1.726	1.7	1.7	2.038
	0.4004	2.92	3.004	2.99	2.92	3.391
	0.6020	5.327	5.219	5.312	5.238	5.693
	0.8006	9.032	8.852	9.032	9.069	9.308
308.15	**0.201**	1.5	1.494	1.5	1.5	1.81
	0.4004	2.534	2.561	2.55	2.511	2.933
	0.6020	4.389	4.38	4.39	4.39	4.746
	0.8006	7.481	7.318	7.357	7.481	7.56
313.15	**0.201**	1.36	1.399	1.36	1.36	1.647
	0.4004	2.304	2.321	2.244	2.212	2.573
	0.6020	3.756	3.838	3.756	3.756	4.082
	0.8006	6.132	6.203	6.145	6.233	6.397
318.15	**0.201**	1.21	1.252	1.21	1.236	1.474
	0.4004	2.039	2.043	1.997	2.001	2.279
	0.6020	3.279	3.323	3.295	3.306	3.591
	0.8006	5.312	5.283	5.27	5.303	5.547
323.15	**0.201**	1.1	1.138	1.1	1.122	1.347
	0.4004	1.816	1.825	1.782	1.784	2.036
	0.6020	2.857	2.916	2.857	2.879	3.135
	0.8006	4.53	4.556	4.479	4.523	4.756
328.15	**0.201**	1.02	1.02	1.02	1.02	1.257
	0.4004	1.625	1.616	1.593	1.58	1.847
	0.6020	2.462	2.55	2.47	2.472	2.717

	0.8006	3.812	3.937	3.816	3.812	4.003
333.15	**0.201**	0.92	0.926	0.92	0.92	1.14
	0.4004	1.44	1.439	1.422	1.409	1.644
	0.6020	2.128	2.227	2.16	2.161	2.382
	0.8006	3.261	3.371	3.261	3.252	3.452
MDEA(x_1) -ETOH						
293.15	**0.2010**	3.295	3.18	3.283	3.284	3.371
	0.4004	8.525	8.533	8.423	8.073	8.493
	0.6020	21.286	21.459	21.205	21.088	21.648
	0.8006	49.48	49.974	49.362	49.367	50.307
298.15	**0.2010**	2.895	2.829	2.886	2.883	3.126
	0.4004	7.188	7.281	7.218	7.208	7.688
	0.6020	17.49	17.56	18.416	17.917	18.781
	0.8006	40.86	39.226	40.718	39.49	41.112
303.15	**0.2010**	2.561	2.475	2.552	2.552	2.946
	0.4004	6.188	6.103	6.223	6.055	6.699
	0.6020	14.175	14.111	14.051	14.05	14.604
	0.8006	29.63	30.21	29.574	29.628	29.606
308.15	**0.2010**	2.269	2.116	2.261	2.261	2.624
	0.4004	5.468	5.072	5.324	5.222	5.946
	0.6020	11.69	11.402	11.626	11.623	12.686
	0.8006	23.67	23.732	23.534	23.629	24.56
313.15	**0.2010**	1.984	1.961	1.977	1.977	2.306
	0.4004	4.466	4.494	4.542	4.493	4.938
	0.6020	9.7	9.659	9.613	9.622	10.252
	0.8006	18.81	19.22	18.807	18.776	19.522
318.15	**0.2010**	1.799	1.743	1.992	1.992	2.336
	0.4004	4.315	3.899	4.329	4.325	4.796
	0.6020	8.606	8.181	8.555	8.665	8.956
	0.8006	16.026	15.892	15.833	15.999	15.646
323.15	**0.2010**	1.565	1.565	1.559	1.56	1.849
	0.4004	3.618	3.396	3.63	3.465	3.74
	0.6020	7.04	6.915	7.197	7.048	7.35
	0.8006	12.99	13.034	12.968	12.947	13.286
328.15	**0.2010**	1.354	1.394	1.356	1.35	1.599
	0.4004	2.952	2.968	2.949	2.962	3.155

	0.6020	5.993	5.93	5.963	5.954	6.158
	0.8006	10.93	10.968	10.905	10.806	11.107
333.15	**0.2010**	1.251	1.254	1.252	1.247	1.485
	0.4004	2.699	2.591	2.707	2.583	2.778
	0.6020	4.819	5.025	4.821	4.83	5.072
	0.8006	8.34	9.02	8.275	8.327	8.76
DEA(x_1) -ETOH						
293.15	**0.2002**	5.347	5.508	5.613	5.347	5.154
	0.4001	20	21.951	19.467	19.795	20.887
	0.6000	86.5	82.132	87.033	90.771	84.891
	0.8000	318.9	296.559	318.634	290.574	301.041
298.15	**0.2002**	4.63	4.722	5.549	4.63	5.117
	0.4001	17.14	17.426	15.302	10.35	17.978
	0.6000	59.48	60.37	61.318	59.577	59.034
	0.8000	210.5	201.65	209.581	210.945	180.501
303.15	**0.2002**	4.034	4.054	4.055	4.034	4.604
	0.4001	13.56	14.106	13.517	10.602	15.205
	0.6000	44.98	46.093	45.022	45.33	45.984
	0.8000	143	144.986	142.979	143.425	129.765
308.15	**0.2002**	3.254	3.407	3.231	3.254	3.732
	0.4001	11.35	11.35	11.396	11.26	12.008
	0.6000	36.07	35.507	36.024	38.832	36.125
	0.8000	106	106.813	106.023	105.62	99.581
313.15	**0.2002**	3.125	3.098	3.15	3.125	3.609
	0.4001	8.93	9.699	8.881	8.629	10.646
	0.6000	28.54	28.517	28.589	29.226	28.56
	0.8000	80.5	80.536	80.475	80.582	71.9
318.15	**0.2002**	2.873	2.699	2.885	2.873	3.329
	0.4001	7.56	8.101	7.536	7.386	9.377
	0.6000	23.06	22.835	23.084	23.179	23.126
	0.8000	62	61.763	61.988	62	54.406
323.15	**0.2002**	2.493	2.381	2.508	2.493	2.902
	0.4001	6.77	6.821	6.739	6.723	7.769
	0.6000	18.45	18.355	18.481	18.494	18.596
	0.8000	46.37	47.347	46.355	44.595	42.049
328.15	**0.2002**	2.269	2.078	2.072	2.269	2.656

	0.4001	6.06	5.736	6.455	6.056	6.731
	0.6000	14.77	14.867	14.375	14.885	14.942
	0.8000	32.99	36.908	33.187	32.876	31.855
333.15	**0.2002**	2.083	1.855	2.074	2.083	2.45
	0.4001	5.92	4.939	5.937	5.876	5.993
	0.6000	12.28	12.35	12.263	13.319	12.667
	0.8000	26.5	29.551	26.509	26.5	25.68

The predicted viscosity of the studied binary mixtures from Jouyban-Acree Model presented a good agreement with the experimental viscosity values, with average absolute relative deviation of 1.081, 1.620 and 1.518 for MEA-ETOH, MDEA-ETOH and, DEA-ETOH mixtures, respectively. The value of regressed parameters for the entire range of temperature are presented in **Table 6-20**.

Table 6-20:Regressed Parameters of Jouyban-Acree Model for binary mixtures at 293.15–333.15 K and P=0.101MPa

MEA-ETOH		**MDEA-ETOH**		**DEA-ETOH**	
A_0	0.165	A_0	0.873	A_0	1.107
A_1	23.780	A_1	98.530	A_1	-39.946
A_2	8.596	A_2	7.017	A_2	279.326
SD	0.065				
AARD%	1.081	**AARD%**	1.620	**AARD%**	1.518

The comparison of the calculated viscosity from 2nd order polynomial version of Jouyban-Acree Model to experimental viscosity of MEA-ETOH, MDEA-ETOH and DEA-ETOH mixture is shown in **Figure 6-10**.

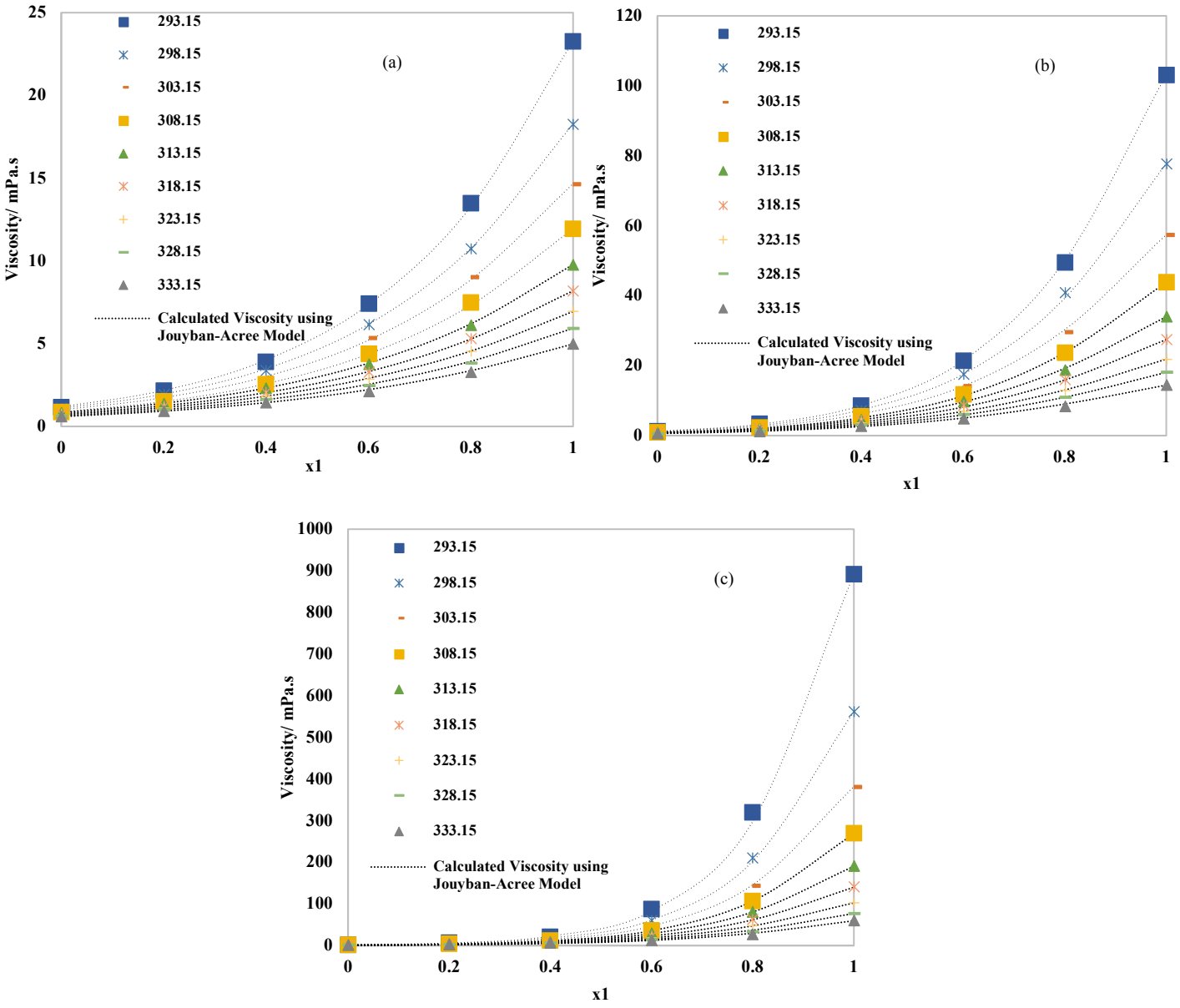

Figure 6-10: Comparison of the calculated viscosity using Jouyban-Acree Model to experimental values for a) MEA(x_1)-ETOH, b) MDEA(x_1)-ETOH and, c) DEA(x_1)-ETOH solutions

A second order version of Herreaz model was used to correlate the experimental viscosity of the studied mixtures. The values of the regressed parameters calculated using this model together with the %AARD are tabulated in **Table 6-21**.

Also, the comparison of the calculated viscosity using this Model to experimental viscosity of MEA-ETOH, MDEA-ETOH, and DEA-ETOH mixture as a function of amine mole fraction are presented in **Figure 6-11.**

Table 6-21: Herreaz fitting coefficients of the viscosity and %AARD for binary solutions at T=293.15 -333.15 K and P=0.1 mPa

T	**293.15**	**298.15**	**303.15**	**308.15**	**313.15**	**318.15**	**323.15**	**328.15**	**333.15**
MEA-ETOH									
A_0	0.694	0.679	0.754	0.764	0.762	0.751	0.739	0.703	0.697
A_1	-1.057	-0.926	-1.106	-1.117	-1.056	-0.916	-0.835	-0.749	-0.647
A_2	0.551	0.442	0.581	0.615	0.549	0.431	0.372	0.359	0.263
%AARD	0.295								
MDEA-ETOH									
A_0	0.618	0.648	0.641	0.669	0.671	0.705	0.715	0.718	0.630
A_1	-1.245	-1.207	-1.123	-1.122	-1.028	-0.991	-0.966	-0.939	-0.637
A_2	0.738	0.664	0.599	0.588	0.483	0.467	0.379	0.343	0.152
%AARD	0.286								
DEA-ETOH									
A_0	0.427	0.547	0.520	0.502	0.569	0.599	0.542	0.490	0.467
A_1	-1.050	-1.484	-1.319	-1.099	-1.315	-1.374	-1.083	-0.832	-0.567
A_2	0.678	1.046	0.892	0.652	0.840	0.888	0.631	0.425	0.158
%AARD	1.341								

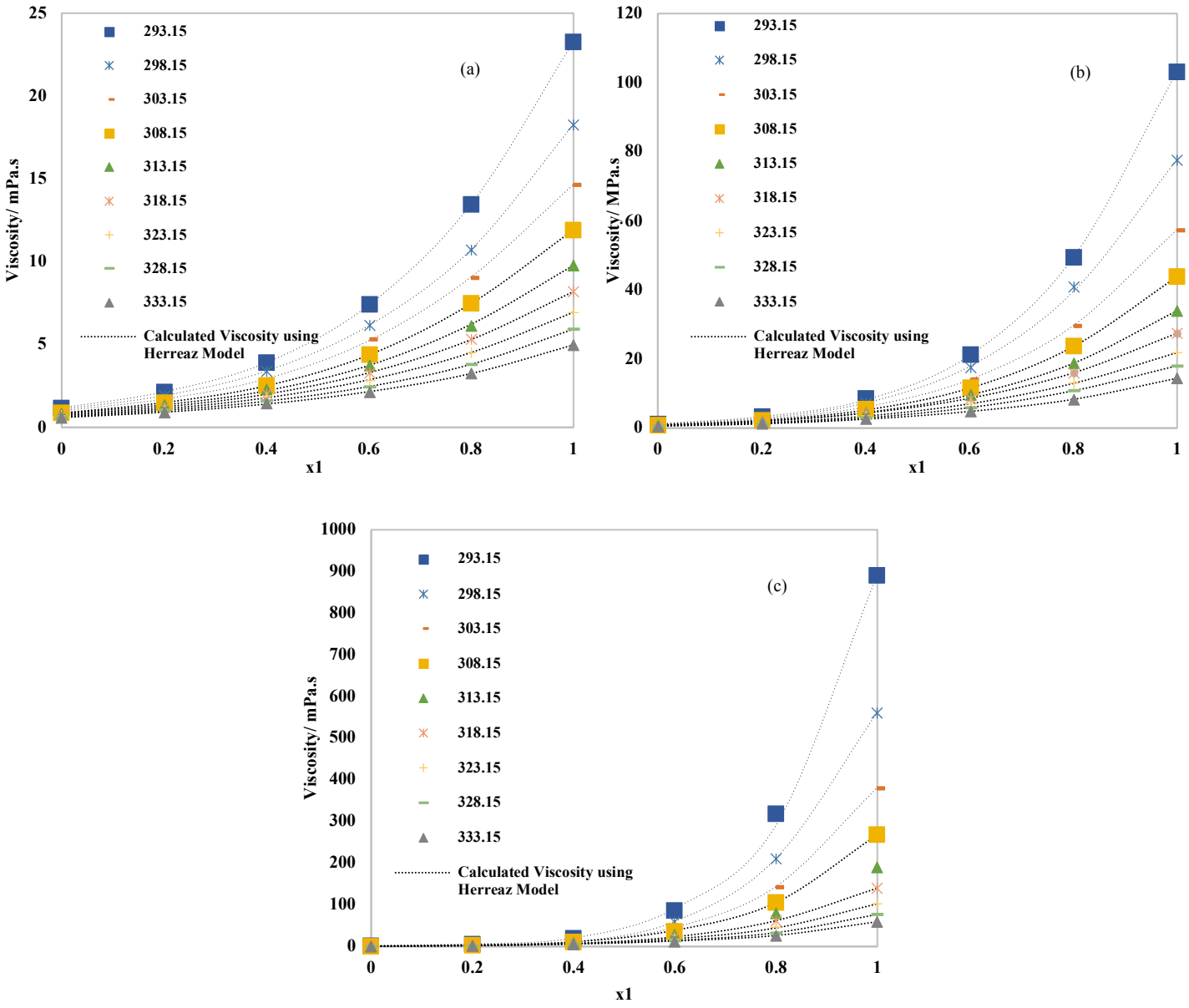

Figure 6-11: Comparison of the calculated viscosity using Herreaz model to experimental values for a) MEA(x_1)-ETOH, b) MDEA(x_1)-ETOH and, c) DEA(x_1)-ETOH solutions

The 2nd order Redlich-Kister type of equation was applied to correlate the viscosity of the binary mixtures of MEA-ETOH, MDEA-ETOH and DEA-ETOH. For all studied mixtures, this equation correlated the experimental data satisfactory, with average absolute relative deviation values of 0.118 for MEA-ETOH, 0.207 and 1.242 for MDEA-ETOH and DEA-ETOH, respectively. The values of the regressed parameters at each temperature for studied binary mixtures are reported in **Table 6-22**.

Table 6-22: Redlich− Kister fitting coefficient of the viscosity and %AARD for the studied binary Mixtures at T= 293.15− 323.15 K and P = 0.101MPa

T	293.15	298.15	303.15	308.15	313.15	318.15	323.15	328.15	333.15
MEA-ETOH									
A_0	-27.440	-20.492	-15.319	-12.223	-9.646	-7.653	-6.276	-5.221	-4.141
A_1	-9.844	-7.031	-4.546	-4.095	-3.050	-2.104	-1.923	-1.991	-1.536
A_2	-0.041	-0.072	-0.070	-0.285	-0.295	-0.305	-0.604	-0.600	-0.613
%AARD	0.118								
MDEA-ETOH									
A_0	-154.739	-110.786	-79.054	-57.725	-42.981	-31.898	-24.397	-20.456	-15.436
A_1	-78.387	-42.235	-35.460	-23.526	-15.910	-11.309	-6.686	-4.720	-6.664
A_2	-17.825	2.834	-8.089	-3.885	-2.424	-1.557	-1.999	0.900	-4.825
%AARD	0.207								
DEA-ETOH									
A_0	-1618.609	-1002.286	-665.330	-457.650	-318.248	-228.567	-161.554	-116.595	-85.878
A_1	-1148.830	-687.064	-462.403	-300.965	-189.447	-127.285	-89.735	-76.554	-56.813
A_2	-429.404	-227.607	-187.051	-118.629	-49.607	-23.857	-22.965	-44.028	-34.982
%AARD	1.242								

The comparison of the calculated viscosity using this Model to experimental viscosity of MEA-ETOH, MDEA-ETOH, and DEA-ETOH mixtures as a function of amine mole fraction are presented in **Figure 6-12**.

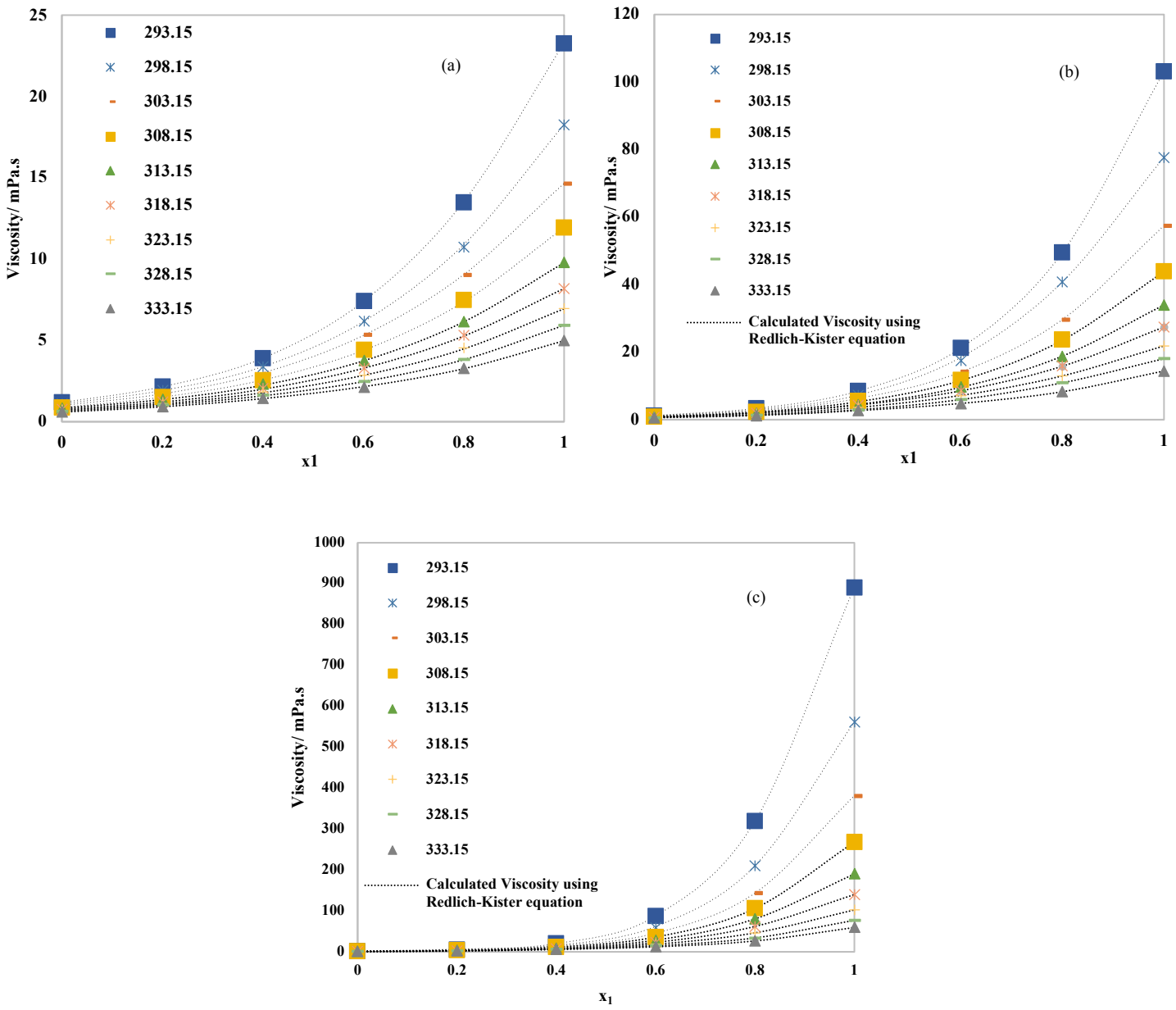

Figure 6-12: Comparison of the calculated viscosity using Redlich-Kister Model to experimental values for a) MEA(x_1)-ETOH, b) MDEA(x_1)-ETOH and, c) DEA(x_1)-ETOH solutions

Table 6-23 reveals the calculated interaction parameters using McAlister (three-body) model of the studied binary mixtures. This model correlates the experimental viscosity data satisfactorily.

Table 6-23: Interaction parameters of McAlister (three-body) model along with %AARD for the studied binary Mixtures at T = 293.15− 323.15 K and P = 0.101MPa									
T(K)	**293.15**	**298.15**	**303.15**	**308.15**	**313.15**	**318.15**	**323.15**	**328.15**	**333.15**
MEA+ETOH									
v_{12}	10.151	8.162	7.313	5.689	4.984	4.496	3.830	3.005	2.650
v_{21}	3.538	3.112	2.703	2.505	2.106	1.827	1.664	1.671	1.475
%AARD	0.166								
MDEA+ETOH									
v_{12}	39.328	34.320	21.333	19.197	15.728	11.017	11.034	9.396	6.834
v_{21}	5.564	5.224	5.696	5.130	4.010	5.125	3.086	2.493	2.460
%AARD	0.243								
DEA+ETOH									
v_{12}	214.886	97.597	70.434	61.154	40.674	29.622	24.106	17.169	13.978
v_{21}	10.338	13.712	12.787	9.109	9.643	9.581	7.825	7.684	7.249
%AARD	0.400								

The comparison of the calculated viscosity from these Models to experimental viscosity of MEA-ETOH, MDEA-ETOH, and DEA-ETOH mixture as a function of amine mole fraction are presented in **Figure 6-13.**

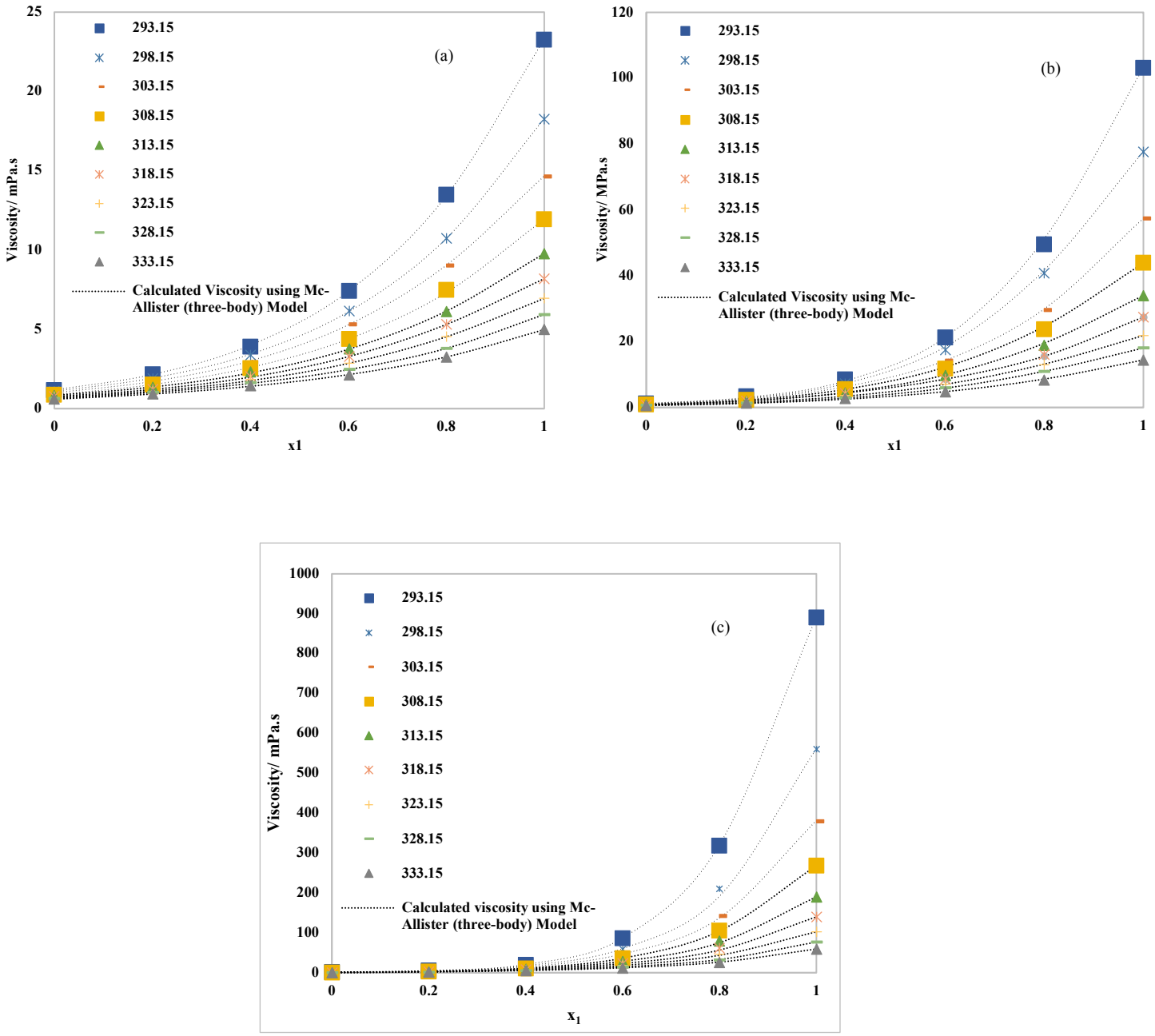

Figure 6-13: Comparison of the calculated viscosity using Mc-Allister(three-body) Model to experimental values for a) MEA(x_1)-ETOH, b) MDEA(x_1)-ETOH and, c) DEA(x_1)-ETOH solutions

Table 6-24 reveals a comparison of average absolute relative deviation among different models for MEA-ETOH, MDEA-ETOH, and DEA-ETOH mixtures.

The value of %AARD for all the three binary systems indicate that although all the models can correlate the experimental viscosity very satisfactory, the best result of viscosity is attributed to the Redlich-Kister model.

Table 6-24 : Comparison of %AARD among different models for MEA-ETOH, MDEA-ETOH, and DEA-ETOH mixtures

Model	MEA-ETOH	MDEA-ETOH	DEA-ETOH
Jouyban-Acree Eq(3-96)	1.081	1.620	1.052
Redlich-Kister Eq(3-85)	0.118	0.207	1.242
Herreaz Eq(3-97)	0.295	0.286	1.341
McAlister(three-body) Eq(3-94)	0.166	0.243	0.4

Figure 6-14 shows the parity chart for viscosity of the binary systems for all correlation methods. All the models show very small deviation.

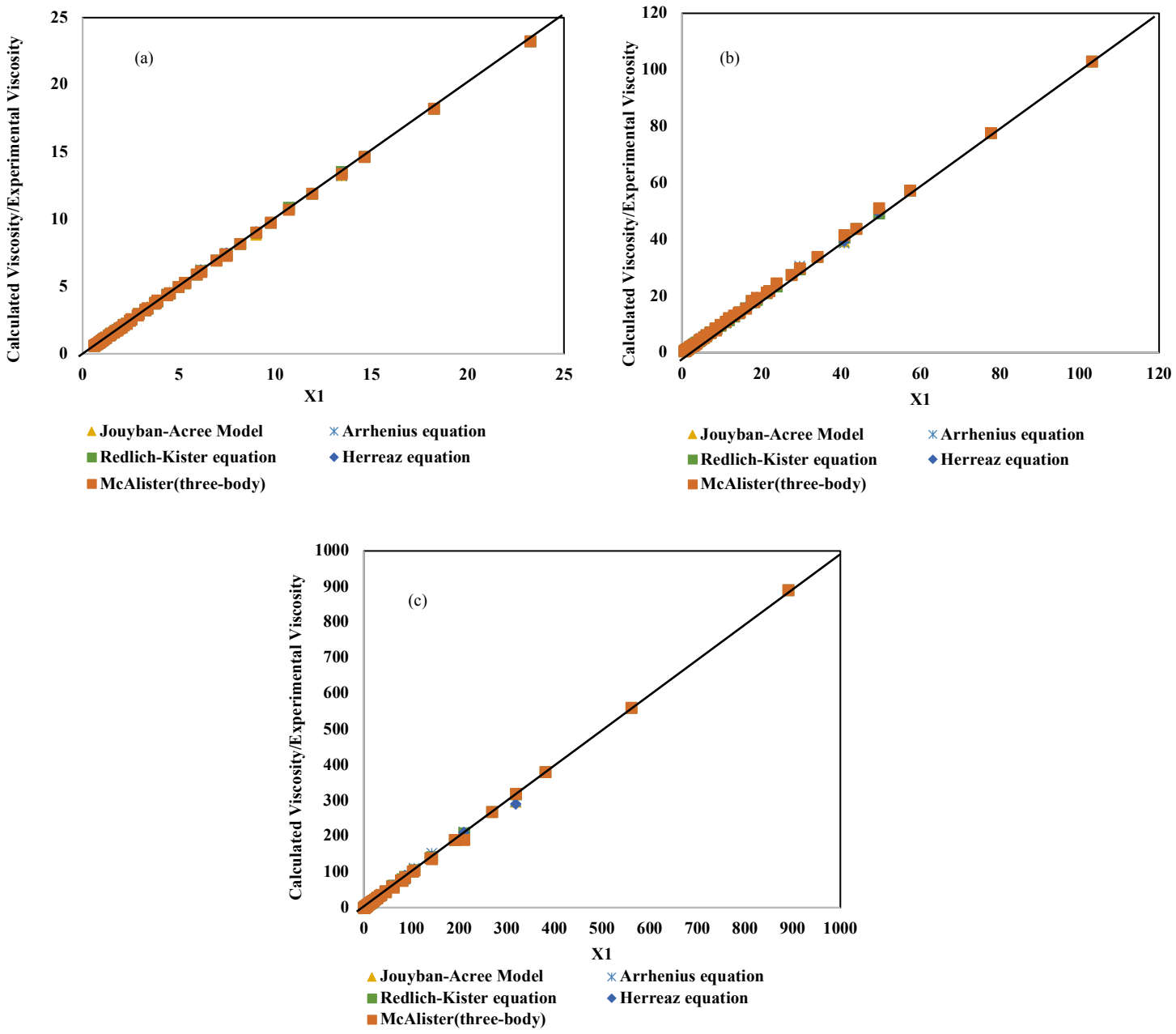

Figure 6-14: Parity chart for viscosity of for a) MEA-ETOH, b) MDEA-ETOH and, c) DEA-ETOH systems

6.4.3 **Refractive index Correlation**

The refractive indices of the studied binary mixtures were correlated using different models including Lorentz-Lorenz, Gladstone-Dale, Heller, Weiner, Arago-Biot, Eykman and Newton which are given in section (3-6-3) in chapter 3.

Comparison of the calculated refractive indices of binary mixtures of MEA-ETOH, MDEA-ETOH and DEA-ETOH using different correlations to experimental refractive indices at temperatures ranging from 293.15 to 333.15 K and P=0.101MPa are listed in **Table 6-25**. A close look of the data presented in this table shows that all correlations correlate the experimental values perfectly with the deviations ranged from 0.16 % to maximum 0.44 % for the MEA-ETOH mixture, 0.15 % to maximum 0.36 % for the MDEA-ETOH and, 0.44 % to maximum 0.91 % for the MEA-ETOH mixture which are satisfactory.

Further, it can be observed that the lowest deviation from experimental data is attributed to the Weiner relation for all three binary mixtures.

Table 6-25 :Comparison the experimental refractive indices of binary mixtures to calculated one using different models at 293.15–333.15 K and P=0.101MPa									
T(K)	**X_1**	**Exp**	**Lorentz-Lorenz Eq(3-100)**	**Goldstone-Dale Eq(3-99)**	**Weiner Eq(3-102)**	**Heller Eq(3-101)**	**Arago-Biot Eq(3-103)**	**Eyring – John Eq(3-104)**	**Newton Eq(3-105)**
MEA(X_1)-ETOH									
293.15	**0.201**	1.38515	1.38160	1.38211	1.38809	1.38141	1.38211	1.38185	1.38265
	0.4004	1.40489	1.40073	1.40147	1.40573	1.40096	1.40147	1.40110	1.40222
	0.602	1.42257	1.41941	1.42012	1.42280	1.41979	1.42012	1.41976	1.42083
	0.8006	1.43885	1.43719	1.43765	1.43892	1.43749	1.43765	1.43742	1.43809
298.15	**0.201**	1.38359	1.37850	1.37898	1.38506	1.37827	1.37898	1.37873	1.37949
	0.4004	1.40357	1.39693	1.39765	1.40207	1.39712	1.39765	1.39728	1.39839
	0.602	1.42087	1.41560	1.41632	1.41915	1.41597	1.41632	1.41596	1.41704
	0.8006	1.43726	1.43402	1.43450	1.43587	1.43433	1.43450	1.43426	1.43497
303.15	**0.201**	1.38171	1.37650	1.37698	1.38309	1.37626	1.37698	1.37673	1.37749
	0.4004	1.40185	1.39495	1.39568	1.40012	1.39515	1.39568	1.39531	1.39642
	0.602	1.41923	1.41365	1.41438	1.41722	1.41402	1.41438	1.41401	1.41510
	0.8006	1.43546	1.43211	1.43260	1.43397	1.43242	1.43260	1.43235	1.43307
308.15	**0.201**	1.37990	1.37440	1.37487	1.38090	1.37416	1.37487	1.37462	1.37537
	0.4004	1.39992	1.39270	1.39341	1.39780	1.39288	1.39341	1.39305	1.39415
	0.602	1.41738	1.41126	1.41197	1.41478	1.41162	1.41197	1.41161	1.41268
	0.8006	1.43363	1.42959	1.43007	1.43143	1.42989	1.43007	1.42983	1.43053
313.15	**0.201**	1.37821	1.37236	1.37284	1.37888	1.37213	1.37284	1.37259	1.37334
	0.4004	1.39813	1.39066	1.39137	1.39576	1.39084	1.39137	1.39101	1.39211
	0.602	1.41541	1.40922	1.40993	1.41275	1.40958	1.40993	1.40957	1.41065
	0.8006	1.43183	1.42756	1.42804	1.42940	1.42787	1.42804	1.42780	1.42851
318.15	**0.201**	1.37670	1.37029	1.37077	1.37686	1.37006	1.37077	1.37052	1.37127
	0.4004	1.39675	1.38862	1.38933	1.39376	1.38880	1.38933	1.38897	1.39007
	0.602	1.41364	1.40723	1.40794	1.41079	1.40759	1.40794	1.40758	1.40867
	0.8006	1.43007	1.42564	1.42612	1.42750	1.42595	1.42612	1.42588	1.42659
323.15	**0.201**	1.37560	1.36820	1.36868	1.37480	1.36796	1.36868	1.36843	1.36919
	0.4004	1.39522	1.38655	1.38727	1.39172	1.38673	1.38727	1.38690	1.38801
	0.602	1.41231	1.40520	1.40591	1.40877	1.40556	1.40591	1.40555	1.40664
	0.8006	1.42885	1.42366	1.42414	1.42553	1.42396	1.42414	1.42390	1.42462

328.15	**0.201**	1.37430	1.36614	1.36661	1.37279	1.36589	1.36661	1.36636	1.36712
	0.4004	1.39389	1.38453	1.38525	1.38975	1.38471	1.38525	1.38488	1.38600
	0.602	1.41092	1.40324	1.40396	1.40685	1.40361	1.40396	1.40360	1.40470
	0.8006	1.42765	1.42179	1.42227	1.42367	1.42209	1.42227	1.42203	1.42275
333.15	**0.201**	1.37333	1.36395	1.36443	1.37066	1.36370	1.36443	1.36418	1.36495
	0.4004	1.39270	1.38241	1.38313	1.38767	1.38259	1.38313	1.38275	1.38389
	0.602	1.40930	1.40119	1.40191	1.40483	1.40155	1.40191	1.40154	1.40265
	0.8006	1.42627	1.41981	1.42029	1.42170	1.42011	1.42029	1.42005	1.42078
%AARD			0.43481	0.39218	0.16376	0.42384	0.39218	0.41395	0.34866
MDEA(X_1)-ETOH									
293.15	**0.2002**	1.40067	1.39831	1.39924	1.40576	1.39847	1.39924	1.39877	1.40018
	0.4013	1.426	1.42412	1.42512	1.42909	1.42464	1.42512	1.42463	1.42611
	0.5998	1.44424	1.44298	1.44374	1.44597	1.44346	1.44374	1.44337	1.44446
	0.8	1.45776	1.45764	1.45804	1.45900	1.45792	1.45804	1.45785	1.45841
298.15	**0.2002**	1.39895	1.39438	1.39527	1.40198	1.39448	1.39527	1.39482	1.39618
	0.4013	1.42435	1.41988	1.42089	1.42507	1.42038	1.42089	1.42039	1.42188
	0.5998	1.44269	1.43923	1.44002	1.44240	1.43972	1.44002	1.43963	1.44077
	0.8	1.45528	1.45471	1.45513	1.45617	1.45500	1.45513	1.45493	1.45553
303.15	**0.2002**	1.39708	1.39237	1.39326	1.40000	1.39247	1.39326	1.39281	1.39418
	0.4013	1.42272	1.41790	1.41891	1.42311	1.41840	1.41891	1.41841	1.41991
	0.5998	1.4411	1.43728	1.43807	1.44047	1.43777	1.43807	1.43768	1.43883
	0.8	1.45335	1.45280	1.45322	1.45426	1.45309	1.45322	1.45301	1.45362
308.15	**0.2002**	1.39542	1.39056	1.39145	1.39825	1.39065	1.39145	1.39099	1.39237
	0.4013	1.42165	1.41619	1.41720	1.42144	1.41668	1.41720	1.41669	1.41821
	0.5998	1.44009	1.43565	1.43644	1.43887	1.43614	1.43644	1.43605	1.43721
	0.8	1.45198	1.45124	1.45167	1.45272	1.45153	1.45167	1.45146	1.45207
313.15	**0.2002**	1.39376	1.38851	1.38940	1.39623	1.38860	1.38940	1.38894	1.39032
	0.4013	1.42023	1.41415	1.41516	1.41942	1.41465	1.41516	1.41465	1.41617
	0.5998	1.43835	1.43365	1.43444	1.43688	1.43414	1.43444	1.43405	1.43521
	0.8	1.45036	1.44927	1.44970	1.45076	1.44956	1.44970	1.44949	1.45010
318.15	**0.2002**	1.39283	1.38612	1.38699	1.39374	1.38620	1.38699	1.38654	1.38790
	0.4013	1.4191	1.41156	1.41256	1.41677	1.41205	1.41256	1.41205	1.41356
	0.5998	1.43765	1.43093	1.43171	1.43412	1.43141	1.43171	1.43132	1.43247

	0.8	1.44813	1.44646	1.44688	1.44793	1.44675	1.44688	1.44667	1.44728
323.15	**0.2002**	1.39182	1.38401	1.38488	1.39167	1.38409	1.38488	1.38443	1.38580
	0.4013	1.41835	1.40948	1.41047	1.41471	1.40996	1.41047	1.40997	1.41148
	0.5998	1.43629	1.42888	1.42967	1.43209	1.42936	1.42967	1.42927	1.43043
	0.8	1.44686	1.44446	1.44488	1.44594	1.44474	1.44488	1.44467	1.44528
328.15	**0.2002**	1.39105	1.38189	1.38277	1.38959	1.38197	1.38277	1.38231	1.38369
	0.4013	1.41776	1.40740	1.40840	1.41266	1.40788	1.40840	1.40789	1.40940
	0.5998	1.43543	1.42685	1.42764	1.43008	1.42734	1.42764	1.42725	1.42841
	0.8	1.44523	1.44249	1.44291	1.44398	1.44278	1.44291	1.44270	1.44332
333.15	**0.2002**	1.39	1.37954	1.38041	1.38722	1.37962	1.38041	1.37996	1.38133
	0.4013	1.41694	1.40498	1.40598	1.41023	1.40546	1.40598	1.40547	1.40698
	0.5998	1.43432	1.42441	1.42519	1.42763	1.42488	1.42519	1.42480	1.42596
	0.8	1.44383	1.44002	1.44044	1.44151	1.44031	1.44044	1.44023	1.44085
%AARD			0.35508	0.30179	0.15366	0.33195	0.30179	0.32836	0.25258
DEA(X_1)-ETOH									
293.15	**0.2002**	1.40923	1.39647	1.39747	1.40544	1.39655	1.39747	1.39697	1.39849
	0.4001	1.43627	1.42345	1.42463	1.42971	1.42402	1.42463	1.42404	1.42579
	0.6	1.45002	1.44498	1.44594	1.44888	1.44557	1.44594	1.44547	1.44685
	0.8	1.46530	1.46259	1.46311	1.46441	1.46295	1.46311	1.46286	1.46360
298.15	**0.2002**	1.40796	1.39269	1.39366	1.40193	1.39270	1.39366	1.39317	1.39465
	0.4001	1.43495	1.41929	1.42048	1.42587	1.41983	1.42048	1.41989	1.42166
	0.6	1.44823	1.44135	1.44235	1.44552	1.44196	1.44235	1.44186	1.44331
	0.8	1.46369	1.45997	1.46053	1.46195	1.46035	1.46053	1.46026	1.46106
303.15	**0.2002**	1.40637	1.39078	1.39176	1.40012	1.39079	1.39176	1.39126	1.39276
	0.4001	1.43345	1.41750	1.41870	1.42416	1.41805	1.41870	1.41810	1.41989
	0.6	1.44672	1.43968	1.44069	1.44390	1.44029	1.44069	1.44020	1.44166
	0.8	1.46218	1.45842	1.45899	1.46042	1.45880	1.45899	1.45871	1.45952
308.15	**0.2002**	1.40532	1.38891	1.38989	1.39834	1.38891	1.38989	1.38939	1.39090
	0.4001	1.43231	1.41571	1.41692	1.42244	1.41626	1.41692	1.41632	1.41813
	0.6	1.44524	1.43800	1.43901	1.44226	1.43862	1.43901	1.43852	1.43999
	0.8	1.46067	1.45684	1.45741	1.45886	1.45723	1.45741	1.45714	1.45796
313.15	**0.2002**	1.40362	1.38700	1.38798	1.39652	1.38700	1.38798	1.38748	1.38900
	0.4001	1.43102	1.41391	1.41513	1.42070	1.41446	1.41513	1.41452	1.41634

	0.6	1.44424	1.43631	1.43733	1.44061	1.43692	1.43733	1.43682	1.43832
	0.8	1.45907	1.45525	1.45583	1.45730	1.45565	1.45583	1.45555	1.45638
318.15	**0.2002**	1.40262	1.38496	1.38595	1.39457	1.38495	1.38595	1.38544	1.38698
	0.4001	1.43012	1.41195	1.41318	1.41882	1.41251	1.41318	1.41256	1.41441
	0.6	1.44335	1.43445	1.43548	1.43880	1.43508	1.43548	1.43497	1.43648
	0.8	1.45815	1.45351	1.45409	1.45558	1.45391	1.45409	1.45381	1.45465
323.15	**0.2002**	1.40178	1.38289	1.38388	1.39258	1.38288	1.38388	1.38337	1.38492
	0.4001	1.42893	1.40996	1.41119	1.41688	1.41051	1.41119	1.41057	1.41243
	0.6	1.44267	1.43255	1.43359	1.43695	1.43318	1.43359	1.43308	1.43460
	0.8	1.45737	1.45172	1.45231	1.45381	1.45212	1.45231	1.45202	1.45287
328.15	**0.2002**	1.40077	1.38084	1.38184	1.39062	1.38083	1.38184	1.38132	1.38288
	0.4001	1.42786	1.40799	1.40923	1.41499	1.40855	1.40923	1.40861	1.41048
	0.6	1.44195	1.43069	1.43173	1.43513	1.43132	1.43173	1.43121	1.43275
	0.8	1.45670	1.44995	1.45055	1.45207	1.45036	1.45055	1.45026	1.45111
333.15	**0.2002**	1.39962	1.37860	1.37959	1.38842	1.37858	1.37959	1.37908	1.38064
	0.4001	1.42616	1.40577	1.40701	1.41279	1.40632	1.40701	1.40638	1.40827
	0.6	1.44177	1.42850	1.42955	1.43296	1.42913	1.42955	1.42903	1.43057
	0.8	1.45557	1.44781	1.44841	1.44994	1.44822	1.44841	1.44812	1.44898
%AARD			0.83761	0.77139	0.44177	0.810439	0.77139	0.90765	0.70558

In addition to the above-mentioned relations, two semi-empirical models including modified Graber equations and Jouyban-Acree model were also applied to correlate the experimental refractive indices of the studied binary mixtures.

Comparison of the correlated refractive indices of binary mixtures of MEA-ETOH, MDEA-ETOH and DEA-ETOH using Jouyban-Acree and modified Graber Models to experimental refractive indices at temperatures of 293.15 to 333.15 K and P=0.101MPa are presented in **Table 6-26**.

Table 6-26 :Comparison the experimental refractive indices of binary mixtures to calculated refractive index using Jouyban-Acree and Graber models at 293.15–333.15 K and P=0.101MPa					
T(K)	**x_1**	**Experimental density**	**Calculated refractive indices using Modified Graber equation (8 parameters) Eq(3-91)**	**Calculated refractive indices using Modified Graber equation (6 parameters) Eq(3-90)**	**Calculated refractive indices using Jouyban-Acree Model Eq(3-92)**
MEA(x_1)-ETOH					
293.15	**0.2010**	1.38515	1.38578	1.38378	1.38706
	0.4004	1.40489	1.40614	1.40568	1.40519
	0.6020	1.42257	1.42405	1.42495	1.42257
	0.8006	1.43885	1.43984	1.44153	1.43868
298.15	**0.2010**	1.38359	1.38405	1.38241	1.38512
	0.4004	1.40357	1.40437	1.40389	1.40338
	0.6020	1.42087	1.42224	1.42278	1.42085
	0.8006	1.43726	1.43800	1.43903	1.43707
303.15	**0.2010**	1.38171	1.38203	1.38107	1.38320
	0.4004	1.40185	1.40239	1.40213	1.40158
	0.6020	1.41923	1.42031	1.42065	1.41916
	0.8006	1.43546	1.43611	1.43659	1.43547
308.15	**0.2010**	1.37990	1.37994	1.37974	1.38130
	0.4004	1.39992	1.40017	1.40040	1.39980
	0.6020	1.41738	1.41796	1.41857	1.41748
	0.8006	1.43363	1.43363	1.43420	1.43389
313.15	**0.2010**	1.37821	1.37790	1.37844	1.37942
	0.4004	1.39813	1.39813	1.39870	1.39803
	0.6020	1.41541	1.41594	1.41653	1.41581
	0.8006	1.43183	1.43162	1.43186	1.43232
318.15	**0.2010**	1.37670	1.37584	1.37715	1.37755
	0.4004	1.39675	1.39613	1.39704	1.39628
	0.6020	1.41364	1.41400	1.41452	1.41416
	0.8006	1.43007	1.42974	1.42956	1.43076

323.15	**0.2010**	1.37560	1.37375	1.37589	1.37570
	0.4004	1.39522	1.39408	1.39540	1.39454
	0.6020	1.41231	1.41200	1.41256	1.41253
	0.8006	1.42885	1.42779	1.42731	1.42922
328.15	**0.2010**	1.37430	1.37169	1.37464	1.37386
	0.4004	1.39389	1.39208	1.39379	1.39282
	0.6020	1.41092	1.41009	1.41063	1.41091
	0.8006	1.42765	1.42595	1.42511	1.42769
333.15	**0.2010**	1.37333	1.36932	1.37341	1.37204
	0.4004	1.39270	1.38982	1.39221	1.39112
	0.6020	1.40930	1.40795	1.40873	1.40930
	0.8006	1.42627	1.42394	1.42295	1.42617
MDEA(x_1)-ETOH					
293.15	0.2002	1.40067	1.40253	1.40000	1.40075
	0.4013	1.42600	1.42947	1.42598	1.42606
	0.5998	1.44424	1.44637	1.44467	1.44428
	0.8000	1.45776	1.45818	1.45845	1.45686
298.15	0.2002	1.39895	1.40079	1.39872	1.39923
	0.4013	1.42435	1.42775	1.42440	1.42448
	0.5998	1.44269	1.44442	1.44286	1.44268
	0.8000	1.45528	1.45632	1.45647	1.45528
303.15	0.2002	1.39708	1.39860	1.39747	1.39772
	0.4013	1.42272	1.42556	1.42283	1.42291
	0.5998	1.44110	1.44259	1.44108	1.44110
	0.8000	1.45335	1.45447	1.45452	1.45371
308.15	0.2002	1.39542	1.39665	1.39623	1.39623
	0.4013	1.42165	1.42373	1.42129	1.42136
	0.5998	1.44009	1.44093	1.43932	1.43953
	0.8000	1.45198	1.45295	1.45261	1.45215
313.15	0.2002	1.39376	1.39454	1.39500	1.39475
	0.4013	1.42023	1.42167	1.41977	1.41983

	0.5998	1.43835	1.43897	1.43759	1.43798
	0.8000	1.45036	1.45106	1.45072	1.45061
318.15	0.2002	1.39283	1.39221	1.39380	1.39328
	0.4013	1.41910	1.41920	1.41828	1.41831
	0.5998	1.43765	1.43642	1.43589	1.43643
	0.8000	1.44813	1.44839	1.44886	1.44908
323.15	0.2002	1.39182	1.39004	1.39260	1.39182
	0.4013	1.41835	1.41709	1.41680	1.41680
	0.5998	1.43629	1.43440	1.43421	1.43491
	0.8000	1.44686	1.44646	1.44703	1.44756
328.15	0.2002	1.39105	1.38788	1.39143	1.39038
	0.4013	1.41776	1.41499	1.41535	1.41530
	0.5998	1.43543	1.43241	1.43255	1.43339
	0.8000	1.44523	1.44455	1.44523	1.44606
333.15	0.2002	1.39000	1.38531	1.39026	1.38895
	0.4013	1.41694	1.41244	1.41391	1.41382
	0.5998	1.43432	1.42993	1.43092	1.43189
	0.8000	1.44383	1.44212	1.44345	1.44457
DEA(x_1)-ETOH					
293.15	**0.2002**	1.40923	1.41021	1.40802	1.40942
	0.4001	1.43627	1.43886	1.43627	1.43632
	0.6000	1.45002	1.45454	1.45489	1.45325
	0.8000	1.46530	1.46478	1.46802	1.46489
298.15	**0.2002**	1.40796	1.40844	1.40698	1.40804
	0.4001	1.43495	1.43721	1.43484	1.43489
	0.6000	1.44823	1.45309	1.45321	1.45182
	0.8000	1.46369	1.46347	1.46616	1.46347
303.15	**0.2002**	1.40637	1.40637	1.40595	1.40667
	0.4001	1.43345	1.43531	1.43344	1.43348
	0.6000	1.44672	1.45144	1.45156	1.45040
	0.8000	1.46218	1.46203	1.46434	1.46206

308.15	**0.2002**	1.40532	1.40437	1.40495	1.40532
	0.4001	1.43231	1.43345	1.43207	1.43209
	0.6000	1.44524	1.44981	1.44994	1.44900
	0.8000	1.46067	1.46057	1.46255	1.46067
313.15	**0.2002**	1.40362	1.40229	1.40396	1.40398
	0.4001	1.43102	1.43153	1.43072	1.43070
	0.6000	1.44424	1.44813	1.44836	1.44760
	0.8000	1.45907	1.45907	1.46080	1.45928
318.15	**0.2002**	1.40262	1.40015	1.40299	1.40265
	0.4001	1.43012	1.42952	1.42940	1.42933
	0.6000	1.44335	1.44633	1.44680	1.44622
	0.8000	1.45815	1.45744	1.45908	1.45791
323.15	**0.2002**	1.40178	1.39798	1.40204	1.40133
	0.4001	1.42893	1.42748	1.42810	1.42797
	0.6000	1.44267	1.44450	1.44527	1.44485
	0.8000	1.45737	1.45577	1.45739	1.45655
328.15	**0.2002**	1.40077	1.39581	1.40110	1.40002
	0.4001	1.42786	1.42544	1.42682	1.42662
	0.6000	1.44195	1.44267	1.44378	1.44350
	0.8000	1.45670	1.45411	1.45573	1.45521
333.15	**0.2002**	1.39962	1.39327	1.40017	1.39873
	0.4001	1.42616	1.42302	1.42557	1.42528
	0.6000	1.44177	1.44044	1.44230	1.44215
	0.8000	1.45557	1.45203	1.45410	1.45387

The Combined expanded uncertainty $U(n_D)=0.00010$

The values of regressed parameters of modified Graber equations and Jouyban-Acree Model for binary mixtures together with the values for %AARD are tabulated in **Table 6-27**. As it is clear from this table, all the models for three binary mixtures correlate the experimental refractive index values satisfactory. The maximum deviation from the measured refractive index data is attributed to the Jouyban-Acree Model for all three mixtures and the least deviation is related to modified Graber equation (6 parameters).

Table 6-27: Regressed parameters of different Methods for the studied amines and ethanol mixtures at 293.15–333.15 K and P=0.101MPa					
Modified Graber equation (8 parameters) Eq(3-91)		**Modified Graber equation (6 parameters) Eq(3-90)**		**Jouyban-Acree Model Eq(3-92)**	
MEA-ETOH					
A_1	-0.15054	A_1	0.13787	A_0	0.02268
A_2	0.00762	A_2	-0.13756	A_1	-1.92636
A_3	0.42524	A_3	-0.11033	A_2	0.32815
A_4	-0.12678	A_4	1.45765		
A_5	0.66372	A_5	-0.00588		
A_6	-0.34163	A_6	0.00177		
A_7	0.20511				
A_8	-0.02159				
AARD%	0.0423	**AARD%**	0.0901	**AARD%**	0.11433
MDEA-ETOH					
A_1	0.04192	A_1	0.12523	A_0	0.06838
A_2	-0.00640	A_2	-0.08610	A_1	-10.26953
A_3	0.43544	A_3	-0.86379	A_2	0.34447
A_4	0.29101	A_4	1.44376		
A_5	0.55970	A_5	-0.00515		
A_6	-0.52150	A_6	0.00424		
A_7	-0.43631				
A_8	-0.00090				
AARD%	0.0747	**AARD%**	0.0828	**AARD%**	0.2377
DEA-ETOH					
A_1	0.04359	A_1	-0.10818	A_0	0.08266
A_2	-0.00570	A_2	-0.09769	A_1	-16.66795
A_3	0.43993	A_3	-0.36577	A_2	0.32880
A_4	0.24546	A_4	1.39603		
A_5	0.55053	A_5	-0.00238		
A_6	-0.52905	A_6	0.00559		
A_7	-0.38744				

A_8	-0.00092				
AARD%	0.0806	**AARD%**	0.1303	**AARD%**	0.2751

Also **Figure 6-15** to **Figure 6-17** show the comparison of the calculated refractive indices using Jouyban- Acree and Graber models to experimental refractive index of MEA-ETOH, MDEA-ETOH , and DEA-ETOH mixtures as a function of amine mole fraction .

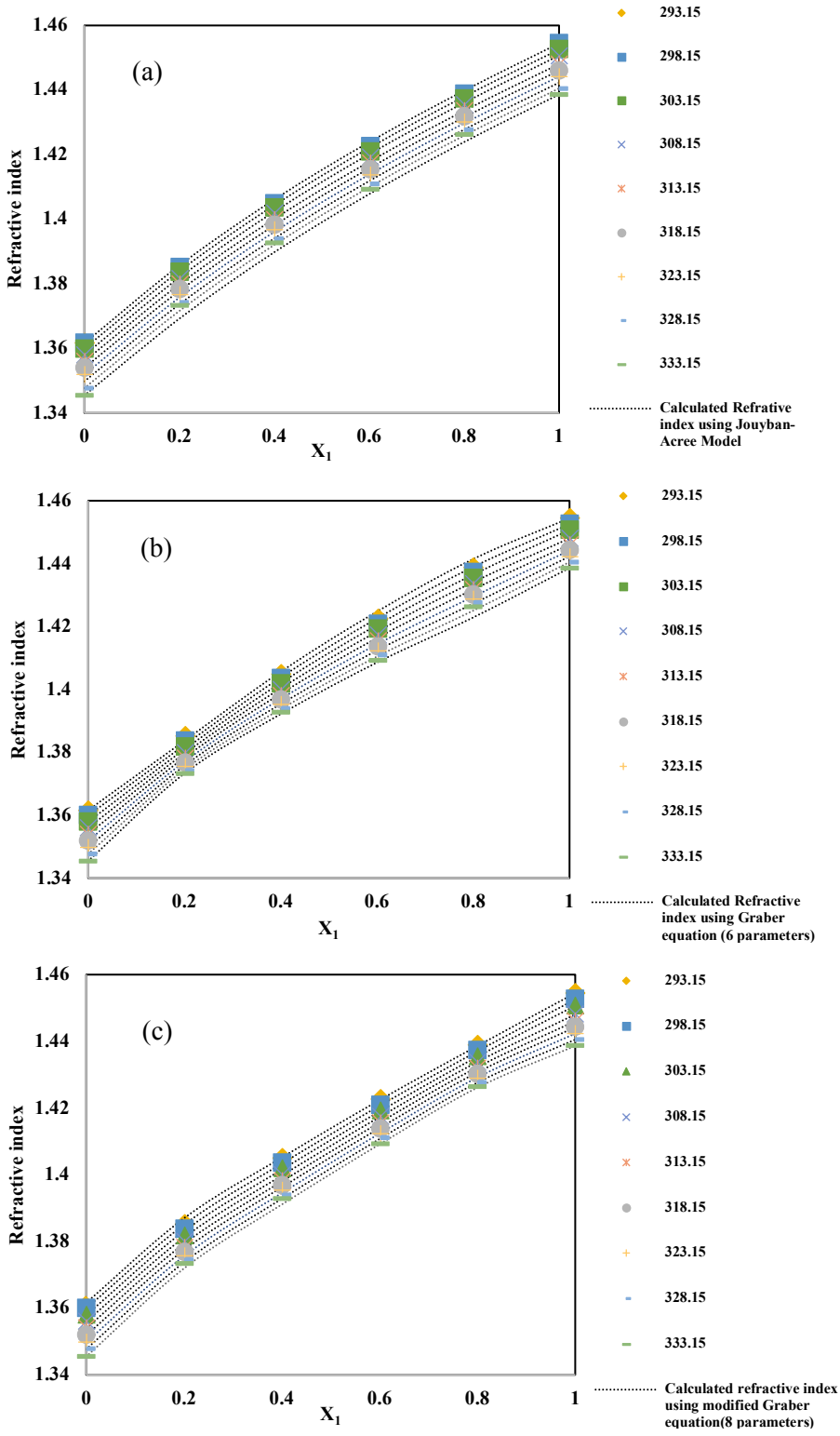

Figure 6-15: Calculated refractive index of MEA(x1)-ETOH mixture using a) Jouyban-Acree Model ,b) Modified Graber equation(6 parameters) , and c) Modified Graber equation(8 parameters)

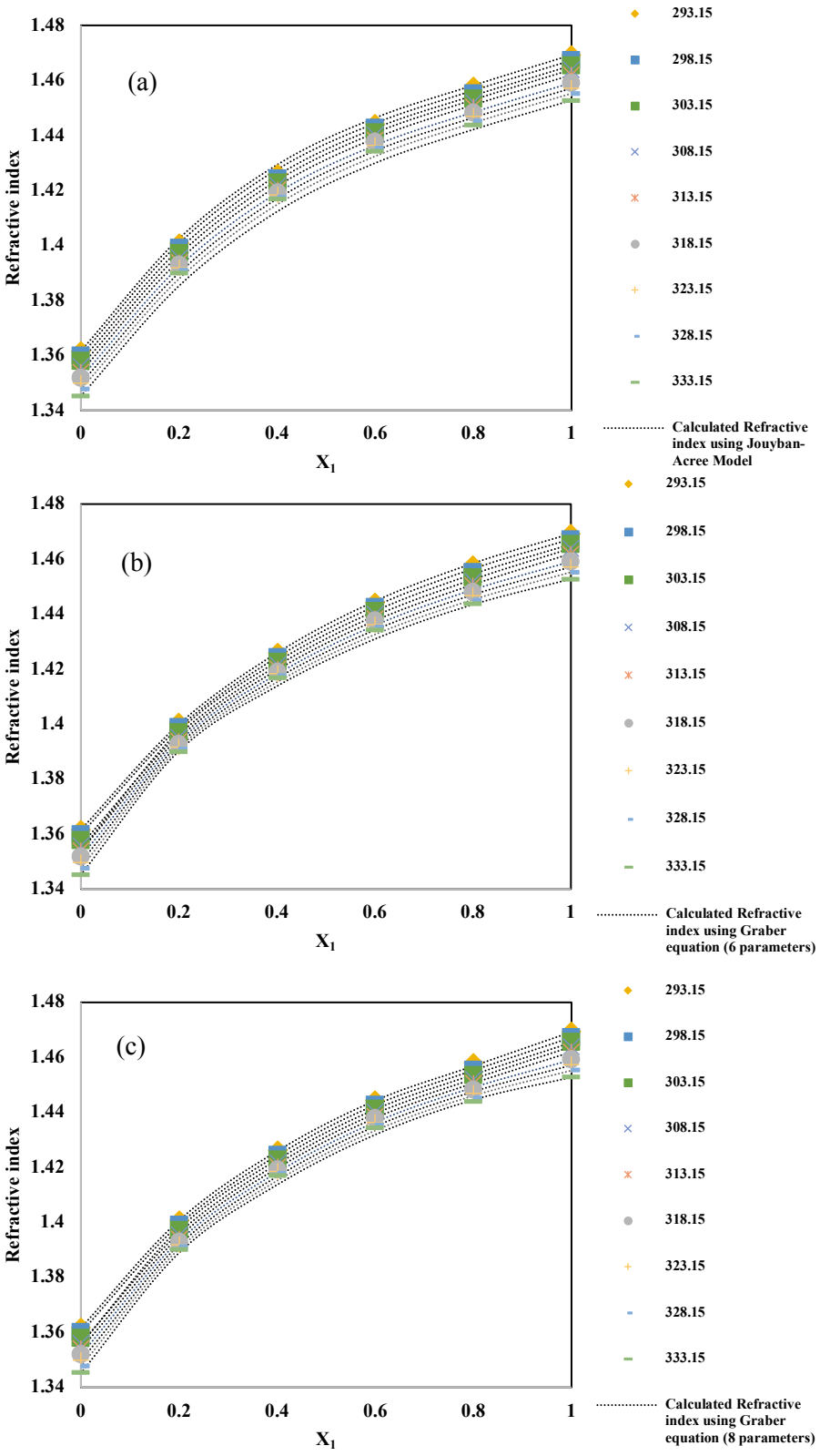

Figure 6-16:Calculated refractive index of MDEA(x_1)-ETOH mixture using a) Jouyban-Acree Model ,b) Modified Graber equation(6 parameters) , and c) Modified Graber equation(8 parameters)

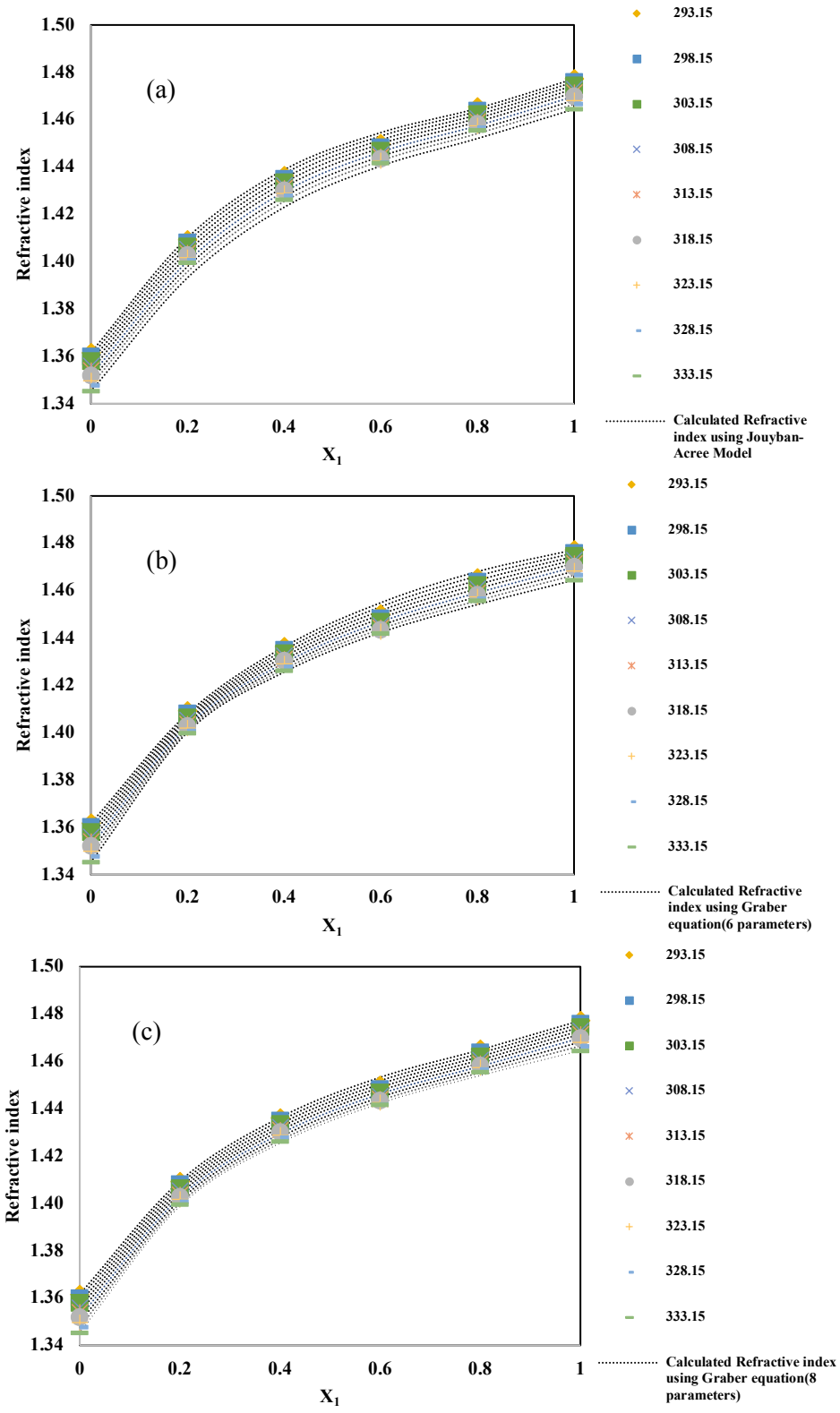

Figure 6-17: calculated refractive index of DEA(x1)-ETOH mixture using a) Jouyban-Acree Model ,b) Modified Graber equation(6 parameters) , and c) Modified Graber equation(8 parameters)

CHAPTER SEVEN: CONCLUSIONS AND RECOMMENDATIONS

7. Conclusions and recommendations

7.1 Conclusions

Fundamental knowledge of the thermo-physical properties of a simple and cost-effective solvent is required for the process of CO_2 capture by chemical absorption as the most commonly used CO_2 capture process in industry. In this study, hybrid solvents, the mixtures of alkanolamine and ethanol, were investigated due to their low solvent regeneration energy. Ethanol was used in hybrid solvents due to its low toxicity and high availability. Also, three commonly used alkanolamines for CO_2 capturing including Monoethanolamine (MEA), Methyldiethanolamine (MDEA), and Diethanolamine (DEA) were investigated in this study.

In this work, densities, viscosities and refractive indices of the binary mixtures of MEA+ETOH, MDEA+ETOH and DEA+ETOH were measured over the entire range of composition and for the temperatures ranging from 293.15 to 333.15 K, with the interval of 5 K. These physical properties showed a significant dependence on solvent mass fraction and temperature. Some conclusions were drawn as follows:

- The density values of the studied solutions increase with an increase in amine concentrations in all temperatures due the higher molar mass of amines against ethanol that leads to an increase in density of the mixture with adding a greater number of amines. On the other hand, at any constant amine concentration, the densities of the solutions decrease as the temperature increases which is attributed to the increase in volume of the solution, while the mass remains constant.
- At any constant temperature, the viscosity values of the studied solutions increase upon increase in alkanolamine concentration due to their higher viscosity than ethanol. However, the viscosity value of the system decreases with the increase in the temperature due to the increase in the mobility of the system with increase in temperature.

- Refractive index values of the solutions decrease upon increasing the temperature at any constant concentration but increase with the increase in the concentration of alkanolamines at any constant temperature.

In fact, by measuring the thermodynamic properties of a solution, the deviation of the solution from the ideality can be obtained. In addition, the molecular interactions as well as structural arrangement can be interpreted. To achieve these goals, excess molar volume, partial molar volume, partial molar volume at infinite dilution, and apparent molar volume were evaluated from the density experimental data. Also, the deviation in viscosity and refractive index from ideality were calculated in this study.

The values of V^E for all the solutions were negative and absolute values of V^E decrease with increase in temperature. The temperature dependent negative values of V^E reveal that the volume shrinkage takes place when alkanolamine and ethanol are mixed. The value and sign of V^E depend on which of the chemical, physical and geometrical factors in the mixture are predominant over the others. In this study, the absolute values of V^E for the systems follow the order: MEA+ETOH> MDEA+ETOH >DEA+ETOH based on the following interpretations:

- The self- associated bonds of MEA molecules are weaker than that in DEA and MDEA, therefore, at certain temperature, the number of available MEA species to form a cross complex with ethanol is larger than DEA and MDEA. Consequently, the volume contraction in MEA+ETOH mixture is larger than that of MDEA+ETOH and DEA+ETOH.
- The self-associated bonds for MDEA molecules are weaker than DEA due to the strict hindrance effect of the methyl group attached to the N atom of MDEA, therefore, the number of available MDEA species at the certain temperature is higher than DEA and hence, volume contraction is larger for MDEA+ETOH mixture than DEA+ETOH mixture.
- Based on the geometrical effect, the smaller molecule of ethanol can better pack in the voids presents in large molecules of MDEA and DEA compared to MEA which leads to increase in the volume contraction as well as the absolute value of V^E, hence, the volume

contraction in DEA+ETOH mixture is larger than that of MDEA+ETOH and MEA+ETOH.

- The overall V^E value of MEA+ETOH mixture is the most negative among all amines. This trend indicates that the chemical effect seems to be dominant over other factors in the presently investigated mixtures.
- The value of V^E becomes less negative with increase in temperature. When temperature increases the self- and cross-associated bonds of the components decrease and the value of V^E become less negative.

Partial molar volumes at infinite dilution were also calculated from two different methods. Results indicate that the values of the partial molar volume at infinite dilution for presently studied mixtures calculated from equations 6-8 and 6-9 are in a good agreement with the values obtained from equations 6-10 and 6-11. All values of the partial molar volumes at infinite dilution are less than corresponding molar volumes of pure components due to the packing effect and formation of hydrogen bond between solvent and solute.

After measurement of the experimental data for densities, viscosities and refractive indices of the investigated binary mixtures at different temperatures, some correlations were used to correlate the experimental data.

Redlich-Kister type of equation was used to calculate the value of excess molar volume for the studied mixture. The results show that this equation can be precisely used to correlate the excess molar volume with the average absolute deviation less than 0.008 for all mixtures at different investigated temperatures.

Three different models including modified Graber equations (6 and 8 parameters) and Jouyban-Acree Model were applied to correlate the densities of the mixtures. The %AARD values obtained from the Modified Graber methods are very close for all three mixtures. Hence, it is expected that the concentration of the second component (x_2), which is ethanol in this study, does not impact the density properties of the mixtures noticeably. Also, the %AARD of Jouyban−Acree Model are

larger than Graber methods for MDEA+ETOH and DEA+ETOH, however, this amount is the lowest for MEA+ETOH mixture.

The viscosity deviations of the binary mixtures of MEA+ETOH, MDEA+ETOH and DEA+ETOH were measured in the temperature range of 293.15 to 333.15 K and correlated with the Redlich-Kister type of equation. The value of $\Delta\eta$ for all the solutions are negative and increase with increase of temperature for all mixtures. The negative value of viscosity deviation is attributed to the weak interactions between unlike molecules. Also, the difference in the molecular size of the unlike components affects the sign and value of viscosity deviation. Hence, in this study, the smallest value of viscosity deviation corresponds to DEA+ETOH and the highest value is related to MEA+ETOH binary mixture.

The viscosities of the studied binary mixtures were also correlated using different models including McAllister Model, Jouyban-Acree Model, Herraez Model, and Redlich-Kister equation. Results show that % AARD of the presently used models for all the systems are among 0.1 to 2.1 mPa.s which indicate that all the models can estimate the experimental viscosity data satisfactorily. Among these models the best results for present mixtures is attributed to the Redlich-Kister model with the lowest %AARD of 0.12 mPa.s for MEA+ETOH, 0.21 mPa.s for MDEA+ETOH and 1.24 mPa.s for DEA+ETOH solution. It should be mentioned that in comparison of different models, number of adjustable parameters should also be considered. Of course, correlations with high number of adjustable parameters can yield better results.

The experimental data for refractive indices of the studied mixtures were correlated using different models including Lorentz-Lorenz, Gladstone-Dale, Heller, Weiner, Arago-Biot, Eykman and Newton. All these correlations estimate the experimental data well within the acceptable %AARD ranged from 0.16 % to maximum 0.44 % for the MEA+ETOH mixture, 0.15 % to maximum 0.36 % for the MDEA+ETOH and, 0.44 % to maximum 0.91 % for the MEA+ETOH mixture. Further, the lowest deviation from experimental data was determined from the Weiner relation.

The modified Graber equations (6 and 8 parameters) and Jouyban-Acree model were also applied to correlate the experimental refractive indices of the studied mixtures. All the models for three

binary mixtures estimate the experimental refractive index values perfectly. The maximum deviation from the measured refractive index data is attributed to the Jouyban-Acree Model with %AARD of 0.11 for MEA+ETOH, 0.24 for MDEA+ETOH and 0.27 for DEA+ETOH solution. The lowest deviation from experimental data is attributed to the modified Graber equation (8 parameters) with %AARD of 0.04 for MEA+ETOH, 0.07 for MDEA+ETOH and 0.08 for DEA+ETOH solution.

7.2 Recommendations for future work

In future, the binary mixtures of other alkanolamines (which are normally synthesized) with ethanol can be studied. Also, ternary systems of MEA/DEA/MDEA+Ethanol+Water and also multi-component systems of hybrids of MEA, DEA and MDEA+ Ethanol+Water can be studied. Depending on the availability of different equipment, the reliability for generating the experimental data against the Anton-Paar equipment can be studied. We used least squares method for fitting the adjustable parameters of the models and the correlations studied in this work, which is normally used in literature. It is suggested that the capability of advanced fitting and optimization methods like genetic algorithm, etc., are also investigated. In this study, the most commonly used and recommended models and correlations were investigated. It is suggested to look at advanced models e.g. Artificial Neural Networks (ANN), etc., for modeling the studied systems in future. Finally, it should be mentioned that interpretation of macroscopic properties by molecular interactions may be controversial when a limited number of properties are analyzed and the observed effects may not be characteristic. In his analysis, some other literature data, such as vapor- liquid equilibrium, surface tension or dielectric constant could be taken into account.

References

[1] R. Cooper, J. McCarthy, and B. Metz, "Climate Change 2001: The Scientific Basis," in *Foreign Affairs*, vol. 81, no. 1, 2002, p. 208.

[2] A. Yamasaki, "An Overview of CO2 Mitigation Options for Global Warming-Emphasizing CO2 Sequestration Options," *J. Chem. Eng. Japan - J CHEM ENG JPN*, vol. 36, pp. 361–375, Apr. 2003, doi: 10.1252/jcej.36.361.

[3] G. Balachandar, N. Khanna, and D. Das, "Chapter 6 - Biohydrogen Production from Organic Wastes by Dark Fermentation," A. Pandey, J.-S. Chang, P. C. Hallenbecka, and C. B. T.-B. Larroche, Eds. Amsterdam: Elsevier, 2013, pp. 103–144.

[4] Stephen A. Rackley, *CCS technology glossary*. Butterworth-Heinemann, 2017.

[5] "Global Monitoring Laboratory - Carbon Cycle Greenhouse Gases." https://gml.noaa.gov/ccgg/trends/ (accessed Sep. 21, 2021).

[6] S. Dinda, "Development of solid adsorbent for carbon dioxide capture from flue gas," *Sep. Purif. Technol.*, vol. 109, pp. 64–71, 2013, doi: 10.1016/j.seppur.2013.02.027.

[7] M. K. Mondal, H. K. Balsora, and P. Varshney, "Progress and trends in CO2 capture/separation technologies: A review," *Energy*, vol. 46, no. 1, pp. 431–441, 2012, doi: https://doi.org/10.1016/j.energy.2012.08.006.

[8] G. M. L. US Department of Commerce, NOAA, "Global Monitoring Laboratory - Carbon Cycle Greenhouse Gases." https://www.esrl.noaa.gov/gmd/ccgg/trends/gl_full.html (accessed Mar. 13, 2020).

[9] D. Y. C. Leung, G. Caramanna, and M. M. Maroto-Valer, "An overview of current status of carbon dioxide capture and storage technologies," *Renew. Sustain. Energy Rev.*, vol. 39, no. November, pp. 426–443, 2014, doi: 10.1016/j.rser.2014.07.093.

[10] Intergovernmental Panel on Climate Change, "CARBON DIOXIDE CAPTURE AND STORAGE." Accessed: Jul. 13, 2020. [Online]. Available: https://archive.ipcc.ch/pdf/special-reports/srccs/srccs_wholereport.pdf.

[11] D. Y. C. Leung, G. Caramanna, and M. M. Maroto-Valer, "An overview of current status of carbon dioxide capture and storage technologies," *Renew. Sustain. Energy Rev.*, vol. 39, pp. 426–443, 2014, doi: https://doi.org/10.1016/j.rser.2014.07.093.

[12] R. Sabouni, H. Kazemian, and S. Rohani, "Carbon dioxide capturing technologies: a review

focusing on metal organic framework materials (MOFs)," *Environ. Sci. Pollut. Res.*, vol. 21, no. 8, pp. 5427–5449, Apr. 2014, doi: 10.1007/s11356-013-2406-2.

[13] O. Dr. Bolland, *Carbon dioxide capture*, no. October. 2009.

[14] Costas P. Pappis, *Climate Change, Supply Chain Management and Enterprise Adaptation:Implications of Global Warming on the Economy*. 2010.

[15] A. A. Olajire, "CO2 capture and separation technologies for end-of-pipe applications – A review," *Energy*, vol. 35, no. 6, pp. 2610–2628, 2010, doi: https://doi.org/10.1016/j.energy.2010.02.030.

[16] J. D. Figueroa, T. Fout, S. Plasynski, H. McIlvried, and R. D. Srivastava, "Advances in CO2 capture technology—The U.S. Department of Energy's Carbon Sequestration Program," *Int. J. Greenh. Gas Control*, vol. 2, no. 1, pp. 9–20, 2008, doi: https://doi.org/10.1016/S1750-5836(07)00094-1.

[17] G. S. Kumar, M. Viswandham, A. V. S. S. K. S. Gupta, and G. S. Kumar, "a Review of Pre-Combustion Co2 Capture in Igcc," *Int. J. Res. Eng. Technol.*, vol. 02, no. 05, pp. 847–853, 2013, doi: 10.15623/ijret.2013.0205020.

[18] S. D. Kenarsari *et al.*, "Review of recent advances in carbon dioxide separation and capture," *RSC Adv.*, vol. 3, no. 45, pp. 22739–22773, 2013, doi: 10.1039/c3ra43965h.

[19] Z. (Henry) Liang *et al.*, "Recent progress and new developments in post-combustion carbon-capture technology with amine based solvents," *Int. J. Greenh. Gas Control*, vol. 40, pp. 26–54, 2015, doi: 10.1016/j.ijggc.2015.06.017.

[20] W. Kuckshinrichs and J. F. Hake, *Carbon capture, storage and use: Technical, economic, environmental and societal perspectives*. 2015.

[21] Feron, P. H.M. and Hendriks, C. A., "CO2 Capture Process Principles and Costs," *Oil Gas Sci. Technol. - Rev. IFP*, vol. 60, no. 3, pp. 451–459, 2005, doi: 10.2516/ogst:2005027.

[22] A. B. Rao and E. S. Rubin, "A Technical, Economic, and Environmental Assessment of Amine-Based CO2 Capture Technology for Power Plant Greenhouse Gas Control," *Environ. Sci. Technol.*, vol. 36, no. 20, pp. 4467–4475, Oct. 2002, doi: 10.1021/es0158861.

[23] D. M. D. Alessandro, B. Smit, and J. R. Long, "Carbon Dioxide Capture Carbon Dioxide Capture : Prospects for New Materials Angewandte," pp. 6058–6082, 2010, doi: 10.1002/anie.201000431.

[24] A. S. Bhown and B. C. Freeman, "Analysis and Status of Post-Combustion Carbon Dioxide

Capture Technologies," *Environ. Sci. Technol*, pp. 8624–8632, 2011, doi: 10.1021/es104291d.

[25] K. A. Mumford, Y. Wu, K. H. Smith, and G. W. Stevens, "Review of solvent based carbon-dioxide capture technologies," *Front. Chem. Sci. Eng.*, vol. 9, no. 2, pp. 125–141, 2015, doi: 10.1007/s11705-015-1514-6.

[26] W. M. Budzianowski, "Single solvents, solvent blends, and advanced solvent systems in CO2 capture by absorption: A review," *Int. J. Glob. Warm.*, vol. 7, no. 2, pp. 184–225, 2015, doi: 10.1504/IJGW.2015.067749.

[27] X. Luo, A. Hartono, and H. Svendsen, "Comparative kinetics of carbon dioxide absorption in unloaded aqueous monoethanolamine solutions using wetted wall and string of discs columns," *Chem. Eng. Sci.*, vol. 82, pp. 31–43, Sep. 2012, doi: 10.1016/j.ces.2012.07.001.

[28] C. Yu, C. Huang, and C. Tan, "A Review of CO 2 Capture by Absorption and Adsorption," pp. 745–769, 2012, doi: 10.4209/aaqr.2012.05.0132.

[29] A. Brunetti, F. Scura, G. Barbieri, and E. Drioli, "Membrane technologies for CO 2 separation," *J. Memb. Sci.*, vol. 359, no. 1–2, pp. 115–125, 2010, doi: 10.1016/j.memsci.2009.11.040.

[30] S. Topham *et al.*, *Carbon Dioxide*. 2014.

[31] T. Study, "CO 2 CAPTURE IN THE CEMENT," no. July, 2008.

[32] R. Singh, "Chapter 3 - Hybrid membrane systems – applications and case studies," R. B. T.-H. M. S. for W. P. Singh, Ed. Amsterdam: Elsevier Science, 2005, pp. 131–196.

[33] S. S. Clair Gough, *Carbon Capture and its Storage: An Integrated Assessment*, 1st editio. London, 2006.

[34] M. Tambe, M. M. Maroto-valer, and A. J. Finn, "Study of design parameters affecting the performance of CO 2 purification units in oxy-fuel combustion," *Int. J. Greenh. Gas Control*, vol. 12, pp. 441–449, 2013, doi: 10.1016/j.ijggc.2012.11.016.

[35] G. Göttlicher and R. Pruschek, "Comparison of CO2 removal systems for fossil-fuelled power plant processes," *Energy Convers. Manag.*, vol. 38, pp. S173–S178, 1997, doi: https://doi.org/10.1016/S0196-8904(96)00265-8.

[36] R. Porrazzo, G. White, and R. Ocone, "Techno-economic investigation of a chemical looping combustion based power plant," *Faraday Discuss.*, vol. 192, no. 0, pp. 437–457, 2016, doi: 10.1039/C6FD00033A.

[37] M. Q. ul I. Zafar, "Oxygen Carriers Materials for Chemical-Looping Technologies - Reactivity and Kinetics Muhammad Qamar ul Islam Zafar," CHALMERS UNIVERSITY OF TECHNOLOGY, 2007.

[38] P. Wang, N. Means, D. Shekhawat, D. Berry, and M. Massoudi, "Chemical-Looping Combustion and Gasification of Coals and Oxygen Carrier Development: A Brief Review," pp. 10605–10635, 2015, doi: 10.3390/en81010605.

[39] J. Adánez, L. F. de Diego, F. García-Labiano, P. Gayán, A. Abad, and J. M. Palacios, "Selection of Oxygen Carriers for Chemical-Looping Combustion," *Energy & Fuels*, vol. 18, no. 2, pp. 371–377, Mar. 2004, doi: 10.1021/ef0301452.

[40] M. M. Hossain and H. I. De Lasa, "Chemical-looping combustion (CLC) for inherent CO 2 separations — a review," vol. 63, 2008, doi: 10.1016/j.ces.2008.05.028.

[41] E. D. Sloan Jr., C. A. Koh, and C. A. Koh, *Clathrate Hydrates of Natural Gases*, 3rd editio. CRC Press, Taylor & Francis Group, New York, 2007.

[42] E. D. Sloan, "Gas Hydrates: Review of Physical/Chemical Properties," *Energy & Fuels*, vol. 12, no. 2, pp. 191–196, Mar. 1998, doi: 10.1021/ef970164+.

[43] L. J. Florusse *et al.*, "Stable low-pressure hydrogen clusters stored in a binary clathrate hydrate," *Science (80-.).*, vol. 306, no. 5695, pp. 469–471, Oct. 2004, doi: 10.1126/science.1102076.

[44] M. H. F. Sluiter, H. Adachi, R. V. Belosludov, V. R. Belosludov, and Y. Kawazoe, *Ab initio study of hydrogen storage in hydrogen hydrate clathrates*, vol. 45, no. 5. 2004.

[45] P. Linga, R. Kumar, J. A. Ripmeester, P. Enlezos, and B. Engineering, "HYDRATE PROCESSES FOR CO 2 CAPTURE AND SCALE UP USING A NEW APPARATUS," 2008.

[46] P. Linga, R. Kumar, and P. Englezos, "The clathrate hydrate process for post and pre-combustion capture of carbon dioxide," vol. 149, pp. 625–629, 2007, doi: 10.1016/j.jhazmat.2007.06.086.

[47] H. D. Schulz and M. Zabel, "Gas Hydrates in Marine Sediments," *Mar. Geochemistry*, no. August 2015, pp. 1–574, 2006, doi: 10.1007/3-540-32144-6.

[48] T. Hughes, "Plug Formation and Dissociation of Mixed Gas Hydrates and Methane Semi-Clathrate Hydrate Stability," UNIVERSITY OF CANTERBURY, 2008.

[49] E. Oko, M. Wang, and A. S. Joel, "Current status and future development of solvent-based

carbon capture," *Int. J. Coal Sci. Technol.*, vol. 4, no. 1, pp. 5–14, 2017, doi: 10.1007/s40789-017-0159-0.

[50] F. Vega, M. Cano, S. Camino, L. M. G. Fernández, E. Portillo, and B. Navarrete, "Solvents for Carbon Dioxide Capture," *Carbon Dioxide Chem. Capture Oil Recover.*, Aug. 2018, doi: 10.5772/intechopen.71443.

[51] R. Idem *et al.*, "Pilot Plant Studies of the CO2 Capture Performance of Aqueous MEA and Mixed MEA/MDEA Solvents at the University of Regina CO2 Capture Technology Development Plant and the Boundary Dam CO2 Capture Demonstration Plant," *Ind. Eng. Chem. Res.*, vol. 45, no. 8, pp. 2414–2420, Apr. 2006, doi: 10.1021/ie050569e.

[52] C. Tsouris, "Separation of CO2 from Flue Gas: A Review AU - Aaron, Douglas," *Sep. Sci. Technol.*, vol. 40, no. 1–3, pp. 321–348, Jan. 2005, doi: 10.1081/SS-200042244.

[53] H. Liu, "Comprehensive Evaluation of the Physical and Chemical Properties of 1-dimethylamino-2-propanol for Post Combustion CO 2 Capture," University of Regina, 2018.

[54] S. Garg, A. M. Shariff, M. S. Shaikh, B. Lal, A. Aftab, and N. Faiqa, "Selected physical properties of aqueous potassium salt of L-phenylalanine as a solvent for CO2 capture," *Chem. Eng. Res. Des.*, vol. 113, pp. 169–181, 2016, doi: 10.1016/j.cherd.2016.07.015.

[55] D. Camper *et al.*, "Room-Temperature Ionic Liquid # Amine Solutions : Tunable Solvents for Efficient and Reversible Capture of CO Room-Temperature Ionic Liquid - Amine Solutions : Tunable Solvents for Efficient and Reversible Capture of CO 2," pp. 2–5, 2008, doi: 10.1021/ie801002m.

[56] A. L. Kohl and R. B. Nielsen, "Gas purification: Chapter 2 - Alkanolamines for Hydrogen Sulfide and Carbon Dioxide Removal," in *Gas purification*, A. L. Kohl and R. B. B. T.-G. P. (Fifth E. Nielsen, Eds. Houston: Gulf Professional Publishing, 1997, pp. 40–186.

[57] C. K. Foo *et al.*, "Density and viscosity of aqueous mixtures of N-methyldiethanolamines (MDEA), piperazine (PZ) and ionic liquids," *J. Mol. Liq.*, vol. 209, pp. 596–602, 2015, doi: https://doi.org/10.1016/j.molliq.2015.05.041.

[58] P. Singh, J. P. M. Niederer, and G. F. Versteeg, "Structure and activity relationships for amine-based CO2 absorbents-II," *Chem. Eng. Res. Des.*, vol. 87, no. 2, pp. 135–144, 2009, doi: https://doi.org/10.1016/j.cherd.2008.07.014.

[59] S. A. Freeman, R. Dugas, D. H. Van Wagener, T. Nguyen, and G. T. Rochelle, "Carbon

dioxide capture with concentrated, aqueous piperazine," *Int. J. Greenh. Gas Control*, vol. 4, no. 2, pp. 119–124, 2010, doi: https://doi.org/10.1016/j.ijggc.2009.10.008.

[60] G. Sartori and D. W. Savage, "Sterically hindered amines for carbon dioxide removal from gases," *Ind. Eng. Chem. Fundam.*, vol. 22, no. 2, pp. 239–249, May 1983, doi: 10.1021/i100010a016.

[61] I. Kim and H. F. Svendsen, "Heat of Absorption of Carbon Dioxide (CO2) in Monoethanolamine (MEA) and 2-(Aminoethyl)ethanolamine (AEEA) Solutions," *Ind. Eng. Chem. Res.*, vol. 46, no. 17, pp. 5803–5809, Aug. 2007, doi: 10.1021/ie0616489.

[62] A. Hartono, E. F. da Silva, and H. F. Svendsen, "Kinetics of carbon dioxide absorption in aqueous solution of diethylenetriamine (DETA)," *Chem. Eng. Sci.*, vol. 64, no. 14, pp. 3205–3213, 2009, doi: https://doi.org/10.1016/j.ces.2009.04.018.

[63] A. Hartono, K. A. Hoff, T. Mejdell, and H. F. Svendsen, "Solubility of carbon dioxide in aqueous 2.5 M of diethylenetriamine (DETA) solution," *Energy Procedia*, vol. 4, pp. 179–186, 2011, doi: https://doi.org/10.1016/j.egypro.2011.01.039.

[64] J. G. M.-S. Monteiro *et al.*, "Kinetics of CO2 absorption by aqueous 3-(methylamino)propylamine solutions: Experimental results and modeling," *AIChE J.*, vol. 60, no. 11, pp. 3792–3803, Nov. 2014, doi: 10.1002/aic.14546.

[65] A. B. Rao and E. S. Rubin, "Identifying Cost-Effective CO2 Control Levels for Amine-Based CO2 Capture Systems," *Ind. Eng. Chem. Res.*, vol. 45, no. 8, pp. 2421–2429, Apr. 2006, doi: 10.1021/ie050603p.

[66] D. P. Hagewiesche, S. S. Ashour, H. A. Al-Ghawas, and O. C. Sandall, "Absorption of carbon dioxide into aqueous blends of monoethanolamine and N-methyldiethanolamine," *Chem. Eng. Sci.*, vol. 50, no. 7, pp. 1071–1079, 1995, doi: https://doi.org/10.1016/0009-2509(94)00489-E.

[67] B. P. Mandal, M. Guha, A. K. Biswas, and S. S. Bandyopadhyay, "Removal of carbon dioxide by absorption in mixed amines: modelling of absorption in aqueous MDEA/MEA and AMP/MEA solutions," *Chem. Eng. Sci.*, vol. 56, no. 21, pp. 6217–6224, 2001, doi: https://doi.org/10.1016/S0009-2509(01)00279-2.

[68] M. Caplow, "Kinetics of carbamate formation and breakdown," *J. Am. Chem. Soc.*, vol. 90, no. 24, pp. 6795–6803, Nov. 1968, doi: 10.1021/ja01026a041.

[69] E. Y. Kenig, "CO 2 -Alkanolamine Reaction Kinetics : A Review of Recent Studies," no.

11, pp. 1467–1474, 2007, doi: 10.1002/ceat.200700268.

[70] T. L. Donaldson and Y. N. Nguyen, “Carbon Dioxide Reaction Kinetics and Transport in Aqueous Amine Membranes,” *Ind. Eng. Chem. Fundam.*, vol. 19, no. 3, pp. 260–266, Aug. 1980, doi: 10.1021/i160075a005.

[71] P. Tontiwachwuthikul, A. Meisen, and C. J. Lim, “Solubility of carbon dioxide in 2-amino-2-methyl-1-propanol solutions,” *J. Chem. Eng. Data*, vol. 36, no. 1, pp. 130–133, Jan. 1991, doi: 10.1021/je00001a038.

[72] X. Chen and G. T. Rochelle, “Aqueous piperazine derivatives for CO2 capture: Accurate screening by a wetted wall column,” *Chem. Eng. Res. Des.*, vol. 89, no. 9, pp. 1693–1710, 2011, doi: 10.1016/j.cherd.2011.04.002.

[73] N. Hüser, O. Schmitz, and E. Y. Kenig, “A comparative study of different amine-based solvents for CO2-capture using the rate-based approach,” *Chem. Eng. Sci.*, vol. 157, pp. 221–231, 2017, doi: https://doi.org/10.1016/j.ces.2016.06.027.

[74] Z.-Y. Yang, A. N. Soriano, A. R. Caparanga, and M.-H. Li, “Equilibrium solubility of carbon dioxide in (2-amino-2-methyl-1-propanol+piperazine+water),” *J. Chem. Thermodyn.*, vol. 42, no. 5, pp. 659–665, 2010, doi: https://doi.org/10.1016/j.jct.2009.12.006.

[75] P. Brúder, A. Grimstvedt, T. Mejdell, and H. F. Svendsen, “CO2 capture into aqueous solutions of piperazine activated 2-amino-2-methyl-1-propanol,” *Chem. Eng. Sci.*, vol. 66, no. 23, pp. 6193–6198, 2011, doi: 10.1016/j.ces.2011.08.051.

[76] S. Y. Choi, S. C. Nam, Y. Il Yoon, K. T. Park, and S.-J. Park, “Carbon Dioxide Absorption into Aqueous Blends of Methyldiethanolamine (MDEA) and Alkyl Amines Containing Multiple Amino Groups,” *Ind. Eng. Chem. Res.*, vol. 53, no. 37, pp. 14451–14461, Sep. 2014, doi: 10.1021/ie502434m.

[77] J. T. Cullinane and G. T. Rochelle, “Thermodynamics of aqueous potassium carbonate, piperazine, and carbon dioxide,” *Fluid Phase Equilib.*, vol. 227, no. 2, pp. 197–213, 2005, doi: 10.1016/j.fluid.2004.11.011.

[78] S. A. Freeman, J. Davis, and G. T. Rochelle, “Degradation of aqueous piperazine in carbon dioxide capture,” *Int. J. Greenh. Gas Control*, vol. 4, no. 5, pp. 756–761, 2010, doi: 10.1016/j.ijggc.2010.03.009.

[79] F. Bougie and M. C. Iliuta, “CO2 Absorption in Aqueous Piperazine Solutions:

Experimental Study and Modeling," *J. Chem. Eng. Data*, vol. 56, no. 4, pp. 1547–1554, Apr. 2011, doi: 10.1021/je1012247.

[80] H. Liu *et al.*, "Solubility, Kinetics, Absorption Heat and Mass Transfer Studies of CO2 Absorption into Aqueous Solution of 1-Dimethylamino-2-propanol," *Energy Procedia*, vol. 63, pp. 659–664, 2014, doi: 10.1016/j.egypro.2014.11.073.

[81] H. Liu, M. Xiao, Z. Liang, W. Rongwong, J. Li, and P. Tontiwachwuthikul, "Analysis of Reaction Kinetics of CO2 Absorption into a Novel 1-(2-Hydroxyethyl)-piperidine Solvent Using Stopped-Flow Technique," *Ind. Eng. Chem. Res.*, vol. 54, no. 50, pp. 12525–12533, Dec. 2015, doi: 10.1021/acs.iecr.5b03412.

[82] N. El Hadri, D. V. Quang, E. L. V Goetheer, and M. R. M. Abu Zahra, "Aqueous amine solution characterization for post-combustion CO2 capture process," *Appl. Energy*, vol. 185, pp. 1433–1449, 2017, doi: https://doi.org/10.1016/j.apenergy.2016.03.043.

[83] H. Li, Y. Le Moullec, J. Lu, J. Chen, J. C. V. Marcos, and G. Chen, "Solubility and energy analysis for CO2 absorption in piperazine derivatives and their mixtures," *Int. J. Greenh. Gas Control*, vol. 31, pp. 25–32, 2014, doi: https://doi.org/10.1016/j.ijggc.2014.09.012.

[84] A. Nouacer, F. B. Belaribi, I. Mokbel, and J. Jose, "Solubility of carbon dioxide gas in some 2.5M tertiary amine aqueous solutions," *J. Mol. Liq.*, vol. 190, pp. 68–73, 2014, doi: https://doi.org/10.1016/j.molliq.2013.10.026.

[85] Y. Liang, H. Liu, W. Rongwong, Z. Liang, R. Idem, and P. Tontiwachwuthikul, "Solubility, absorption heat and mass transfer studies of CO2 absorption into aqueous solution of 1-dimethylamino-2-propanol," *Fuel*, vol. 144, pp. 121–129, 2015, doi: https://doi.org/10.1016/j.fuel.2014.11.098.

[86] Z. Xu, S. Wang, and C. Chen, "Kinetics Study on CO2 Absorption with Aqueous Solutions of 1,4-Butanediamine, 2-(Diethylamino)-ethanol, and Their Mixtures," *Ind. Eng. Chem. Res.*, vol. 52, no. 29, pp. 9790–9802, Jul. 2013, doi: 10.1021/ie4012936.

[87] A. V Rayer and A. Henni, "Heats of Absorption of CO2 in Aqueous Solutions of Tertiary Amines: N-Methyldiethanolamine, 3-Dimethylamino-1-propanol, and 1-Dimethylamino-2-propanol," *Ind. Eng. Chem. Res.*, vol. 53, no. 12, pp. 4953–4965, Mar. 2014, doi: 10.1021/ie4041324.

[88] S. Singto *et al.*, "Synthesis of new amines for enhanced carbon dioxide (CO2) capture performance: The effect of chemical structure on equilibrium solubility, cyclic capacity,

kinetics of absorption and regeneration, and heats of absorption and regeneration," *Sep. Purif. Technol.*, vol. 167, pp. 97–107, 2016, doi: https://doi.org/10.1016/j.seppur.2016.05.002.

[89] F. A. Chowdhury, H. Okabe, H. Yamada, M. Onoda, and Y. Fujioka, "Synthesis and selection of hindered new amine absorbents for CO2 capture," *Energy Procedia*, vol. 4, pp. 201–208, 2011, doi: https://doi.org/10.1016/j.egypro.2011.01.042.

[90] J. Rolker and M. Seiler, "Industrial Progress: New Energy-Efficient Absorbents for the CO₂ Separation from Natural Gas, Syngas and Flue Gas," *Adv. Chem. Eng. Sci.*, vol. 01, no. 04, pp. 280–288, 2011, doi: 10.4236/aces.2011.14039.

[91] F. A. Chowdhury, H. Okabe, S. Shimizu, M. Onoda, and Y. Fujioka, "Development of novel tertiary amine absorbents for CO2 capture," *Energy Procedia*, vol. 1, no. 1, pp. 1241–1248, 2009, doi: https://doi.org/10.1016/j.egypro.2009.01.163.

[92] T. Sema, A. Naami, R. Idem, and P. Tontiwachwuthikul, "Correlations for Equilibrium Solubility of Carbon Dioxide in Aqueous 4-(Diethylamino)-2-butanol Solutions," *Ind. Eng. Chem. Res.*, vol. 50, no. 24, pp. 14008–14015, Dec. 2011, doi: 10.1021/ie2008345.

[93] D. Fu, J. Xie, F. Wang, and S. Wang, "Investigation of surface tension and viscosity for aqueous solutions of MEA-MeOH and DEA-MeOH," *J. Chem. Thermodyn.*, vol. 116, no. September, pp. 197–205, 2018, doi: 10.1016/j.jct.2017.08.024.

[94] G. Hee, S. Youl, J. Kyun, W. Hi, J. Kim, and J. Kim, "CO 2 absorption kinetics in a CO 2 -free and partially loaded aqueous ammonia solution," *Chem. Eng. J.*, vol. 250, pp. 83–90, 2014, doi: 10.1016/j.cej.2014.03.120.

[95] V. Darde, K. Thomsen, W. J. M. van Well, and E. H. Stenby, "Chilled ammonia process for CO2 capture," *Int. J. Greenh. Gas Control*, vol. 4, no. 2, pp. 131–136, 2010, doi: https://doi.org/10.1016/j.ijggc.2009.10.005.

[96] F. Qin, S. Wang, A. Hartono, H. F. Svendsen, and C. Chen, "Kinetics of CO2 absorption in aqueous ammonia solution," *Int. J. Greenh. Gas Control*, vol. 4, no. 5, pp. 729–738, 2010, doi: https://doi.org/10.1016/j.ijggc.2010.04.010.

[97] Y. Xu, Z. Wang, X. Liu, and B. Jin, "Modeling of the NH3–CO2–H2O vapor–liquid equilibria behavior with species-group Pitzer activity coefficient model," *Int. J. Greenh. Gas Control*, vol. 31, pp. 113–120, 2014, doi: https://doi.org/10.1016/j.ijggc.2014.09.018.

[98] S. Ma, G. Chen, S. Zhu, T. Han, and W. Yu, "Mass transfer of ammonia escape and CO2

absorption in CO2 capture using ammonia solution in bubbling reactor," *Appl. Energy*, vol. 162, pp. 354–362, 2016, doi: https://doi.org/10.1016/j.apenergy.2015.10.089.

[99] D. P. Hanak, C. Biliyok, and V. Manovic, "Rate-based model development, validation and analysis of chilled ammonia process as an alternative CO2 capture technology for coal-fired power plants," *Int. J. Greenh. Gas Control*, vol. 34, pp. 52–62, 2015, doi: https://doi.org/10.1016/j.ijggc.2014.12.013.

[100] T. N. G. Borhani, A. Azarpour, V. Akbari, S. R. Wan Alwi, and Z. A. Manan, "CO2 capture with potassium carbonate solutions: A state-of-the-art review," *Int. J. Greenh. Gas Control*, vol. 41, pp. 142–162, 2015, doi: https://doi.org/10.1016/j.ijggc.2015.06.026.

[101] R. Moene, L. Schoon, J. van Straelen, and F. Geuzebroek, "Precipitating Carbonate Process for Energy Efficient Post-combustion CO2 Capture," *Energy Procedia*, vol. 37, pp. 1881–1887, 2013, doi: https://doi.org/10.1016/j.egypro.2013.06.068.

[102] H. Knuutila, H. F. Svendsen, and M. Anttila, "CO2 capture from coal-fired power plants based on sodium carbonate slurry; a systems feasibility and sensitivity study," *Int. J. Greenh. Gas Control*, vol. 3, no. 2, pp. 143–151, 2009, doi: https://doi.org/10.1016/j.ijggc.2008.06.006.

[103] J. K. Stolaroff, D. W. Keith, and G. V Lowry, "Carbon Dioxide Capture from Atmospheric Air Using Sodium Hydroxide Spray," *Environ. Sci. Technol.*, vol. 42, no. 8, pp. 2728–2735, Apr. 2008, doi: 10.1021/es702607w.

[104] S.-J. Han, M. Yoo, D.-W. Kim, and J.-H. Wee, "Carbon Dioxide Capture Using Calcium Hydroxide Aqueous Solution as the Absorbent," *Energy & Fuels*, vol. 25, no. 8, pp. 3825–3834, Aug. 2011, doi: 10.1021/ef200415p.

[105] U. E. Aronu, A. Hartono, K. A. Hoff, and H. F. Svendsen, "Kinetics of Carbon Dioxide Absorption into Aqueous Amino Acid Salt: Potassium Salt of Sarcosine Solution," *Ind. Eng. Chem. Res.*, vol. 50, no. 18, pp. 10465–10475, Sep. 2011, doi: 10.1021/ie200596y.

[106] H. Knuutila, U. E. Aronu, H. M. Kvamsdal, and A. Chikukwa, "Post combustion CO2 capture with an amino acid salt," *Energy Procedia*, vol. 4, pp. 1550–1557, 2011, doi: https://doi.org/10.1016/j.egypro.2011.02.024.

[107] U. E. Aronu, E. T. Hessen, T. Haug-Warberg, K. A. Hoff, and H. F. Svendsen, "Vapor–liquid equilibrium in amino acid salt system: Experiments and modeling," *Chem. Eng. Sci.*, vol. 66, no. 10, pp. 2191–2198, 2011, doi: https://doi.org/10.1016/j.ces.2011.02.033.

[108] D. G. Kidnay, A. J., Kidnay, A. J., Parrish, W. R. & McCartney, *fundamentals of Natural gas Processing*, 2nd editio. CRC press, 2011.

[109] S. Mokhatab and W. A. Poe, *Chapter 7 - Natural Gas Sweetening*. Boston: Gulf Professional Publishing, 2012.

[110] K. A. Mumford *et al.*, "Evaluation of the protic ionic liquid, N,N-dimethyl-aminoethylammonium formate for CO2 capture," *Int. J. Greenh. Gas Control*, vol. 32, pp. 129–134, 2015, doi: https://doi.org/10.1016/j.ijggc.2014.11.011.

[111] M. Aghaie, N. Rezaei, and S. Zendehboudi, "A systematic review on CO2 capture with ionic liquids: Current status and future prospects," *Renew. Sustain. Energy Rev.*, vol. 96, pp. 502–525, 2018, doi: https://doi.org/10.1016/j.rser.2018.07.004.

[112] J. F. Brennecke and B. E. Gurkan, "Ionic Liquids for CO2 Capture and Emission Reduction," *J. Phys. Chem. Lett.*, vol. 1, no. 24, pp. 3459–3464, Dec. 2010, doi: 10.1021/jz1014828.

[113] R. Krupiczka, A. Rotkegel, and Z. Ziobrowski, "Comparative study of CO2 absorption in packed column using imidazolium based ionic liquids and MEA solution," *Sep. Purif. Technol.*, vol. 149, pp. 228–236, 2015, doi: https://doi.org/10.1016/j.seppur.2015.05.026.

[114] M. E. Boot-Handford *et al.*, "Carbon capture and storage update," *Energy Environ. Sci.*, vol. 7, no. 1, pp. 130–189, 2014, doi: 10.1039/C3EE42350F.

[115] M. Hasib-ur-Rahman, M. Siaj, and F. Larachi, "Ionic liquids for CO2 capture—Development and progress," *Chem. Eng. Process. Process Intensif.*, vol. 49, no. 4, pp. 313–322, 2010, doi: https://doi.org/10.1016/j.cep.2010.03.008.

[116] F. Karadas, M. Atilhan, and S. Aparicio, "Review on the Use of Ionic Liquids (ILs) as Alternative Fluids for CO2 Capture and Natural Gas Sweetening," *Energy & Fuels*, vol. 24, no. 11, pp. 5817–5828, Nov. 2010, doi: 10.1021/ef1011337.

[117] M. Ramdin, T. W. de Loos, and T. J. H. Vlugt, "State-of-the-Art of CO2 Capture with Ionic Liquids," *Ind. Eng. Chem. Res.*, vol. 51, no. 24, pp. 8149–8177, Jun. 2012, doi: 10.1021/ie3003705.

[118] X. Zhang, X. Zhang, H. Dong, Z. Zhao, S. Zhang, and Y. Huang, "Carbon capture with ionic liquids: overview and progress," *Energy Environ. Sci.*, vol. 5, no. 5, pp. 6668–6681, 2012, doi: 10.1039/C2EE21152A.

[119] Z. Lei, C. Dai, and B. Chen, "Gas Solubility in Ionic Liquids," *Chem. Rev.*, vol. 114, no. 2,

pp. 1289–1326, Jan. 2014, doi: 10.1021/cr300497a.

[120] S. Zeng *et al.*, "Ionic-Liquid-Based CO2 Capture Systems: Structure, Interaction and Process," *Chem. Rev.*, vol. 117, no. 14, pp. 9625–9673, Jul. 2017, doi: 10.1021/acs.chemrev.7b00072.

[121] D. W. Savage, G. Sartori, and G. Astarita, "Amines as rate promoters for carbon dioxide hydrolysis," *Faraday Discuss. Chem. Soc.*, vol. 77, no. 0, pp. 17–31, 1984, doi: 10.1039/DC9847700017.

[122] T. N. G. Borhani, V. Akbari, M. K. A. Hamid, and Z. A. Manan, "Rate-based simulation and comparison of various promoters for CO2 capture in industrial DEA-promoted potassium carbonate absorption unit," *J. Ind. Eng. Chem.*, vol. 22, pp. 306–316, 2015, doi: https://doi.org/10.1016/j.jiec.2014.07.024.

[123] H. Thee, N. J. Nicholas, K. H. Smith, G. da Silva, S. E. Kentish, and G. W. Stevens, "A kinetic study of CO2 capture with potassium carbonate solutions promoted with various amino acids: Glycine, sarcosine and proline," *Int. J. Greenh. Gas Control*, vol. 20, pp. 212–222, 2014, doi: https://doi.org/10.1016/j.ijggc.2013.10.027.

[124] A. Lee *et al.*, "A study of the vapour–liquid equilibrium of CO2 in mixed solutions of potassium carbonate and potassium glycinate," *Int. J. Greenh. Gas Control*, vol. 36, pp. 27–33, 2015, doi: https://doi.org/10.1016/j.ijggc.2015.02.007.

[125] J. Liu, S. Wang, B. Zhao, G. Qi, and C. Chen, "Study on mass transfer and kinetics of CO2 absorption into aqueous ammonia and piperazine blended solutions," *Chem. Eng. Sci.*, vol. 75, pp. 298–308, 2012, doi: https://doi.org/10.1016/j.ces.2012.03.047.

[126] H. Yu, Q. Xiang, M. Fang, Q. Yang, and P. Feron, "Promoted CO2 absorption in aqueous ammonia," *Greenh. Gases Sci. Technol.*, vol. 2, no. 3, pp. 200–208, 2012, doi: 10.1002/ghg.1280.

[127] J. Yu, S. Wang, and H. Yu, "Experimental studies and rate-based simulations of CO2 absorption with aqueous ammonia and piperazine blended solutions," *Int. J. Greenh. Gas Control*, vol. 50, pp. 135–146, 2016, doi: https://doi.org/10.1016/j.ijggc.2016.04.019.

[128] T. Chakravarty, U. K. Phukan, and R. H. Weilund, *Reaction of Acid Gases With Mixtures of Amines*, vol. 81:4. 1985.

[129] R. Sakwattanapong, A. Aroonwilas, and A. Veawab, "Behavior of Reboiler Heat Duty for CO2 Capture Plants Using Regenerable Single and Blended Alkanolamines," *Ind. Eng.*

Chem. Res., vol. 44, no. 12, pp. 4465–4473, Jun. 2005, doi: 10.1021/ie050063w.

[130] P.-Y. Chung, A. N. Soriano, R. B. Leron, and M.-H. Li, "Equilibrium solubility of carbon dioxide in the amine solvent system of (triethanolamine+piperazine+water)," *J. Chem. Thermodyn.*, vol. 42, no. 6, pp. 802–807, 2010, doi: https://doi.org/10.1016/j.jct.2010.02.005.

[131] A. Samanta and S. S. Bandyopadhyay, "Absorption of carbon dioxide into piperazine activated aqueous N-methyldiethanolamine," *Chem. Eng. J.*, vol. 171, no. 3, pp. 734–741, 2011, doi: https://doi.org/10.1016/j.cej.2011.02.008.

[132] G. Puxty and R. Rowland, "Modeling CO2 Mass Transfer in Amine Mixtures: PZ-AMP and PZ-MDEA," *Environ. Sci. Technol.*, vol. 45, no. 6, pp. 2398–2405, Mar. 2011, doi: 10.1021/es1022784.

[133] R. Dugas and G. Rochelle, "Absorption and desorption rates of carbon dioxide with monoethanolamine and piperazine," *Energy Procedia*, vol. 1, no. 1, pp. 1163–1169, 2009, doi: https://doi.org/10.1016/j.egypro.2009.01.153.

[134] M. Nainar and A. Veawab, "Corrosion in CO2 Capture Process Using Blended Monoethanolamine and Piperazine," *Ind. Eng. Chem. Res.*, vol. 48, no. 20, pp. 9299–9306, Oct. 2009, doi: 10.1021/ie801802a.

[135] D.-J. Seo and W.-H. Hong, "Solubilities of Carbon Dioxide in Aqueous Mixtures of Diethanolamine and 2-Amino-2-methyl-1-Propanol," *J. Chem. Eng. Data*, vol. 41, no. 2, pp. 258–260, Jan. 1996, doi: 10.1021/je950197o.

[136] C. Nwaoha *et al.*, "Carbon dioxide (CO2) capture: Absorption-desorption capabilities of 2-amino-2-methyl-1-propanol (AMP), piperazine (PZ) and monoethanolamine (MEA) tri-solvent blends," *J. Nat. Gas Sci. Eng.*, vol. 33, pp. 742–750, 2016, doi: 10.1016/j.jngse.2016.06.002.

[137] C. S. Ume, E. Alper, and F. P. Gordesli, "Kinetics of Carbon Dioxide Reaction with Aqueous Mixture of Piperazine and propanediol," 2013, doi: 10.1002/kin.20752.

[138] A. V Rayer, K. Z. Sumon, T. Sema, A. Henni, R. O. Idem, and P. Tontiwachwuthikul, "Part 5c: Solvent chemistry: solubility of CO2 in reactive solvents for post-combustion CO2," *Carbon Manag.*, vol. 3, no. 5, pp. 467–484, Oct. 2012, doi: 10.4155/cmt.12.47.

[139] H. Chang and C. Shih, "Simulation and Optimization for Power Plant Flue Gas CO2 Absorption-Stripping Systems," *Sep. Sci. Technol.*, vol. 40, no. 4, pp. 877–909, Mar. 2005,

doi: 10.1081/SS-200048014.

[140] K. Goto, H. Okabe, F. Alam, S. Shimizu, and Y. Fujioka, “International Journal of Greenhouse Gas Control Development of novel absorbents for CO 2 capture from blast furnace gas,” *Int. J. Greenh. Gas Control*, vol. 5, no. 5, pp. 1214–1219, 2011, doi: 10.1016/j.ijggc.2011.06.006.

[141] A. T. Zoghi, F. Feyzi, and S. Zarrinpashneh, “Experimental investigation on the effect of addition of amine activators to aqueous solutions of N-methyldiethanolamine on the rate of carbon dioxide absorption,” *Int. J. Greenh. Gas Control*, vol. 7, pp. 12–19, 2012, doi: https://doi.org/10.1016/j.ijggc.2011.12.001.

[142] Z. Feng, M. Jing-Wen, Z. Zheng, W. You-Ting, and Z. Zhi-Bing, “Study on the absorption of carbon dioxide in high concentrated MDEA and ILs solutions,” *Chem. Eng. J.*, vol. 181–182, pp. 222–228, 2012, doi: https://doi.org/10.1016/j.cej.2011.11.066.

[143] Y. Zhao *et al.*, “Density, viscosity, and performances of carbon dioxide capture in 16 absorbents of amine + ionic liquid + H 2O, ionic liquid + H2O, and Amine + H2O systems,” *J. Chem. Eng. Data*, vol. 55, no. 9, pp. 3513–3519, 2010, doi: 10.1021/je100078w.

[144] F. L. Bernard *et al.*, “Anticorrosion Protection by Amine-Ionic Liquid Mixtures: Experiments and Simulations,” *J. Chem. Eng. Data*, vol. 61, no. 5, pp. 1803–1810, May 2016, doi: 10.1021/acs.jced.5b00996.

[145] J. Yang, X. Yu, J. Yan, and S.-T. Tu, “CO2 Capture Using Amine Solution Mixed with Ionic Liquid,” *Ind. Eng. Chem. Res.*, vol. 53, no. 7, pp. 2790–2799, Feb. 2014, doi: 10.1021/ie4040658.

[146] J. Yang, X. Yu, L. An, S.-T. Tu, and J. Yan, “CO2 capture with the absorbent of a mixed ionic liquid and amine solution considering the effects of SO2 and O2,” *Appl. Energy*, vol. 194, pp. 9–18, 2017, doi: https://doi.org/10.1016/j.apenergy.2017.02.071.

[147] A. V. Rayer, A. Henni, and J. Li, “Reaction kinetics of 2-((2-aminoethyl) amino) ethanol in aqueous and non-aqueous solutions using the stopped-flow technique,” *Can. J. Chem. Eng.*, vol. 91, no. 3, pp. 490–498, 2013, doi: 10.1002/cjce.21690.

[148] S.-W. Park, B.-S. Choi, and J.-W. Lee, “Chemical absorption of carbon dioxide with triethanolamine in non-aqueous solutions,” *Korean J. Chem. Eng.*, vol. 23, no. 1, pp. 138–143, 2006, doi: 10.1007/BF02705705.

[149] C.-H. Yu, T.-W. Wu, and C.-S. Tan, “CO2 capture by piperazine mixed with non-aqueous

solvent diethylene glycol in a rotating packed bed," *Int. J. Greenh. Gas Control*, vol. 19, pp. 503–509, 2013, doi: 10.1016/j.ijggc.2013.10.014.

[150] J. Tan, H. Shao, J. Xu, L. Du, and G. Luo, "Mixture absorption system of monoethanolamine-triethylene glycol for CO2 capture," *Ind. Eng. Chem. Res.*, vol. 50, no. 7, pp. 3966–3976, 2011, doi: 10.1021/ie101810a.

[151] V. D. Spasojevic, B. D. Djordjevic, S. P. Šerbanovic, I. R. Radovic, and M. Lj Kijevčanin, "Densities, refractive indices, viscosities, and spectroscopic study of 1-amino-2-propanol + 1-butanol and + 2-butanol solutions at (288.15 to 333.15) K," *J. Chem. Eng. Data*, vol. 59, no. 6, pp. 1817–1829, 2014, doi: 10.1021/je401036f.

[152] G. P. Dubey and K. Kumar, "Thermodynamic properties of binary liquid mixtures of diethylenetriamine with alcohols at different temperatures," *Thermochim. Acta*, vol. 524, no. 1–2, pp. 7–17, 2011, doi: 10.1016/j.tca.2011.06.003.

[153] K. Fu, W. Rongwong, Z. Liang, Y. Na, R. Idem, and P. Tontiwachwuthikul, "Experimental analyses of mass transfer and heat transfer of post-combustion CO 2 absorption using hybrid solvent MEA – MeOH in an absorber," *Chem. Eng. J.*, vol. 260, pp. 11–19, 2015, doi: 10.1016/j.cej.2014.08.064.

[154] G. Jie, Y. Jun, Z. Feifei, C. Xin, T. Ming, and K. Wanzhong, "Study on Absorption and Regeneration Performance of Novel Hybrid Solutions for CO 2 Capture," vol. 18, no. 1, pp. 66–72, 2016.

[155] A. Henni and A. E. Mather, "Solubility of Carbon Dioxide in Methyldiethanolamine + Methanol + Water," *J. Chem. Eng. Data*, vol. 40, no. 2, pp. 493–495, 1995, doi: 10.1021/je00018a030.

[156] K. N. H. Tounsi, A. Barreau, E. Le Corre, P. Mougin, and E. Neau, "Measurement of Carbon Dioxide Solubility in a Solution of Diethanolamine Mixed with Methanol," pp. 9239–9243, 2005, doi: 10.1021/ie0580250.

[157] F. J. Tamajón, E. Álvarez, F. Cerdeira, and D. Gómez-díaz, "CO 2 absorption into N-methyldiethanolamine aqueous-organic solvents," vol. 283, pp. 1069–1080, 2016, doi: 10.1016/j.cej.2015.08.065.

[158] A. Valtz, C. Coquelet, and D. Richon, "Volumetric properties of the monoethanolamine-methanol mixture at atmospheric pressure from 283.15 to 353.15 K," *Thermochim. Acta*, vol. 428, no. 1–2, pp. 185–191, 2005, doi: 10.1016/j.tca.2004.11.015.

[159] D. Roy, M. F. Wahab, M. Talebi, and D. W. Armstrong, “Replacing methanol with azeotropic ethanol as the co-solvent for improved chiral separations with supercritical fluid chromatography (SFC),” *Green Chem.*, vol. 22, no. 4, pp. 1249–1257, 2020, doi: 10.1039/c9gc04207e.

[160] G. F. Versteeg and W. P. M. van Swaaij, “On the kinetics between CO2 and alkanolamines both in aqueous and non-aqueous solutions-II. Tertiary amines,” *Chem. Eng. Sci.*, vol. 43, no. 3, pp. 587–591, 1988, doi: 10.1016/0009-2509(88)87018-0.

[161] M. Lee and T. Lin, “Density and Viscosity for Monoethanolamine + Water, + Ethanol, and+ 2-Propanol,” *ournal Chem. Eng. Data*, vol. 40, no. 1, pp. 336–339, 1995, doi: 10.1021/je00017a074.

[162] R. P. Alicia Garcı´a-Abuı´n, Diego Go´mez-Dı´az, M. Dolores La Rubia, Jose´ M. Navaza, “Density , Speed of Sound , and Isentropic Compressibility of Triethanolamine (or N -Methyldiethanolamine) + Water + Ethanol Solutions from t =(15 to 50) ° C,” *J. Chem. Eng. Data*, vol. 54, pp. 3114–3117, 2009, doi: 10.1021/je900064e.

[163] A. Estrella, D. Go, M. D. La Rubia, M. Navaza, and R. Pacheco, “Density and Speed of Sound of Binary Mixtures of N -Methyldiethanolamine and Triethanolamine with Ethanol,” pp. 2059–2061, 2007, doi: 10.1021/je700245a.

[164] E. Álvarez, D. Gómez-díaz, M. D. La Rubia, and J. M. Navaza, “Surface Tension of Binary Mixtures of N -Methyldiethanolamine and Triethanolamine with Ethanol,” *J. Chem. Eng. Data*, vol. 53, pp. 874–876, 2008, doi: 10.1021/je700647x.

[165] A. Henni, Y. Maham, P. Tontiwachwuthikul, A. Chakma, and A. E. Mather, “Densities and Viscosities for Binary Mixtures of N -Methyldiethanolamine + Triethylene Glycol Monomethyl Ether from 25 ° C to 70 ° C and N -Methyldiethanolamine + Ethanol Mixtures at 40 ° C,” pp. 247–253, 2000, doi: 10.1021/je9902140.

[166] Q. Liu, C. Zhu, T. Fu, and Y. Ma, “Volumetric and Viscometric Properties of Alcohol Amines + Ethanol Binary Mixtures,” *J. Chem. Eng. Data*, vol. 62, no. 10, pp. 3261–3273, 2017, doi: 10.1021/acs.jced.7b00321.

[167] Z. Li, D. Zhao, Y. Zhuang, F. Yang, X. Liu, and Y. Chen, “Volumetric properties of monoethanolamine and alcohol binary mixtures at different temperatures and 0.1 MPa,” *J. Chem. Thermodyn.*, 2019, doi: https://doi.org/10.1016/j.jct.2019.01.025.

[168] D. Ma, Q. Liu, C. Zhu, H. Feng, and Y. Ma, “Volumetric and viscometric properties of

ternary solution of (N-methyldiethanolamine + monoethanolamine + ethanol)," *J. Chem. Thermodyn.*, vol. 134, pp. 5–19, Jul. 2019, doi: 10.1016/j.jct.2019.02.019.

[169] J. M. Smith, H. C. Van Ness, and B. I. Bhatt, *INTRODUCTION TO CHEMICAL ENGINEERING*, 6th ed. 2001.

[170] H. Devoe, *Thermodynamics and Chemistry*, 2nd ed. 2012.

[171] R. Nieto, M. C. Gonzalez, and F. Herrero, "Thermodynamics of mixtures: Functions of mixing and excess functions," *Am. J. Phys.*, vol. 67, no. 12, pp. 1096–1099, 1999, doi: 10.1119/1.19089.

[172] F. Pouryousefi, R. Idem, T. Supap, and P. Tontiwachwuthikul, "Artificial Neural Networks for Accurate Prediction of Physical Properties of Aqueous Quaternary Systems of Carbon Dioxide (CO2)-Loaded 4-(Diethylamino)-2-butanol and Methyldiethanolamine Blended with Monoethanolamine," *Ind. Eng. Chem. Res.*, vol. 55, no. 44, pp. 11614–11621, 2016, doi: 10.1021/acs.iecr.6b03018.

[173] H. Gao, G. Gao, H. Liu, X. Luo, Z. Liang, and R. O. Idem, "Density, Viscosity, and Refractive Index of Aqueous CO2-Loaded and -Unloaded Ethylaminoethanol (EAE) Solutions from 293.15 to 323.15 K for Post Combustion CO2 Capture," *J. Chem. Eng. Data*, vol. 62, pp. 4205–4214, 2017, doi: 10.1021/acs.jced.7b00586.

[174] A. Hartono, E. O. Mba, and H. F. Svendsen, "Physical Properties of Partially CO 2 Loaded Aqueous Monoethanolamine (MEA)," *J. Chem. Eng. Data*, vol. 59, p. 1808−1816, 2014, doi: 10.1021/je401081e.

[175] J. Zhang, P. S. Fennell, and J. P. M. Trusler, "Density and Viscosity of Partially Carbonated Aqueous Tertiary Alkanolamine Solutions at Temperatures between (298.15 and 353.15) K," *J. Chem. Eng. Data*, vol. 60, no. 8, pp. 2392–2399, 2015, doi: 10.1021/acs.jced.5b00282.

[176] Z. Idris and D. A. Eimer, "Density Measurements of Unloaded and CO2-Loaded 3-Amino-1-propanol Solutions at Temperatures (293.15 to 353.15) K," *J. Chem. Eng. Data*, vol. 61, no. 1, pp. 173–181, 2016, doi: 10.1021/acs.jced.5b00412.

[177] R. H. Weiland, J. C. Dingman, D. B. Cronin, and G. J. Browning, "Density and viscosity of some partially carbonated aqueous alkanolamine solutions and their blends," *J. Chem. Eng. Data*, vol. 43, no. 3, pp. 378–382, 1998, doi: 10.1021/je9702044.

[178] O. Redlich and A. T. Kister, "Algebraic Representation of Thermodynamic Properties and

the Classification of Solutions," *Ind. Eng. Chem.*, vol. 40, no. 2, pp. 345–348, 1948, doi: 10.1021/ie50458a036.

[179] T. A. Graber, H. R. Galleguillos, C. Céspedes, and M. E. Taboada, "Density, Refractive Index, Viscosity, and Electrical Conductivity in the Na2CO3 + Poly(ethylene glycol) + H2O System from (293.15 to 308.15) K," *J. Chem. Eng. Data*, vol. 49, no. 5, pp. 1254–1257, Sep. 2004, doi: 10.1021/je034233s.

[180] S. S. Navarro, R. B. Leron, A. N. Soriano, and M. Li, "Thermophysical property characterization of aqueous amino acid salt solution containing serine," *J. Chem. Thermodyn.*, 2014, doi: 10.1016/j.jct.2014.05.019.

[181] J. C. Thermodynamics, A. A. R. Garcia, R. B. Leron, A. N. Soriano, and M. Li, "Thermophysical property characterization of aqueous amino acid salt solutions containing a -aminobutyric acid," *J. Chem. Thermodyn.*, vol. 81, pp. 136–142, 2015, doi: 10.1016/j.jct.2014.10.005.

[182] L. Tirona, R. B. Leron, A. N. Soriano, and M. Li, "Densities , viscosities , refractive indices , and electrical conductivities of aqueous alkali salts of α -alanine," *J. Chem. Thermodyn.*, 2014, doi: 10.1016/j.jct.2014.05.014.

[183] G. Murshid, H. Ghaedi, M. Ayoub, S. Garg, and W. Ahmad, "Experimental and correlation of viscosity and refractive index of non-aqueous system of diethanolamine (DEA) and dimethylformamide (DMF) for CO 2 capture," vol. 250, pp. 162–170, 2018, doi: 10.1016/j.molliq.2017.11.176.

[184] A. Jouyban, A. Fathi Azarbayjani, M. Khoubnasabjafari, and W. Acree, "Mathematical representation of the density of liquid mixtures at various temperatures using Jouyban-Acree model," *Indian J. Chem. - Sect. A Inorganic, Phys. Theor. Anal. Chem.*, vol. 44, pp. 1553–1560, Aug. 2005.

[185] S. S. Karunarathne, D. A. Eimer, and L. E. Øi, "Density, viscosity, and excess properties of MDEA + H2O, DMEA + H2O, and DEEA + H2O mixtures," *Appl. Sci.*, vol. 10, no. 9, 2020, doi: 10.3390/app10093196.

[186] Z. Idris, N. B. Kummamuru, and D. A. Eimer, "Viscosity measurement of unloaded and CO2-loaded aqueous monoethanolamine at higher concentrations," *J. Mol. Liq.*, vol. 243, pp. 638–645, Oct. 2017, doi: 10.1016/J.MOLLIQ.2017.08.089.

[187] Z. Idris, N. B. Kummamuru, and D. a. Eimer, "Viscosity Measurement and Correlation of

Unloaded and CO2-Loaded 3-Amino-1-propanol Solution," *J. Chem. Eng. Data*, vol. 63, pp. 1454–1459, 2018, doi: 10.1021/acs.jced.7b01035.

[188] D. Fu, L. H. Chen, and L. G. Qin, "Experiment and model for the viscosity of carbonated MDEA-MEA aqueous solutions," *Fluid Phase Equilib.*, vol. 319, pp. 42–47, 2012, doi: 10.1016/j.fluid.2012.01.029.

[189] M. H. Li and Y. C. Lie, "Densities and Viscosities of Solutions of Monoethanolamine + N-methyldiethanolamine + Water and Monoethanolamine + 2-Amino-2-methyl-1-propanol + Water," *J. Chem. Eng. Data*, vol. 39, no. 3, pp. 444–447, 1994, doi: 10.1021/je00015a009.

[190] B. P. Mandal, M. Kundu, and S. S. Bandyopadhyay, "Density and viscosity of aqueous solutions of (N-methyldiethanolamine + monoethanolamine), (N-methyldiethanolamine + diethanolamine), (2-amino-2-methyl-1-propanol + monoethanolamine), and (2-amino-2-methyl-1-propanol + diethanolamine)," *J. Chem. Eng. Data*, vol. 48, no. 3, pp. 703–707, 2003, doi: 10.1021/je020206a.

[191] D. Fu, Z. Li, and F. Liu, "Experiments and model for the viscosity of carbonated 2-amino-2-methyl-1- propanol and piperazine aqueous solution," *J. Chem. Thermodyn.*, vol. 68, pp. 20–24, 2014, doi: 10.1016/j.jct.2013.08.025.

[192] R. A. McAllister, "The viscosity of liquid mixtures," *AIChE J.*, vol. 6, no. 3, pp. 427–431, 1960, doi: 10.1002/aic.690060316.

[193] E. L. Heric and J. G. Brewer, "Viscosity of Some Binary Liquid Nonelectrolyte Mixtures," *J. Chem. Eng. Data*, vol. 12, no. 4, pp. 574–583, 1967, doi: 10.1021/je60035a028.

[194] J. V Herráez, R. Belda, O. Díez, and M. Herráez, "An equation for the correlation of viscosities of binary mixtures," *J. Solution Chem.*, vol. 37, no. 2, pp. 233–248, 2008, doi: 10.1007/s10953-007-9226-2.

[195] L. GRUNBERG and A. H. NISSAN, "Mixture Law for Viscosity," *Nature*, vol. 164, no. 4175, pp. 799–800, 1949, doi: 10.1038/164799b0.

[196] J. H. Gladstone, T. P. Dale, and W. E. Gladstone, "XVII. On the influence of temperature on the refraction of light," *Proc. R. Soc. London*, vol. 9, pp. 328–331, Jan. 1859, doi: 10.1098/rspl.1857.0079.

[197] H. A. Lorentz, "On the Lorentz-Lorenz Formula and Model of Dielectric," *Ann. Phys. 9*, pp. 641–665, 1906.

[198] W. Heller, "Remarks on Refractive Index Mixture Rules," *J. Phys. Chem.*, vol. 69, no. 4,

pp. 1123–1129, Apr. 1965, doi: 10.1021/j100888a006.

[199] O. Weiner, “Theory of refraction constants,” *math.-phys. Klasse*, vol. 62, no. 5, p. 256, 1910.

[200] D. F. J. B. J. B. Arago, “Refractive properties of binary mixtures,” *Mem. Acad. Fr*, 1806.

[201] S. S. Kurtz and A. L. Ward, “The refractivity intercept and the specific refraction equation of Newton. I. development of the refractivity intercept and comparison with specific refraction equations,” *J. Franklin Inst.*, vol. 222, no. 5, pp. 563–592, 1936, doi: https://doi.org/10.1016/S0016-0032(36)90986-9.

[202] C. J. F. Bottcher, “Theory of Electric Polarization,” *Elsevier, Amsterdam*, 1952.

[203] H. Eyring and M. S. Jhon, “Significant liquid structures,” New York: John Wiley & Sons, Ltd, 1969.

[204] G. Oster, “The Scattering of Light and its Applications to Chemistry.,” *Chem. Rev.*, vol. 43, no. 2, pp. 319–365, Oct. 1948, doi: 10.1021/cr60135a005.

[205] M. Mundhwa, R. Alam, and A. Henni, “Volumetric Properties, Viscosities, and Refractive Indices for Aqueous 2-((2-Aminoethyl)amino)ethanol Solutions from (298.15 to 343.15) K,” *J. Chem. Eng. Data*, vol. 51, no. 4, pp. 1268–1273, Jul. 2006, doi: 10.1021/je060032n.

[206] F. Pouryousefi and R. O. Idem, “New analytical technique for carbon dioxide absorption solvents,” *Ind. Eng. Chem. Res.*, vol. 47, no. 4, pp. 1268–1276, 2008, doi: 10.1021/ie0709786.

[207] E. Bjørndal, “Acoustic measurement of liquid density with applications for mass measurement of oil,” 2007.

[208] M. R. Riazi, “Characterization and Properties of Petroleum Fractions,” 2007. doi: 10.1520/mnl50-eb.

[209] P. Hidnert and E. L. Peffer, “Density of solids and liquids,” *Natl. Bur. Stand. Circ. 487*, pp. 1–29, 1950.

[210] F. Spieweck and H. Bettin, “Review: Solid and liquid density determination,” *Tech. Mess.*, vol. 59, no. 6, pp. 237–244, 1992, doi: 10.1524/teme.1992.59.6.237.

[211] Wikipedia, “Oscillating U-tube,” 2018. https://en.wikipedia.org/wiki/Oscillating_U-tube (accessed Mar. 23, 2021).

[212] “Oscillating U-tube - Wikipedia.” https://en.wikipedia.org/wiki/Oscillating_U-tube (accessed Mar. 08, 2021).

[213] "U-tube technology in digital laboratory density meters :: Anton Paar Wiki." https://wiki.anton-paar.com/za-en/u-tube-technology-in-digital-laboratory-density-meters/ (accessed Mar. 08, 2021).

[214] "Density and density measurement :: Anton Paar Wiki." https://wiki.anton-paar.com/en/density-and-density-measurement/#overview-of-density-measurement-techniques (accessed Mar. 08, 2021).

[215] "Relative density - Wikipedia." https://en.wikipedia.org/wiki/Relative_density#Pycnometer (accessed Mar. 23, 2020).

[216] "Basics of viscometry :: Anton Paar Wiki." https://wiki.anton-paar.com/en/basic-of-viscometry/ (accessed Mar. 09, 2021).

[217] "How to measure viscosity :: Anton Paar Wiki." https://wiki.anton-paar.com/za-en/how-to-measure-viscosity/ (accessed Mar. 09, 2021).

[218] "Falling ball viscometer, Viscosity, By OpenStax (Page 3/3) | Jobilize." https://www.jobilize.com//physics4/test/falling-ball-viscometer-viscosity-by-openstax?qcr=www.quizover.com (accessed Mar. 09, 2021).

[219] "VISCOSITY MEASUREMENT." https://www.thermopedia.com/content/1244/ (accessed Mar. 09, 2021).

[220] D. Tomida, C. Yokoyama, E. H. Abramson, R. F. Berg, E. F. May, and V. Viscometer, "Viscometer," *PCI-Paint Coatings Ind.*, vol. IX, no. AUG, pp. 96–131, 2014, doi: 10.1007/978-1-4020-5482-2_2.

[221] T. G. Mezger, *The Rheology Handbook*, 4th ed. 2014.

[222] S. K. Mylona, "Absolute Viscosity Measurements," Aristotle University of Thessaloniki School, PhD thesis, 2014.

[223] "Viscometer." https://wikimili.com/en/Viscometer (accessed Mar. 09, 2020).

[224] "Refractometer types :: Anton Paar Wiki." https://wiki.anton-paar.com/en/refractometer-types/ (accessed Mar. 10, 2020).

[225] E. B. Rinker, D. W. Oelschlager, A. T. Colussi, K. R. Henry, and O. C. Sandall, "Viscosity, Density, and Surface Tension of Binary Mixtures of Water and N-Methyldiethanolamine and Water and Diethanolamine and Tertiary Mixtures of These Amines with Water over the Temperature Range 20–100°C," *J. Chem. Eng. Data*, vol. 39, no. 2, pp. 392–395, 1994, doi: 10.1021/je00014a046.

[226] “Density and sound velocity meter: DSA 5000 M :: Anton-Paar.com.” https://www.anton-paar.com/za-en/products/details/density-and-sound-velocity-meter-dsa-5000-m/ (accessed Mar. 08, 2019).

[227] A. Anton Paar, “Instruction Manual DSA 5000 M,” 2011. Accessed: Mar. 23, 2021. [Online]. Available: www.anton-paar.com.

[228] “Rolling-ball viscometer: Lovis 2000 M/ME :: Anton-Paar.com.” https://www.anton-paar.com/za-en/products/details/rolling-ball-viscometer-lovis-2000-mme/ (accessed Mar. 08, 2019).

[229] “Digital Refractometer | ATAGO CO.,LTD.” https://www.atago.net/product/?l=en&f=products-rx-alpha-top.php#ABd58190 (accessed Mar. 08, 2021).

[230] B. N. Taylor, “Guidelines for evaluating and expressing the uncertainty of NIST measurement results,” Gaithersburg, MD, 1994. doi: 10.6028/NIST.TN.1297.

[231] N. Moodley, “Separation and Recovery of a Complexing Agent in the Production of Lithium Hexfluorophosphate,” University of KwaZulu-Natal, 2019.

[232] D. Fu, L. Chen, and L. Qin, “Fluid Phase Equilibria Experiment and model for the viscosity of carbonated MDEA – MEA aqueous solutions,” *Fluid Phase Equilib.*, vol. 319, pp. 42–47, 2012, doi: 10.1016/j.fluid.2012.01.029.

[233] M. Hernández-Mendoza, A. Zúñiga-Moreno, M. E. Manríquez-Ramírez, and O. Elizalde-Solis, “Densities and excess molar volumes of binary systems N,N-dimethylformamide + ethanolamine or N,N-diethylethanolamine,” *J. Solution Chem.*, vol. 43, no. 11, pp. 1981–1996, 2014, doi: 10.1007/s10953-014-0250-8.

[234] A. Garcáa-Abuán, D. Gómez-Dáaz, M. D. La Rubia, and J. M. Navaza, “Density, speed of sound, viscosity, refractive index, and excess volume of N -methyl-2-pyrrolidone + ethanol (or water or ethanolamine) from T = (293.15 to 323.15) K,” *J. Chem. Eng. Data*, vol. 56, no. 3, pp. 646–651, 2011, doi: 10.1021/je100967k.

[235] X. X. Li, G. C. Fan, Z. L. Zhang, Y. W. Wang, and Y. Q. Lu, “Density and viscosity for binary mixtures of diethylene glycol monobutyl ether with monoethanolamine, diethanolamine, and triethanolamine from (293.15 to 333.15) K,” *J. Chem. Eng. Data*, vol. 58, no. 5, pp. 1229–1235, 2013, doi: 10.1021/je4000372.

[236] A. Blanco, A. García-Abuín, D. Gómez-Díaz, J. M. Navaza, and Ó. L. Villaverde, “Density,

speed of sound, viscosity, surface tension, and excess volume of N -ethyl-2-pyrrolidone + ethanolamine (or diethanolamine or triethanolamine) from T = (293.15 to 323.15) K," *J. Chem. Eng. Data*, vol. 58, no. 3, pp. 653–659, 2013, doi: 10.1021/je301123j.

[237] D. Ma, Q. Liu, C. Zhu, H. Feng, and Y. Ma, "Volumetric and viscometric properties of ternary solution of (N-methyldiethanolamine + monoethanolamine + ethanol)," *J. Chem. Thermodyn.*, vol. 134, pp. 5–19, 2019, doi: 10.1016/j.jct.2019.02.019.

[238] M. M. Taib and T. Murugesan, "Density, refractive index, and excess properties of 1-butyl-3- methylimidazolium tetrafluoroborate with water and monoethanolamine," *J. Chem. Eng. Data*, vol. 57, no. 1, pp. 120–126, 2012, doi: 10.1021/je2007204.

[239] Y. M. Tseng and A. R. Thompson, "Densities and Refractive Indices of Aqueous Monoethanolamine, Diethanolamine, Triethanolamine," *J. Chem. Eng. Data*, vol. 9, no. 2, pp. 264–267, 1964, doi: 10.1021/je60021a043.

[240] F. Murrleta-Guevara and A. Trejo Rodríguez, "Liquid density as a function of temperature of five organic solvents," *J. Chem. Eng. Data*, vol. 29, no. 2, pp. 204–206, 1984, doi: 10.1021/je00036a032.

[241] T. G. Amundsen, L. E. Øi, and D. A. Eimer, "Density and viscosity of monoethanolamine + water + carbon dioxide from (25 to 80) °C," *J. Chem. Eng. Data*, vol. 54, no. 11, pp. 3096–3100, 2009, doi: 10.1021/je900188m.

[242] J. Águila-Hernández, A. Trejo, B. E. García-Flores, and R. Molnar, "Viscometric and volumetric behaviour of binary mixtures of sulfolane and N-methylpyrrolidone with monoethanolamine and diethanolamine in the range 303-373 K," *Fluid Phase Equilib.*, vol. 267, no. 2, pp. 172–180, 2008, doi: 10.1016/j.fluid.2008.02.023.

[243] M. Yasmin and M. Gupta, "Density, viscosity, velocity and refractive index of binary mixtures of poly(Ethylene Glycol) 200 with ethanolamine, m-cresol and aniline at 298.15 K," *J. Solution Chem.*, vol. 40, no. 8, pp. 1458–1472, 2011, doi: 10.1007/s10953-011-9731-1.

[244] S. N. Khan, S. M. Hailegiorgis, Z. Man, A. M. Shariff, and S. Garg, "Thermophysical Properties of Aqueous 1-Butyl-3-Methylimidazolium Acetate [BMIM] [AC] + Monoethanolamine (MEA) Hybrid as a Solvent for CO2 Capture," *Procedia Eng.*, vol. 148, pp. 1326–1331, 2016, doi: 10.1016/j.proeng.2016.06.553.

[245] S. Tian, S. Ren, Y. Hou, W. Wu, and W. Peng, "Densities, Viscosities and Excess Properties

of Binary Mixtures of 1,1,3,3-Tetramethylguanidinium Lactate + Water at T = (303.15 to 328.15) K," *J. Chem. Eng. Data*, p. A-H, 2013, doi: 10.1021/je3009073.

[246] Y. Yin, T. Fu, C. Zhu, and Y. Ma, "Volumetric and viscometric study and FT-IR analysis of binary and ternary mixtures of 1-butyl-3-methylimidazolium tetrafluoroborate, methyldiethanolamine and water," *J. Mol. Liq.*, vol. 243, pp. 664–676, 2017, doi: 10.1016/j.molliq.2017.08.088.

[247] X. Wang, K. Kang, W. Wang, and Y. Tian, "Volumetric properties of binary mixtures of 3-(methylamino)propylamine with water, N -methyldiethanolamine, N, N -dimethylethanolamine, and N, N -diethylethanolamine from (283.15 to 363.15) K," *J. Chem. Eng. Data*, vol. 58, no. 12, pp. 3430–3439, 2013, doi: 10.1021/je400679k.

[248] A. Haghtalab and A. Shojaeian, "Volumetric and viscometric behaviour of the binary systems of N-methyldiethanolamine and diethanolamine with 1-butyl-3-methylimidazolium acetate at various temperatures," *J. Chem. Thermodyn.*, vol. 68, pp. 128–137, 2014, doi: 10.1016/j.jct.2013.09.001.

[249] S. S. Karunarathne, D. A. Eimer, K. J. Jens, and L. E. øi, "Density, viscosity, and excess properties of ternary aqueous mixtures of MDEA + MEA, DMEA + MEA, and DEEA + MEA," *Fluids*, vol. 5, no. 1, 2020, doi: 10.3390/fluids5010027.

[250] R. M. DiGuillo, R. J. Lee, S. T. Schaeffer, L. L. Brasher, and A. S. Teja, "Densities and Viscosities of the Ethanolamines," *J. Chem. Eng. Data*, vol. 37, no. 2, pp. 239–242, 1992, doi: 10.1021/je00006a028.

[251] S. A. Razavizadeh, S. Sheikh, and Z. Nassaj Gerowgi, "Measurement of thermophysical properties of pure and mixture of alkanolamines from 288.15-323.15 K," *Phys. Chem. Res.*, vol. 5, no. 2, pp. 269–279, 2017, doi: 10.22036/pcr.2017.41046.

[252] M. Vahidi and B. Moshtari, "Dielectric data, densities, refractive indices, and their deviations of the binary mixtures of N-methyldiethanolamine with sulfolane at temperatures 293.15-328.15 K and atmospheric pressure," *Thermochim. Acta*, vol. 551, pp. 1–6, 2013, doi: 10.1016/j.tca.2012.10.004.

[253] B. Hawrylak, S. E. Burke, and R. Palepu, "Partial molar and excess volumes and adiabatic compressibilities of binary mixtures of ethanolamines with water," *J. Solution Chem.*, vol. 29, no. 6, pp. 575–594, 2000, doi: 10.1023/A:1005198230692.

[254] Y. Maham, T. T. Teng, A. E. Mather, and L. G. Hepler, "Volumetric properties of (water

diethanolamine) systems," *Can. J. Chem.*, vol. 73, no. 403, pp. 1514–1519, 1995.

[255] A. Muhammad, M. I. A. Mutalib, C. D. Wilfred, T. Murugesan, and A. Shafeeq, "Viscosity, refractive index, surface tension, and thermal decomposition of aqueous N-methyldiethanolamine solutions from (298.15 to 338.15) K," *J. Chem. Eng. Data*, vol. 53, no. 9, pp. 2226–2229, 2008, doi: 10.1021/je800282a.

[256] M. M. Akbar and T. Murugesan, "Thermophysical properties for the binary mixtures of 1-hexyl-3- methylimidazolium bis(trifluoromethylsulfonyl)imide [hmim][Tf 2N] + N-methyldiethanolamine (MDEA) at temperatures (303.15 to 323.15) K," *J. Mol. Liq.*, vol. 169, pp. 95–101, 2012, doi: 10.1016/j.molliq.2012.02.014.

[257] S. N. Khan, S. M. Hailegiorgis, Z. Man, A. M. Shariff, and S. Garg, "Thermophysical properties of aqueous N-methyldiethanolamine (MDEA) and ionic liquids 1-butyl-3-methylimidazolium trifluoromethanesulfonate [bmim][OTf], 1-butyl-3-methylimidazolium acetate [bmim][Ac] hybrid solvents for CO2 capture," *Chem. Eng. Res. Des.*, vol. 121, no. March, pp. 69–80, 2017, doi: 10.1016/j.cherd.2017.02.034.

[258] J. M. Bernal-García, L. A. Galicia-Luna, K. R. Hall, M. Ramos-Estrada, and G. A. Iglesias-Silva, "Viscosities for aqueous solutions of N-methyldiethanolamine from 313.15 to 363.15 K," *J. Chem. Eng. Data*, vol. 49, no. 4, pp. 864–866, 2004, doi: 10.1021/je0302250.

[259] E. Álvarez, F. Cerdeira, D. Gómez-Diaz, and J. M. Navaza, "Density, Speed of sound, isentropic compressibility, and excess volume of binary mixtures of 1-amino-2-propanol or 3-amino-1-propanol with 2-amino-2-methyl-1-propanol, diethanolamine, or triethanolamine from (293.15 to 323.15) K," *J. Chem. Eng. Data*, vol. 55, no. 7, pp. 2567–2575, 2010, doi: 10.1021/je900739x.

[260] V. Spasojević, S. Serbanovic, P. Stefanovic, and M. Kijevcanin, "Review of technological methods and experimental determination of thermodynamic and transport properties of reagents for carbon dioxide removal from flue gases," *Hem. Ind.*, vol. 68, pp. 123–134, Jan. 2014, doi: 10.2298/HEMIND130312039S.

[261] S. P. R. A. Udara, A. Neelakantha, A. E. Dag, and C. M. Morten, "Viscosities of Pure and Aqueous Solutions of Monoethanolamine (MEA), Diethanolamine (DEA) and N-Methyldiethanolamine (MDEA)," *Annu. Trans. Nord. Rheol. Soc.*, vol. 21, no. March, pp. 299–306, 2013.

[262] J. Águila-Hernández, A. Trejo, B. E. García-Flores, and R. Molnar, "Viscometric and

volumetric behaviour of binary mixtures of sulfolane and N-methylpyrrolidone with monoethanolamine and diethanolamine in the range 303–373K," *Fluid Phase Equilib.*, vol. 267, no. 2, pp. 172–180, 2008, doi: https://doi.org/10.1016/j.fluid.2008.02.023.

[263] H. Djojoputro and S. Ismadji, "Density and viscosity of binary mixtures of ethyl-2-methylbutyrate and ethyl hexanoate with methanol, ethanol, and 1-propanol at (293.15, 303.15, and 313.15) K," *J. Chem. Eng. Data*, vol. 50, no. 4, pp. 1343–1347, 2005, doi: 10.1021/je0500633.

[264] M. T. Zafarani-Moattar and R. Majdan-Cegincara, "Density, speed of sound, and viscosity of binary mixtures of poly(propylene glycol) 400 + ethanol and + 2-propanol at different temperatures," *J. Chem. Eng. Data*, vol. 53, no. 9, pp. 2211–2216, 2008, doi: 10.1021/je8002767.

[265] A. K. Nain, "Densities and volumetric properties of (formamide + ethanol, or 1-propanol, or 1,2-ethanediol, or 1,2-propanediol) mixtures at temperatures between 293.15 K and 318.15 K," *J. Chem. Thermodyn.*, vol. 39, no. 3, pp. 462–473, 2007, doi: 10.1016/j.jct.2006.07.021.

[266] S. Mrad, C. Lafuente, M. Hichri, and I. Khattech, "Density, Speed of Sound, Refractive Index, and Viscosity of the Binary Mixtures of N , N - dimethylacetamide with Methanol and Ethanol," 2016, doi: 10.1021/acs.jced.5b01000.

[267] A. Arce, E. Rodil, and A. Soto, "Volumetric and viscosity study for the mixtures of 2-ethoxy-2- methylpropane, ethanol, and 1-ethyl-3-methylimidazolium ethyl sulfate ionic liquid," *J. Chem. Eng. Data*, vol. 51, no. 4, pp. 1453–1457, 2006, doi: 10.1021/je060126x.

[268] R. Salinas, J. Pla-franco, and E. Lladosa, "Density, Speed of Sound, Viscosity, and Excess Properties of Binary Mixtures Formed by Ethanol and Bis(tri fl uorosulfonyl)imide-Based Ionic Liquids," 2015, doi: 10.1021/je500594z.

[269] R. Belda, J. V. Herraez, and O. Diez, "A study of the refractive index and surface tension synergy of the binary water/ethanol: Influence of concentration," *Phys. Chem. Liq.*, vol. 43, no. 1, pp. 91–101, 2005, doi: 10.1080/00319100512331327342.

[270] E. Álvarez, D. Gómez-Díaz, M. D. La Rubia, J. M. Navaza, R. Pacheco, and S. Sánchez, "Density and Speed of Sound of Binary Mixtures of *N* -Methyldiethanolamine and Triethanolamine with Ethanol," *J. Chem. Eng. Data*, vol. 52, no. 5, pp. 2059–2061, 2007, doi: 10.1021/je700245a.

[271] S. L. Oswal and H. S. Desai, “Studies of viscosity and excess molar volume of binary mixtures: 2. Butylamine+1-alkanol mixtures at 303.15 and 313.15 K,” *Fluid Phase Equilib.*, vol. 161, no. 1, pp. 191–204, 1999, doi: https://doi.org/10.1016/S0378-3812(99)00165-X.

[272] H. Rafiee and F. Frouzesh, “Volumetric properties for binary and ternary mixtures of allyl alcohol, 1,3 dichloro 2-propanol and 1-ethyl-3-methyl imidazolium ethyl sulfate [Emim][EtSO4] from T = 298.15- 318.15K at ambient pressure,” *Thermochim. Acta*, vol. 611, May 2015, doi: 10.1016/j.tca.2015.04.027.

[273] S. Begum, R. Clarke, M. Ahmed, S. Begum, and M. Saleh, “Volumetric, viscosimetric and surface properties of aqueous solutions of triethylene glycol, tetraethylene glycol, and tetraethylene glycol dimethyl ether,” *J. Mol. Liq.*, vol. 177, pp. 11–18, Jan. 2013, doi: 10.1016/j.molliq.2012.09.015.

[274] V. D. Spasojević, B. D. Djordjević, S. P. Šerbanović, I. R. Radović, and M. L. Kijevčanin, “Densities, Refractive Indices, Viscosities, and Spectroscopic Study of 1-Amino-2-propanol + 1-Butanol and + 2-Butanol Solutions at (288.15 to 333.15) K,” *J. Chem. Eng. Data*, vol. 59, no. 6, pp. 1817–1829, Jun. 2014, doi: 10.1021/je401036f.

[275] F. I. Chowdhury, S. Akhtar, M. A. Saleh, M. U. Khandaker, Y. M. Amin, and A. K. Arof, “Volumetric and viscometric properties of aqueous solutions of some monoalkanolamines,” vol. 223, pp. 299–314, 2016.

[276] A. Henni, J. J. Hromek, P. Tontiwachwuthikul, and A. Chakma, “Volumetric Properties and Viscosities for Aqueous AMP Solutions from 25 °C to 70 °C,” *J. Chem. Eng. Data*, vol. 48, no. 3, pp. 551–556, Mar. 2003, doi: 10.1021/je0201119.

[277] Y. Maham, T. T. Teng, A. E. Mather, and L. G. Hepler, “Volumetric properties of (water + diethanolamine) systems,” *Can. J. Chem.*, vol. 73, no. 9, pp. 1514–1519, Sep. 1995, doi: 10.1139/v95-187.

[278] Y. Maham, T. T. Teng, L. G. Hepler, and A. E. Mather, “Densities, excess molar volumes, and partial molar volumes for binary mixtures of water with monoethanolamine, diethanolamine, and triethanolamine from 25 to 80°C,” *J. Solution Chem.*, vol. 23, no. 2, pp. 195–205, 1994, doi: 10.1007/BF00973546.